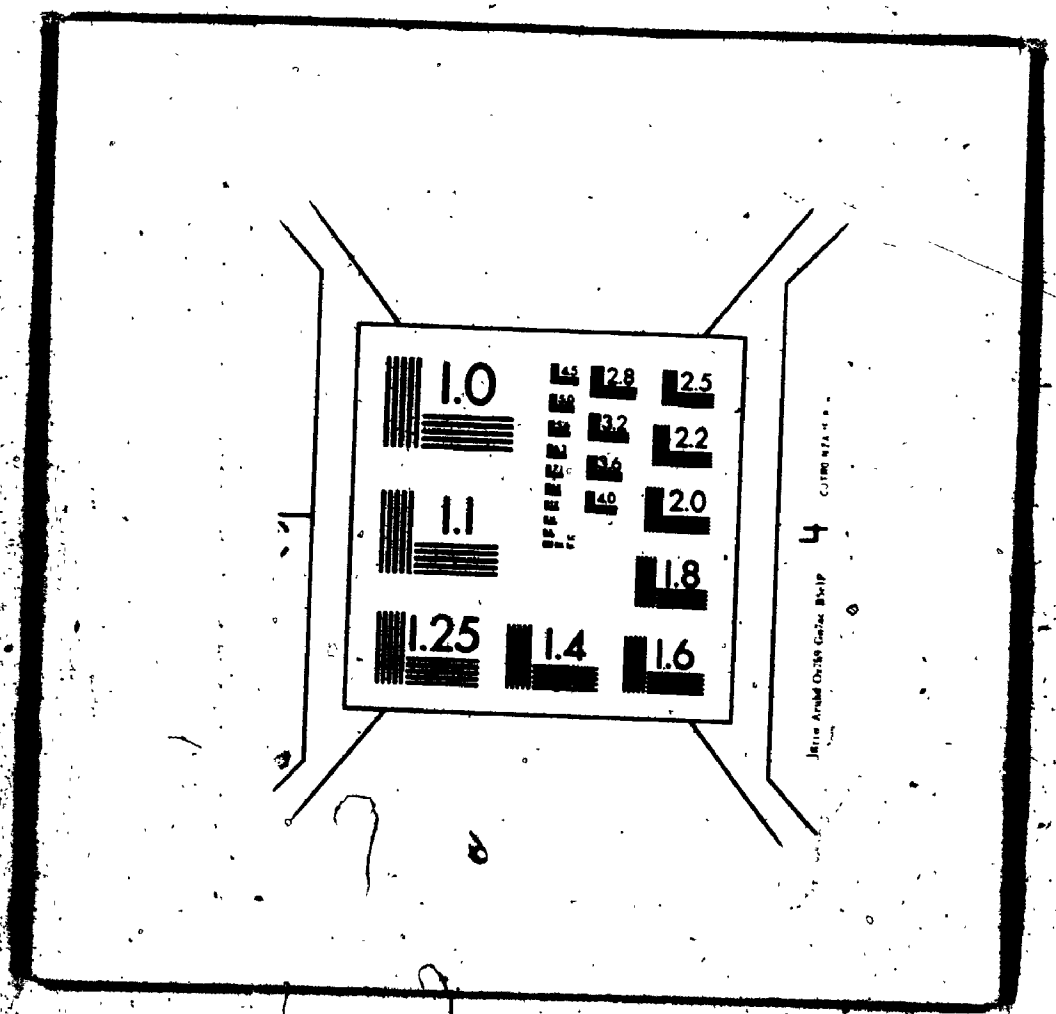
1.0
1.1
1.25
1.4
1.6
1.8
2.0
2.2
2.5
2.8
3.2
3.6
4.0

37346

National Library of Canada / Bibliothèque nationale du Canada

CANADIAN THESES ON MICROFICHE / THÈSES CANADIENNES SUR MICROFICHE

NAME OF AUTHOR/*NOM DE L'AUTEUR* ROBERT HARLAND KEMPTHORNE

TITLE OF THESIS/*TITRE DE LA THÈSE* CONTACT STRESS DISTRIBUTIONS BENEATH A RIGID STRIP FOOTING

UNIVERSITY/*UNIVERSITÉ* CARLETON UNIVERSITY

DEGREE FOR WHICH THESIS WAS PRESENTED/*GRADE POUR LEQUEL CETTE THÈSE FUT PRÉSENTÉE* MASTER OF ENGINEERING

YEAR THIS DEGREE CONFERRED/*ANNÉE D'OBTENTION DE CE DEGRÉ* 1978

NAME OF SUPERVISOR/*NOM DU DIRECTEUR DE THÈSE* Dr. A.P.S. SELVADURAI

Permission is hereby granted to the NATIONAL LIBRARY OF CANADA to microfilm this thesis and to lend or sell copies of the film.

The author reserves other publication rights, and neither the thesis nor extensive extracts from it may be printed or otherwise reproduced without the author's written permission.

L'autorisation est, par la présente, accordée à la BIBLIOTHÈQUE NATIONALE DU CANADA de microfilmer cette thèse et de prêter ou de vendre des exemplaires du film.

L'auteur se réserve les autres droits de publication; ni la thèse ni de longs extraits de celle-ci ne doivent être imprimés ou autrement reproduits sans l'autorisation écrite de l'auteur.

DATED/*DATÉ* Feb. 17/78 SIGNED/*SIGNÉ* RH Kempthorne

PERMANENT ADDRESS/*RÉSIDENCE FIXÉ* 1490 RAVEN AVE.
OTTAWA, ONT
K1Z 7Y8

NL-91 (11-79)

National Library of Canada

Cataloguing Branch
Canadian Theses Division

Ottawa, Canada
K1A 0N4

Bibliothèque nationale du Canada

Direction du catalogage
Division des thèses canadiennes

NOTICE

The quality of this microfiche is heavily dependent upon the quality of the original thesis submitted for microfilming. Every effort has been made to ensure the highest quality of reproduction possible.

If pages are missing, contact the university which granted the degree.

Some pages may have indistinct print especially if the original pages were typed with a poor typewriter ribbon or if the university sent us a poor photocopy.

Previously copyrighted materials (journal articles, published tests, etc.) are not filmed.

Reproduction in full or in part of this film is governed by the Canadian Copyright Act, R.S.C. 1970, c. C-30. Please read the authorization forms which accompany this thesis.

THIS DISSERTATION
HAS BEEN MICROFILMED
EXACTLY AS RECEIVED

AVIS

La qualité de cette microfiche dépend grandement de la qualité de la thèse soumise au microfilmage. Nous avons tout fait pour assurer une qualité supérieure de reproduction.

S'il manque des pages, veuillez communiquer avec l'université qui a conféré le grade.

La qualité d'impression de certaines pages peut laisser à désirer, surtout si les pages originales ont été dactylographiées à l'aide d'un ruban usé ou si l'université nous a fait parvenir une photocopie de mauvaise qualité.

Les documents qui font déjà l'objet d'un droit d'auteur (articles de revue, examens publiés, etc.) ne sont pas microfilmés.

La reproduction, même partielle, de ce microfilm est soumise à la Loi canadienne sur le droit d'auteur, SRC 1970, c. C-30. Veuillez prendre connaissance des formules d'autorisation qui accompagnent cette thèse.

LA THÈSE A ÉTÉ
MICROFILMÉE TELLE QUE
NOUS L'AVONS REÇUE

CONTACT STRESS DISTRIBUTIONS BENEATH A RIGID STRIP FOOTING

by

Robert Harland Kempthorne, B.Eng.

A THESIS SUMBITTED TO THE FACULTY OF GRADUATE STUDIES AND RESEARCH IN PARTIAL FULFILLMENT OF THE REQUIREMENTS FOR THE DEGREE OF MASTER OF ENGINEERING

FACULTY OF ENGINEERING
CARLETON UNIVERSITY
OTTAWA, ONTARIO
JANUARY 1978

The undersigned recommend to the Faculty of Graduate Studies and Research acceptance of the thesis "Contact Stress Distributions Beneath a Rigid Strip Footing" submitted by Robert Harland Kempthorne, B.Eng. in partial fulfillment of the requirements for the degree of Master of Engineering.

Thesis Supervisor

Chairman, Department of Civil Engineering

Carleton University

Ottawa

ABSTRACT

This investigation has centered on the monitoring of a model rigid strip footing resting on a consolidating soil medium with a view to determining the time-dependent response of the contact stress distribution. The monitoring also included the immediate and consolidation settlement of the footing, and the incremental pore water pressures within the soil medium.

The immediate contact stress distributions were found to be highly dependent on the magnitude of the applied stress, relative to the bearing capacity of the soil. At low stress levels the contact stresses were substantially higher adjacent to the edge of the footing, and as the load increased the contact stress distribution became more uniform. Throughout the duration of the main test the contact stress distribution was found to vary within a narrow band, the shape of which resembled the case of an elastic-plastic soil medium. The lack of substantial changes in the shape of the contact stress distribution is thought to be a characteristic of the soft clay used in the experiment.

Additional experiments on a cohesionless soil medium showed that the contact stresses were highly variable but tended to fall within a band that was similar in shape to those observed in previous studies on sand.

ACKNOWLEDGEMENTS

The author acknowledges gratefully his indebtedness to Dr. A.P.S. Selvadurai for his interest and guidance throughout the duration of this research.

The author wishes to express his appreciation of the help and advice given freely by Lev Rothenburg and Jim Rodger. Acknowledgements are due to Drew Allan, Dan Carson, Paul Conlon, Brian Davies, Ken McMartin and Terry Nicholas of the Civil Engineering Department of Carleton University. Acknowledgements are also due to André Drupsteen, Gary Farbar and Bernie Moore, as well as Les Rice, Richard Kempthorne, John Herler, Fred Bertignoll and Henry Kovalchik of the technical staff at Carleton University.

Thanks go to Peter McKay of Dochart Brick and Tile Co., Ltd.

The author appreciated the care and attention of Mrs. Sylvia Carrière in typing the manuscript.

The research would not have been possible without the financial assistance of the National Research Council, through an award of a National Research Council Scholarship.

TABLE OF CONTENTS

page

1. INTRODUCTION 1

2. LITERATURE REVIEW 3

2.0 Introduction 3
2.1 Contact Stress Distribution beneath Foundations 3

2.1.1 Introduction 3
2.1.2 Flexibility of the Structural Foundation 5
2.1.3 Mechanical Properties of the Soil 11

2.1.3.1 Cohesion 12
2.1.3.2 Angle of Internal Friction 13
2.1.3.3 Non-Homogeneity 16
2.1.3.4 Influence of Poisson's Ratio 17

2.1.4 Foundation Geometry 18
2.1.5 Foundation Embedment 20
2.1.6 Depth to Rigid Base 21
2.1.7 Degree of Roughness of the Foundation Interface ... 22
2.1.8 Magnitude, Mode of Load and Stress History of the Soil 25
2.1.9 Efficiency of the Contact Stress Measuring Device . 28
2.1.10 Conclusions on Contact Stress Distribution 33

2.2 Settlement of Foundations on Normally Consolidated Clay ... 35

2.2.1 Immediate Settlement 35
2.2.2 Consolidation Settlement 38
2.2.3 Consolidation of a Layer under a Uniform Strip Load 45
2.2.4 Pore Water Pressure Predictions 46
2.2.5 Pore Water Pressure Measurement 49

3. EXPERIMENTAL PROGRAM 55

3.1 Present Research Work 55
3.2 Experimental Apparatus 58

3.2.1 Test Tank 58
3.2.2 Steel Plate 61
3.2.3 Pressure Transducers 66
3.2.4 Method of Load Application 68
3.2.5 Data Acquisition 71
3.2.6 Displacement Transducers 75
3.2.7 Pore Water Pressure Apparatus 76

3.3 Cohesive Soil 82

3.3.1 General Characteristics 82
3.3.2 Atterberg Limits 83
3.3.3 Specific Gravity 83

page

3.3.4 Particle Size Distribution 83
3.3.5 Compaction and Placement 85
3.3.6 Initial Conditions 89
3.3.7 Clay Properties 89

3.4 Quartz Sand 95

3.4.1 General Characteristics 95
3.4.2 Placement Method 102
3.4.3 Direct Shear Tests on Sand 111

4. TEST RESULTS AND DISCUSSION 114

4.1 Introduction 114
4.2 Cohesionless Soil Medium 115

4.2.1 Introduction 115
4.2.2 Plate Settlement 116
4.2.3 Contact Stress Distribution—Cohesionless Soil 120

4.3 Preliminary Test of Plate on Clay 131
4.4 Plane Strain Test 137

4.4.1 Surcharge 137
4.4.2 Immediate Plate Settlement 148
4.4.3 Surface Displacement Profile 155
4.4.4 Immediate Contact Stress Distribution 163
4.4.5 Pore Pressure Response 170

4.4.5.1 Immediate Pore Water Pressure Response ... 170
4.4.5.2 Pore Water Pressure Dissipation 187

4.4.6 Consolidation Settlement 190

4.4.6.1 Total Consolidation Settlement 190
4.4.6.2 Rate of Consolidation Settlement 197

4.4.7 Variation of the Contact Stress Distribution with Time 199

4.5 Static Contact Stresses 206

5. CONCLUSIONS AND RECOMMENDATIONS 220

5.1 Summary and Conclusions 220
5.2 Recommendations for Future Work 222

REFERENCES 225

APPENDICES 239

LIST OF FIGURES

Figure		*page*
2.1	Finite beam on an isotropic elastic solid medium (Borowicka, 1938)	7
2.2	Contact stresses for flexible versus rigid strip footings	8
2.3	General contact stress distributions beneath rigid foundation	14
2.4	Contact stress distribution under a rigid strip foundation on a soil layer of limited thickness (after Tsytovich, 1976)	23
2.5	Effect of surface drainage on excess pore pressure (Schiffman *et al.*, 1969)	40
2.6	Lateral distribution of excess pore pressure (Schiffman *et al.*, 1969)	41
2.7	Lateral distribution of maximum shear stress (Schiffman *et al.*, 1969)	42
2.8	Effect of layer thickness on degree of consolidation of a uniformly loaded flexible strip footing (after Gibson *et al.*, 1970)	44
3.1	Idealization of strip footing	57
3.2	Diagram of test tank and load apparatus	59
3.3	Diagram of rigid steel test plate	62
3.4	Diagram of pressure transducer installed in test plate	65
3.5	Characteristic pressure transducer "footprint" (after Davidson, 1975)	69
3.6	Piezometer	77
3.7	Pore water pressure measuring system — 6-cell chamber	78
3.8	Pore water pressure measuring system — 1-cell chamber	79
3.9	Pore pressure lines installed in tank	80
3.10	Plasticity chart (after A. Casagrande)	84

Figure		*page*
3.11	Grain size distribution of sand and clay	86
3.12	Moisture content versus dry density for "Arnprior" clay	87
3.13	Moisture content versus Young's modulus for remolded, extruded "Arnprior" clay	92
3.14	Moisture content versus shear strength of remolded, extruded "Arnprior" clay	93
3.15	Direct shear tests results for remolded, extruded "Arnprior" clay	94
3.16	Standard consolidation test No. 1	96
3.17	Standard consolidation test No. 2 and 3	97
3.18	Standard consolidation test No. 4	98
3.19	Standard consolidation test No. 5	99
3.20	Standard consolidation test No. 6	100
3.21	Graph of placement density versus size of hopper hole diameter	108
3.22	Graph of placement density versus height of fall	110
3.23	Direct shear test results for Flint-grade and Banding-grade sand	112
4.1	Typical load-deflection curves for plate on Flint-grade and Banding-grade sand	117
4.2	Comparison of model plate settlement with observed settlement of footings on sand for various relative densities (Burland *et al.*, 1977)	119
4.3	Summary of tests on sand, maximum applied stress = 147 kPa	121
4.4	Summary of highs and lows during first load cycle	122
4.5	Summary of highs and lows during second load cycle	123
4.6	Method of averaging of contact stresses for plate on sand	125
4.7	Weighted percentage of area on plate for each pressure transducer — sand tests	126

Figure		*page*
4.8	Graph of applied stress versus settlement for preliminary test on clay	133
4.9	Contact stress distribution for preliminary test on clay (q_0 = 145 kPa)	134
4.10	Contact stress distribution for preliminary test on clay (q_0 = 200 kPa)	135
4.11	Settlement versus stress due to surcharge applied before plane strain test	139
4.12	Graph of surcharge deflection versus time in plane strain test	140
4.13	Centreline and edge pore water pressure dissipation during surcharge loading of plane strain tank	144
4.14	Degree of pore water pressure dissipation with depth after seven days of surcharge loading of plane strain tank	147
4.15	Initial undrained settlement during plane strain test	150
4.16	One-dimensional settlement in control box	152
4.17	Idealized load-settlement curve for uniformly loaded flexible strip footing resting on n/c clay layer with H/B = 1.5	154
4.18	Surface settlement profile for strip footing	157
4.19	First test on clay, surface displacement profile (Δq_0 = 24.6 kPa)	158
4.20	Second test on clay, surface displacement profile (Δq_0 = 5.5 kPa)	159
4.21	Second test on clay, surface displacement profile (Δq_0 = 13.1 kPa)	160
4.22	Second test on clay, surface displacement profile (Δq_0 = 16.6 kPa)	161
4.23	Contact stress distribution between walls of plane strain apparatus	164
4.24	Immediate contact stress distribution during plane strain test, centre region of plate	166
4.25	Initial normalized contact stress distributions during first test on clay	168

Figure		*page*
4.26	Graph of contact stress distributions beneath a rigid die, for various corner curvatures (from Goodier and Loutzenheiser, 1965)	169
4.27	Centreline influence factors for calculation of principal stresses below flexible strip footing	172
4.28	Edge influence factors for calculation of principal stresses below flexible strip footing	173
4.29	Estimated pore pressure parameter A versus depth below plate	176
4.30	Predicted $\Delta u/q_0$ below centreline of plate	178
4.31	Predicted $\Delta u/q_0$ below edge of plate	179
4.32	Centreline influence factor for calculation of total octahedral normal stress	182
4.33	Edge influence factor for calculation of total octahedral normal stress	183
4.34	Influence factors for calculation of vertical stress below plate	186
4.35	Dissipation of pore water pressure below centreline of plate	188
4.36	Dissipation of pore water pressure below edge of plate	189
4.37	Consolidation settlement during first plane strain test	195
4.38	Degree of consolidation settlement with time (after Davis and Poulos, 1972)	198
4.39	Normalized contact stress distribution throughout first plane strain test	201
4.40	Contact stress versus time for individual pressure transducers during first plane strain test	203
4.41	Incremental contact stress distribution across centre region for reloading of plate after five-week test on clay	205
4.42	Contact stress distributions during second plane strain test (Δq_0 = 52 kPa)	210
4.43	Vane shear strength results from plane strain apparatus	211

Figure		*page*
4.44	Incremental contact stress distribution for third test on clay	213
4.45	Measured versus average contact stress from third test on clay	214
4.46	Summation of incremental contact stress distributions during third test on clay	216
4.47	Contact stress distributions predicted from Schultze (1961) and Zeevaert (1972)	218

LIST OF PLATES

Plate		*page*
1	Load apparatus, plane strain tank and data acquisition system in temperature and humidity control room	59
2	Top view of rigid test plate with sixteen pressure transducers	63
3	Bottom view of rigid test plate showing locations of flush diaphragms of pressure transducers	64
4	Pressure transducers	67
5	"B & F" forty-channel data acquisition system with timer	72
6	Sand placement in plane strain tank by hopper	104
7	Preliminary test on clay layer	132
8	"Arnprior" clay being extruded from pugmill	138
9	Piezometer placed in clay	142
10	Six-chamber pore water pressure measuring device	143
11	Test plate installed over plane strain apparatus with displacement transducers in place	149
12	Removal of side wall of plane strain tank for placement of plastic sheeting and film of oil	207

LIST OF TABLES

Table		*page*
1	Summary of triaxial and direct shear tests on clay	90
2	Summary of consolidation tests	101
3	Flint-grade sand density calibration tests	105
4	Banding-grade sand density calibration tests	106
5	Summary of contact stress distributions for sand	128
6	Immediate pore water pressure observations	145
7	Predicted pore water pressures below plate	177
8	Comparison between Δu and $\Delta\sigma_{oct}$ computed by various methods	181
9	A parameter back-figured from observed pore water pressures	185
10	Predicted consolidation settlement	192
11	Contact stress across centreline with time	202

LIST OF SYMBOLS

A,B	Pore Pressure Parameters
B	Foundation Width
b	B/2
C	Constant
C_c	Compression Index
C_r	Recompression Index
C_u	Coefficient of Uniformity
CU	Consolidated-Undrained Shear Test
c_w	Shear Strength
c_v	Coefficient of Consolidation
$\bar{c}$	Adjusted Coefficient of Consolidation
D	Depth of Embedment of Foundation
D_x	Grain Size with x Percent Finer Soil Particles
D_R	Relative Density
e	Void Ratio
e_0	Initial Void Ratio
E	Young's Modulus
E'	Young's Modulus of Soil Skeleton
E_r	Reload Young's Modulus
E_s	Equivalent Young's Modulus for Granular Soil in Compression
E_t	Tangential Young's Modulus
E_u	Undrained Young's Modulus
F	Intake Factor for Piezometer
f	Initial Shear Stress Ratio

FSO	Full-Scale Output
G	Shear Modulus
G_s	Specific Gravity
H	Depth of Compressible Layer
h	Thickness of Foundation
I	Moment of Inertia
I_z	Influence Factor for Undrained Loading
k	Permeability of Soil
K_r	Relative Flexibility of Soil and Foundation
ℓ	Length of Foundation
N	Blow Count from the Standard Penetration Test
N_c, N_q, N_γ	Bearing Capacity Factors
OCR	Overconsolidation Ratio
OD	Outside Diameter
Q	Total Load on Foundation
q_c	Static, Dutch Cone Bearing Capacity, in kg/cm^2
q_0	Applied Foundation Stress
Δq_0	Increment in Applied Foundation Stress
Δq_x	Contact Stress at Position x
$\bar{q}_x$	q_x/q_0
R	Radius of Curvature at Edge of Foundation
R^2	Coefficient of Multiple Determination
S	Degree of Saturation
t	Time
T_v	One-Dimensional Time Factor
Ta	Adjusted Time Factor
Δu	Increment in Pore Pressure

U	Degree of Consolidation
UU	Unconsolidated Undrained Compression Test
V	Volume Factor for Compressibility of Piezometer System
x	Horizontal Distance from Centre of Strip Foundation
z	Vertical Distance Below Foundation Level
ϕ	Angle of Internal Friction
γ	Unit Weight of Soil
γ_w	Unit Weight of Water
ϵ	Curvature Contact Distance at Edge of Foundation *or* Equilization Ratio for Piezometer
ν	Poisson's Ratio
ν_s	Poisson's Ratio of the Soil
ν_b	Poisson's Ratio of the Foundation
ν'	Poisson's Ratio of the Soil Skeleton
ρ	Settlement
ρ_i	Initial Settlement
$\sigma_x, \sigma_y, \sigma_z$	Normal Stresses
$\sigma_1, \sigma_2, \sigma_3$	Major, Intermediate, Minor Principal Stresses
σ_{oct}	Change in Octahedral Normal Stress
σ	Stress Increment Measured by the Pressure Transducer
$\hat{\sigma}$	Standard Deviation
σ'	Effective Stress
τ	Shear Stress

LIST OF APPENDICES

No.		*page*
1	Summary of Research Concerned with Contact Stress beneath a Foundation	239
2	Pore Pressure Equations	249
3	Field Observations of Pore Water Pressure Measurement	252
4	Test Plate Rigidity	254
5	Pressure Transducer Specifications and Calibration	256
6	Displacement of Pressure Transducer Diaphragm	261
7	Load Cell Specifications and Calibration	262
8	Displacement Transducer Specifications and Calibration	263
9	"Arnprior" Clay Chemical and Mineral Analysis	265
10	Bearing Capacity of a Strip Foundation	266
11	Computer Program CONTAC	269
12	Summary of Initial Settlement Predictions for Strip Footing	273
13	Computer Program DELTAH	274
14	Computer Program STRES2	282

CONVERSION OF UNITS

Symbols and Conversion Factors for SI Units

m = metre = 39.37 inches

mm = millimetre = 0.03937 inches

N = Newton = 0.22481 pound force

kN = Newton = 224.81 pound force

Conversion from Imperial to SI Units

1 inch = 25.4 mm

1 foot = 304.8 mm = 0.3048 m

1 lb force = 4.4482 N

1 kip = 4448.2 N = 4.4482 kN

Conversion of Units for Pressure and Stress

1 psi = 1 lb force per square inch = 6.8947 kPa

or

1 kPa = 1 Kilo Newton per square metre = 0.14504 psi

1. INTRODUCTION

The analysis of the interaction between structural foundations and the supporting soil media are of fundamental importance to both structural and foundation engineering. From a complete analysis of this interaction problem information can be derived concerning the contact stresses and displacements at the soil-foundation interface, as well as the distribution of stresses and strains within the supporting soil medium. The conventional design of the structural foundation is based on an assumed contact stress distribution, and on a desire to maintain total and differential settlements at a tolerable level. The analytical and experimental research done in the past has been mainly concerned with the time-independent problem, i.e. the soil-foundation interaction analysis can be performed without regard to changes which occur with time in either the structure or the properties of the soil medium. This assumption has been encouraged from experimental studies performed predominantly on granular soil mediums where the soil properties are essentially constant with time. This has been accompanied with a lack of long-term measurements on full-scale structures.

The importance of the time-dependent response of the soil medium is decidedly more evident for saturated cohesive soils, where primary and secondary consolidation influence the total settlement. The degree of consolidation settlement is governed by the consolidation characteristics of the soil and on the drainage paths available for dissipation of any developed excess pore water pressures. Since the mechanical behaviour of the soil medium changes with time, it is plausible to assume

that both the contact stresses and displacements at the soil foundation interface are time dependent. Analyses presently used to incorporate time dependence are based on simplified assumptions regarding the contact stress distribution beneath the foundation, and on the state of strain in the soil medium. For example, the raft design would be based on either the undrained or drained strength and deformation parameters of the soil with no allowance with time for the intermediate spatial variations.

The main objective of this thesis is to investigate the manner in which the contact stress distribution can be influenced by the consolidating effects of the supporting soil medium. The structural foundation used in the investigation is considered to be rigid on the bases of the relative rigidity, K_r, proposed by Borowicka (1938). Tests have been performed on both cohesive and cohesionless soil media.

The particular problem being examined in this series of experiments is intended to model the behaviour of a section of uniformly loaded rigid strip footing under plane strain conditions. The contact between the rigid plate and soil medium is assumed to be smooth. The thickness of the soil layer was approximately 2.5 times the footing width, which will be shown to be representative of a deep layer with a rigid base that has only marginal effect on performance of the foundation.

2. LITERATURE REVIEW

2.0 *Introduction*

The main objective of this chapter is to present a summary of the published and unpublished literature on contact stress measurements beneath model and prototype structural foundations resting on real or idealized soil media in order to clearly establish the influence various parameters may have on the measured contact stress distribution. Concern is expressed not only for work that has been done to date, but also areas of study that require more research before there can be developed an efficient procedure for the practical design of structural foundations.

In addition, some of the techniques presently used to present settlement are briefly introduced because deflections are an equally important part of the soil-foundation interaction problem. A comparison will be made between the observed settlements of the test plate and the settlements predicted from some of the theoretical methods. This will include a review of several articles concerning pore water pressure predictions and their measurement.

2.1 *Contact Stress Distribution beneath Foundations*

2.1.1 *Introduction*

When a load is applied to a foundation, there is a reaction exerted by the supporting soil medium. This soil reaction causes shear stresses and bending stresses in the foundation. To design for these stresses, the magnitude and distribution of the contact stresses must be known.

Both uniform and planar distributions of contact stress have usually been assumed in the past because it greatly simplifies the analysis.

The stress occurring at the interface between a structural foundation and the supporting soil medium is commonly referred to as "contact pressure" or "contact stress".* Usually only the normal stress distribution is implied, but under certain conditions, tangential stresses also occur at the interface. We may expect the contact stress distribution at the interface of the foundation to depend on the following factors:

(a) Flexibility of the foundation;

(b) Mechanical properties of the soil;

(c) Geometry of the foundation;

(d) Foundation embedment;

(e) Depth to undeformable base or rigid stratum;

(f) Degree of roughness at the foundation interface;

(g) Magnitude of load, mode of load, and stress history of the soil.

This section is intended to clearly establish the influence of each of the above factors on the contact stress distribution beneath model and prototype structural foundations resting on real or idealized soil media. Articles of direct relevance to the stated problem are briefly introduced, and a summary of these articles is presented in tabular form in Appendix 1.

*The use of the term "pressure" is unconventional in terms of mechanics of solids nomenclature. The tractions that act on the interface are stress vectors. As such, the distribution constitutes a contact stress.

2.1.2 *Flexibility of the Structural Foundation*

A foundation can ideally be described as perfectly rigid or perfectly flexible. A "rigid" foundation is one in which there is no differential displacement between various points along the contact surface, i.e. an original plan contact surface remains plane under any distribution of external forces. A "flexible" foundation offers no resistance in bending to the external loads; hence, there is large differential displacement throughout the contact surface. A perfectly rigid foundation, while desirable, is rarely achieved in practice. Raft foundations approaching this have been built by increasing the depth of concrete in the foundation to 2 m or more (Gerrard *et al.*, 1971).

The analysis of contact stresses beneath foundations which possess intermediate flexibility is performed by employing both analytical and numerical methods of stress analysis developed in the theory of elasticity. The determination of contact stresses were first analyzed using advanced theory of elasticity. The effect of the flexural rigidity of the footing was investigated by Borowicka (1936) for a uniformly loaded circular foundation resting on a semi-infinite isotropic elastic medium, and later (Borowicka, 1938; see Selvadurai, 1978) for a strip foundation subject to either a uniform load or central line load. The relative stiffness, K_r, of the strip footing is given by

$$K_r = \frac{4}{3} \frac{(1-\nu_s^2)}{(1-\nu_b^2)} \frac{E_b}{E_s} \left(\frac{t}{B}\right)^3$$

where E_b = Young's modulus of the beam
E_s = Young's modulus of the soil
ν_s = Poisson's ratio of the soil
ν_b = Poisson's ratio of the beam
t = Thickness of the beam
B = Width of the beam.

The graphical results are presented in Fig. 2.1. A perfectly flexible footing ($K_r = 0$) was shown to have a uniform contact stress distribution, and as the rigidity increased, the contact stress is redistributed with lower stresses at the centre and higher edge stresses. A perfectly rigid footing gives the same result as that first given by Boussinesq (1885) for the circular footing and by Sadowsky (1928) for the strip footing (see Timoshenko and Goodier, 1970). Sadowsky (1928) showed that the contact stress distribution increased from $2q_0/\pi$ at the centre to infinity at the edge (q_0 is the average stress, equal to the total load applied per unit length divided by the width of the footing). In reality, the infinite contact stress at the edge cannot be achieved because the soil material undergoes plastic yield and the stresses are redistributed over the base (see Fig. 2.2).

In all subsequent work, the rigidity of the foundation has been analyzed in terms of the *relative* rigidity of the foundation compared to the soil medium. This has usually included a ratio of the modulus of the foundation and the soil medium, a ratio of the respective Poisson's ratios, and a dimensionless term relating the thickness of the footing to its width. The use of this method usually allowed the analysis of other factors such as adhesion at the soil foundation interface or soil non-homogeneity to be taken into account (Parkes, 1957; Barden, 1962). The application of finite element techniques to the soil-foundation interaction problem have frequently used a ratio of elastic modulii as a relative rigidity parameter. The advantage is that the use of computer analysis will give approximate solutions to more general problems such as homogeneous anisotropy and isotropy, varying compressibility with depth and soil stratification (Cheung and Nag, 1968; Le Lievre and

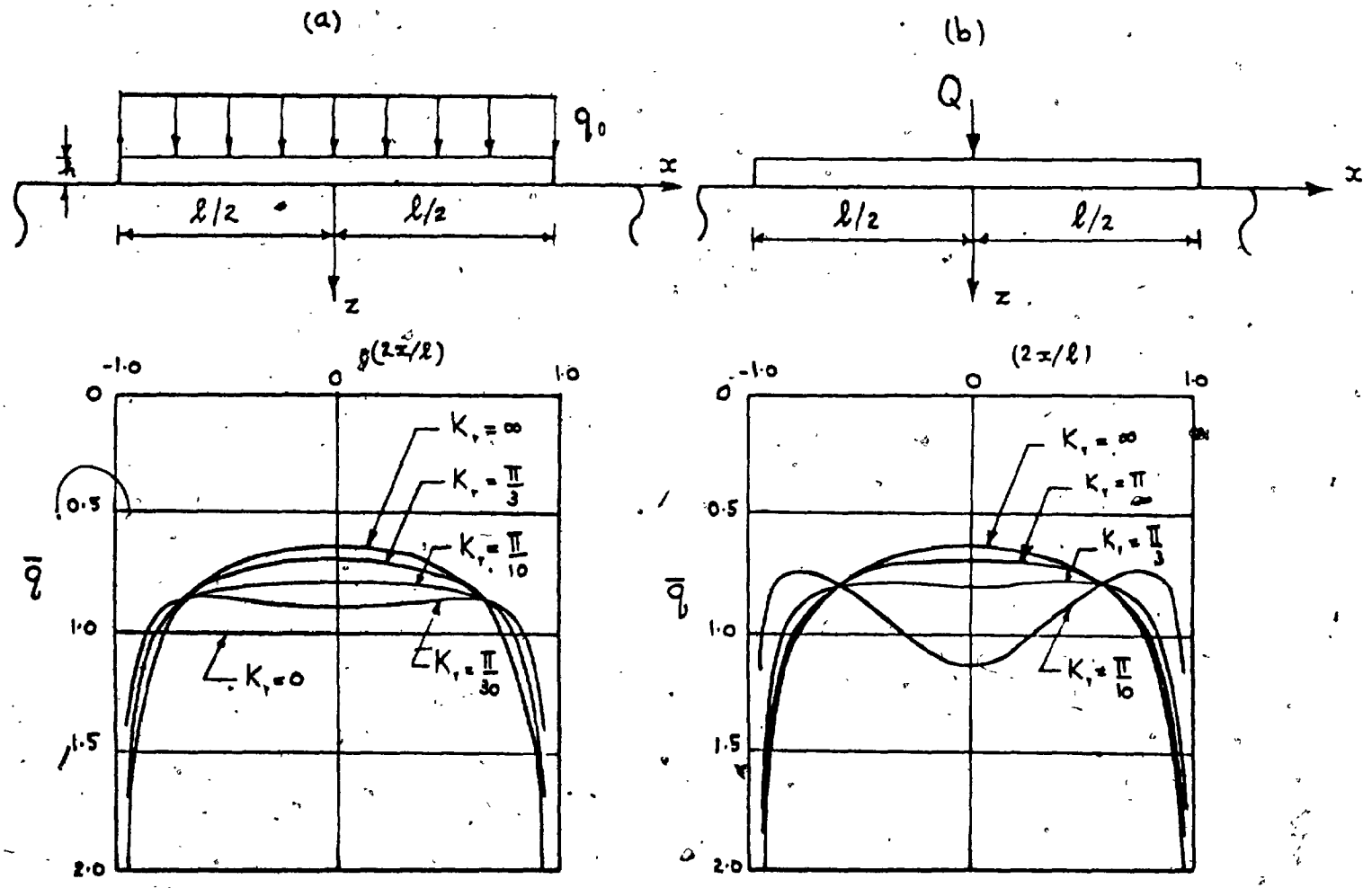

FIGURE 2.1

Finite Beam on an Isotropic Elastic Solid Medium, Plane Strain Contact Stress Distribution beneath a Finite Beam with a Smooth Interface [after Borowicka, 1938; from Selvadurai (1978)]

(a) Finite beam subjected to a uniform load of stress intensity q_0; contact stress $q_x = \bar{q} \cdot q_0$

(b) Finite beam subjected to a central load Q; contact stress $q_x = \bar{q}\,\frac{Q}{b\ell}$

Q = total load acting over the width (b) of the beam; $K_r = \frac{4(1-\nu_s^2)}{3(1-\nu_b^2)}\,\frac{E_b}{E_s}\left(\frac{h}{\ell}\right)^3$

FLEXIBLE FOUNDATION

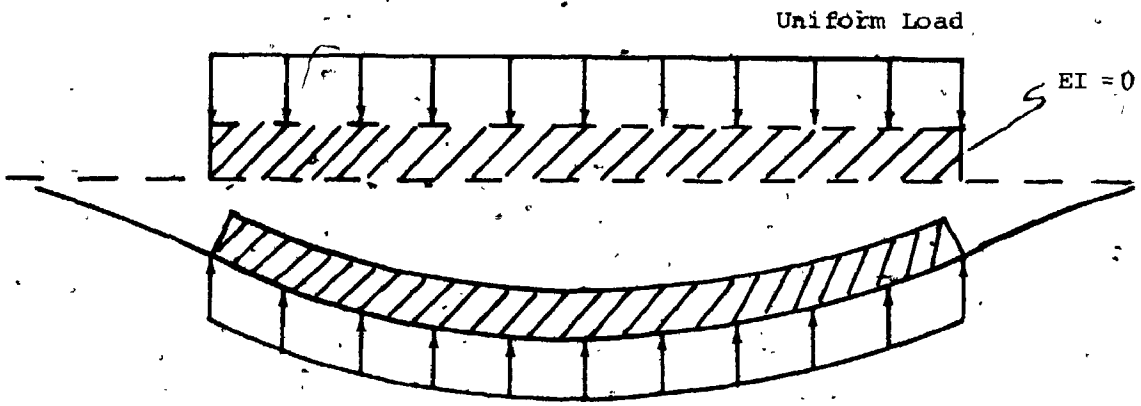

Uniform Contact Stress
Non-Uniform Settlement
No Bending Moment Induced

RIGID FOUNDATION

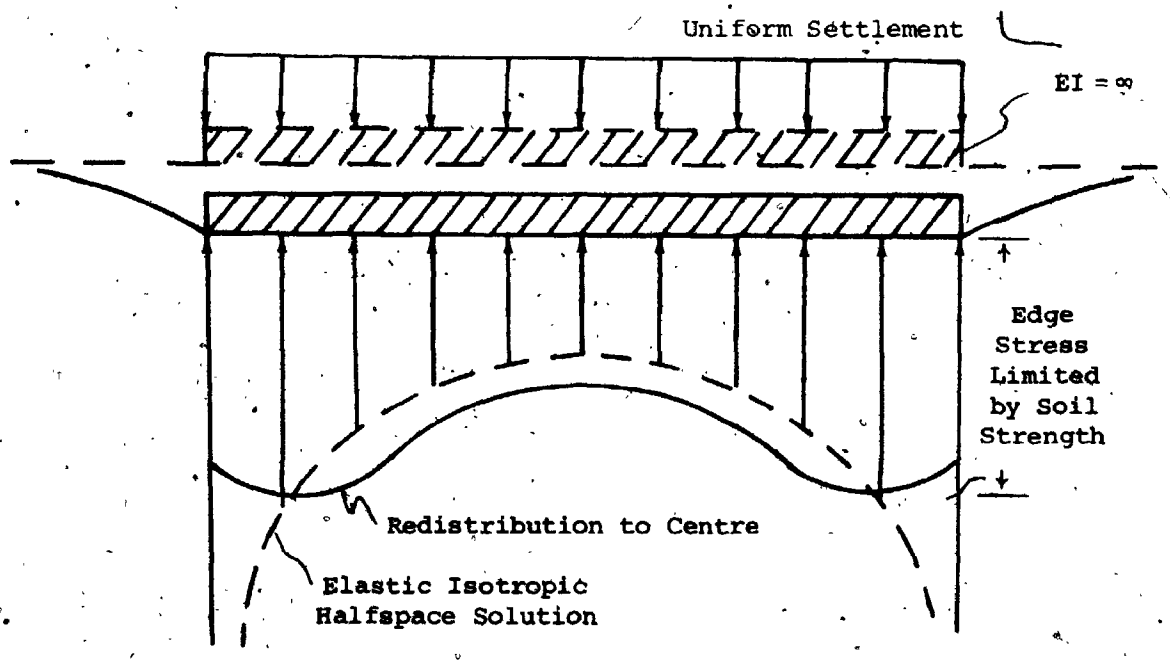

FIGURE 2.2

Contact Stresses for Flexible versus Rigid Strip Footings

Vigneswaran, 1972; Hooper, 1974; Wood and Larnack, 1974; Boswell and Scott, 1975).

The effect of foundation rigidity on contact stress distribution has been observed in the field by Gerrard *et al.* (1971). Two raft foundations with similar subsoil conditions were reported, and preliminary investigations showed that the more rigid raft had high edge stresses, but the second raft showed a more uniform distribution indicative of a flexible raft. A mat-supported silo group investigated by Crowser *et al.* (1974) was considered to be rigid and the edge stresses were computed to be up to three times as great as the centre stresses. Cracking in the silo walls was observed, so the supposedly rigid structure was, in fact, "flexible". Almost all of the other field observations assume a "rigid" foundation, but it is interesting to conjecture how many other rafts and mat foundations are actually flexible (Teng, 1949; L'Herminier, 1957; Kaufman and Sherman, 1964; Krivorotov, 1973).

Model studies to determine the effect of beam flexibility on contact stresses and bending moments have been performed by Lenczner (1962), Vesić (1963), Barden (1963) and Shelyapin and Sergeev (1967). The general result was that the stiffer the beam, the higher the edge contact stresses. The effect of the flexibility of a circular plate on contact stress distribution was reported by Smith (1970).

One of the advantages of model experiments lies in the control that can be exercised over various parameters. As an example, the relative flexibility of the test plate can be established with a greater degree of certainty than the full-scale counterpart. In full-scale tests, assumptions regarding the Young's modulus and Poisson's ratio of the foundation are important, but can be overshadowed by the assumptions of

the *effective* moment of inertia when cracking of the concrete in the foundation is taken into account.

Frequently, only the rigidity of the foundation is included in the calculation of structural rigidity, but this rigidity can be altered when the stiffness of the superstructure is included in the analysis. Sommer (1965) proposed a method for including the flexural rigidity of the superstructure in the calculation of settlements, contact stresses and bending moments. The variation in contact stress distribution due to the increase in rigidity is not directly determined, because the method requires an assumption of the stress distribution beforehand. Heil (1969) later extended this method to include the effects of creep of concrete. The results showed that the rigidity of the column-load foundation transfer increased the total rigidity of the structure. In addition, the rigidity was decreased by the creep of the concrete, causing a reduction in the induced bending moments but only small changes in the contact stress distribution. The contribution of the superstructure to total foundation stiffness was also analyzed by Chamecki (1956) and Grasshoff (1961). Two alternative methods of analysis for variable structure-foundation stiffness are outlined by Lee and Harrison (1970) involving an iterative procedure until the statics and compatibility requirements of the whole system are complete. De Simone and Gould (1972) stress the importance of the structure in increasing the foundation rigidity and reducing differential settlement for two full-scale mat foundations in Cambridge, Massachusetts.

In 1966 a method was proposed by the American Concrete Institute (A.C.I.—1966) for the design of combined footings and mats. This analysis includes the stiffness of the framed members and shear walls with

the stiffness of the foundation. The method was included in the design of a raft for a very stiff fifteen-storey building in Ottawa (Eden, McRostie and Hall, 1973) and in the designs by De Simone and Gould (1972). There are presently more sophisticated analyses available for design and analysis of raft foundations (see Hain and Lee, 1974; Selvadurai, 1978) but the ACI-1966 method was the first step towards establishing a code common to all designers in the U.S.A.

To summarize the previous paragraphs, the flexural rigidity of the foundation has a significant effect on the contact stress distribution. For an elastic supporting medium, flexible foundations subjected to a uniform load would, by definition, have a uniform contact stress. As the rigidity increases, higher edge stresses will occur, and the magnitude of the edge stress is dependent on the ability of the supporting soil to withstand these stresses. In practice, it is difficult to assign a value to the relative rigidity of the foundation-soil system, and approximate methods and assumptions are necessary regarding the Young's modulii and Poisson's ratios of the soil and foundation.

2.1.3 *Mechanical Properties of the Soil*

The mechanical properties of the soil appears to have the greatest influence on the distribution of contact stress. These properties can be expressed in terms of strength characteristics such as the cohesion and the angle of internal friction, and "elementary" deformability characteristics such as the Young's modulus and the Poisson's ratio. The consolidation characteristics of the soil medium have been neglected in the past, and their influence on contact stress is less known.

2.1.3.1 *Cohesion*

For a rigid foundation resting on an idealized elastic soil, the application of any finite load should produce infinitely high edge stresses. The contact stress distribution for a cohesive soil resembles that of an elastic medium, but the actual edge stress is determined by the ability of the soil to withstand this stress. Terzaghi (1943) assumes that when plastic flow occurs at the edge, the value of the edge contact stress can equal the maximum bearing stress of the soil, q_u. An analysis based on the theory of plasticity indicates that for a strip footing resting on a purely cohesive material ($\phi = 0$), $q_u = (\pi+2)\ c_u$, where c_u is the undrained shear strength of the soil medium. As a result of this yielding, redistribution of contact stress takes place over the contact surface, resulting in higher stresses at the centre than those predicted from elastic theory. There have been numerous articles written that acknowledge the presence of a plastic zone near the edge of the foundation, and the extent of the zone is dependent on the magnitude of the applied or external stress in relation to the bearing capacity. A model of the soil-foundation interaction proposed by Schultze (1961) takes into account the influence of both elastic and plastic effects. Here the maximum value of the edge contact stress is again limited to the bearing capacity of the soil. Further elastic-plastic analyses have been presented by Gorbunov-Possadov (1965), Zeevaert (1972), Biernatowski (1973) and Snarskii (1974).

Experimental model studies and field studies involving cohesive soil media tend to substantiate the concept of elastic and plastic regions. Reports of model footings on cohesive soils are few, but as early as 1933 tests on a rigid circular footing resting on a stiff

London clay were conducted by Faber. The results showed characteristically high edge stresses. Converse (1933) performed a field test on an 0.91-m square concrete block over a clay-loam, and found that the contact stress distribution depended on the magnitude of the load. More recent tests on model beams or footings involving contact stress measurement have been reported by Lazebnik and Smirnov (1964), Akai and Otsuki (1974) and Rivkin and Gusenitsa (1976). Full-scale field observations of the occurrence of high edge stresses produced by a rigid foundation resting on a cohesive soil are more frequent and have been reported by Teng (1949), L'Herminier (1957), Schultze (1961), Lazebnik (1970, 1973), Gosbell (1970), Gerrard *et al.* (1971), Eden *et al.* (1973) and Crowser *et al.* (1974). In all the above cases, the high edge stresses are attributed to the degree of cohesion of the soil and to the relatively high rigidity of the foundation.

2.1.3.2 *Angle of Internal Friction*

It may be noted that in the theoretical models that limit the edge contact stress distribution, as the cohesion of the soil decreases the high edge stresses are reduced, and in a purely cohesionless soil, the edge stresses of a foundation located at the soil surface are theoretically reduced to zero. The shape of the contact stress distribution for a cohesionless soil depends on the width of the foundation and varies from a parabolic distribution for narrow foundations to a "saddle" shape for wide foundations (see Fig. 2.3). This is due to the fact that the effect of loss of cohesion is limited to the edge only, where the failure takes place by the shearing action of the soil particles. (See, for example, Koegler and Scheidig, 1927; Faber, 1933; Muhs, 1965; Murzenko,

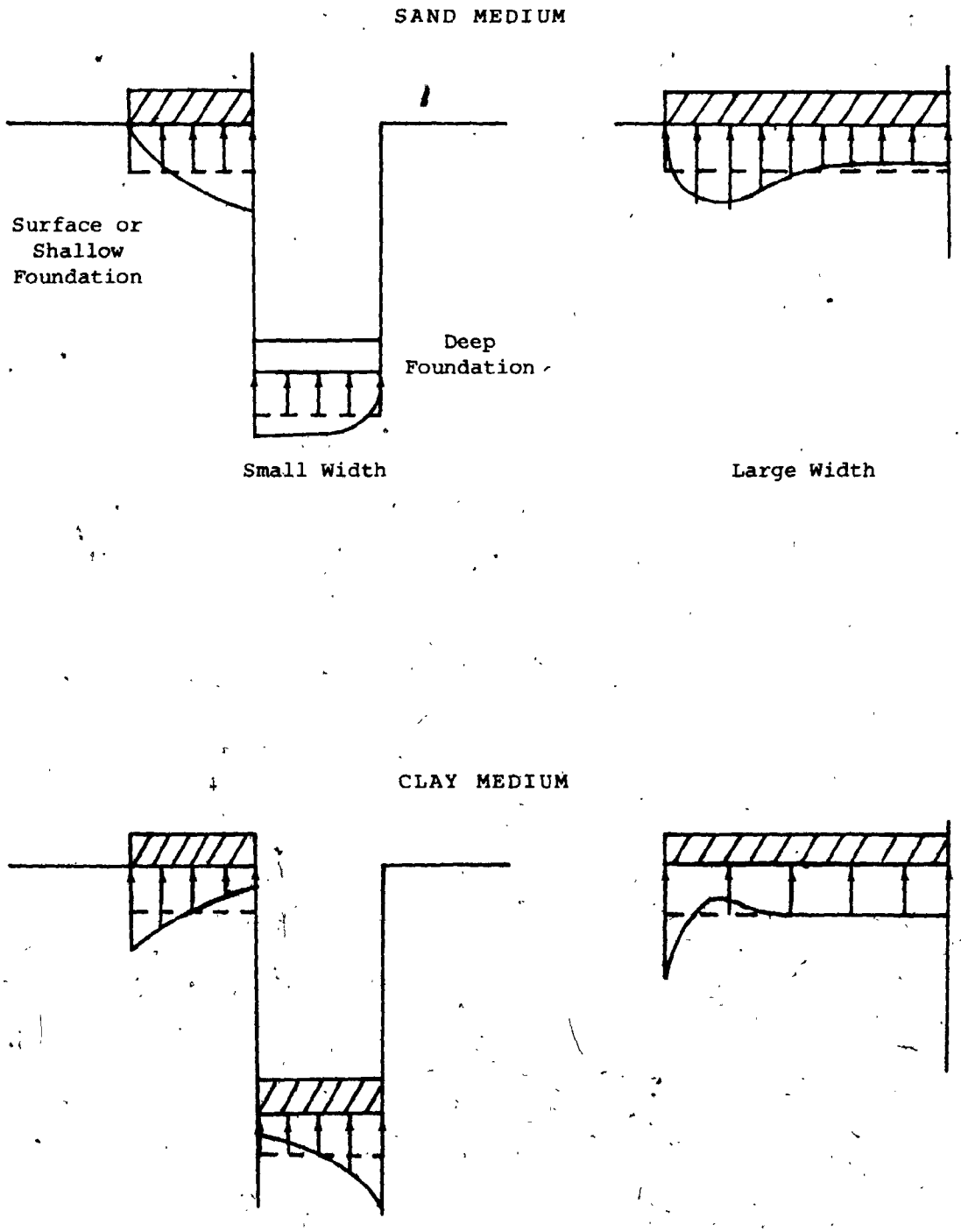

FIGURE 2.3

General Contact Stress Distributions Beneath Rigid Foundations

1965; Lazebnik and Smirnov, 1965; Ho and Lopez, 1969; Nwabuokei, 1976).

The effective angle of internal friction is dependent on a number of factors including the size and shape of the soil particles, the particle density, particle size distribution, the water content in the voids and the rate, magnitude and mode of stress application. Much of the experimental work on contact stress distribution has been performed on various types of sands, ideally represented as a cohesionless material. For any given type of sand, the angle of internal friction depends primarily on the density of the material, where in general, the greater the density, the higher the angle of internal friction. In order to make comparisons between cohesionless soils with different properties, the density of the soil is commonly expressed in terms of relative density, D_R, or in more general classifications such as loose, medium, dense, or very dense (Terzaghi and Peck, 1967; Peck *et al.*, 1974).

There are very few systematic studies of the effect of soil density on the contact stress distribution. Most of the model tests have been performed on sand that was either in its compact or dense state, and the density was not varied. Muhs (1965) states that tests were performed on loose, compact and dense sand, but the results are reported only for the compact sand. Nwabuokei (1976) completed tests on medium and dense sands, and the shape of the curves was not greatly affected by the change in density. Krivorotov (1976) noted that the contact stresses are dependent on the initial density of the soil. As the load is increased, the density of the sand medium directly beneath the plate changes, i.e., compact sand becomes less dense at the edges, whereas loose sand is compacted. At low stress levels, the contact stress

distribution is nearly uniform for both loose and dense sand, but as the load is increased, the shape takes the form of a "saddle", and is more noticeable if the sand is initially compact.

In full-scale observations, most sands encountered will be in the medium to dense state, so the general observations made by researchers to date have applications in most design problems. The contact stress observed in many cases is highly variable, irregular or non-symmetric, and this is usually attributed to either errors in the measuring device or to soil inhomogeneity (Teng, 1949; Kaufman and Sherman, 1964; Sikso and Johnson, 1964; Gerrard *et al.*, 1971; Lazebnik, *et al.*, 1973; Krivorotov, 1973).

2.1.3.3 *Non-Homogeneity*

Several investigators including Gibson (1967, 1974), Gibson and Sills (1971), Burland *et al.* (1973), Carrier and Christian (1973), Hopper (1974) and Boswell and Scott (1975) have reinforced the fact that spatial variations in the material properties (deformability or strength) can exist within the soil medium. One form of spatial variation known as non-homogeneity generally refers to a linear increase in Young's modulus with depth, of the form $E(z) = E(0) + kz$. Here z is the depth below the surface, $E(z)$, $E(0)$ are the values of Young's modulus at depth z and at the surface respectively, and k is a constant. This is only one variety of non-homogeneity that could be studied, but there is experimental evidence to support its application in soil mechanics (see Burland *et al.*, 1973).

The results of the above assumption of non-homogeneity were analyzed by a finite element method by Carrier and Christian (1973) for a

rigid circular plate. Hooper (1974) extended this for plate flexibility and partial adhesion between the circular plate and soil. Boswell and Scott (1975) provided influence co-efficients for contact stress and settlement, again for a circular plate. The use of a finite element method is very useful when analyzing problems of non-homogeneity, and other users of this method for layered soil systems include Hoeg *et al.* (1968), Radhakrishnan and Reese (1969), and Wood and Larnack (1974). Many papers have been primarily concerned with the settlment of the foundation, and the contact stress distribution is not given.

The general pattern of contact stress distribution remains the same for varying amounts of soil non-homogeneity, but the effect of increasing Young's modulus with depth causes the shape to be more uniform. Surface displacements are more localized and differential displacements for uniformly-loaded flexible rafts are reduced. The differential raft displacements become more sensitive to the distribution of applied loads, and bending moments are significantly reduced if the degree of non-homogeneity is substantial. In the special case when the Young's modulus is zero at the surface and increases linearly with depth in an incompressible half-space, a uniform strip or circular loading will produce uniform settlement and contact stress beneath the entire foundation.

2.1.3.4 *Influence of Poisson's Ratio*

In general, the contact stress distribution between two deformable bodies is dependent on the elastic constants, E and ν, of *both* materials. This can be illustrated in terms of a flexibility coefficient, K_r, such as used by Borowicka (1938) and others, as previously explained in Section 2.1.2. For a perfectly rigid plate ($K_r \rightarrow \infty$) the contact stress

distribution is independent of the elastic constants of the soil medium. From the definition of K_r given in Section 2.1.2, it is evident that K_r is directly proportional to the Young's modulii of the soil and foundation, but Poisson's ratio has a less significant effect. For example, reducing Poisson's ratio of the soil from 0.5 to 0.0 would only increase K_r by one-third. This increase in rigidity causes the contact stresses to decrease in the centre region of the plate, and increase at the edge. Carrier and Christian (1973) showed this effect to be marginal. Variations in Poisson's ratio have a more noticeable effect on the total and differential settlement of the foundation (Gibson and Sills, 1971). The problem of spatial variation in Poisson's ratio is more complex and usually only the resultant effect on settlement or plate bending moments is presented (Hooper, 1975).

2.1.4 *Foundation Geometry*

The zone of influence of high edge stresses is in many cases limited to a localized area at the perimeter of the foundation. With narrow, rigid foundations such as footings, these edge effects tend to overlap such that a distinctive concave parabolic or "saddle"-shaped contact stress distribution is observed with both cohesive and cohesionless soils at the working stress range. As the width increases, the rigidity of the foundation can be introduced with the use of a dimensionless ratio of foundation thickness to width, t/B. The "overlapping" effect of the edge stresses is reduced as the width increases, thereby producing a region in the centre that will have a lower, more uniform contact stress distribution. In many instances, it is impossible to separate the effect of the "overlapping" of edge stresses from the reduction in high

edge stresses due to increased flexibility of the foundation.

For the ideal elastic case, the contact stress becomes more uniform across the width of the foundation as the shape changes from a circle to a strip, but the high edge stresses are still present. De Beer (1957) attempted to show that the distribution in the longitudinal direction of a rigid rectangular beam will be similar to the elastic case, and that the assumption of uniform distribution in the transverse direction will give a longitudinal distribution that does not differ greatly from that obtained by assuming a parabolic distribution. Studies concerning the three-dimensional calculation of contact stresses are relatively few in number (Sakurai and Kitamura, 1970). Most of the investigations have been developed for simpler cases where axisymmetric loading conditions apply. One exception is in a paper by Sakurai and Kitamura (1970) where the contact stress distribution is calculated beneath a rigid rectangular plate of varying dimensions.

Irregular foundation geometry is difficult to analyze for contact stress distributions, so approximate methods have been devised. Kogan and Satsuk (1964) used a plate analogy for irregular foundation profiles, and Borodochev and Tarikov (1972) employed an electrical modelling technique for irregular foundation plans. More often, engineering judgement is used to simplify the problem (see Kaufman and Sherman, 1964; Sikso and Johnson, 1964).

There have been a number of observations of contact stress distributions beneath model foundations and many conclusions have been drawn from these results. It is always, however, necessary to question whether the results are directly applicable to full-scale foundations. In some areas of soil mechanics, the significance of scale effects are

recognized as important and empirical corrections are generally employed. The most common example is in determining the bearing capacity of a foundation from plate load tests. A study of the effect of scale in model foundations was conducted by Graham and Stuart (1971) and the results lead to the conclusion that the dimensionless bearing capacity coefficients depend strongly on footing width. It will be shown that the distribution of contact stress is dependent on the magnitude of applied stress relative to the bearing capacity. Thus, the contact stress distribution is indirectly related to the absolute dimensions of the foundation.

2.1.5 *Foundation Embedment*

As the depth of embedment of the foundation increases, the confining stresses also increase. For a foundation embedded in a cohesionless medium, the soil at the edges is now able to withstand a finite amount of shear. Hence it is possible to have normal contact stresses across the entire foundation width, the magnitude of which are directly related to the degree of overburden.

This effect was observed in the experiments by Faber (1933) whereby the edge contact stresses were increased when a surcharge equivalent to 7 m of soil was applied to the surface of region outside the foundation width. Schultze (1961) reported several cases of contact stress measurement where the distribution was relatively uniform for foundations with a large depth of embedment, resting in cohesionless soils. Muhs (1965) also emphasizes the importance of depth of embedment by relating it to the angle of internal friction of the soil, and thus to the bearing capacity of the foundation. Ho and Lopez (1968) observed that

embedment of a circular plate in sand produced a contact stress distribution that was more uniform (versus parabolic) than in surface tests, but that there appeared to be a "critical" embedment depth, after which a further increase in the depth of embedment did not change the contact stress distribution significantly. Hartikainen (1973) found only a marginal change in the contact stress distribution when a model footing was embedded in loose sand. One theoretical solution to the problem of an embedded rigid circular plate showed that the contact stress is lower in the centre region and higher at the edge (relative to the surface case) but the effect is small (Likhovtsev, 1976).

It should be noted that depth of embedment has usually been expressed as a relative depth, i.e. the ratio of embedment to foundation width. Of greater importance is the absolute value of the embedment of the foundation, as it determines the extent of the confining stresses acting at the foundation edge, which in turn controls the strength characteristics of the soil.

2.1.6 *Depth to Rigid Base*

The contact stress distribution is influenced by the extent or thickness of deformable soil medium supporting the structural foundation, i.e. the depth to which a rigid base such as a rock stratum exists below a foundation. Although the importance of the layer thickness in settlement analysis is acknowledged (Simons, 1974), the calculation of induced stresses in the layer are influenced by the boundary conditions used in the analyses (i.e. displacement or stress conditions at the soil rigid base interface). Similar variations may exist in computed contact stress distributions so only the observable trends will be mentioned.

Conway *et al.* (1966) were able to calculate the effect of a rigid base for a rigid, axially loaded, flat-ended indenter with or without friction at the foundation interface. Numerical values were presented for several indenter widths to layer depth ratios, and the effect of the rigid base on contact stresses did not become significant until the depth was about equal to the width of the strip. In general, as the depth to the rigid base decreased, the contact stresses increased in the centre region (see Fig. 2.4 for a similar analysis by Tsytovich, 1976). This was again illustrated in a finite element solution of the same problem presented by Milović *et al.* (1970) (for different depths of soil layers). Some experimental evidence was given by Mysholivskii and Khlopetskii (1975) for tests of a flexible beam resting on sand of varying depths. The results showed that the contact stresses increased beneath the applied load as the depth to the rigid base decreased.

2.1.7 *Degree of Roughness of the Foundation Interface*

The effect of the roughness of the foundation interface was analyzed by Parkes (1957) for a two-dimensional case of a large raft resting on a semi-infinite soil subjected to a vertical loading. For a smooth surface, the shear stresses will be zero, and the shear stresses developed at a rough boundary will depend on Poisson's ratio of the soil, the relative flexibility of the raft, soil system and the distribution of the external loading. Furthermore, if Poisson's ratio is 1/2 (i.e., elastic material is incompressible, such as that occurring during undrained elastic deformation of the soil), the contact stresses are the same whether the interface is rough or smooth. For smaller values of Poisson's ratio, the contact stresses for a rough raft are slightly greater than

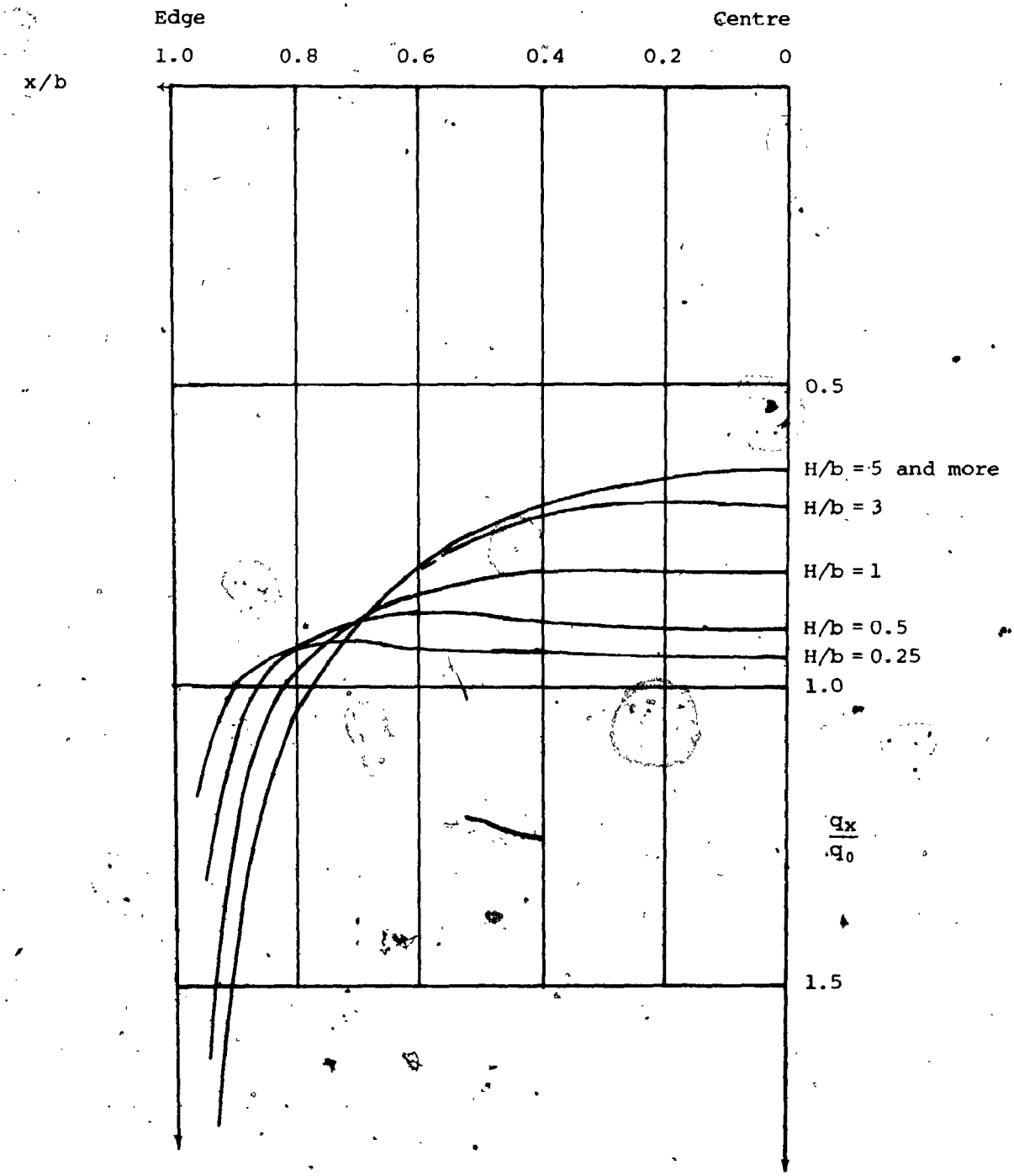

FIGURE 2.4

Contact Stress Distribution under a Rigid Strip Foundation on a Soil Layer of Limited Thickness (from Tsytovich, 1976)

those of a smooth raft because the shear stresses at the interface reduce the curvature of the raft, giving it the same effect as an increase in rigidity.

The effect of foundation roughness has been further described by Sedykh (1964) and Gorbunov-Possadov (1965). The degree of roughness affects the shape of the failure plane, and higher bearing capacities are possible. The magnitude and shape of the tangential stresses are dependent on the cohesion of the soil medium and applied load. Cheung and Nag (1968) applied the finite element method to the analysis of plates and beams resting on an elastic medium; their investigations show that the introduction of horizontal contact stresses reduced the tensile bending stress in a relatively rigid beam by over 30 percent. The significance of the reduction in tensile stress reduces as the beam becomes more flexible. Further investigations along these lines are also reported by Yamaguchi *et al.* (1968), Schiffman (1969) and Carrier and Christian (1973). Again these investigations indicate that the contact stress distribution was practically unaffected by the degree of roughness of the foundation. The displacements were, however, significantly altered by the interface roughness. Carrier and Christian (1973) concluded that roughness is important when the soil is both homogeneous and Poisson's ratio is less than 0.3. Hooper (1974), also using the finite element method, showed that the contact stress was greater in the centre portion of a rigid circular punch resting on a homogeneous elastic half-space if there was adhesive contact. The extent of this increase was limited, due to the effect of slip at the soil-foundation boundary.

There are several methods of measuring the tangential stress occurring at the soil foundation interface, but the model studies to

date have not investigated the effect of varying the surface roughness (Muhs, 1965; Nwabuokei, 1976). There is need for further experimental research in this area.

2.1.8 *Magnitude, Mode of Load and Stress History of the Soil*

The influence of the magnitude of load is usually analyzed in terms of two extreme cases: (1) loads of small intensity (i.e. compared to the ultimate load) acting on a stiff foundation, so that elastic solutions will apply, and (2) loads of magnitude approaching the bearing capacity of the foundation. Increasing the magnitude of the applied stress on a rigid foundation can alter the shape of the contact stress distribution. The maximum load that can be applied is limited to the bearing capacity of the soil. For cohesive soils, the high edge stresses remain high, but the stress in the central region increases until the contact stresses throughout the foundation become more uniform.

For narrow foundations resting on cohesionless soils, the typical parabolic stress distribution shape is continued with increasing load. Faber (1933) found that there was a fairly constant ratio of approximately 2.5 between the maximum stress occurring and average stress applied. Schultze (1961) showed that the contact stress distribution was highly dependent on the load applied in relation to the ultimate bearing capacity. At working stress levels, with a factor of safety of 3.0, the distributions are typically concave parabolic, or saddle-shaped, which at ultimate load changes to a full parabola for sands and a uniform distribution for cohesive soils. This was further confirmed in model studies on sand by Muhs (1965), Murzenko (1965), Lazebnik (1965), Ho and Lopez (1968), Okulova (1968), Hartikainen (1973), Rivkin (1976)

and Nwabuokei (1976).

There have been numerous idealized models of the soil behaviour varying from purely elastic to a purely plastic medium, and combinations thereof. A truly representative model to determine contact stresses for all cases of loading and soil conditions has not yet been developed but progress is being made (Schultze, 1961; Barden, 1962; Gorbunov-Passadov, 1965; Smoltczyk, 1967; Gibson, 1967; Cheung and Nag, 1968; Shirotov, 1972; Carrier and Christian, 1973; Malyshev, 1973; Biernatowski, 1973; Selvadurai, 1976; Hooper, 1974; Snarskii, 1974). The finite element investigation by Wood and Larnach (1974) lead to the conclusion that as the factor of safety decreased (i.e., the load is increased) the edge pressure is decreased due to local soil failure, and the centre of the raft receives a corresponding increase. Contact stress for cohesive soils approaches a uniform distribution as general soil failure is reached, and cohesionless soils have an increase in the centre contact stress (maximum value not specified).

The distribution of applied load only affects the contact stress when the foundation is flexible. Borowicka (1938) compared the difference between a uniformly distributed load and a point load for various degrees of foundation flexibility of a strip. More recently, an example of design contact stresses beneath a hypothetical structure with a relatively flexible mat foundation was given by Laumans and Schad (1976) using the finite element method. Here the loads were transferred to the mat foundation through the columns, the contact stresses are generally higher directly beneath the loading points.

The effect of a cyclic load on contact stress distribution for a cohesionless soil was observed by Murzenko (1965), Ho and Lopez (1968),

and Hartikainen (1973). In general, each load cycle causes a redistribution of the contact stresses. If the original stress distribution was saddle-shaped, the stress increases in the central region and decreases at the edges, resulting in a more uniform distribution. The greatest effect of repeated loading occurs during the first two cycles, after which the magnitude of the change is comparatively small in relation to other factors that affect contact stress distributions.

Measurements of contact stress under dynamic loading conditions are reported by Chae *et al.* (1965), Drenevich and Hall (1966), and more recently by Akai and Otsuki (1974). The contact stresses are redistributed more uniformly in the case of sand tests, but the analysis for a cohesive medium has not been presented. The problem is complicated by the build-up of pore water pressures in the soil, and most of the research to date with dynamic loading has been concerned with the bearing capacity of the foundation rather than the examination of the distribution of contact stresses.

In engineering practice the load application depends on the construction sequence. For large projects, such as dams, canal locks or raft foundations, the load may be applied over a period of months or even years. Contact stresses beneath foundations resting on cohesionless soils will not be significantly affected by the rate of loading; however, little is known about how the consolidation characteristics of a cohesive soil can affect the contact stress. Examples of civil engineering projects in which contact stresses have been monitored over time have been reported by Teng (1949), Schultze (1961), Kaufman and Sherman (1964), Sikso and Johnson (1964), Gerrard *et al.* (1971), Gosbell (1971), Eden, McRostie and Hall (1973), Krivorotov (1973) and Crowser *et al.*

(1974). In most cases the monitoring has ended when construction was complete. Eden *et al.* (1973) found that there was little appreciable change over time in the high edge stresses of the foundation, indicating that there was not appreciable redistribution of the contact stress as consolidation of the clay layer took place. Sikso and Johnson (1964) relate contact stress observations with theoretical observations based on applied loads, and in some cases found that the measured contact stress increased with time, but usually remained constant. A general conclusion cannot be made in this case, because of the questionable accuracy of the measuring cells.

2.1.9 *Efficiency of the Contact Stress Measuring Device*

The selection of a device to measure the stresses occurring at the soil foundation interface is part of a larger problem of measuring the induced stresses within an earth mass subjected to an external load. An excellent summary of the uses of contact stress measuring devices was given by Hvorslev (1976). Hanna (1973) outlines the factors that can be used to judge the performance of embedded earth pressure cells and boundary pressure cells:

(1) Simple principle of design and operation

(2) Durability in the field or lab environment

(3) Accuracy both for long-term and short-term measurements

(4) A proven record in the field

(5) Ease of calibration and re-calibration

(6) Non-sensitive to environment changes

(7) Minimum interference due to installation in the ground

(8) Simple installation procedures

(9) Minimum overall cost.

The error of a contact stress measuring device can be expressed as $(\sigma_c - q_x)/q_x$, where σ_c represents the stress increment measured by the cell, and q_x is the actual change in contact stress. In order to reduce this error, basic design features have been developed. Probably the most important requirement of the measuring device is that its registration should induce a minimum of interference into the soil medium. This has led to the design of pressure transducers that are very rigid relative to the soil so that only small deflections are necessary for a signal response. The use of solid state electronic components enables small strains to be measured accurately.

Most studies are concerned with normal contact stresses only, but it is possible to measure the shear stresses at the soil foundation interface with special devices such as the "Cambridge" load cell used for example by Hambley and Roscoe (1969), or the cell developed by Muhs and Bub (1965) using an elaborate system of ball bearings to measure the stresses in three independent directions. There are several methods used to measure normal contact stress, and a good summary of these devices has been presented by Bozozuk (1970), Hanna (1973), Lazebnik *et al.* (1973), Doohan (1975) and Nwabuokei (1976). Common names for these devices are the pneumatic earth pressure cell, beam-type pressure cells, pressure transducers and Cambridge transducers. This discussion does not intend to go into detail on the advantages and disadvantages of each of these types of measuring devices, but will introduce some of the characteristics of the contact stress measuring cells used in the current experiments.

The flush diaphragm pressure transducer was described by Hvorslev

(1976) in a comparison of many currently available earth pressure cells. Their principle of operation was simpler than most of the other types of cells, but their use was restricted to fairly fine-grained and uniform soils because stones in the soil may cause eccentric load concentrations and also damage the diaphragm. Most of Hvorslev's work is associated with full-scale earth pressure cells, or cells fully embedded in the soil, but parts are related to this discussion. It was shown that a pressure cell always under-registers the applied stress. The amount of underregistration decreases as the rigidity of the cell diaphragm increases. An estimate was given as to the amount of protrusion necessary to cause 100 percent registration for given values of deformation modulii of the soil and pressure cell.

Both contact stresses and pore water pressures were measured in this thesis by flush diaphragm pressure transducers. It is worthwhile discussing some of the factors that influence their performance. Votava (1974) provides an introduction into the various types of instruments that are used to measure a wide variety and range of pressures. More detail was provided by Sandford (1976). Here it was explained that transducers with bonded strain gauges are usually composed of a miniature Wheatstone's bridge circuit with output voltage directly proportional to input excitation voltage. Since the sensitivity of the instrument is usually expressed in millivolts per volt input, a stronger, more measurable output signal is produced from a higher input voltage. There is a limit to the input voltage magnitude because heat is generated by the strain gauges and errors become large.

The basic principle of the strain gauge transducer is that under conditions of zero applied stress on the measuring diaphragm the

Wheatstone bridge circuit is electrically balanced. When stress is applied, the diaphragm deflects, causing a change in strain of the resistance gauges and producing a proportionate change in the output signal. Since the output signal is dependent on the input voltage, it is required that the excitation voltage remain constant during operation.

The influence of the environmental conditions (such as temperature and humidity) on the pressure transducer performance was discussed by Davidson (1975). Ideally, there should be a linear response between the stress applied to the diaphragm and the output measured by the transducer. Deviation from this linearity is commonly known as non-linearity, hysteresis and repeatability. Drift and shift are commonly used terms and should be explained. Sandford (1976) defines these terms as follows:

> NON-LINEARITY — the amount by which the measured output of a transducer, subjected to any load within its capacity, differs from an ideally linear output as defined by a straight line. The transducer output is measured on increasing load only.
>
> HYSTERESIS — the amount by which a transducer output, when measured under an increasing load, differs from its output under an equal but decreasing load.
>
> REPEATABILITY — the maximum difference between any two values of output for any given load within the capacity rating as measured on successive runs under identical conditions of load, time, temperature, and so on.
>
> DRIFT AND SHIFT — drift in the output signal of a transducer may result from any cause, but the cause is usually thermal. Drift will disappear when the cause is removed. Shift is a permanent change in the output. It remains when the cause is removed.

The manufacturer usually specifies the maximum error due to

non-linearity, repeatability and hysteresis as a percentage of full-scale output (FSO). For example, a ± 1.0 percent combined error in a 1000-kPa pressure transducer would mean that the error is ± 10 kPa throughout the 1000-kPa span range, i.e., at 100 kPa applied stress, the error is ± 10 percent. This is unacceptable in many cases, so in practice it is common to accurately calibrate the pressure transducer over the pressure range that is required.

Davidson (1975) found that temperature changes in the environment were most likely to have the largest influence on the measured output. Temperature can affect the resistivity of the strain gauges in the pressure cell, the power supply voltage, and the output voltage measured by the data acquisition system. The effect of temperature can be reduced if the pressure transducer is temperature-compensated by the use of dummy bridges.

Creep of the pressure transducer diaphragm during constant applied stress will result in the output voltage changing with time. Davidson (1975) noted the effect on output, showing that it is dependent on both the magnitude of the applied stress and on the number of cycled loads of the diaphragm. It is difficult to quantify the change in output due solely to the creep of the pressure transducer, and the manufacturers do not include it in their performance characteristics. Verma (1976) attempted to measure the effect of creep, and for his application found it to be negligible.

The contact stress measuring cell is registering the *average* stress over its sensitive surface. If the size of the measuring area is small from a global point of view, the output of the measuring device can be taken as representing the stress at a "point". The contact

stress *distribution* can be obtained by combining the results of a large number of cells. Pahl (1977) estimated the number of cells required to establish a statistically significant contact stress distribution, if assumptions were made regarding the accuracy of the measuring device and shape of the distribution. The results show that the number of cells required is probably more than the number used in the field and model studies in the past. An example of the large variation in contact stress at seemingly identical locations along the interface was presented by Krivorotov (1976) in tests conducted on sands. The standard deviation of the edge measurements varied from 30 to 67 percent of the average contact stress. Lazebnik *et al.* (1966) showed that the type of measuring apparatus influenced the observed contact stress and hence, the conclusions drawn.

This section has briefly introduced some of the uncertainties involved in experimentally measuring the contact stress distribution. In many cases, the theoretical models have advanced further than the experimental analysis has an ability to measure. It is difficult or impossible to draw valid conclusions from experimental work that has inherent errors of magnitude greater than the influence of the parameter being measured. For this reason, a clear understanding of the limitations of the measuring device is necessary, and should be discussed when presenting any such research work.

2.1.10 *Conclusions on Contact Stress Distribution*

The distribution of contact stress along a soil-foundation interface can vary significantly from a simplified assumption of uniform contact pressure. The parameters that can affect the distribution are:

(1) flexibility of the structural foundation

(2) mechanical properties of the soil

(3) geometry of the foundation

(4) foundation embedment

(5) thickness of deformable soil layer

(6) degree of roughness at the foundation interface

(7) load magnitude, mode and distribution.

Much of the research done to date has been concerned with soil media idealized as a purely elastic material, and the latest developments have extended this to honogeneous anisotropy and isotropy, compressibility decreasing with depth, and certain cases of stratification. Several articles have developed an approximate method of dealing with loads that approach the ultimate bearing capacity; the soil is modelled as having both elastic and plastic characteristics. To provide observational data to aid in constructing a more realistic model of soil-foundation interaction, researchers have performed model experiments that usually isolated one or more of the parameters which affect the distribution of contact stress. This has been extended to observations of large structures in the field. The problem with all the laboratory and field experiments lies in the difficulty of measuring the actual contact stress distribution with a device that will not interfere with the soil medium.

More experimental research is required in nearly all aspects of the parameters affecting contact stress distribution. This must be complemented with an extensive field observation program. Only then can a truly representative model of soil-foundation interaction be developed, in order to predict contact stress distribution to be used in the design

of structural foundations.

2.2 *Settlement of Foundations on Normally Consolidated Clay*

This study is concerned not only with the contact stress distribution beneath a rigid strip footing, but also with the observed settlement. For cohesive materials there is usually an immediate elastic settlement followed by a time-dependent settlement due to either expulsion of the porewater from the medium, or a compression of the clay structure, or both concurrently. This time-dependent settlement is commonly referred to as primary or secondary consolidation. Although the magnitude of the secondary consolidation may be substantial, the effect will not be investigated.

The number of methods of analysis in calculating settlement have expanded to make it difficult to present a comprehensive review in the limited space available. There have been several "State of the Art" reports written over the years that summarize the current methods used for settlement of foundations on clay, such as Lambe (1964), Seed (1965), Davis and Poulos (1968), Simons (1974) and Burland *et al.* (1977). Recent activity has been directed towards the analysis of a soil medium whose characteristics depart from the assumptions of an ideal isotropic, homogeneous elastic half-space or layer. The determination of the appropriate parameters to be used in the analysis has also received attention. With regard to the settlement analysis used in this study, the clay is assumed to be homogeneous, isotropic and elastic.

2.2.1 *Immediate Settlement*

The immediate settlement of a uniformly loaded rigid strip footing

resting on a layer of saturated cohesive clay is usually expressed in the form:

$$\rho_i = \frac{q_0 B}{E_u} \quad (I)$$

where ρ_i = immediate settlement
q_0 = applied stress
B = foundation width
E_u = undrained Young's modulus of the soil
I = influence factor dependent on:
— Poisson's ratio , $\nu_s = \frac{1}{2}$
— position of settlement point on foundation
— geometry of the foundation
— depth of foundation.

A literature review was made of the published values of influence factors that were applicable. It was difficult to find the solution that corresponded to the exact geometry and loading conditions of the experimental test, but many of the results are similar. The assumptions that went into the various methods are presented in point form and the results are compared in Chapter 4.

SUMMARY OF AVAILABLE IMMEDIATE SETTLEMENT SOLUTIONS FOR *Strip* FOOTINGS

(1) Janbu *et al.* (1956) (see Bowles, 1968)
— rigid base at various depths
— flexible load, but average taken
— interface condition not specified
— Poisson's ratio variable
— correction available for overconsolidated soil

(2) Harr (1966)
— rigid base at various depths
— flexible load
— interface rough or smooth, average given
— Poisson's ratio variable
— settlement at edge and centreline given

(3) Gibson (1967)
— non-homogeneous elastic half-space
— homogeneous case given

Gibson *(cont'd)*
- — flexible load
- — develop rigid case
- — incompressible medium (Poisson's ratio = 0.5)
- — predicts infinite settlement at all points, but the shape of the settlement can be determined.

(4) Poulos (1967)
- — rigid base at various depths
- — flexible load
- — vertical and horizontal displacement
- — interface between soil and rigid base is rough
- — Poisson's ratios: 0.5, 0.4, 0.2, 0
- — stresses given at five positions in the soil

(5) Milović *et al.* (1970)
- — finite element analysis
- — rigid footing
- — rigid base
- — rough footing, rough base
- — Poisson's ratios: 0.45, 0.3, 0.005
- — stresses given in soil beneath centreline

(6) D'Appolonia, Poulos and Ladd (1971)
- — corrections to elastic theory to take into account yielding of the clay layer
- — requires
  - — E_u, undrained modulus
  - — q_u, ultimate bearing capacity
  - — f , initial shear stress ratio between the initial in-situ shear stress before any external load is applied and and the undrained shear strength

It will be shown that the various solutions to the immediate settlement influence factors are not always in close agreement, largely due to the differences in assumptions regarding the conditions occurring at the boundaries of the soil medium. There is a possible greater source of error, however, involving the determination of the undrained modulus E_u from laboratory or field in-situ tests. This was illustrated by Shields and Bauer (1975) when estimating the immediate settlement of spread footings on a sensitive marine clay. Results for unconsolidated undrained (UU), consolidated undrained (CU) and stress path triaxial tests were compared with field pressuremeter tests, plate bearing tests

and a full-scale footing test. Plate bearing tests were in best agreement with the full-scale footing results, but the consolidated undrained triaxial test was also similar. The laboratory determination of E_u was emphasized by Simons (1974) to be highly dependent on a number of factors, such as the stress history of the soil, the stress level, the rate of strain and sample disturbance.

Davis and Poulos (1968) calculate the total final settlement for a homogeneous isotropic soil medium by relating the Young's modulus of the soil skeleton, E', to the undrained Young's modulus, E_u, and substituting the value into the equation for immediate settlement. The problem lies in determining appropriate values of E_u and E'.

2.2.2 *Consolidation Settlement*

Terzaghi's (1943) classical theory of consolidation is widely used to predict both the ultimate settlement and the rate of settlement of a saturated clay layer. All of the settlement is assumed to be due to one-dimensional strain, which results from the increase in effective stress as the excess pore pressures are dissipated. The immediate increase in pore pressures are assumed to be equal to the change in total vertical stress. Skempton and Bjerrum (1957) modified the method to take into account the relationship between the excess pore pressures and the major and minor principal stresses. Lambe (1965) proposed that the settlement analysis be computed from measurements of the vertical strain due to undrained loading and drained loading of the soil sample in triaxial tests. Davis and Poulos (1968) offered a variation of determining the settlement from triaxial tests. These methods all require estimates of the increase in stress due to the external loading, which is usually

based on classical elasticity theory.

The problem of the consolidation settlement of a uniformly loaded strip footing resting on a frictionless semi-infinite medium was analyzed by Schiffman *et al.* (1969). The three-dimensional theory of Biot (1941) assumes the soil behaviour to be similar to that of an isotropic, homogeneous fully saturated clay with an elastic soil skeleton and incompressible fluid. One case treated by Schiffman *et al.* (1969) was for an impervious boundary, forcing the pore water pressure to be dissipated laterally, rather than a combination of lateral and vertical directions, as in the case of free drainage at the surface (Fig. 2.5). As the depth below the footing increases, the effect of the impervious boundary decreases.

Figure 2.6 illustrates the initial excess pore pressure distribution at a depth of $z/b = 0.5$, and the distribution at various time intervals. A brief explanation of the physical process can be interpreted in the following manner: The pore water beneath the footing is forced to migrate away from the centre towards the edge. At the edge the excess pore water pressure is dissipating at the same time, but the continual flow of water from the centre reduces the rate of dissipation.

As explained in the article, the classical theory of one-dimensional consolidation (see Terzaghi, 1943) maintains that the total stresses are constant throughout consolidation, and hence the maximum shear stresses are constant. Under three-dimensional conditions, there is a substantial change over time in the maximum shear stress beneath the plate. This concept is illustrated in Figure 2.7 for a depth of $z/b = 0.5$ beneath the footing. At the edge, where the effect is most pronounced, the maximum shear stress increases by 80 percent over the

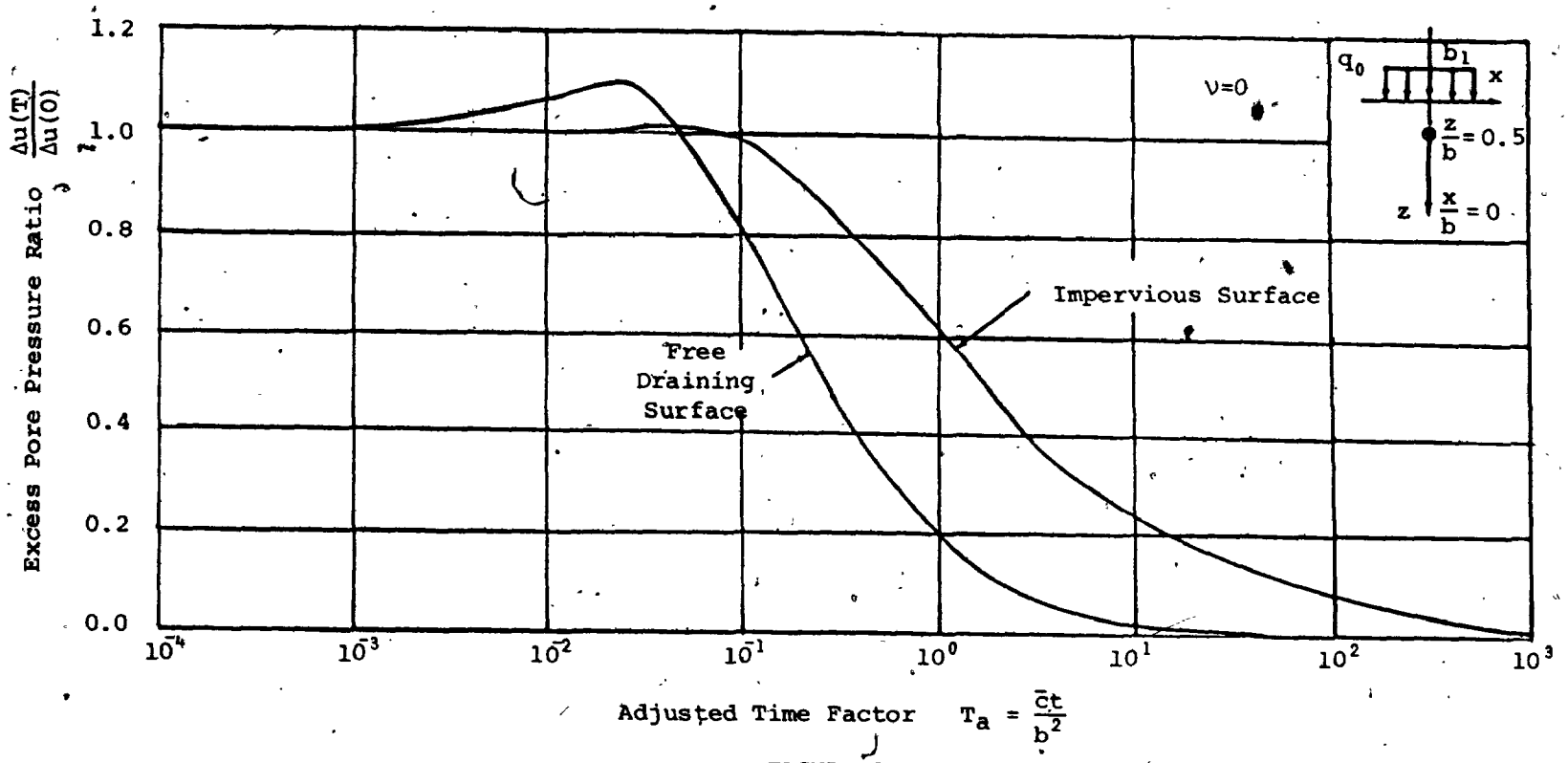

FIGURE 2.5
Effect of Surface Drainage on Excess Pore Pressure, Plane Strain Consolidation, Normally Loaded Halfplane (after Schiffman *et al.*, 1969)

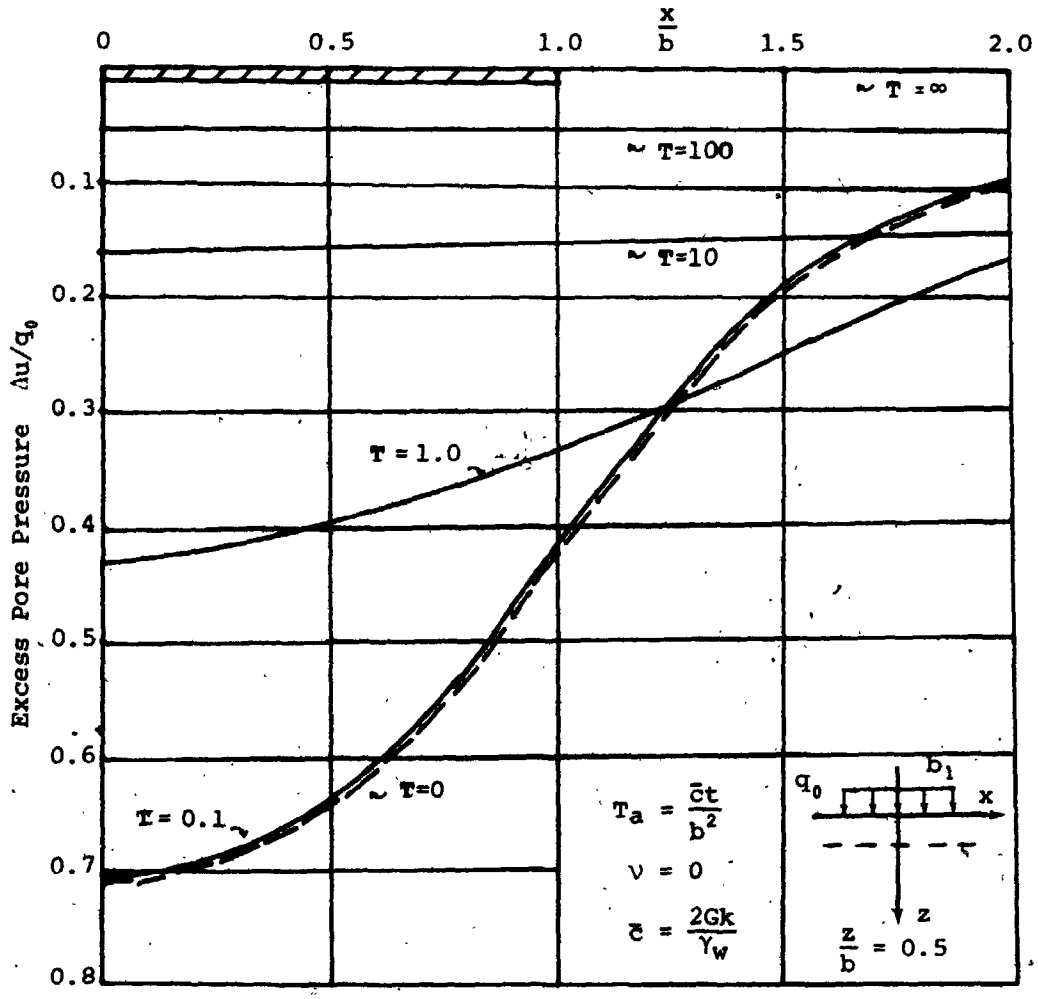

FIGURE 2.6

Lateral Distribution of Excess Pore Pressure, Plane Strain Consolidation, Normally Loaded Half-plane, Impervious Surface (after Schiffman *et al.*, 1969)

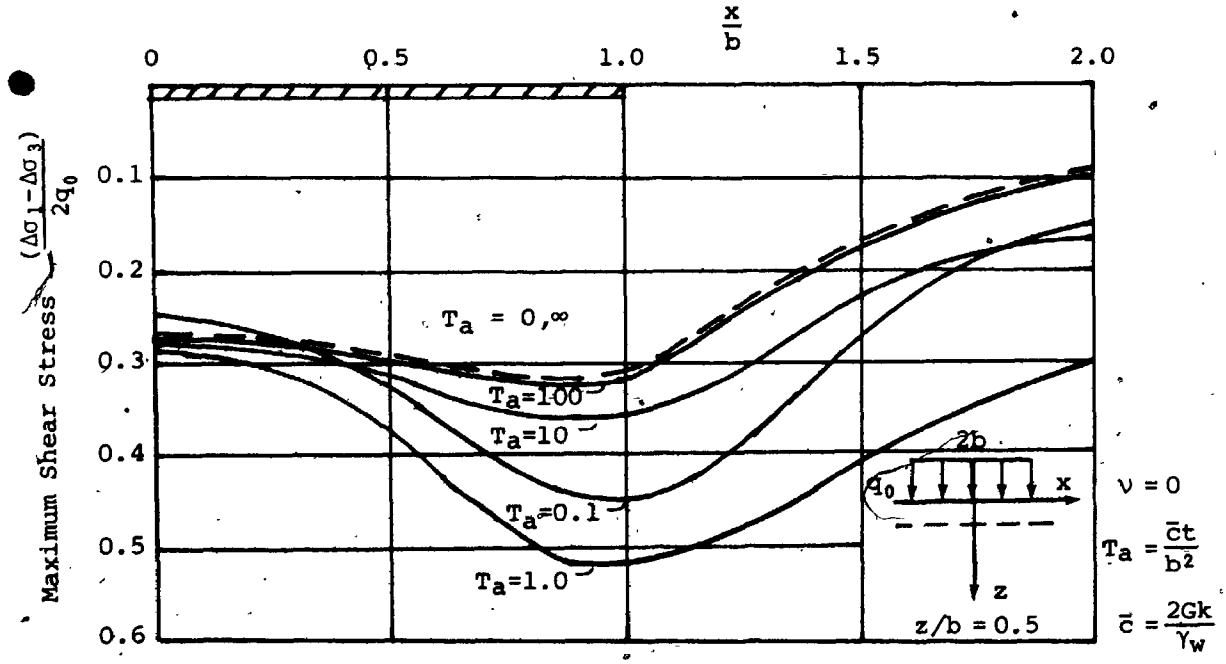

FIGURE 2.7

Lateral Distribution of Maximum Shear Stress, Plane Strain Consolidation, Normally Loaded Half-plane, Impervious Surface (after Schiffman *et al.*, 1969)

initial value, and then decreases to its original value. It is usually assumed that plastic yielding will not occur beneath a uniformly loaded flexible strip for low levels of applied average stress, but the results of the consolidation analysis indicate that local yielding or instability may occur at some time during the consolidation process, even at low stress levels.

The results given by Schiffman *et al.* (1969) are not directly applicable to the experiments performed as a part of this study. The results for a *rigid* footing would be desirable, and the conditions occurring at the contact surface for both rigid and flexible loadings are more related to this study. The results given by Schiffman *et al.* (1969) are important because they illustrate that under three-dimensional conditions, there is a change in *total* stresses throughout the medium during consolidation. Under non-uniform loading, the assumption of lateral drainage away from the centreline may not be valid near the surface of the soil medium, and the problem becomes more complex. There is justification, however, to believe that the contact stresses will not remain constant during the consolidation process, but the magnitude of the change is not known.

Gibson *et al.* (1970) extended the analysis of Schiffman *et al.* (1969) to include the case of a smooth, impervious base at various depths below the uniform strip load. Of relevance to this study is the fact that, for the case of free drainage at the surface, and a rigid base at $z/b = 5$, the rate of dissipation of pore water pressure was essentially the same as that of the semi-infinite medium (Fig. 2.8).

Hwang *et al.* (1971) have examined the same problem treated by Schiffman *et al.* (1969), using the finite element technique developed

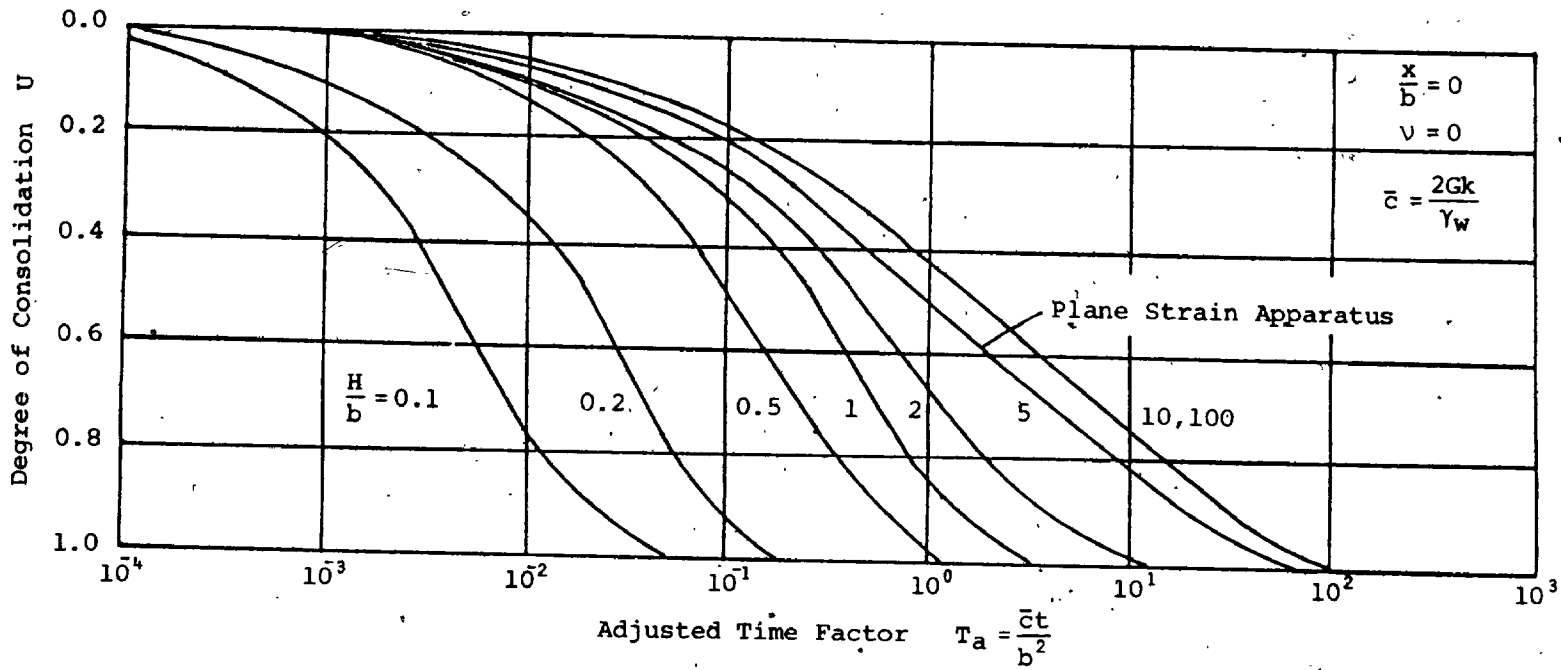

FIGURE 2.8

Effect of Layer Thickness on Degree of Consolidation of a Uniformly Loaded Flexible Strip Footing (after Gibson *et al.*, 1970)

for consolidation problems. In the analysis the geometry used in the modelling of the region was, unfortunately, different from the setup used in this study. There was excellent agreement of the finite element results with the existing analytical solutions so extension of the problem to various layer depths and drainage conditions would be possible.

2.2.3 *Consolidation of a Layer Under a Uniform Strip Load*

The results of a finite element program used to study the consolidation of a layer under a strip load was presented by Christian *et al.* (1972). It was intended to show the effects of (a) aspect ratio of layer thickness to load width, (b) Poisson's ratio of the soil skeleton, and (c) degree of orthotropic permeability, on the primary consolidation settlement of a strip load on an elastic soil. The basic assumptions are the same as those used in Biot's (1941) theory of consolidation (and Terzaghi's (1943) one-dimensional theory).

It was found that if the edge boundary was located away from the strip centreline a distance five times the thickness of the clay layer, these conditions appeared to model a clay layer of infinite lateral extent (provided the interface between the soil and rigid base was rough).

The phenomenological results of varying load width may be of practical importance. One of the limiting cases is that of a uniform load applied to the entire surface of the layer, where the total settlement and rate of settlement is identical to the one-dimensional theory. As the width of the loaded area decreases, i.e. as the rigid base moves farther from the surface, there is a greater amount of intermediate settlement in relation to total settlement. This effect is dominant in the case of an infinite layer where the initial settlement is infinite. The

intermediate case of a layer of finite extent has finite values of immediate and primary consolidation settlement. The ratio of width to layer thickness, b/H, has a major effect on the *rate* of settlement, where it was shown that as the layer depth increases the settlement rate increases correspondingly faster than predicted by one-dimensional theory. Under the same circumstances, the excess pore water pressure dissipation lags behind the degree of consolidation settlement.

Christian *et al.* (1972) clearly point out the uncertainties involved in using the one-dimensional approach to initial and primary consolidation computation when the thickness of the layer is large in comparison with the width of the loaded area.

The effect of anisotropic permeability was also studied, and was found to affect the rate of settlement in the early stages, but the total settlement is the same for all cases.

The work also cautions that the results may not be applicable if there is considerable plastic yielding present. Such effects can be manifest in the rigid foundation problem, in which case the consolidation analysis becomes more difficult.

Non-uniform contact stress results in pore pressure gradients beneath the plate. The pore pressure dissipation and hence rate of settlement is highly dependent on the paths available for pore water drainage.

2.2.4 *Pore Water Pressure Predictions*

The principle of effective stress has been used extensively in the past for stability and settlement analysis, and involves two basic steps: (1) determination of the shear strength parameters, c' and ϕ'; and

(2) determination of pore water pressure. This section is concerned with the determination of pore water pressure, both in the laboratory and in the field.

In order to predict excess pore pressures developed by an undrained loading of a cohesive soil, three requirements are necessary:

(1) the relationship between the change in total stress and excess pore pressure must be established;

(2) the conditions of drainage which exist in the field must be determined;

(3) the relationship between the externally applied load and the corresponding change in total stress must be established.

Most of the analytical work done to date assumes the soil material to be linearly elastic. The principle of superposition is assumed applicable whereby the sequence of loading operations bears no influence on the resulting pore pressure increases. There have been several articles which show there are two distinct regions—an "elastic" range where pore pressures are dependent on both the octahedral normal stress and octahedral shear stress, and a "plastic" range where pore pressures vary with changes in the principal stresses (see Hoeg *et al.*, 1969; D'Appolonia *et al.*, 1971; Dascal and Tournier, 1975).

The most general form of the pore water pressure equation is:

$$\Delta u = \beta \Delta \sigma_{oct} + \alpha \Delta \tau_{oct}$$

where $\Delta\sigma_{oct}$ = change in octahedral normal stress
$\Delta\tau_{oct}$ = change in octahedral shear stress

and β,α are experimental constants.

A summary of the various analytical methods used to predict the

increase in pore water pressure is presented in Appendix 2. To determine if pore pressure increases occurring in the field could be predicted, several published field observations were summarized and compared with the predicted pore pressure increases obtained from laboratory experiments. They are presented in tabular form in Appendix 3. The pore pressures tended to agree with the predicted increases if the analysis took into account changes in all three principal stresses.

In almost all cases, the measured field pore pressures were lower than predicted, and it was generally proposed that this was due to pore pressure dissipation. The assumption of "undrained" loading rarely satisfied under field conditions, either due to the presence of sand layers or other drainage paths. With unsaturated soil conditions, it is still difficult to predict 'average' pore pressure increases. The applied field load is seldom applied at the same rate as performed in the laboratory, and is dependent on the rate of construction activity. The dependence of the A parameter (Skempton, 1954) on the stress history, rate of strain, method of testing and other factors results in a reduction in the accuracy and reliability of the value (see Bishop and Henkel, 1962; Lambe, 1962; Crawford, 1963; Ladd and Lambe, 1963; Lee *et al.*, 1969; Bishop, 1973, 1976). The soil medium usually exhibited non-homogeneous and anisotropic properties, features that are difficult to account for in the laboratory.

A combination of the above factors can be offered as a possible explanation as to why the predicted pore pressures are not always in agreement with field measurements. By taking into account as many of the factors as possible affecting the increased pore pressures the discrepancies between the predicted and observed can be reduced.

At present, the analytical techniques for predicting pore pressure increases have generally led to a trend being observed, but more field observations are necessary to substantiate the trend. The predictions of pore pressure increases are dependent on the analysis used to compute the increment in the principal stresses. The variability of the soil conditions emphasizes the importance of determining the actual site conditions. Any attempt at applying theoretical idealizations to field conditions will also be controlled by the methods used to determine the pore pressure parameters, both in the laboratory and in the field.

2.2.5 *Pore Water Pressure Measurement*

Pore water pressures are measured in the field in order to provide a check of the stability analysis during construction of structural foundations, embankments and excavations. Not only are the observations important at the time of construction, but they are useful as historical records to be compared with theoretical predictions. They help to establish the validity of the assumptions used in the models and increase the reliability of the estimated pore pressure increases in the future.

Pore water pressures can be measured with piezometers, hollow filter elements placed in the soil providing a cavity usually filled with water. A summary of the various instruments and techniques used to measure the pressure in the cavity was presented by Bishop *et al.* (1969). It was explained that there are two main types of pore pressure measuring systems: (1) open boreholes or standpipes, where the piezometer is connected to the measuring source by tubes filled with water; and (2) electrical measurement, where the change in pore pressure is registered by a deflection of a diaphragm. The advantages and disadvantages of

each were discussed, showing that the particular field or laboratory application determines which system is better.

The measurement of pore pressure in model foundations has the same principles and sources of error as full-scale tests. The comments made by Vaughan (1974) in respect of the principles involved are briefly introduced. For saturated soils the main concern is to ensure the pore pressure in the cavity is representative of the pore pressure in the surrounding soil. Gibson (1963) expressed the relationship between soil compressibility and piezometer response in terms of an equalization ratio, ϵ, where

$$\epsilon = \exp\left[\frac{-Fkt}{V\gamma_w}\right]$$

where F = intake factor, dependent on size and geometry of the piezometer
k = coefficient of permeability
t = time
V = volume factor for compressibility of the piezometer system, defined as flow into the piezometer for unit pressure change in the cavity
γ_w = unit weight of water.

At 100 percent equalization between the pore pressure in the piezometer cavity and the surrounding soil, $\epsilon = 0$.

This equation is important because it illustrates the features controlling the response time of a piezometer. It is desirable that in the piezometer the intake factor, F, be maximized and the volume factor, V, be minimized. The optimization of the intake factor is constrained by the assumption that the piezometer is measuring the average pore pressure over a volume sufficiently small to be represented as a "point"

relative to the dimensions of the problem being examined. This is especially important where high pore pressure gradients exist in the soil. Minimizing the volume factor V can be accomplished by making the measuring system as "stiff" as possible (i.e. decreasing the volume of "dead" water between the piezometer and the pressure sensor (Burland and Roscoe, 1969)). "Stiff" implies that the connecting lines and sensing device have a minimum increase in volume under an increase in pore water pressure, i.e., very little flow of water through the piezometer is necessary. There is a conflict between maximizing the intake factor, F, and minimizing the volume factor, V, and a compromise must be reached.

The compromise solution depends largely on the situation encountered. The initial equalization of the pressure between the piezometer cavity and surrounding soil immediately after placement will require less time if less soil is disturbed, because the remolded soil generally has a lower permeability. Smaller piezometers are desirable when large pore pressure gradients are possible. They also reduce the error involved due to different deformability characteristics between the piezometer and soil. Vaughan (1974) believes that changes in principal stresses are most apt to be affected by the inclusion of a piezometer producing local stress concentrations similar to those encountered in embedded earth pressure cells (Hvorslev, 1976). As long as total stress changes are small, the error in measured pore pressures will be negligible.

The problem of equalization of piezometer cavity pressure with unsaturated soil was explained by Vaughan (1974), when pore air pressures are present. Pore water pressure is more important to measure because it usually controls the effective stress and directly responds to pore

water drainage. In unsaturated material the air (having a higher pressure) will migrate to the cavity of the piezometer and replace the water. The amount of water displaced will be reduced if high air entry filters are used around the piezometer cavity. For sealed systems the use of high air entry value filters will not stop air diffusion into the cavity (Williams, 1967). Initially the air in the piezometer cavity will be at the same pressure as the water, lower than the air in the surrounding soil, so diffusion will continue. As long as there is a continuous circuit of water from the piezometer to the pressure sensor, pore water pressure will be measured. Eventually the air will fill the cavity, forming a "bubble", and this pressure will continue to rise until the air pressure in the bubble is the same as the air pressure in the adjacent soil.

The problem of air entering the piezometer can be reduced by (1) increasing the volume of water in the piezometer cavity, (2) employing a high air entry value filter, and (3) providing a system for de-airing the lines.

The magnitude of the problem of air in the system will be greater for lower degrees of saturation of the soil and lower pore pressures.

When pore pressures are being measured in the laboratory, the size of the soil sample is usually small. In triaxial, direct shear and oedometer tests the average pore pressure can be measured on the boundary of of the sample with the use of porous rigid filters such as porous stones or ceramic discs. Measurement of the pore water pressure within the sample is more complex, and a review of several articles was made to determine the existing techniques.

Hilf (1956) stated the requirements of a miniature pore pressure

sensor as follows: "The ideal porous tip would have a pore diameter small enough to exclude air, a high conductivity to reach equilibrium in a short time, a shape conducive to insertion without appreciably affecting the geometry of the specimen, and a toughness to withstand shearing forces." The porous tip found most suitable was a stainless steel needle 3/32 inch OD 3 inches long with the end plugged with No. 200 stainless steel mesh. A slurry of white slip casting clay was baked on the end, and the needle was boiled in water for 15 minutes before use. Crawford (1963) also used a 1.2 mm OD hypodermic needle on sensitive Leda clay, after previously freezing the de-aired water in the needle to minimize entry of soil during insertion. Richardson and Whitman (1963) used a 1/8 inch OD 7/8 inch long porous stone, while Barden and McDermott (1965) used a 1/4 inch OD 0.6 inch long ceramic probe. All of these papers were concerned with the pore pressure increases occurring within a soil sample tested in a triaxial cell. A thin tube usually connected the sensor with an external pore pressure measuring device, such as a null indicator or pressure transducer.

Burland and Roscoe (1969) reduced the volume of water between the piezometer and pore pressure measuring device by using sealed miniature pressure transducers housed at the base of either a No. 17 gauge 1½ inch long hypodermic needle filled with cotton, or at the base of a 3/16 inch diameter ceramic disc. These instruments were very sensitive to changes in pore water pressure, having the advantage of compact size and fast response time. The importance of minimizing the air in the piezometer cavity was demonstrated by the increased time lag in the pore pressure response of one device. This study was important for the transient pore pressure response under one-dimensional drainage occurring in an

oedometer cell.

There are very few papers written on the measurement of pore water pressures in the soil medium beneath *model* footings under plane strain or axi-symmetrical conditions for either immediate or transient pore pressure response. One such study was carried out by Aboshi (1955) (as reported by Yamaguchi and Murakami, 1976). Aboshi (1955) studied the transient response of 30 piezometers located symmetrically beneath a 0.5 m circular rigid plate. The clay was placed within a test tank of dimensions 1.00 m × 0.90 m × 0.90 m, with free drainage over the entire surface. It was observed that the pore pressure increased temporarily during the early stages of consolidation, and the time until this peak occurred was longer for points farther away from the drainage surface. It is unfortunate that more information was not provided for comparison with currently available theoretical models.

The immediate pore water pressure response to a rigid circular 0.6 m model footing loaded in the field was reported by Thamm (1976). The maximum excess pore pressures beneath the edge of plate were best predicted by the increase in octahedral normal stresses, in agreement with many full-scale observations (Hoeg *et al.*, 1969; D'Appolonia *et al.*, 1971; Moh *et al.*, 1972).

3. EXPERIMENTAL PROGRAM

3.1 *Present Research Work*

The survey of previously published literature revealed that there was a scarcity of observations of contact stresses beneath a foundation resting on a cohesive soil medium, for both model foundations and full-scale structures. It was also evident that the theoretical analysis had not been developed to take into account the effect on contact stresses of changes in the soil stratum over time. For this reason a program of investigation was started to observe the manner in which contact stresses respond to a consolidating soil medium. The problem being modelled was that of a smooth rigid strip footing tested under plane strain conditions.

In Section 2.1 a number of factors were introduced that appear to have an effect on the contact stress distribution. Of these, this experimental work was restricted to analyzing only a limited number of the variables. For example, the foundation flexibility was fixed and can be considered rigid. The width of the foundation was fixed. A strip footing was modelled. The footing was always placed at the surface and the effect of the thickness of the soil layer was not investigated. There were no attempts to vary the degree of roughness at the interface of the footing and soil. The load application rate can be considered as static and was applied vertically to the centre axis of the footing. By limiting the number of factors to be analyzed, the effect of the main parameters under consideration can be studied more closely.

The primary investigation concerned the time-dependent response of a rigid strip footing, as idealized in Figure 3.1. This problem can be modelled by taking two "planes" at right angles to the longitudinal axes of the strip and subjecting the soil between the two planes to a vertical stress at the surface. Plane strain conditions will hold provided there is no friction along each plane and no strain of the soil along the axial direction (E-E). Considerable effort was made to develop the equipment to model these conditions (see Section 3.2.1).

A total of eleven tests were performed on sand in order to check the performance of the equipment prior to the main test on clay. Each test involved preparing the sand in the test flume to a uniform density and applying a cyclic load to the test plate placed on the surface of the soil. Contact stresses and plate settlement were observed at various load increments.

A test was performed on a 0.4 m layer of compacted clay in a 1.2 m square test frame. This was a preliminary test to provide experience in the operation of the equipment and establish the experimental procedure for subsequent tests on clay. Contact stresses and plate settlement were recorded.

The main test involved the loading of the test plate over a compacted clay layer in the "plane strain" apparatus. The load was applied over a short period of time and allowed to remain for a period of five weeks. During this time the contact stresses, plate settlement and pore water pressures were monitored.

Two subsequent short-term tests were performed on the same bed of compacted clay in order to determine the influence of side wall friction. The tests also provided information on the surface displacement profile,

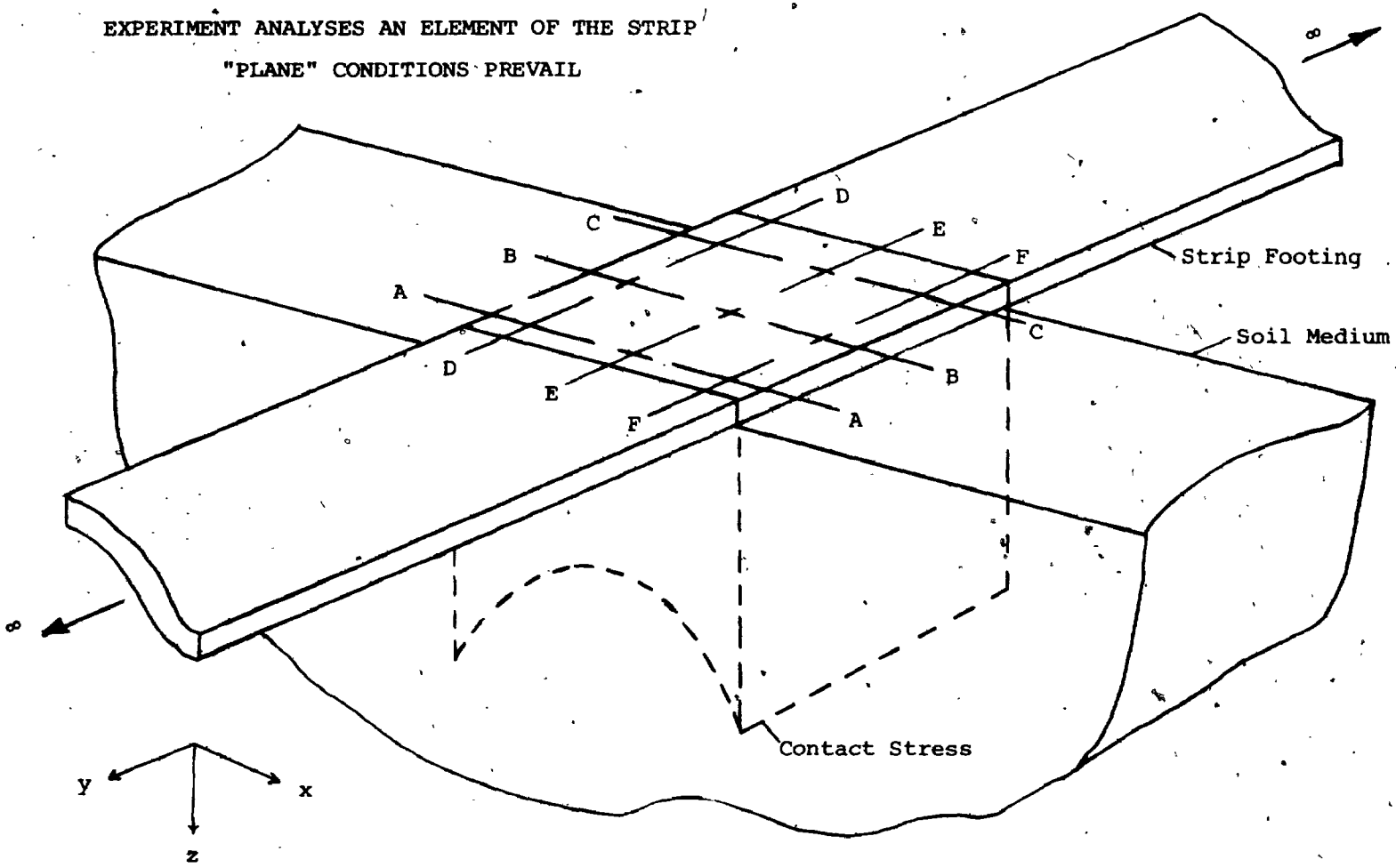

FIGURE 3.1

Idealization of Strip Footing

and on the influence of applied stress level on the contact stress distribution.

The experiments supplied observational data on a number of important aspects of the soil-foundation interaction problem. This chapter will describe in more detail the equipment used to carry out these tests. A summary of the properties of the soil material used in these tests will also be presented.

3.2 *Experimental Apparatus*

3.2.1 *Test Tank*

With the exception of a preliminary test, all tests were performed in a rigid test tank with inside dimensions of 1.52 m × 0.38 m × 1.07 m depth (Fig. 3.2 and Plate 1). The base ends were made of C15 × 33.9 channels, and the walls were 6.4 mm thick steel sheets. They were fastened at 0.15 m intervals with 9.53 mm hexagonal bolts. Since plane strain conditions imply no outward movement of the steel walls, additional stiffness was incorporated by two lengths of 3 × 3 × 3/8 inch angles welded to each side of the tank, and by removable 6 × 4 × 0.375 inch rectangular hollow steel sections. The inside of the test tank was lined with two sheets of polished No. 16 gauge stainless steel to reduce friction. The tank was waterproofed for the clay tests by using a flexible silicone sealant, and a layer of silicone grease was applied to the stainless steel walls. The total weight of the test flume was estimated at 620 kg, and when filled with sand or clay the weight increased to more than 1600 kg. This was considered to be sufficiently great to preclude the necessity for anchorage to the concrete floor.

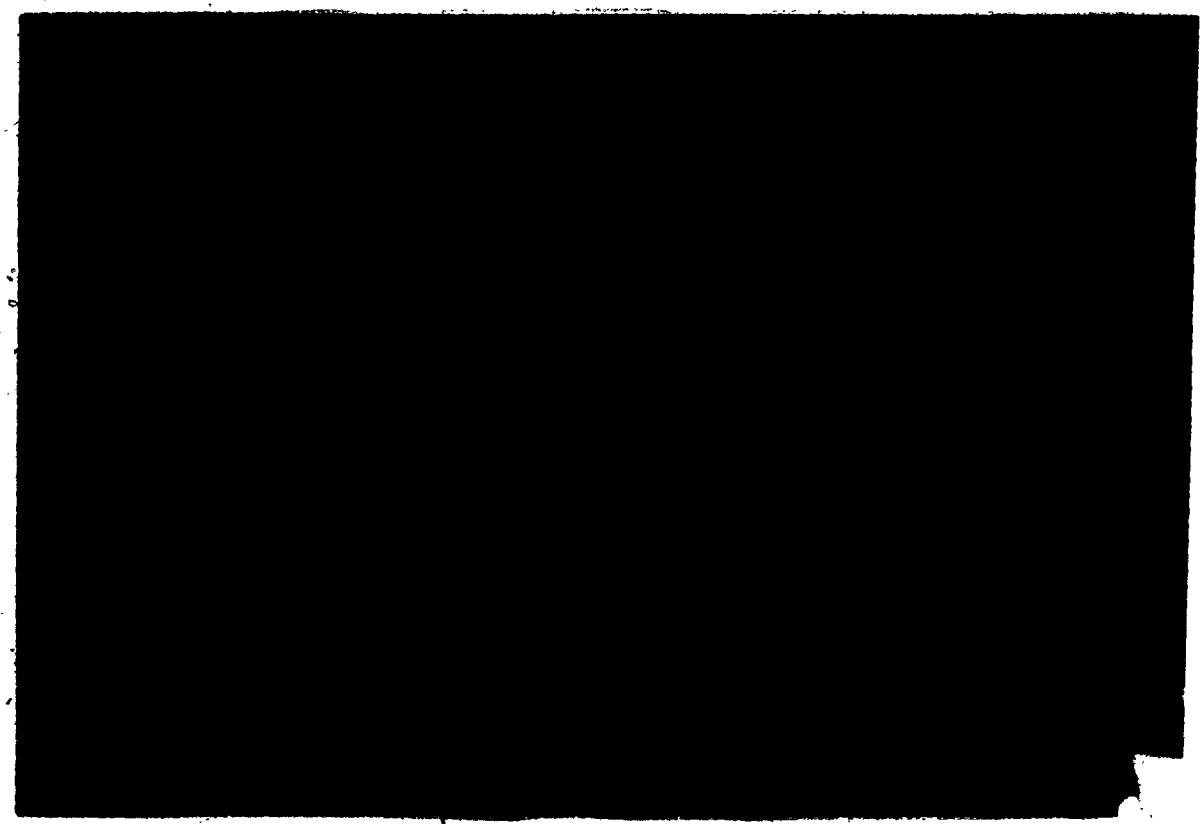

PLATE 1

Load Apparatus, Plane Strain Tank and Data Acquisition System in Temperature and Humidity Control Room

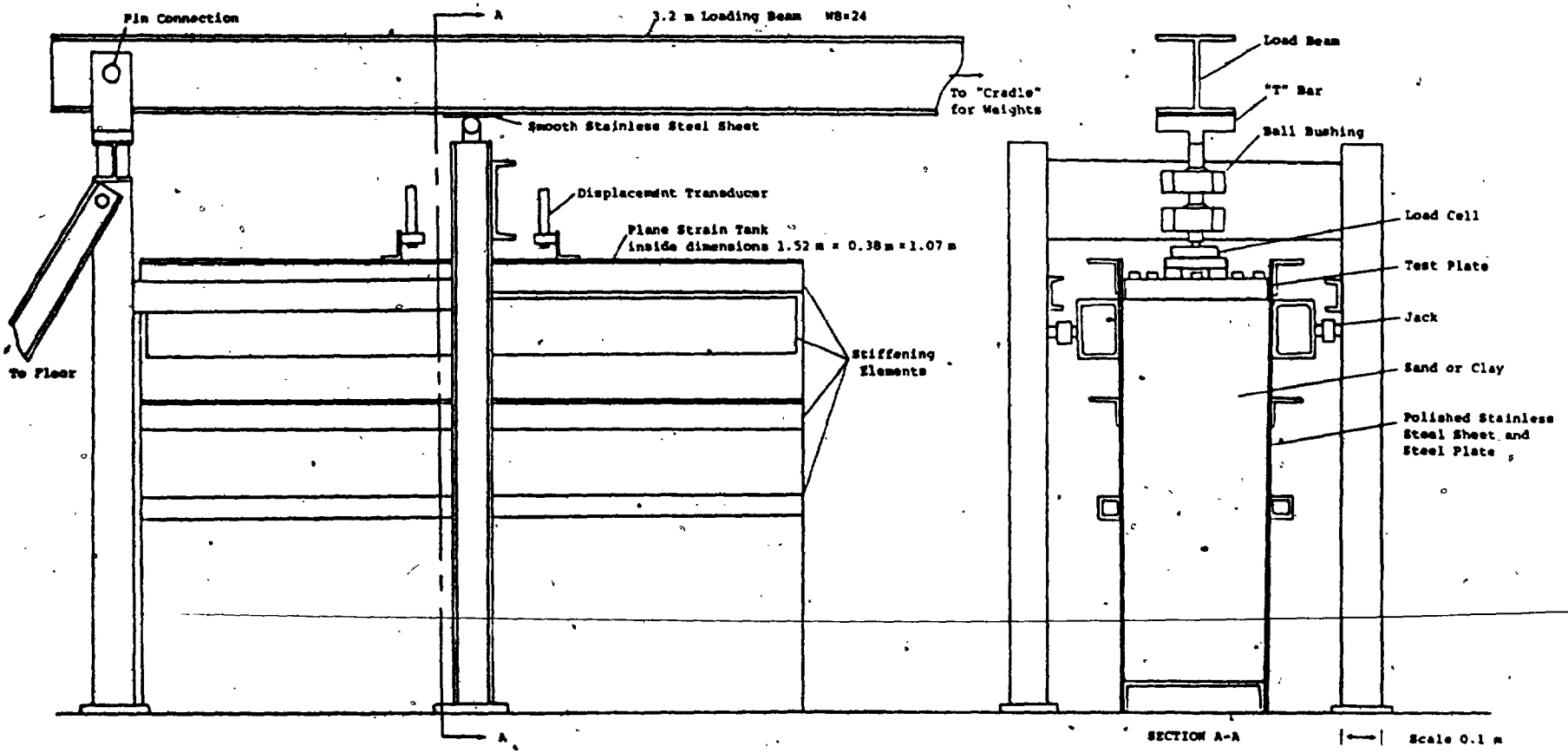

FIGURE 3.2
Diagram of Test Tank and Load Apparatus

3.2.2 *Steel Plate*

A 377 mm square steel plate 51 mm thick weighing 55 kg was used to model the "rigid" foundation. Before any machining was performed, the plate was stress relieved at the metallurgical laboratories of the Department of Energy, Mines and Resources, Ottawa, by heating to a temperature of about 550°C for several hours and then allowing to cool in the furnace. Holes were then drilled into the plate at sixteen locations to accommodate the 18.92 mm diameter pressure cells (Fig. 3.3 and Plates 2 and 3). These locations were chosen with a view to providing a centreline contact stress distribution at six different positions. The other ten pressure cell locations were chosen to check the assumption of equivalent contact stresses along the axis of the strip footing, and with a purpose of using the test plate for three-dimensional experiments, in which the device serves as a square plate.

A cross-section of the pressure transducer installation is shown in Figure 3.4. This method employs a threaded brass collar and neoprene o-ring to allow adjustment of the pressure cell elevation. The first experiments on sand showed the importance of ensuring that the measuring surface of the pressure cells are as flush as possible with the bottom of the plate.

The bottom surface of the test plate was ground by milling to a fine finish. This ensured that the plate surface was both plane and smooth. Since the contact pressures were theoretically shown to depend on the degree of adhesion at the interface (Hooper, 1974; Yamaguchi *et al.*, 1968), it was decided to model one of the limiting cases, that of a smooth foundation with no adhesion, and hence no shear stresses on the interface. Although in practice the foundation is probably rough,

SECTION A-A

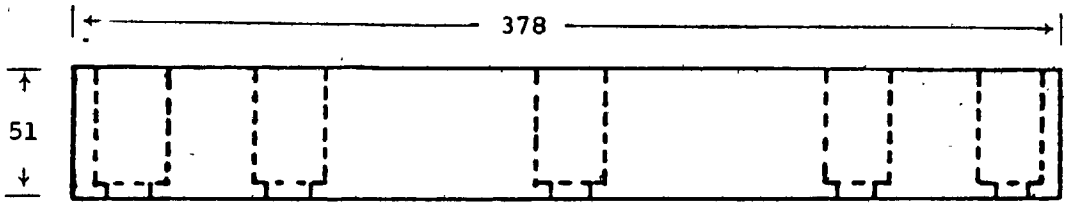

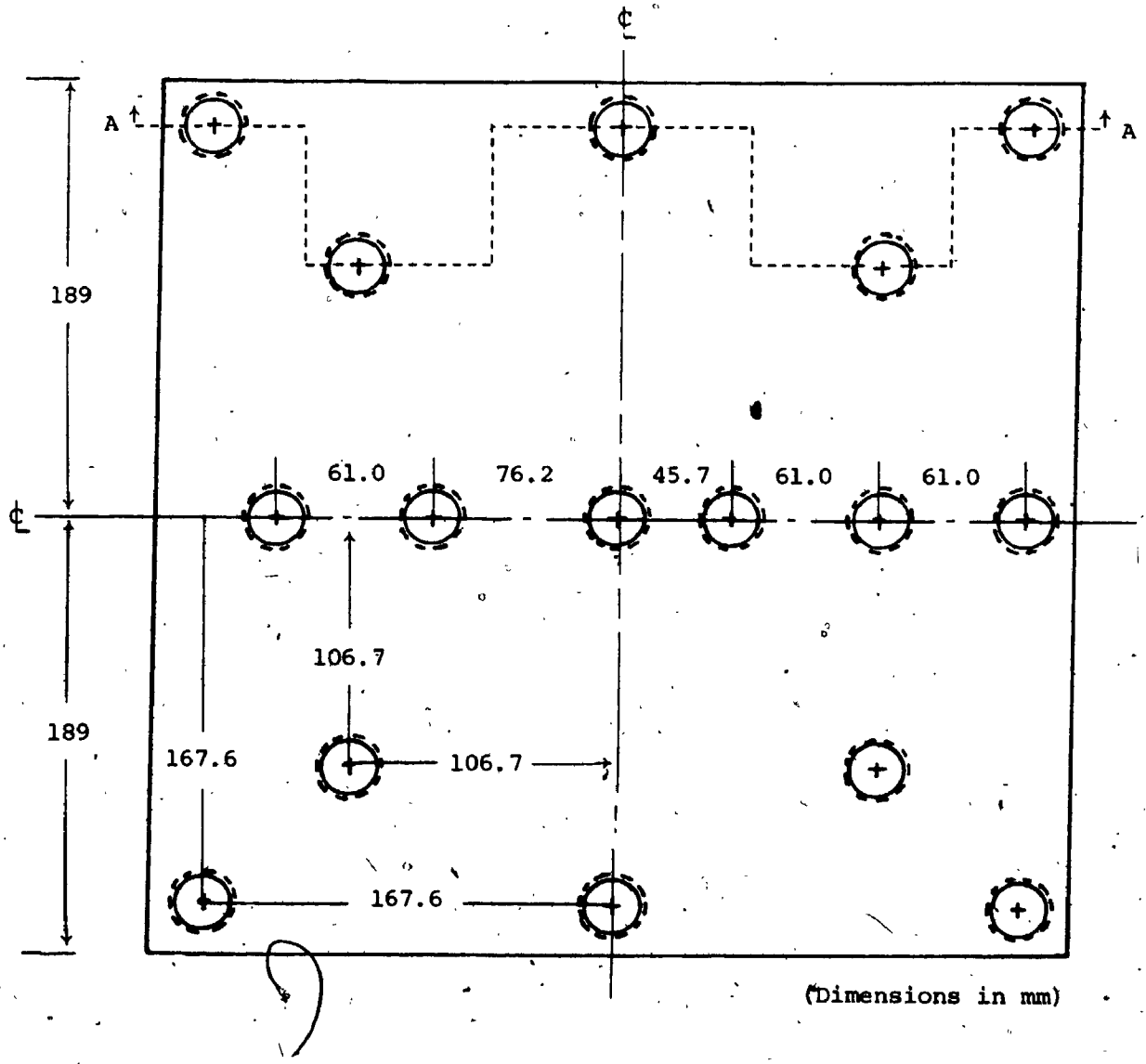

FIGURE 3.3

Diagram of Rigid Steel Test Plate

PLATE 2

Top View of Rigid Test Plate with 16 Pressure Transducers

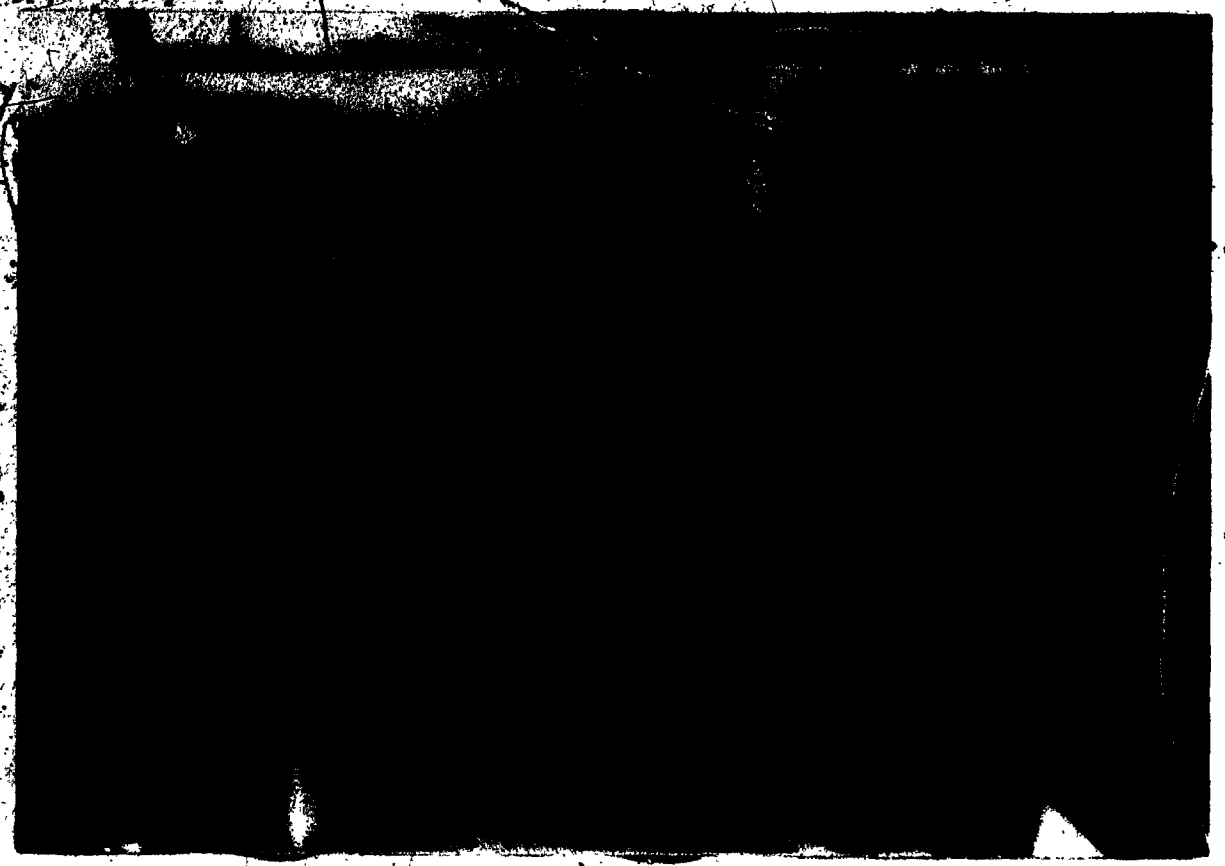

PLATE 3

Bottom View of Rigid Test Plate Showing Locations of Flush Diaphragms of Pressure Transducers

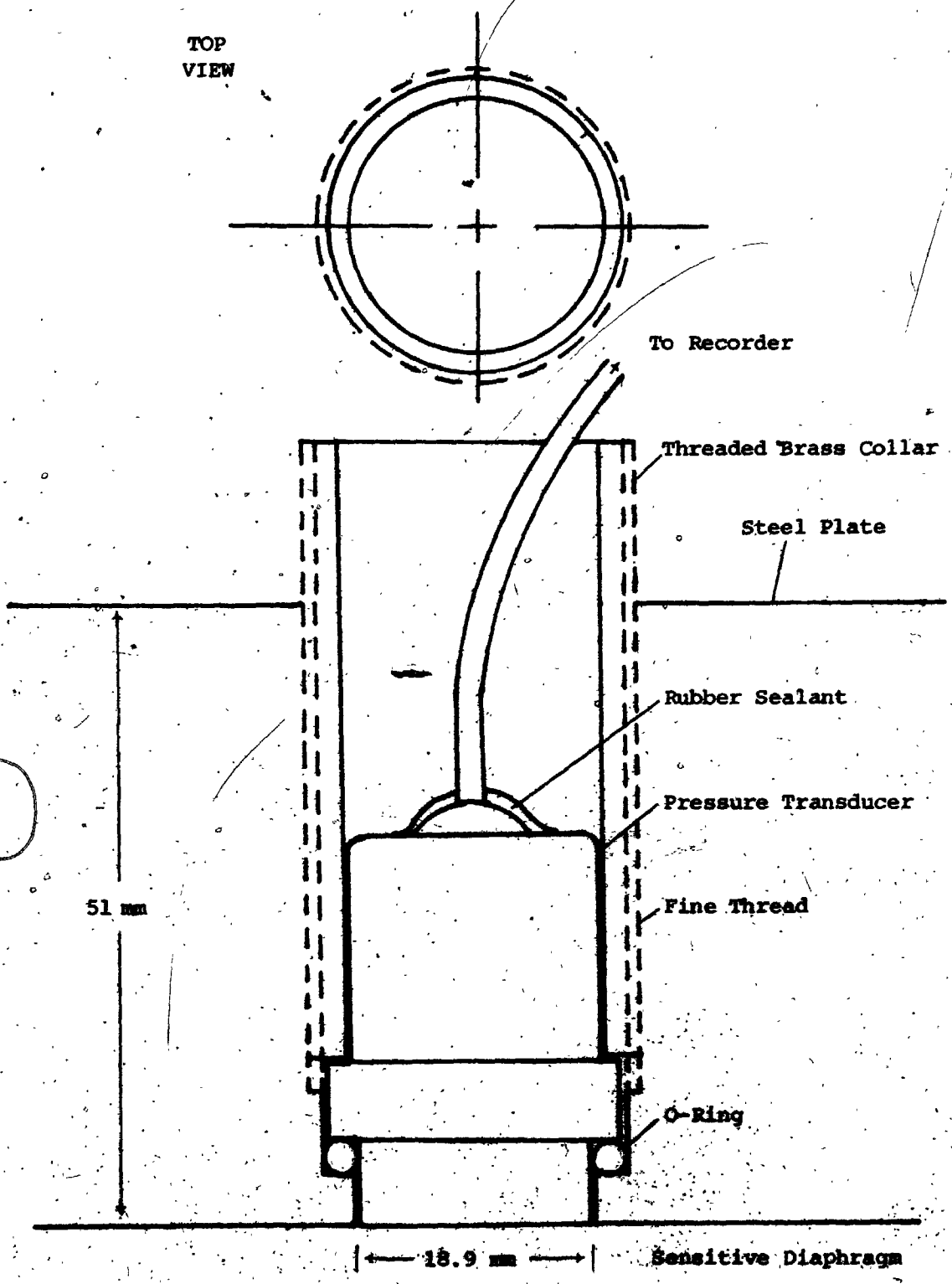

FIGURE 3.4

Diagram of Pressure Transducer Installed in Test Plate

complete adhesion is difficult to model and may not be the "true" condition. It may be fruitful to vary the interface condition in future tests.

Other machining on the test plate included threaded holes for eyebolts to aid in lifting the plate, and holes for anchoring the load cell measuring the total load applied.

In Appendix 4 an estimate was made of the amount of differential deflection of the plate when a uniform load was applied. Calculations were also made for the Relative Rigidity, K_r, by the methods of Borowicka (1938) and ACI (1966). The results indicate that the plate can be considered *rigid*.

3.2.3 *Pressure Transducers*

The pressure transducers used to measure the contact stress were produced by Kulite Semiconductor Products, New Jersey and were available through Willer Engineering Ltd., Toronto (model number IPT750-100). The pressure transducers had a working stress range of 0 to 100 psi (0 to 690 kPa) (see Plate 4 and Appendix 5). Burn (1963) discusses a similar (but not identical) pressure transducer for measuring pore water pressures. In answer to a reply to the manufacturer for more information, it was found that the transducer was a half-bridge piezo-resistive device having two active strain gauge elements bonded directly to the sensitive stainless steel diaphragm. Although the surface diameter of the active face was 18.92 mm, the active area was only 7.62 mm diameter and 0.213 mm thick. From Timoshenko (1940), the volume of the displaced diaphragm can be calculated, as given in Appendix 6. The transducer is very accurate, with the error of combined non-linearity, hysteresis and

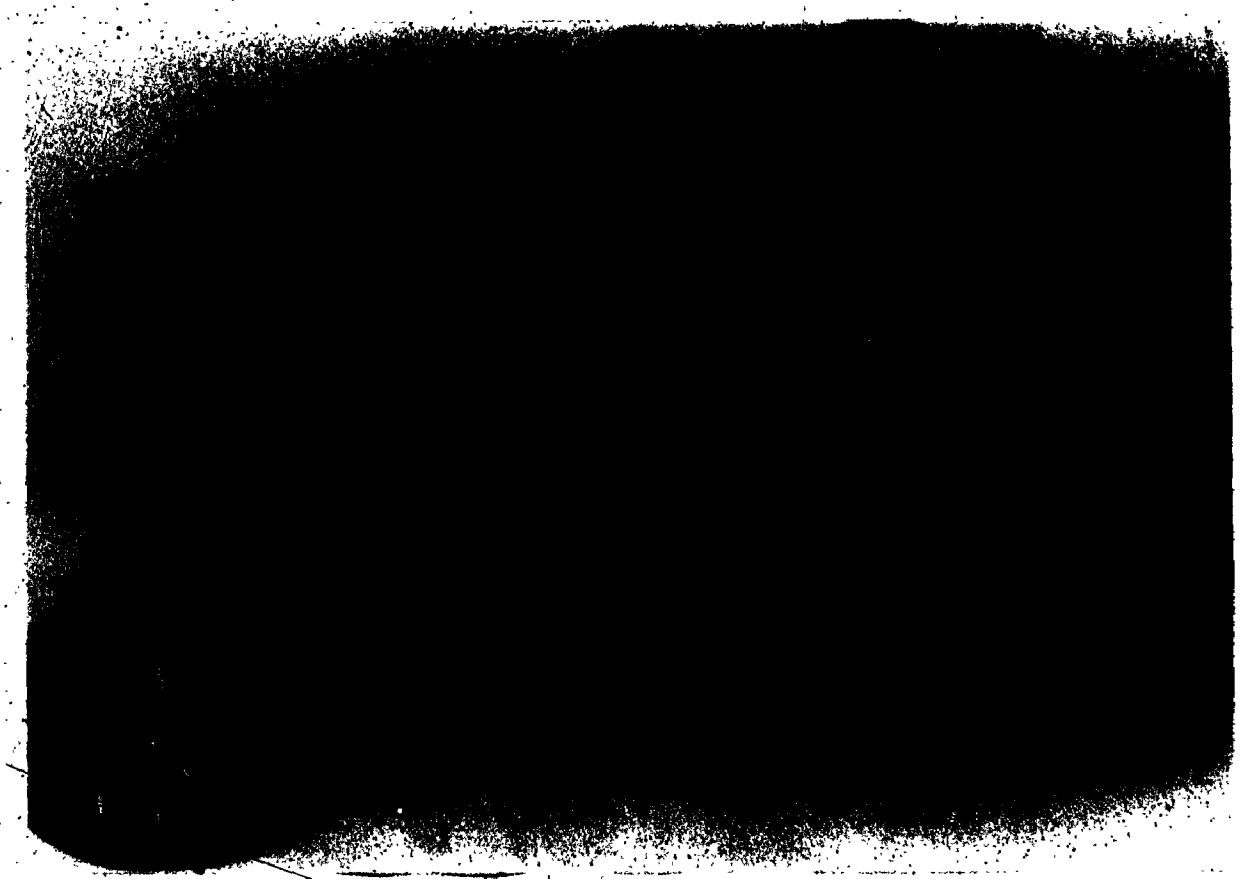

PLATE 4

Pressure Transducers

repeatability given as a maximum of ± 0.5 percent of the full-scale output.

As explained in the literature review of pressure transducer performance, the ± 0.5 percent implies that the accuracy at all values is ± 0.5 psi (+ 3.5 kPa). To overcome this problem, the cells were calibrated over a narrower range of pressures, i.e. from 0 to 50 psi (345 kPa) and 0 to 10 psi (69 kPa) (see Appendix 5). Within these ranges it is possible to reduce the error given as a function of full-scale output. This is illustrated in Figure 3.5.

Although the pressure transducers are temperature-compensated in the range of 27°C to 80°C, the error resulting from changes in ambient room temperature on the rest of the measuring system was reduced by performing all the experiments in a humidity- and temperature-controlled room. This room had plan dimensions of 6.9 m × 4.5 m, and control was provided by two humidifiers and two de-humidifiers, with several fans to circulate the air. Space-heaters were available, but it was found that sealing the room from the rest of the laboratories resulted in a constant temperature of 25°C ± 1°C. The humidity was monitored automatically on two chart recorders. The absolute value of the relative humidity measured by the recorders was kept at approximately 60 percent, with the maximum variation during testing less than ± 5 percent.

3.2.4 *Method of Load Application*

Since the load was being applied over a period of several weeks in the main experiment on clay, it was imperative that the load remained constant with time. Then, if there were any observable changes in the contact stresses, they could be attributed to the soil and not to the

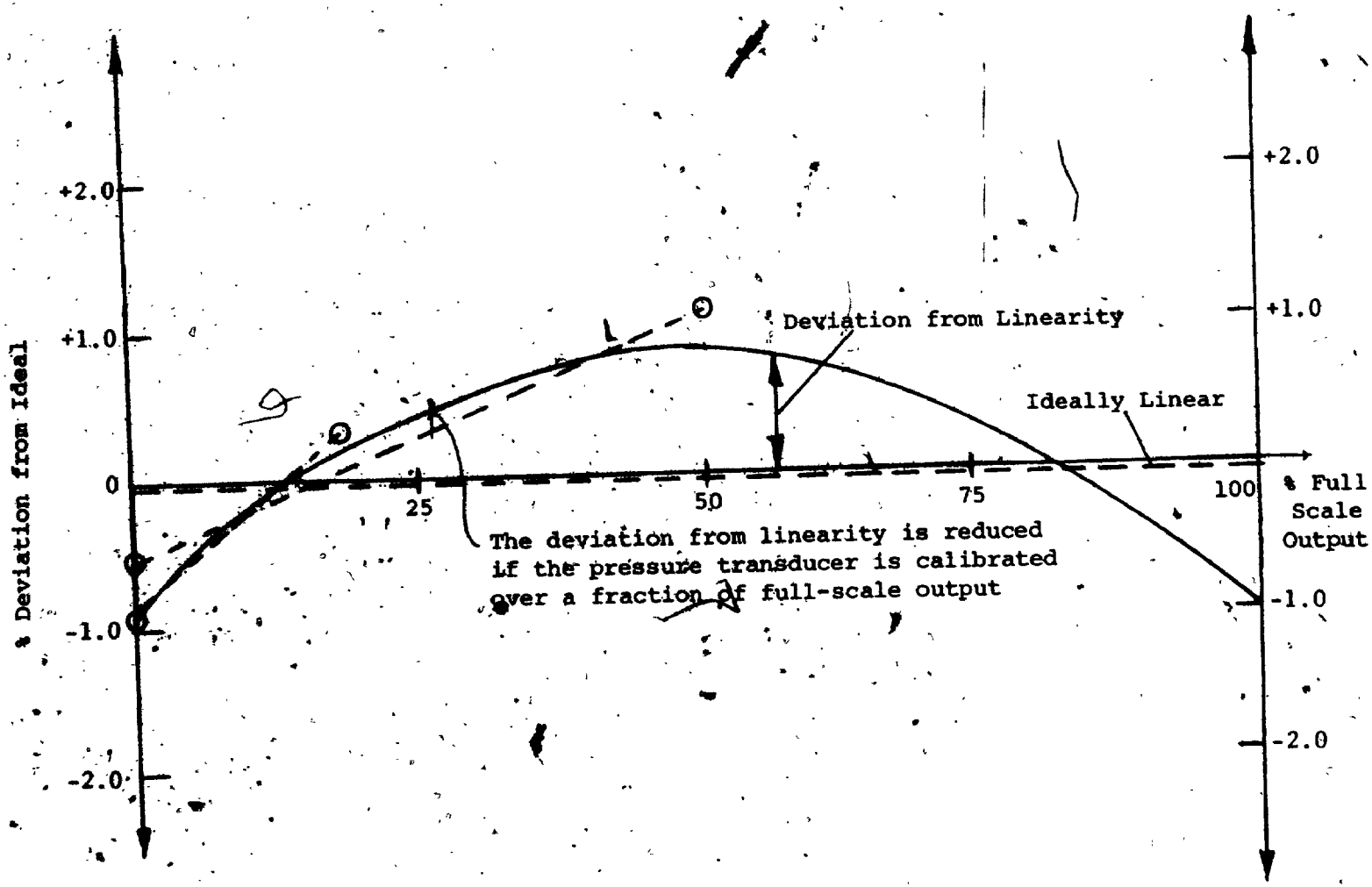

FIGURE 3.5

Characteristic Pressure Transducer "Footprint"
(after Davidson, 1975)

applied load. The loading apparatus is shown in Plate 1, and consists of a cantilever beam with a pin connection at one end and a "cradle" for weights at the free end. By placing the test plate and tank in between, a leverage action can be obtained. The magnitude of the applied load can be varied by changing the weights in the "cradle". This method does not have the ease of varying the applied load as in some techniques (such as hydraulic jacks), but it does possess the significant advantage of ensuring that the static load remains constant with time.

The load is transferred to a "T" bar as shown in Figure 3.2. The top of the bar is removable and free to be aligned at right angles to the beam. As the test plate settles into the soil, the loading beam "rolls" over the round top portion of the "T" bar and the load is still transferred vertically to the plate. The "T" bar is kept vertically aligned throughout the test by two Thompson precision series A ball bushings enclosed in two pillow blocks. These pillow blocks are in turn mounted on a C9 x 13.4 channel positioned over the plate and tank by two rigid columns anchored firmly to the floor and to the end loading frame. The precision ball bushings allow vertical movement and rotation of the "T" bar but limit the horizontal deflections. To verify this, the channel deflection was monitored, and the maximum horizontal deflection measured was less than 0.001 inch.

The "T" bar was attached rigidly to a 10,000-lb (44480 kN) capacity load cell (model number 1210-AJ) by a threaded connection. This connection was designed to minimize both the tilting of the test plate and horizontal deflection.

The load cell specifications and calibration results are given in Appendix 7. The purpose of the load cell was to measure the load

increment applied directly to the rigid test plate by the centilever beam. On the basis of simple statics the applied load was calculated from the beam and weights and compared with the results of the load cell. The agreement was usually within one percent, indicating that the amount of load lost due to friction in the ball bushings was negligible.

The entire loading apparatus was designed to ensure that a constant static load was applied vertically to the centre of the test plate, allowing the plate to settle uniformly only in the vertical direction.

3.2.5 *Data Acquisition*

The system-measuring and recording the experimental data had to be capable of reading 22 pressure transducers, 16 positioned in the test plate and 6 in the pore-water pressure chambers. In addition, the 10,000-pound (44480 kN) capacity load cell and 5 linear variable displacement transducers had to be monitored. Temperature and humidity in the room was measured separately with an automatic chart recorder.

The data acquisition was accomplished with a multi-channel digital strain indicator and recorder produced by B & F Instruments and supplied by Intertechnology Ltd., Toronto (see Plate 5). The type was the B & F Model SY-161 Mini-System (hereafter referred to as "B & F") with up to 40 channels available for recording. With the four-arm strain gauges of the pressure transducers, the voltage excitation required was 7.50 volts, which produces a nominal 100 mV output full scale. The supply voltage of each channel could be varied if desired.

Automatic recording and monitoring was possible with the addition of a "timer" (constructed by the Carleton University Electronics Laboratories) capable of activating the starting switch at prescribed equal

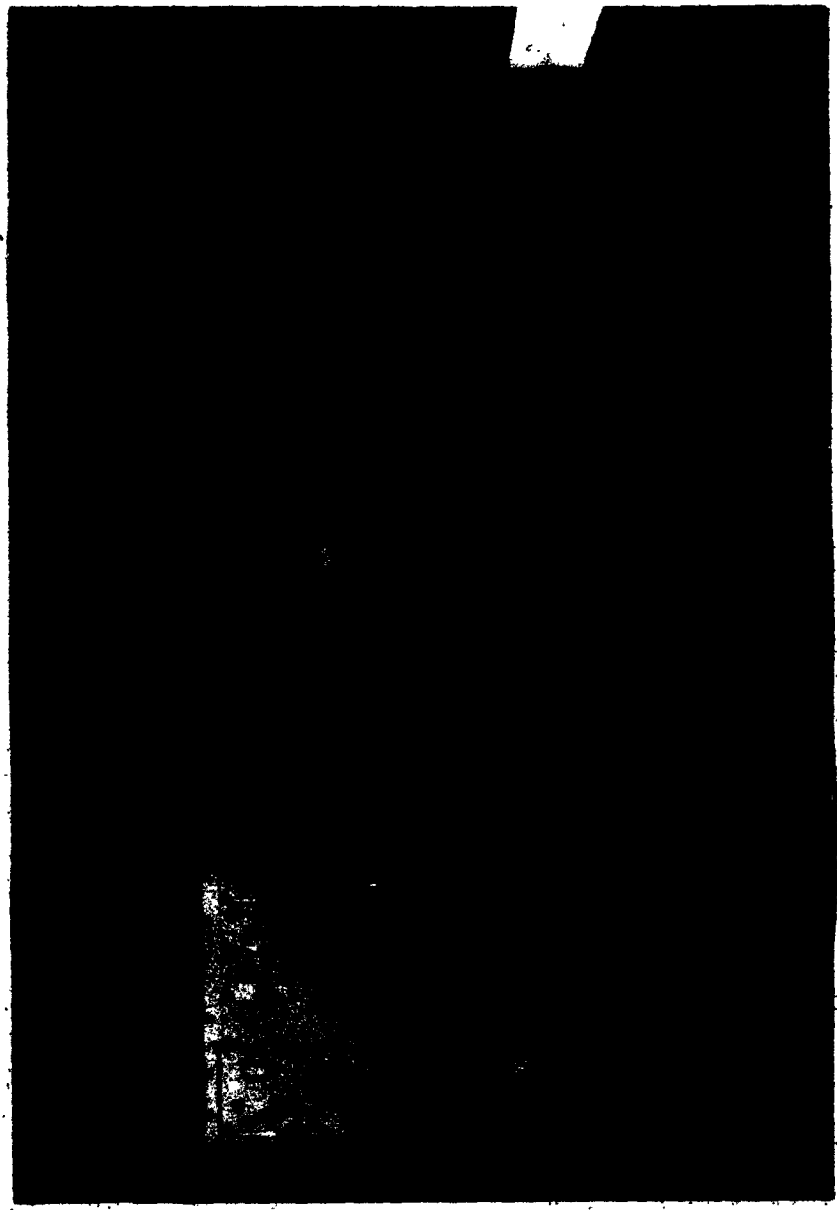

PLATE 5

"B & F" 40-Channel Data Acquisition
System with Timer

intervals of 1, 2, 5, 10, 30 or 60 minutes.

The "B & F" data acquisition system supplied the excitation voltage to the pressure transducers and read the output voltages. The output voltages were measured, displayed and recorded on tape. Each pressure cell has a "zero" shift or measurable voltage output even under conditions of zero applied pressure. The "B & F" recorder allows the "zero" reading to be shifted to any arbitrary value by the use of a balance control on each channel. For each transducer the balance control was used to set the initial "no pressure" voltage display to approximately zero. Any increase in the applied pressure would result in an increase in the output voltage. This change could then be related to the actual pressure increase by the calibration constant of the transducer.

To obtain the relationship between change in voltage and change in "B & F" microstrain, a sensitive digital voltmeter was applied across the output of each channel. Adjusting the balance control increased both the displayed micro-strain and the voltage on the digital voltmeter. By relating an increment in "B & F" microstrain to an increment in voltage measured by the digital voltmeter, and then relating the voltage increment to an increment in pressure by a calibration constant, the "B & F" could be used to accurately record the increments in applied pressure of the transducer.

The accuracy of the "B & F" was given by the manufacturers as ± 1 micro-strain digit (out of ± 2000 units); however, the total system accuracy was much less because the errors of each system are additive. By taking into account the drift due to temperature, the variation in applied input voltage, the creep of the transducer, the error in establishing the calibration constants and the inherent error of the

pressure transducers, the confidence in the output of the measuring system is considerably reduced. The magnitude of many of these errors is unknown, but an estimate would be ± 0.2 to ± 0.3 psi (± 1 to ± 2 kPa) for the tests on clay where the applied pressures are less than 50 kPa. An estimate of this kind must be made if any conclusions are to be drawn from the results of the experiments.

The first ten channels of the "B & F" system were modified to measure the output of the displacement transducers (DCDT's). At first the two types of transducers were incompatible because the full-scale output of the pressure transducers was about ± 100 mV, compared to ± 5.0 volts for the DCDT's. The electronics workshop of Carleton University was able to make the full-scale output on the "B & F" (± 2000 micro-strain) equivalent to ± 1 volt on the ×5 scale for channels 0 to 9. This implied an increment in strain of 2000 units was approximately equivalent to 3.0 inches (75 mm). By reducing the span to ×2 or ×1, 2000 units could be made to represent 1.2 inches or 0.6 inches, respectively. For most experiments, the ×2 scale was used, giving a range of ± 1.2 inches (± 30.5 mm). The exact relationship between the digital increment and displacement depended on the individual calibration constant of the transducer.

Modifications were required on the "B & F" system because the amplifier within the unit had a fixed gain of 666. The maximum reading of the strain gauge indicator was 2.000 V. Thus an input of about 3 mV on the ×1 scale range would give 3 × 666 = 2000 mV output reading on the "B & F". On the ×5 range, the minimum input required to saturate the output reading was only 15 mV. Since the pressure transducers had a full-scale output of 100 mV for approximately 100 psi (690 kPa), some

form of attenuator had to be introduced to keep the strain indicator from going over scale.

There were three possible alternatives to the use of the existing "B & F" system. An attenuator could have been built for each pressure transducer such that the output signal was modified before it entered the "B & F" input conditioner. This method had the advantage that no modifications were necessary to the "B & F" apparatus, but on the advice from the engineering electronics workshop at Carleton University, it was decided to build a single attenuator after the amplifier stage in the "B & F" strain indicator. This method was considered to be more accurate because a larger signal was being modified. The third alternative would have been to reduce the excitation voltage to the pressure transducer and thus reduce the output signal entering the "B & F" unit. No modifications would have been necessary, but the linearity and precision of the pressure transducer output may have been reduced.

3.2.6 *Displacement Transducers*

The duration of the main test necessitated automatic monitoring of the displacement of the test plate in addition to the contact pressures. Six transducers capable of measuring displacement (DCDT's) were purchased from Hewlett Packard Ltd., Ottawa. A DCDT consists of a core that is free to move within the bore of a coil assembly. The position of the core determines the voltage output. In principle, the coil assembly contains an oscillator that converts DC input power into AC. This AC power excites the primary coil windings. As the core is displaced, the voltage induced in the secondary windings changes proportionately. A demodulator and filter then converts the AC output back to

DC, as required by the "B & F" system.

The manufacturer specifies that there is no hysteresis and the deviation from linearity is less than 0.5 percent of full-scale output. The DCDT's purchased had a stroke range of ± 3.0 inches (± 75 mm) and required a 6.0 volt DC input. Mounting blocks were designed to hold the transducers rigidly in the vertical position. More detailed specifications and calibration results are given in Appendix 8.

3.2.7 *Pore Water Pressure Apparatus*

The pore water pressure sensor in the clay consists of a piezometer composed of a No. 16 gauge × 38.1 m stainless steel hypodermic needle modified to prevent the clay material from blocking the opening. A No. 200 stainless steel wire mesh was placed on a sheet of paper, followed by a smaller piece of No. 202 filter paper produced by Reeve Angel. The needle tip was placed on top and "5-minute" epoxy glue was applied around the opening. Upon drying, soaking the needle in water would remove the outer sheet of paper, exposing an opening approximately 3 mm × 6 mm (see Fig. 3.6).

The other end of the needle was epoxied inside $\frac{1}{8}$-inch (3.18 mm) OD copper tubing that varied in length from 1 to 2 metres, depending on the position of the piezometer in the clay layer. The copper tubing led to a system of valves and chambers enclosing several pressure transducers (Figs. 3.7 and 3.8).

There were two separate systems of measuring the pore water pressure. One system measured the pore water pressures at five locations directly below the centre of the plate, and the other system measured the pore water pressures at five locations beneath one of the edges (see

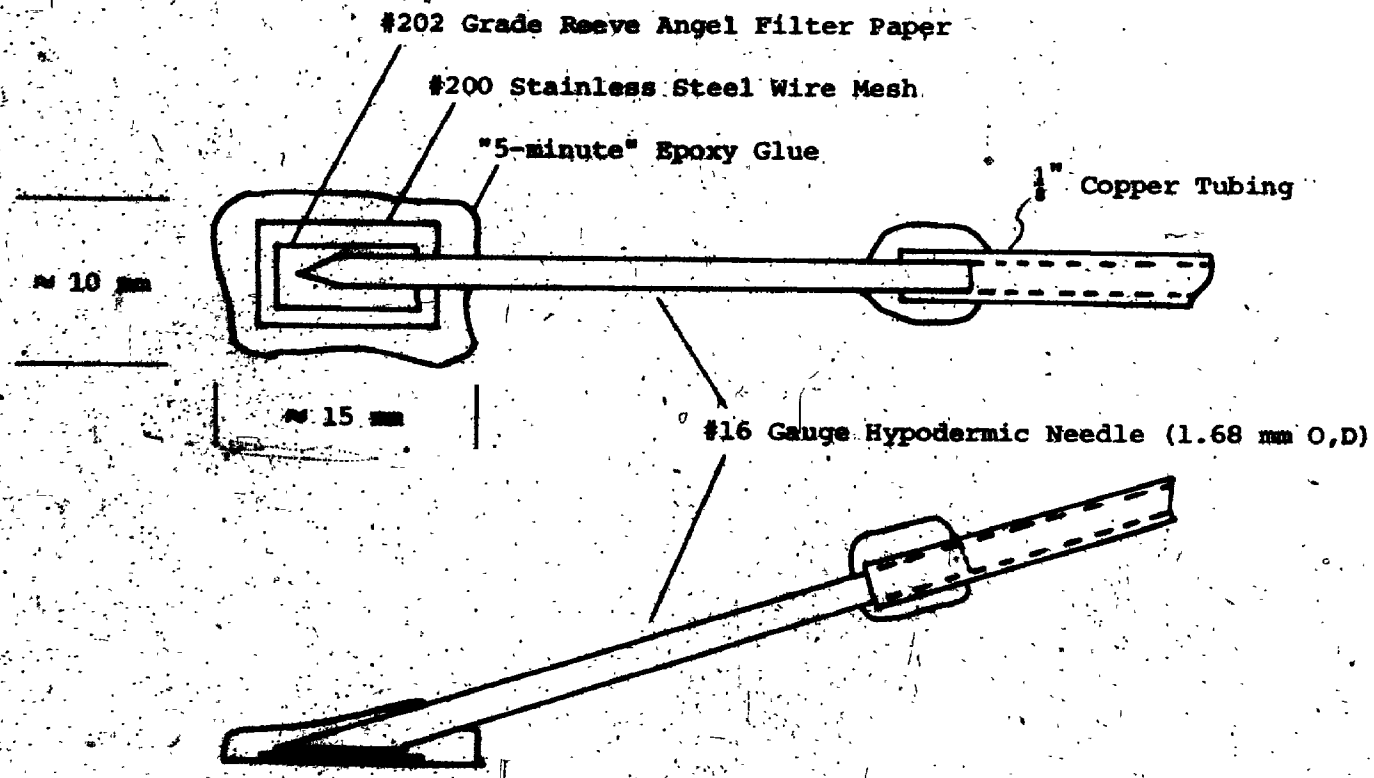

FIGURE 3.6
Piezometer

2

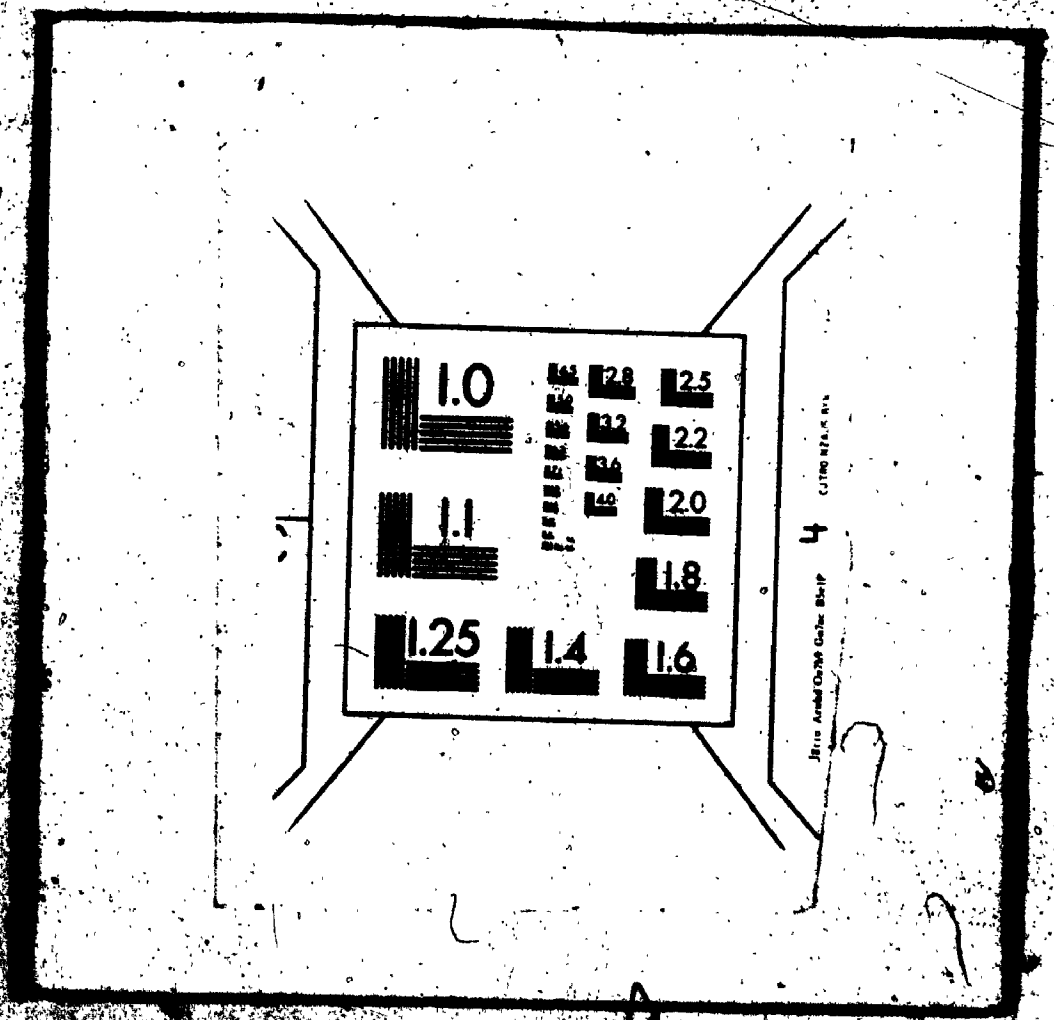

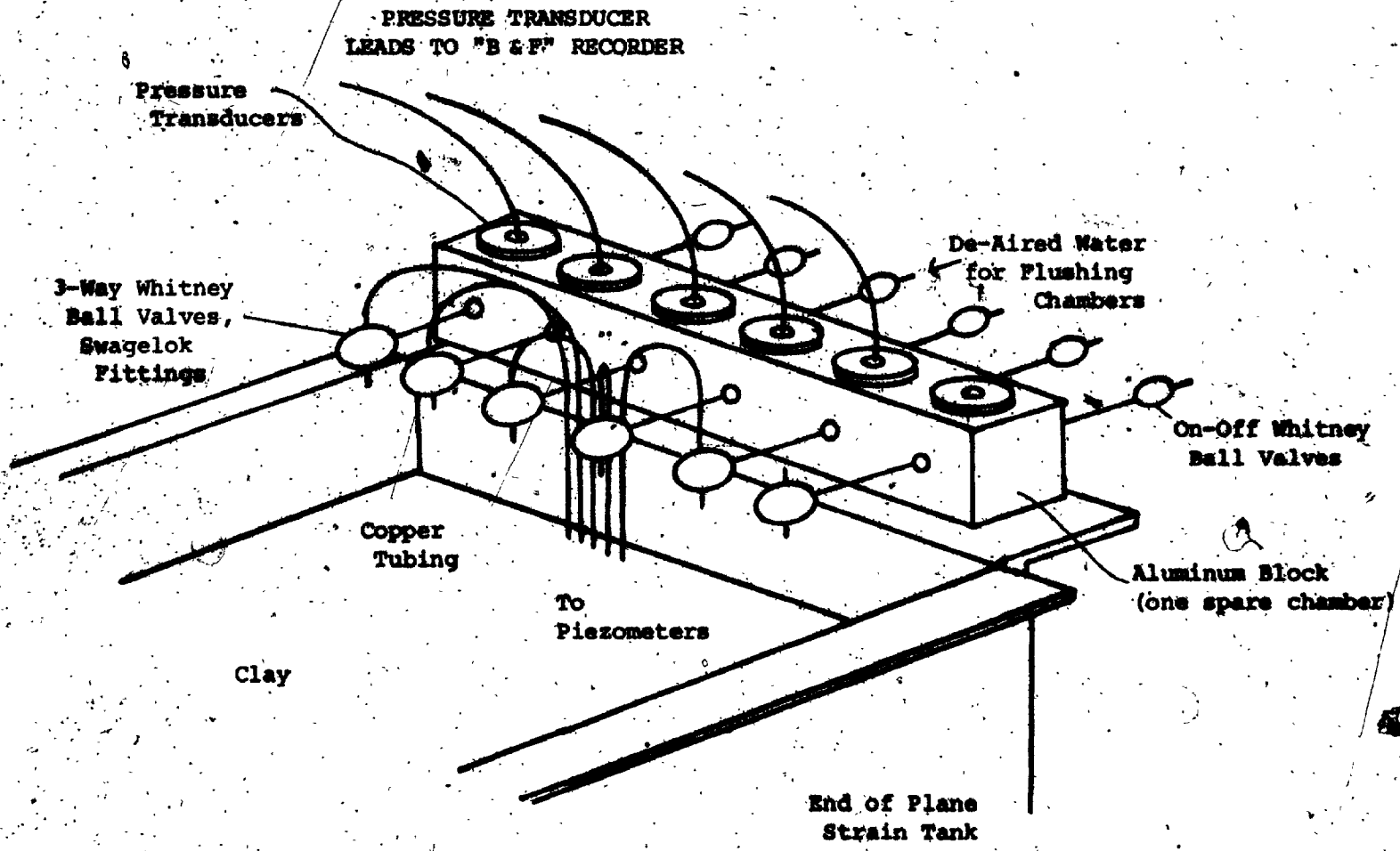

FIGURE 3.7

Pore Water Pressure Measuring System — 6-Cell Chamber

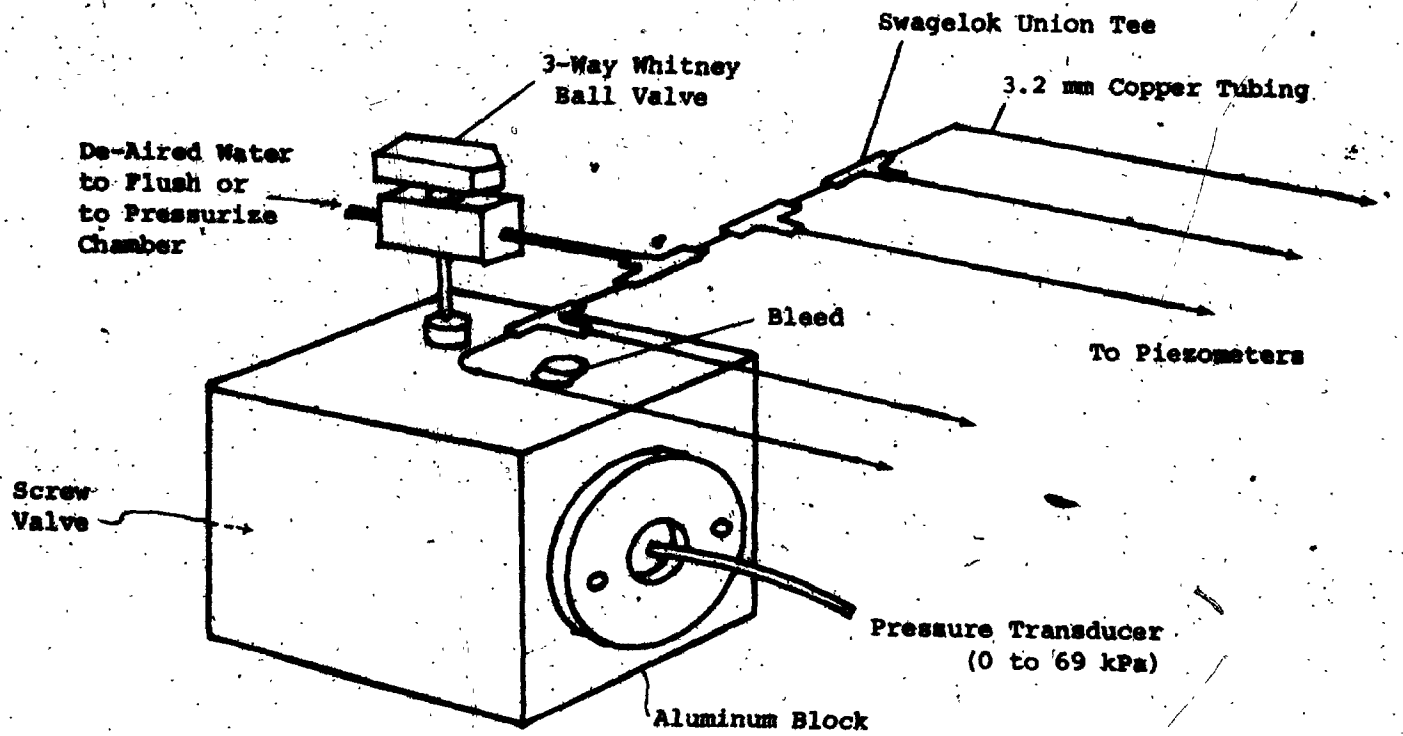

FIGURE 3.8

Pore Water Pressure Measuring System — 1-Cell Chamber
(modelled after Burn, 1963)

Piezometer Number	Depth Below Plate (mm)	z/b
1	90	0.47
2	215	1.13
3	355	1.87
4	570	3.00
5	820	4.30
6	90	0.47
7	215	1.13
8	355	1.87
9	570	3.00
10	720	3.80

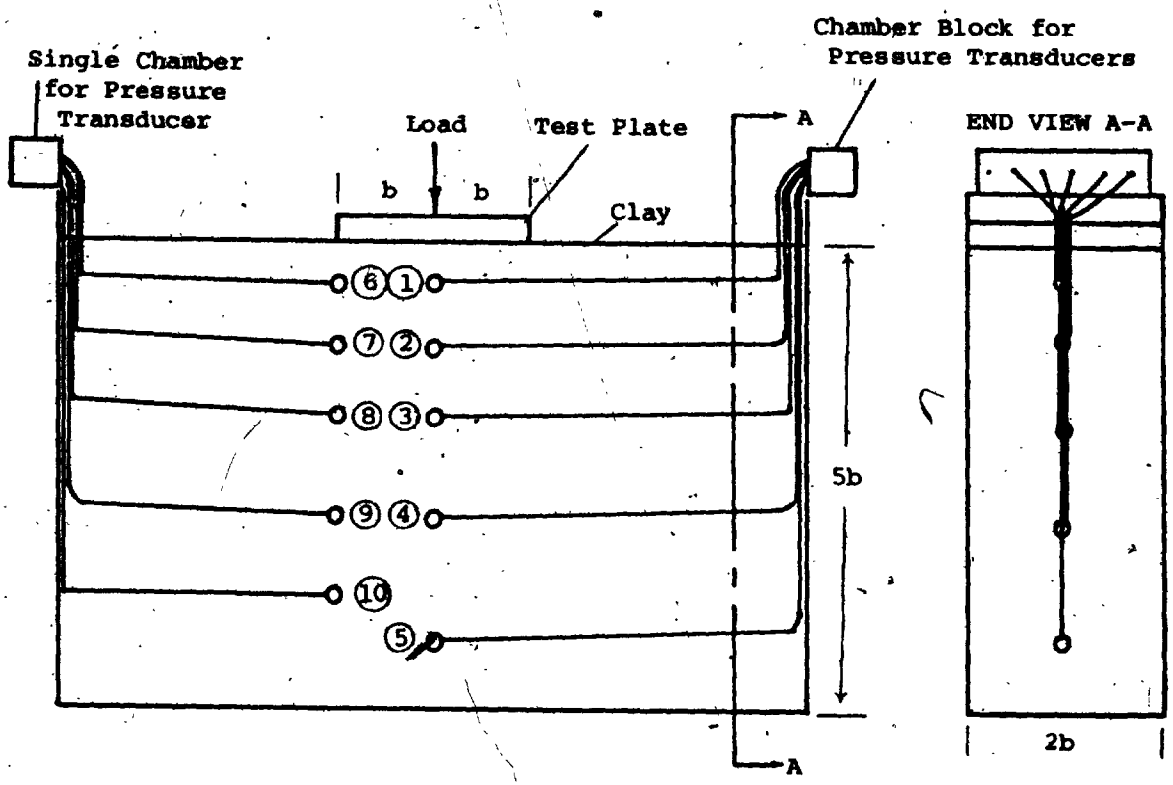

FIGURE 3.9

Pore Pressure Lines Installed in Tank

Fig. 3.9). The first method requires a separate pressure transducer and chamber for each piezometer but the second method uses a single pressure transducer for all five piezometers. In either case, the apparatus has the advantage of being compact and stiff, such that the increase in pore water pressure at the piezometer will be transferred to the pressure transducer with a minimum loss due to volume increases in the lines. Another advantage of this method is the fast response rate of the system to the increase in the pore water pressure at the piezometer, provided the lines are fully saturated. The use of pressure transducers to measure pore water pressures in the laboratory has become common practice (see Burn, 1963). One of the disadvantages of this closed system is that the lines cannot be de-aired. The performance of the piezometer will be discussed in Chapter 4.

When placing the piezometers in the test tank, care was taken to ensure that the lines were saturated with water. De-aired water was prepared by applying a vacuum to distilled water, and this water was then allowed to flow freely through the copper lines before placement. After installing the piezometer at the desired elevation in the clay layer, the three-way valve connecting the line to the pressure cell chamber was closed. The apparatus permits flushing of the pressure cell chamber but the line connecting the piezometer to the chamber cannot be de-aired after installation.

These two pore pressure systems have been designed with the view to measuring the pore water pressure increase in a *saturated* clay due to an externally applied stress. The pore water pressure in the piezometer is assumed to be equal to the pore water pressure in the soil. The degree of saturation of the clay was estimated to be an average of 98

percent, recognizing the fact that there is a finite measurable amount of air in the soil. This is important because it has been shown that, with time, air will migrate to the largest cavity available (Williams, 1967). The air in the soil may be small enough to justify the assumption of a saturated material, but the measured response of the soil to the external stress may disagree with actual pore pressure increase. These possible errors will be discussed in Chapter 4.

3.3 *Cohesive Soil*

3.3.1 *General Characteristics*

The soil material used in the main test was a remolded "Leda" clay obtained from a pit located near Arnprior, Ontario and owned by Dochart Brick and Tile Company, Ltd. Information on the geology of the clay was available from Guillet (1967). Here it was explained that the clay sediments were deposited on the bed of the Champlain Sea, making it a stratified marine clay interbedded with silt and sand lenses. The properties of sensitive marine clay from the St. Lawrence lowlands has been studied extensively by many authors (see, for example, Eden and Crawford, 1957; Crawford, 1961; Mitchell, 1970; Bozozuk and Leonards, 1972) but these results are not directly applicable to the current investigation. The clay used in the experiments was remolded and extruded at a moisture content lower than occurring in the field. The properties of the material were more representative of a normally consolidated clay.

Approximately 1600 kg of clay material was obtained from a section designated by Guillet (1967) as the "Big Bank" located in the west end of the pit at an elevation of about 5 m below ground surface. The

description of the clay was similar to that of the "Little Bank", another section of the pit whose soil was described as "olive-grey, drying buff; uniform, plastic, stoneless; stratified in 2-inch layers; clay grading downwards to fine sand; black organic and rusty stains on joint planes and cracks." Mineral analyses by Guillet (1967) showed that the predominant clay mineral was illite, with a moderate amount of montmorillonite and a trace of chlorite. A more complete chemical and mineral composition is given in Appendix 9 for a typical section of the test pit where the samples were obtained.

3.3.2 *Atterberg Limits*

Liquid and plastic limits were determined by the ASTM recommended procedure designated D423-66 and D424-69 of the Annual Book of ASTM standards. On the basis of five liquid limit and four plastic limit tests, the average liquid limit was 48 percent and the average plastic limit was 24 percent. The results are plotted in Figure 3.10 showing the relationship between the plasticity index and liquid limit. The clay falls into the category of an "inorganic clay of medium plasticity", under the Unified Soil Classification System (see Wu, 1976).

3.3.3 *Specific Gravity*

A total of six tests were performed on the "Arnprior" clay by the method outlined in ASTM standard D854-58. The range in specific gravity was from 2.79 to 2.84, with the average being 2.81.

3.3.4 *Particle Size Distribution*

The particle size distribution was determined in three separate tests, one by the author and two by Farbar (1977). The method used was

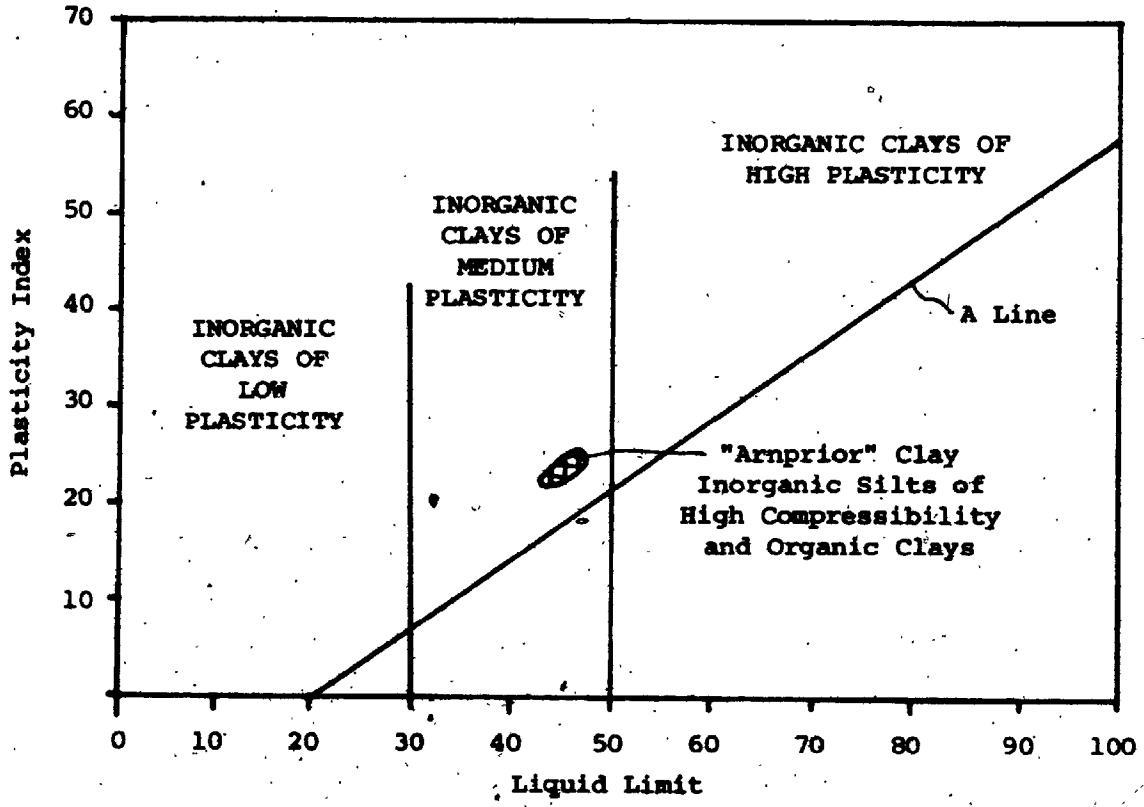

A Line Casagrande $PI = 0.73(W_{LL}-20)$

FIGURE 3.10

Plasticity Chart
(after A. Casagrande, see Akroyd, 1957)

outlined by Bowles (1970), with the dispersing agent being $NaPO_3$. In the hydrometer test only the material passing the No. 200 sieve was used, and the results are presented in Figure 3.11. The percentage silt ranged from 25 to 35 percent, and the amount of colloidal particles (less than 0.002 mm) varied from 55 to 60 percent. This value is probably higher than the actual value because the soil has been dried, pulverized and sieved before performing the particle size distribution test.

3.3.5 *Compaction and Placement*

The relationship between the dry density of the soil and its water content is presented in Figure 3.12. The standard compaction test was used for moisture contents less than 35 percent (see, for example, Bowles, 1970). The maximum dry density varies with the amount of compaction effort used in the test, but appears to occur at a moisture content of 23 to 25 percent. This can be compared with a chart given by Ingles (1974) relating the optimum moisture content with the liquid and plastic limits. For a given plastic limit of 24 percent and liquid limit of 48 percent, the chart gives an optimum moisture content of 19 percent from the standard compaction test. This chart was recommended only for a first estimate of the optimum moisture content and has been averaged from a large number of different types of soils. What is important is that the optimum moisture content appears to be less than 25 percent. At these low moisture contents, the degree of saturation is less than desired for the experiment, but even at relatively high moisture contents of 35 percent, the degree of saturation will be less than 95 percent.

The dry density obtained from the samples extruded through the pug mill is also shown in Figure 3.12. A higher degree of saturation is

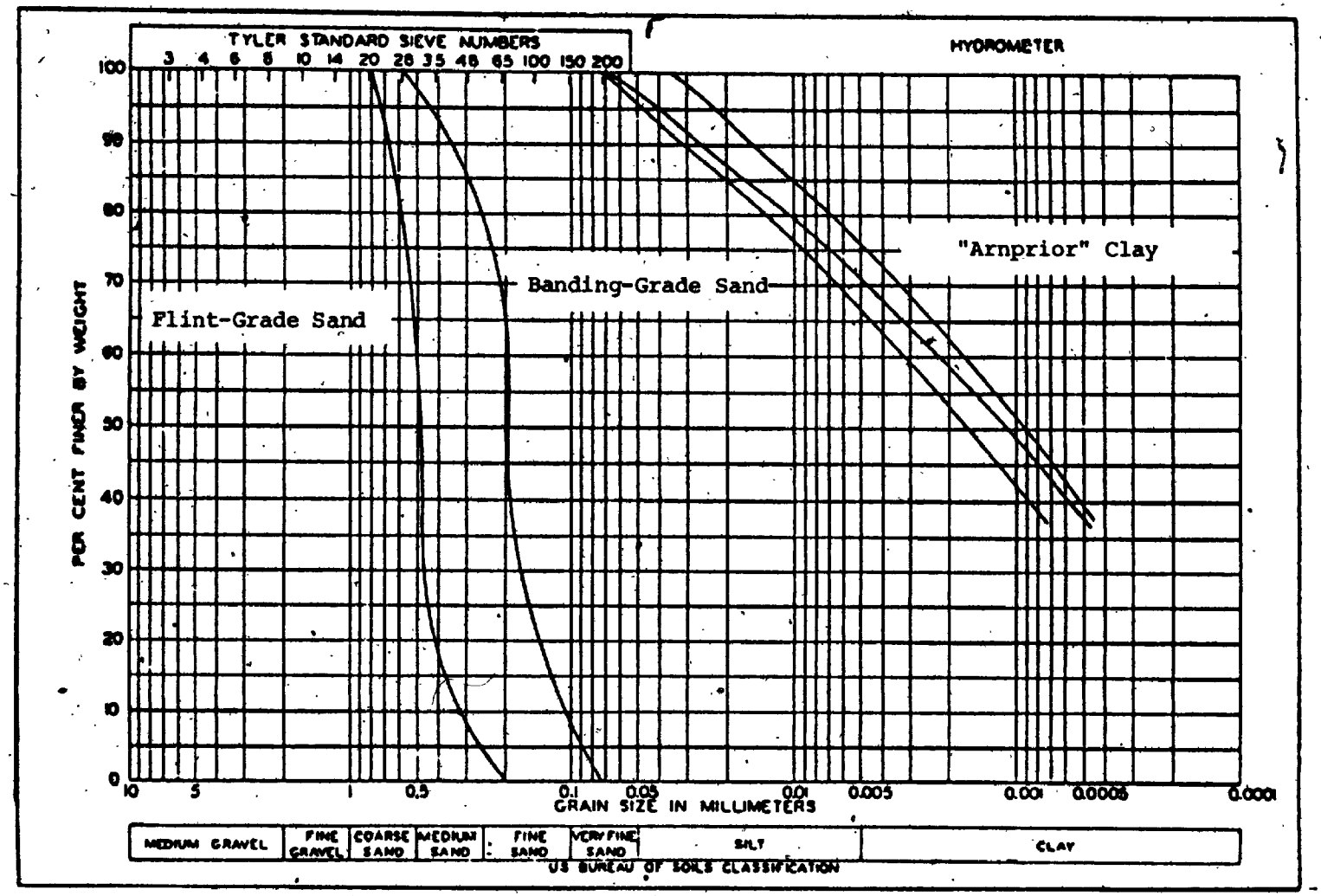

FIGURE 3.11

Grain Size Distribution of Sand and Clay

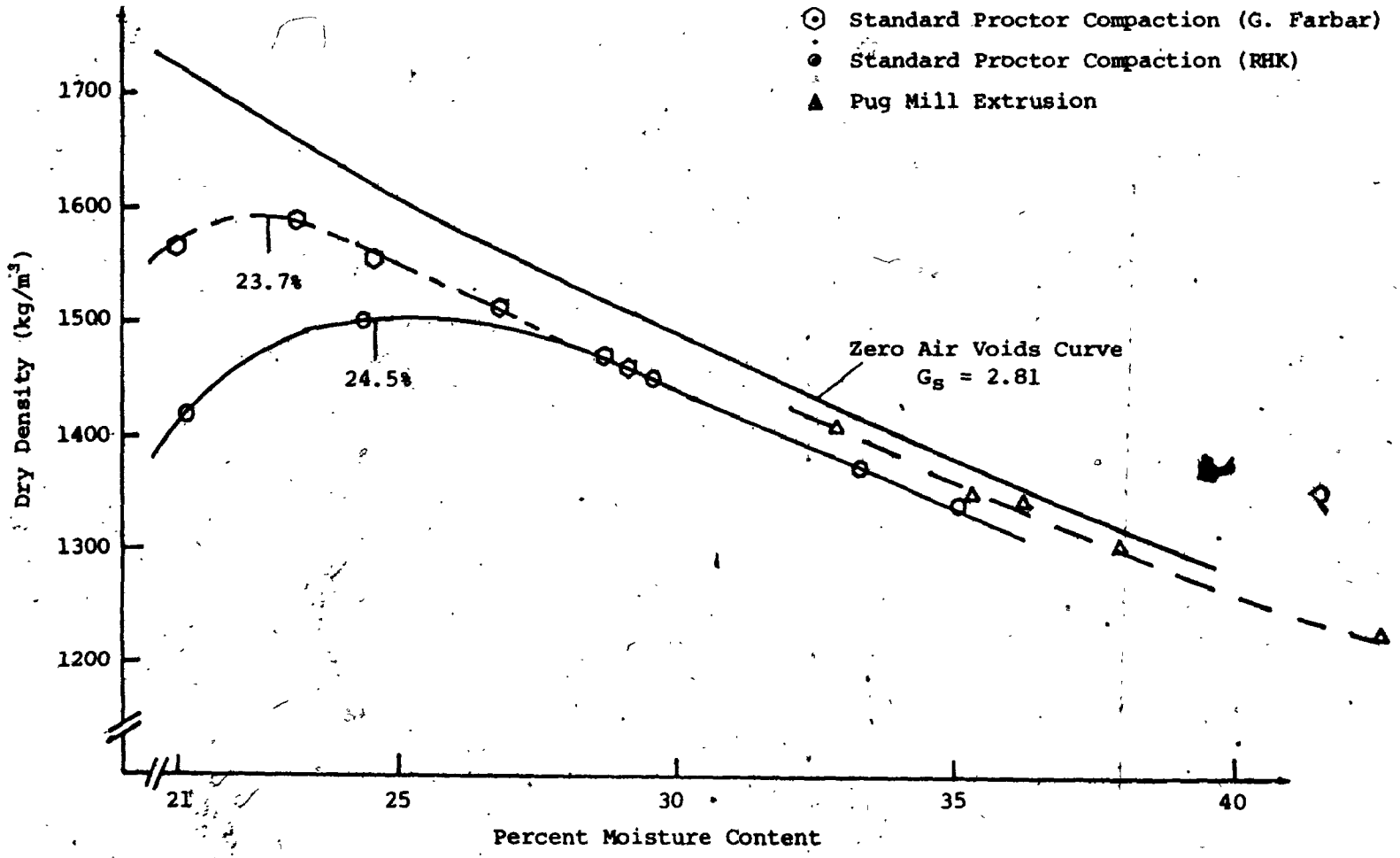

FIGURE 3.12

Moisture Content versus Dry Density for Arnprior Clay

obtained because the method of compaction is more representative of a *kneading* action rather than the impact method of the standard compaction test. Although the kneading *per se* is not known to increase the degree of saturation, it is apparent that more compactive effort is used during the extrusion process than in the standard compaction method.

This study was mainly concerned with the time-dependent response of a *saturated* clay when subjected to a load in the form of a rigid strip footing. The situation in which the voids in the clay are completely filled with water is a special case of the problem of a three-phase medium, i.e., solid clay particles intermixed with air and water. The presence of air in the soil fabric complicates the problem of measuring the initial pore water pressure, and the condition of a fully saturated soil medium occurs more frequently in foundation practice so it was desirable to maximize the degree of saturation of the compacted soil in the test tank.

Tests conducted by Farbar (1977) and Moore (1977) on remolded "Arnprior" clay with a moisture content of 26 to 28 percent showed that a degree of saturation of 90 to 95 percent could be obtained by breaking the clay mass into small particles and tamping the clay into their test apparatus. To achieve a higher degree of saturation and uniformity a pug mill was used to extrude the clay into 76-mm diameter cylinders 0.3 m to 0.4 m long. The pug mill was rated at 225 kg per hour, but it required that the moisture content of the clay be high. By experimenting with various moisture contents, the minimum moisture content that the machine could handle without undue strain was about 38 percent. This produced an average degree of saturation of approximately 98 percent, with a measured low of 96 percent and a high approaching 100 percent

saturation.

The test tank was sealed against water leakage by a silicone sealant, and the polished stainless steel sides were coated with a layer of silicone vacuum grease approximately 0.1 mm thick; this procedure was similar to that adopted by Burland and Roscoe (1969). As the clay was extruded it was placed in the up-right test tank with each layer uniformly tamped with a 5-kg hammer. Although the extruded clay had a high degree of saturation, the total average degree of saturation of the soil in the tank would be reduced if the air voids between the 76-mm diameter clay cylinders were not filled. It was originally intended to extrude 50-mm square lengths, but because the clay moisture content was high, it was soft enough to be molded in place.

3.3.6 *Initial Conditions*

An accurate account was made of all the clay used in the experiment. For the plane strain tank a total of 1075 kg was placed in a volume of 0.586 m^3 for an initial total density of 1835 kg/m^3. The volume was calculated after the surcharge had been applied. Since the moisture content of the clay was controlled at 39 ± 1 percent, and the average degree of saturation was 98 ± 2 percent, then with $G_s = 2.81$ the initial void ratio (e_0) was computed to be in the range of 1.12 to 1.17. When required in future calculations, an average value of e_0 was taken as 1.15.

3.3.7 *Clay Properties*

A summary of several unconsolidated undrained triaxial tests and direct shear tests is presented in Table 1. The triaxial tests covered a wide

TABLE 1

SUMMARY OF TRIAXIAL AND DIRECT SHEAR TESTS ON CLAY

TEST NO.	MOISTURE CONTENT (%)	CELL PRESSURE (kPa)	$\frac{(\sigma_1-\sigma_3)\max}{2}$ (kPa)	E_r 6TH CYCLE (kPa)	E 1% STRAIN (kPa)	SPECIMEN
			Unconsolidated Undrained Triaxial Tests			
1	33.1	20.7	24.5	22,800	3,160	From "control" box
2	43.8	20.7	9.5	3,800	1,000	Extruded only
3	41.0	69.0	12.0	3,180	2,070	" "
4	33.9	34.5	20.7	20,100	4,260	" "
5	34.2	69.0	23.5	30,400	4,780	" "
6	35.6	240.0	30.7	11,040	5,210	" "
7	33.0	69.0	27.6	5,860	3,860	From beneath plate
8	33.6	69.0	29.5	24,150	5,180	" " "
			One-Dimensional Compression Tests			
9	37.3	0	12.9	E_t = 1,450	1,210	Taken from plane strain tank
10	38.3	0	13.6	E_t = 1,660	1,380	" " "
11	39.0	0	14.8	E_t = 1,730	1,380	" " "
12	37.9	0	13.6	E_t = 1,690	1,380	" " "
13	34.3	0	22.1	E_t = 9,250	3,590	" " "
14	32.7	0	21.7	E_t = 10,210	3,660	" " "
15	37.9	0	15.9	E_t = 4,140	1,900	" " "
			Direct Shear Tests			
A	35.0	σ_z = 42.0	22.1	—	—	
B	34.6	σ_z = 71.1	28.3	—	—	
C	34.8	σ_z = 106.3	35.7	—	—	

range of moisture contents in order to show the sensitivity of the undrained shear strength c_u and Young's modulus, E_u, to the initial moisture content of the clay. This is illustrated in Figures 3.13 and 3.14. In general, the higher the initial molding water content, the lower the shear strength and Young's modulus.

It is apparent from Figure 3.13 that the Young's modulus of the soil is not an easy parameter to determine. It is highly dependent on the method of testing and several papers have been written on this subject (see, for example, Ladd, 1964; Soderman *et al.*, 1968). Sample disturbance has frequently been cited as a major source of error but in this experimental study, the clay has been remolded and sample disturbance is at a maximum for both the laboratory specimens and soil materials in the test tank. The definition of the modulus of elasticity is probably the most important factor, so, in agreement with the recommendations of Perloff (1975) and Soderman *et al.* (1968), the reload modulus E_r has been used. In the unconsolidated undrained triaxial tests, the load was cycled at least six times up to a stress level of about one-half the maximum deviatoric stress. The E_r value was taken as the slope of the tangent occurring on the loading of the final cycle, at a stress level of about one-half of the previous cyclic stress increment. For the unconfined compression tests, the modulus was taken as the slope of tangent at a stress of about one-third of the maximum stress. For comparison, the secant modulus at one percent strain is also given in Table 1 and Figure 3.13.

The results show that there is a large variation in the computed Young's modulus, E_r, of the soil, which for a moisture content of 39 percent ranges from 5000 kPa to 10,000 kPa. The unconfined compression

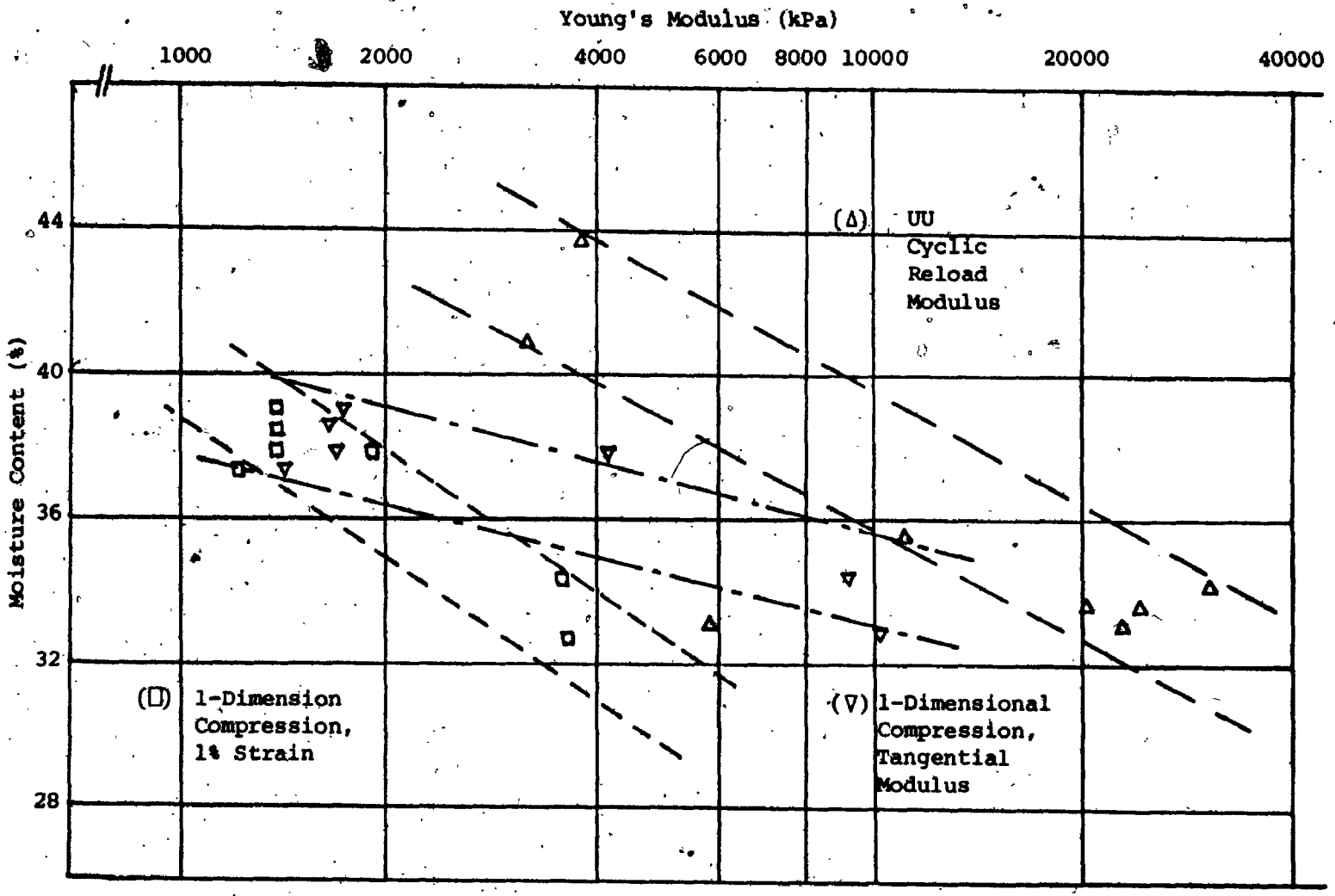

FIGURE 3.13

Moisture Content versus Young's Modulus for Remolded, Extruded "Arnprior" Clay

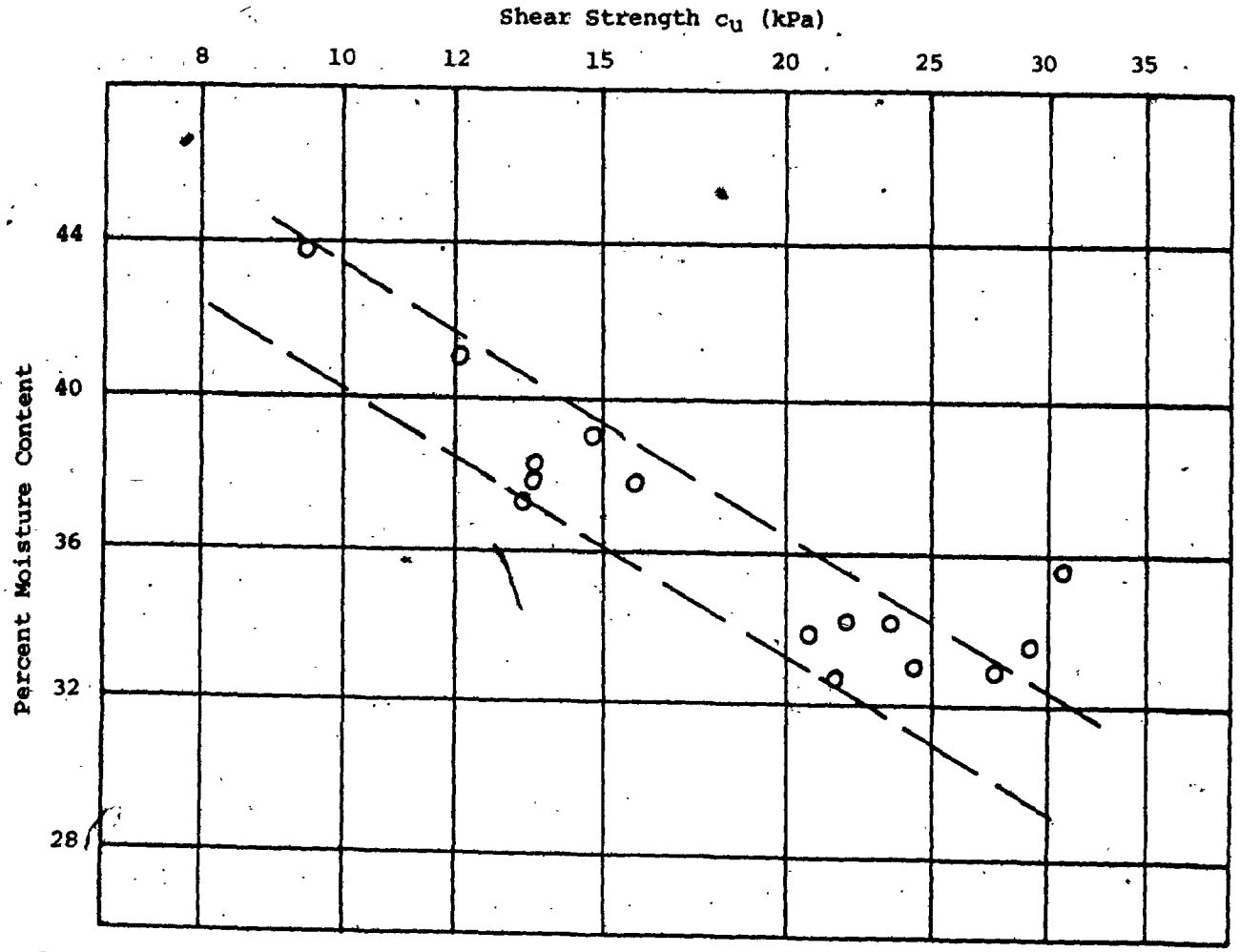

FIGURE 3.14

Moisture Content versus Shear Strength of Remolded, Extruded "Arnprior" Clay

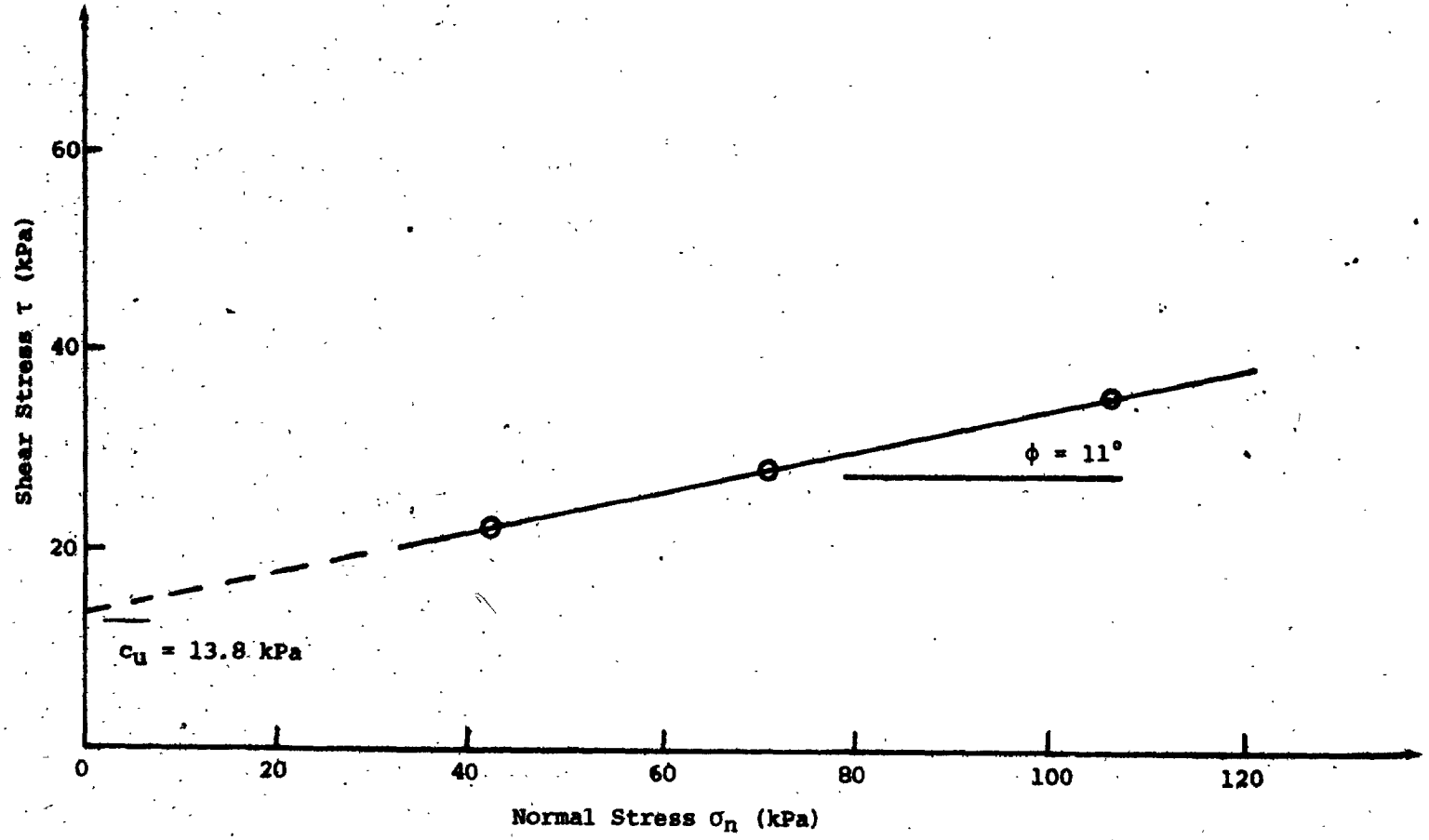

FIGURE 3.15

Direct Shear Test Results for Remolded, Extruded "Arnprior" Clay

tests give a much lower range of between 1000 kPa to 2000 kPa. These results will be compared with the observed plate deformation in Chapter 4.

Figure 3.14 similarly shows that the undrained shear strength can be expected to vary between 12 kPa to 16 kPa at a moisture content of 39 percent. The shear strength obtained from the direct shear test was 13.8 kPa, as shown in Figure 3.15. In-situ vane tests were performed in the plane strain apparatus after the main tests were complete, and will be presented later.

Six standard one-dimensional consolidation tests were performed at various initial moisture contents and initial void ratios. They are presented in Figures 3.16 to 3.20. In general, the remolded extruded clay does not have a clearly defined preconsolidation pressure, but there is a "virgin" slope that can be taken as the compression index, C_c, for a normally consolidated clay. The results are given in Table 2. The coefficient of consolidation, c_v, at high effective stresses ranged from 0.043 mm^2/sec to 0.065 mm^2/sec in all the tests.

3.4 *Quartz Sand*

3.4.1 *General Characteristics*

Two grades of commercially available "Ottawa" sand designated as *Flint* and *Banding* were used in this study. The particle size distributions are given in Figure 3.11.

The Flint-grade sand was a dry, medium to fine white quartz sand composed predominantly of subrounded particles (after Youd, 1973). The coefficient of uniformity was 1.7, representative of a poorly graded sand. The minimum density was 1530 kg/m^3 and maximum density was 1780

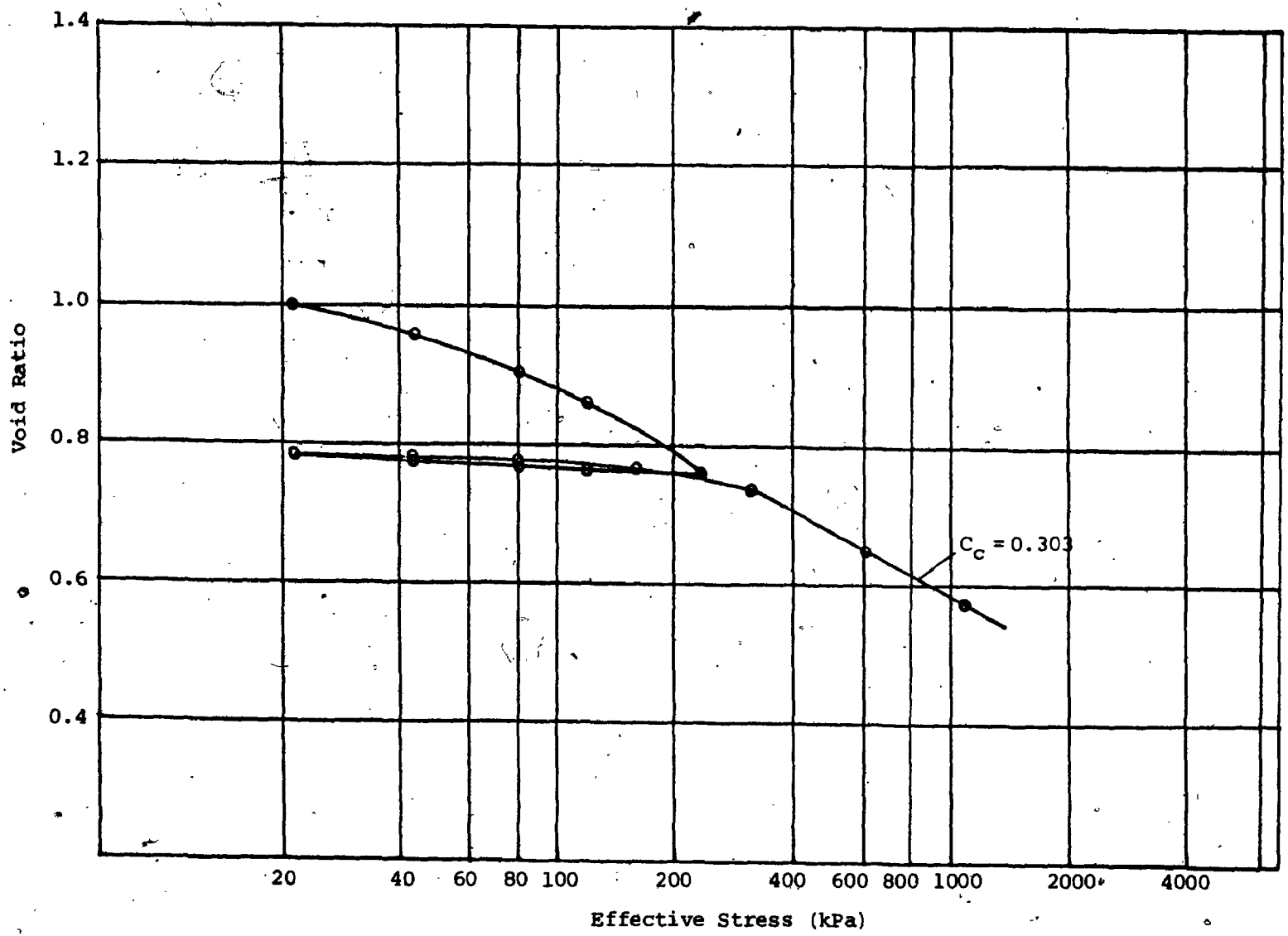

FIGURE 3.16
Standard Consolidation Test No. 1 (Initial Moisture Content = 36.2%)

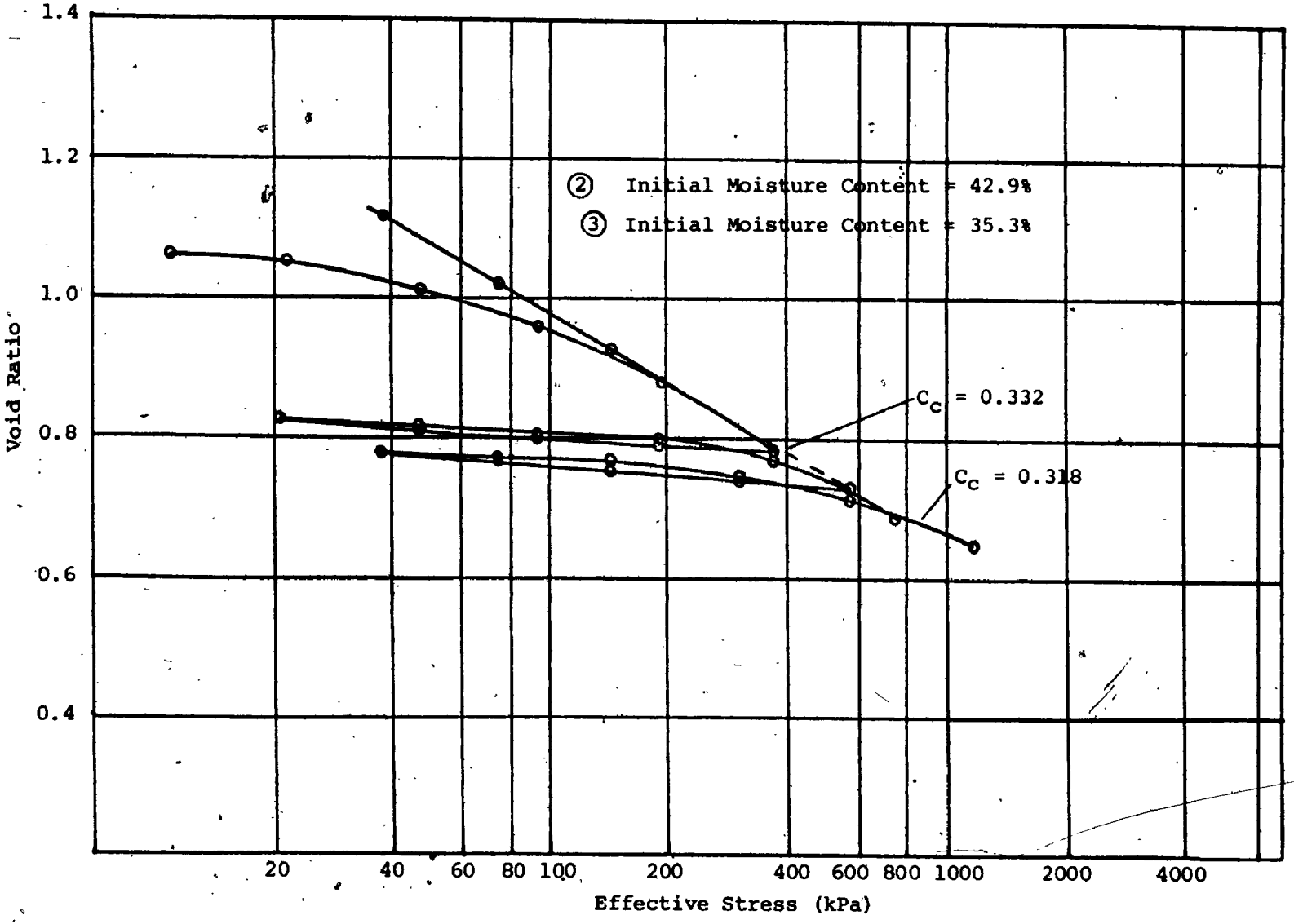

FIGURE 3.17
Standard Consolidation Test No. 2 and 3

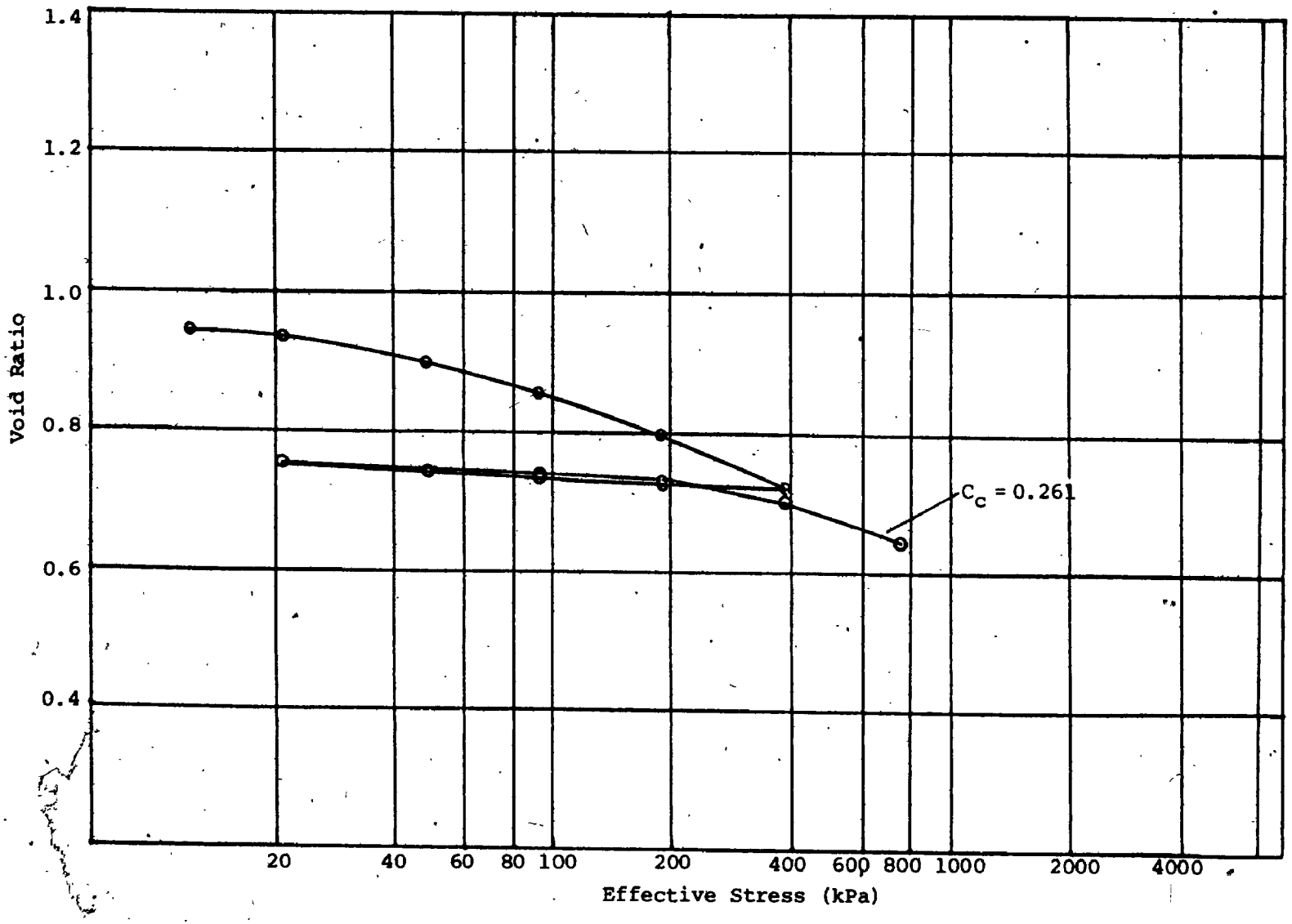

FIGURE 3.18
Standard Consolidation Test No. 4 (Initial Moisture Content = 32.9%)

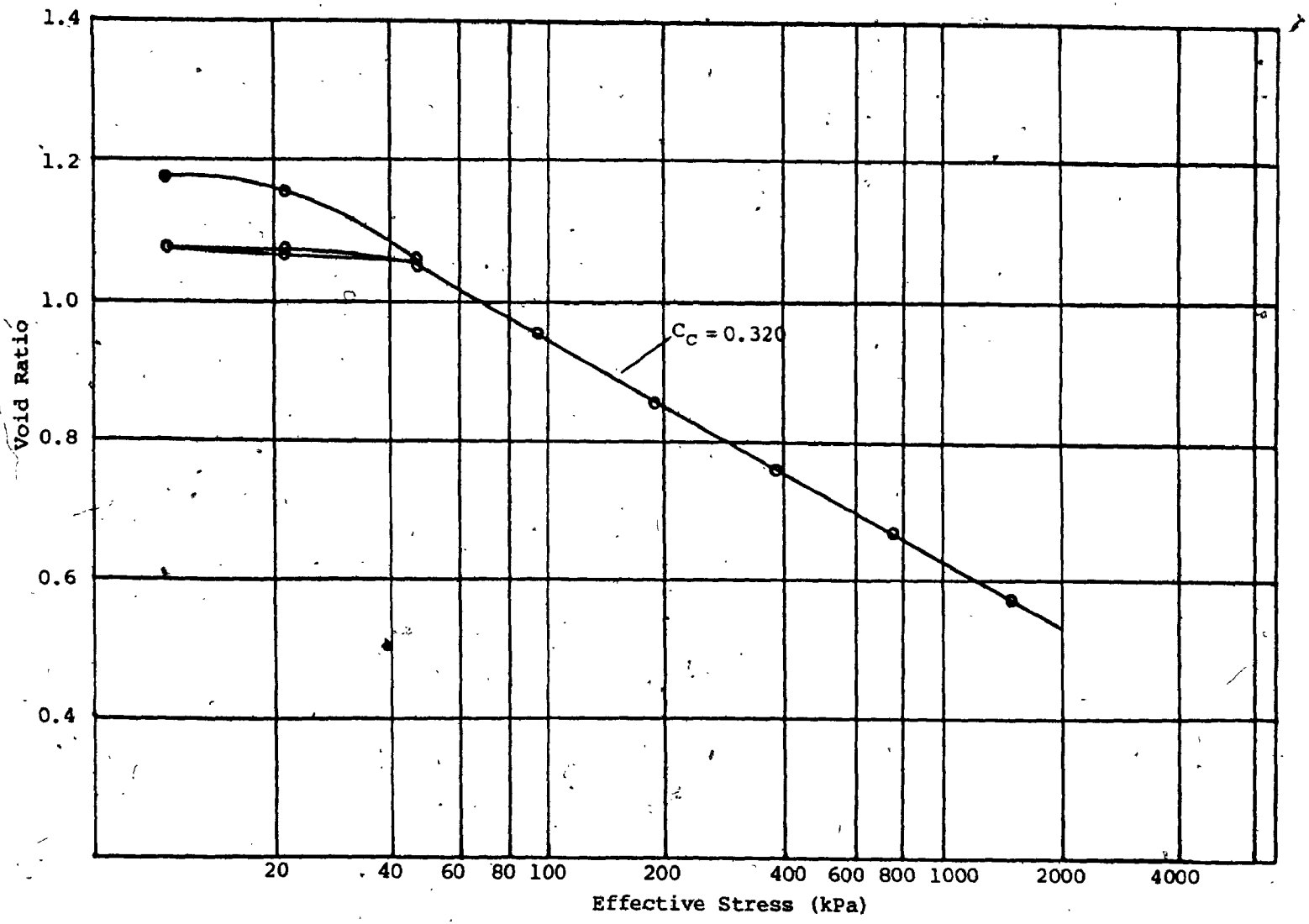

FIGURE 3.19
Standard Consolidation Test No. 5 (Initial Moisture Content = 43.9%)

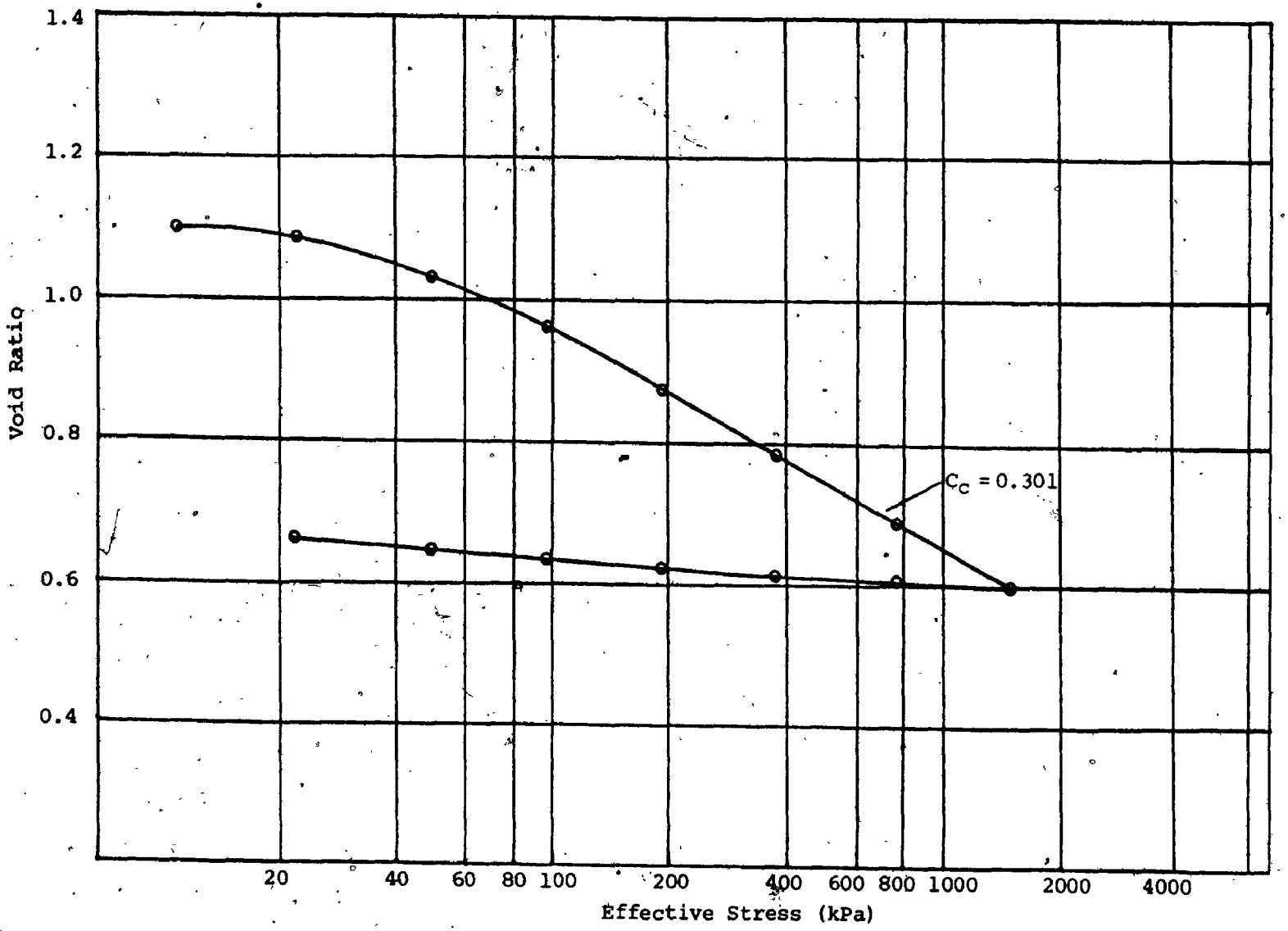

FIGURE 3.20
Standard Consolidation Test No. 6 (Initial Moisture Content = 38.0%)

TABLE 2

SUMMARY OF CONSOLIDATION TESTS

Test Number	*Initial Moisture Content*	*S* %	*Initial Void Ratio*	*Compression Index* C_c	*Recompression Index* C_R
1	36.20	97.5	1.037	0.303	0.036
2	42.90	99.8	1.249	0.318	0.035
3	35.29	98.3	1.065	0.332	0.038
4	32.91	100.0	0.953	0.261	0.031
5	43.91	99.8	1.202	0.320	0.040
6	37.97	99.39	1.121	0.301	na
Average		99.38		0.306	0.036

NOTE

Sample No. 4 was taken approximately 75 mm below test plate after end of 5-week test.

Sample No. 6 was taken approximately 0.45 m below surface of clay after end of supplementary tests.

All other samples were taken directly from extruded cores.

kg/m^3, as obtained by the method outlined by Bowles (1970). With a specific gravity of 2.66, as given by Hasnain (1974), the maximum void ratio was 0.74 and minimum was 0.50.

The dry Banding-grade sand was a fine, poorly graded white quartz sand with a particle shape considered as subangular to subrounded. Its uniformity coefficient was 2.1. The minimum density obtained was 1510 kg/m^3, with a maximum density of 1745 kg/m^3. Thus the limiting void ratios are 0.76 to 0.52.

3.4.2 *Placement Method*

Since the angle of internal friction of a cohesionless material is highly dependent on the density of the soil, it was important that the sand used in the model experiments was deposited in such a manner that the density would not vary substantially within the tank. This would also enable duplicate tests to be performed under similar soil conditions. The placement or large quantities of dry sand while controlling the density has been a problem for many researchers in the past (see, for example, Walker and Whitaker, 1967; Atefi, 1975; Shields *et al.*, 1977).

It has been found that one of the best methods of ensuring that a bed of sand has a uniform density is to control the *rate* and *velocity* of the sand while allowing the particles to "rain" onto the bed. In general, the greater the rate of deposition, the greater the porosity of the sand. The velocity of the soil particles is controlled by the height of fall of the sand, and in general, the greater the height of fall, the greater the density of the sand. There are a number of variations of the method used to deposit the sand, and this investigation

focused on only one such technique, modelled after Atefi (1975) and Drupsteen (1977).

The deposition of the sand in the plane strain apparatus was performed by allowing the sand particles to "rain" onto the bed at a controlled rate of deposition. This was accomplished by placing the sand in a wooden hopper that traversed the top of the test tank (see Plate 6). At the base of the hopper there was a steel plate with a regular pattern of holes. The hole diameter and hole spacing controlled the intensity of sand deposition. Drupsteen (1977) showed that increasing the hole diameter or increasing the number of holes per unit area increased the rate of deposition and resulted in a less dense soil bed. Drupsteen (1977) also showed that there appeared to be a critical height of fall; increasing the height beyond this critical value did not significantly increase the density of the sand.

Tables 3 and 4 summarize the results of several density calibration tests on Flint-grand and Banding-grade sands. The calibrations were performed with round 42-cm^3 capacity aluminum density tins with the top edge sharpened to reduce any edge effects. The tins were placed at various elevations in the test tank and the hopper was passed over the tins several times before they were filled. The tins were removed, scraped level in one smooth pass of a knife edge, and weighed. A number of duplicate tests were performed for each elevation, including the use of larger 300-cm^3 cylindrical density tins. The larger density tins produced average results within the range observed by the smaller density tins. Recent work by Lai (1977) showed that the in-situ density of sand beds can best be measured with the use of density tins. It was considered to be the density reference test producing the most

PLATE 6

Sand Placement in Plane Strain Tank by Hopper

TABLE 3

FLINT-GRADE SAND DENSITY CALIBRATION TESTS (kg/m^3)

(A)

EFFECT OF HEIGHT OF FALL WITH 1.6 MM HOLE DIAMETER

Trial Number	*Height of Fall (m)*	*Density Tin Number* 1	2	3	4	*Average*
1		1747	1753	1751	1753	
2	0.69	1742	1753	1744	1756	
3		1753	1743	1738	1753	
Average		1747	1750	1744	1754	1749
4		1778	1749	1746	1766	
5	0.46	1738	1743	1744	1766	
6		1748	1756	1749	1763	
Average		1753	1749	1746	1765	1753
7		1742	1750	1740	1746	
8	0.23	1754	1740	1744	1755	
9		1748	1745	1741	1763	
Average		1756	1745	1742	1755	1750
10		1729	1733	1735	1752	
11	0.13	1726	1742	1737	1762	
12		1718	1739	1742	1763	
Average		1724	1729	1738	1759	1738
In-Situ Test	0.53	1767	1752	1750	1775	

(B)

EFFECT OF HOLE DIAMETER ON DENSITY

Hole Size (mm)	*Height of Fall (m)*	*Average Density (kg/m^3)*	*Source*
1.60	0.43	1753	RHK
2.38	0.44	1737	from Drupsteen (1977)
2.78	0.44	1731	" " "
3.18	0.44	1716	" " "
3.57	0.44	1712	" " "

TABLE 4

BANDING-GRADE SAND DENSITY CALIBRATION TESTS
(kg/m^3)

(A)
EFFECT OF HEIGHT OF FALL USING SIEVE #30
(0.59 mm hole diameter)

Trial No.	*Height of Fall (m)*	*Density Tin Number* 1	2	3	4	*Average*
1	0.56	1707	1701	1716	1710	1709
2	0.43	1710	1714	1713	1712	1712
3	0.30	1725	1727	1719	1673	1711
4	0.13	1682	1682	1689	1686	1685

(B)
EFFECT OF HOLE DIAMETER ON DENSITY

Hole Size (mm)	*Height of Fall*	*Density Tin Number* 1	2	3	4	*Average*
1.6	0.69	1519	1524	1498	1543	1521
0.84	0.69	1535	1555	1522	1562	1544
0.59	0.56	1707	1701	1716	1710	1709
0.59	0.69	1703	1709	1696	1717	1706
0.59	0.69	1716	1701	1677	1713	1702
0.42	0.69	1726	1732	1715	1732	1726

consistent results, but there may be variations due to non-uniform deposition and particles rebounding from the bottom of the density tins. Different sizes and shapes of density tins were used by Lai (1977) but the variations between the results were not presented.

For this investigation, the effect of density on contact stress distribution was not studied so the problem was reduced to finding a suitable screen hole diameter and hole spacing for the hopper that would produce a medium dense or dense bed of sand. Figure 3.21 shows that the density of the Flint-grade sand was only marginally influenced by the size of the hole diameter. A 1.6-mm hole diameter at regular 2.8-mm spacing was chosen to produce a sand density of 1750 kg/m^3. This produces a Relative Density D_r of 90 percent, based on the minimum and maximum densities obtained by the method outlined by Bowles (1970). The minimum and maximum densities reported have been shown by several researchers to be dependent on a number of factors, such as similarity between soil specimens, test procedure and test equipment (Holtz, 1973; Selig and Ladd, 1973; Tavenas, 1973). A comparison can be made with the empirical work by Youd (1973). With the subrounded Flint-grade sand having a coefficient of uniformity of 1,7, the minimum and maximum void ratios are estimated to be 0.45 and 0.80 respectively. Using these values with an in-situ density of 1750 kg/m^3, the Relative Density D_r is reduced to 81 percent from 90 percent. This is a significant change, but the sand density can still be considered as being "dense", "very dense" or "very compact", depending on the criteria used for classification (Holtz, 1973).

Figure 3.21 shows that for a fine Banding-grade sand the size of hole opening has a significant effect on the density of the soil. Since a dense sand deposit was desired, a hole opening of 0.59 mm was chosen,

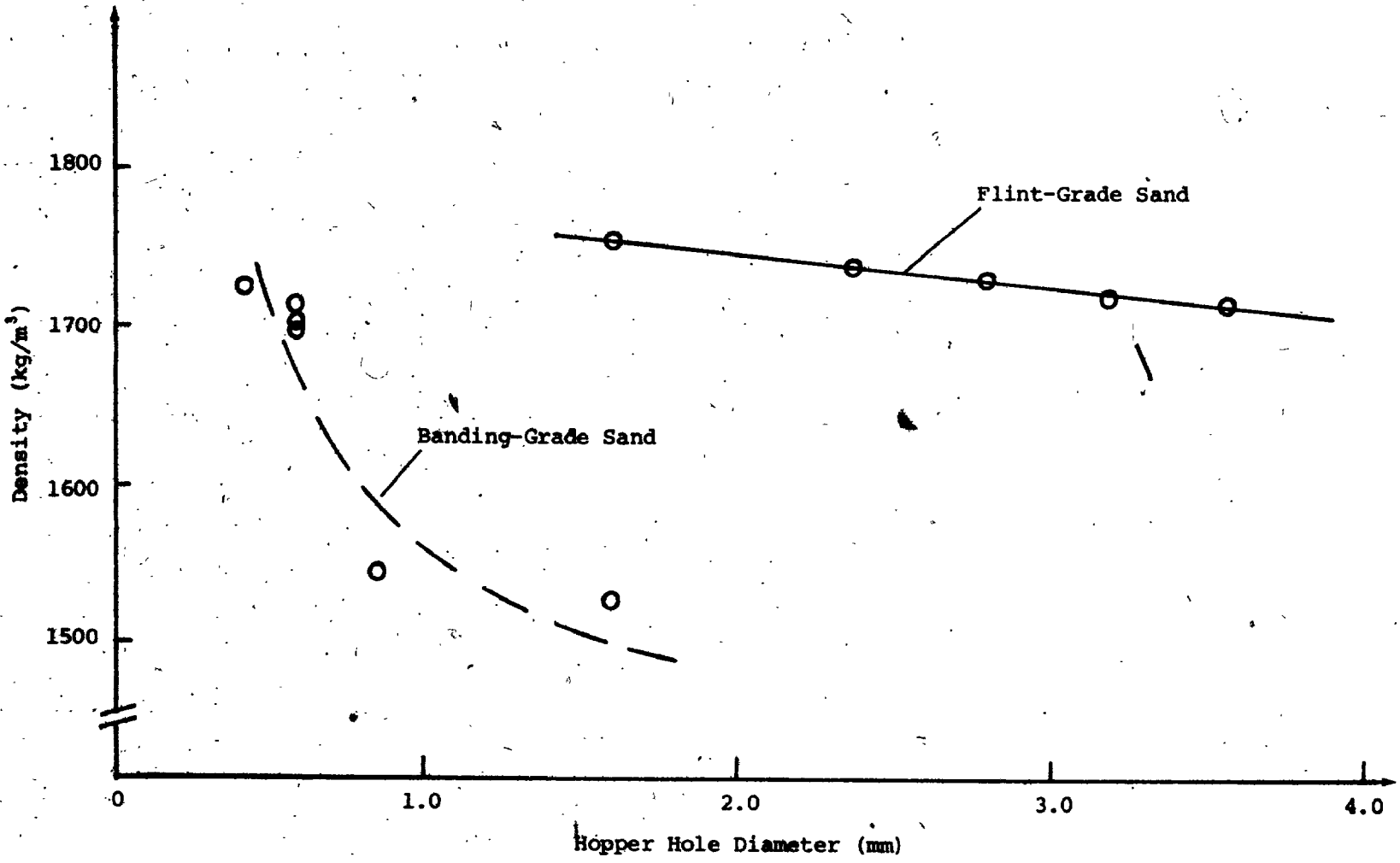

FIGURE 3.21

Graph of Placement Density versus Size of Hopper Hole Diameter

similar to the standard No. 30 sieve size. An average sand density of 1700 kg/m^3 was obtained, producing a Relative Density of 83 percent. Again, comparing this with Youd (1973) for an estimated minimum and maximum void ratio of 0.40 and 0.76 respectively, the Relative Density was computed to be 55 percent. This is considerably less than determined from the method outlined by Bowles (1970). The important point here is that there is evidence that the Banding-grade was not as "relatively" dense as the Flint-grade sand. It will be expected that the angle of internal friction will be less for the Banding-grade sand, and more settlement per unit stress will occur.

The size of hole diameter can be related to the average particle diameter of the two grades of sand. The Flint-grade sand averaged 0.5 mm with a hole opening of 1.6 mm, producing a ratio of hole diameter to average particle diameter of 3.2. The Banding-grade sand averaged 0.2 mm in diameter. With a No. 30 sieve the size of opening was 0.6 mm, again producing a ratio of hole diameter to average particle diameter of 3. Smaller ratios would reduce the intensity of sand rain and increase the density, but at some point the larger particles in these poorly graded sands would not be able to pass through the holes. Thus a compromise must be reached between the desired density and average hole opening diameter.

The relationship between the height of fall and sand density is given in Figure 3.22. With both the Flint-grade and Banding-grade sand, the density remains essentially constant for heights greater than 0.2 m. For this reason it was not necessary to maintain the height of fall throughout the test, as was necessary in some methods used by previous researchers. Atefi (1975) showed that the height of fall was not a

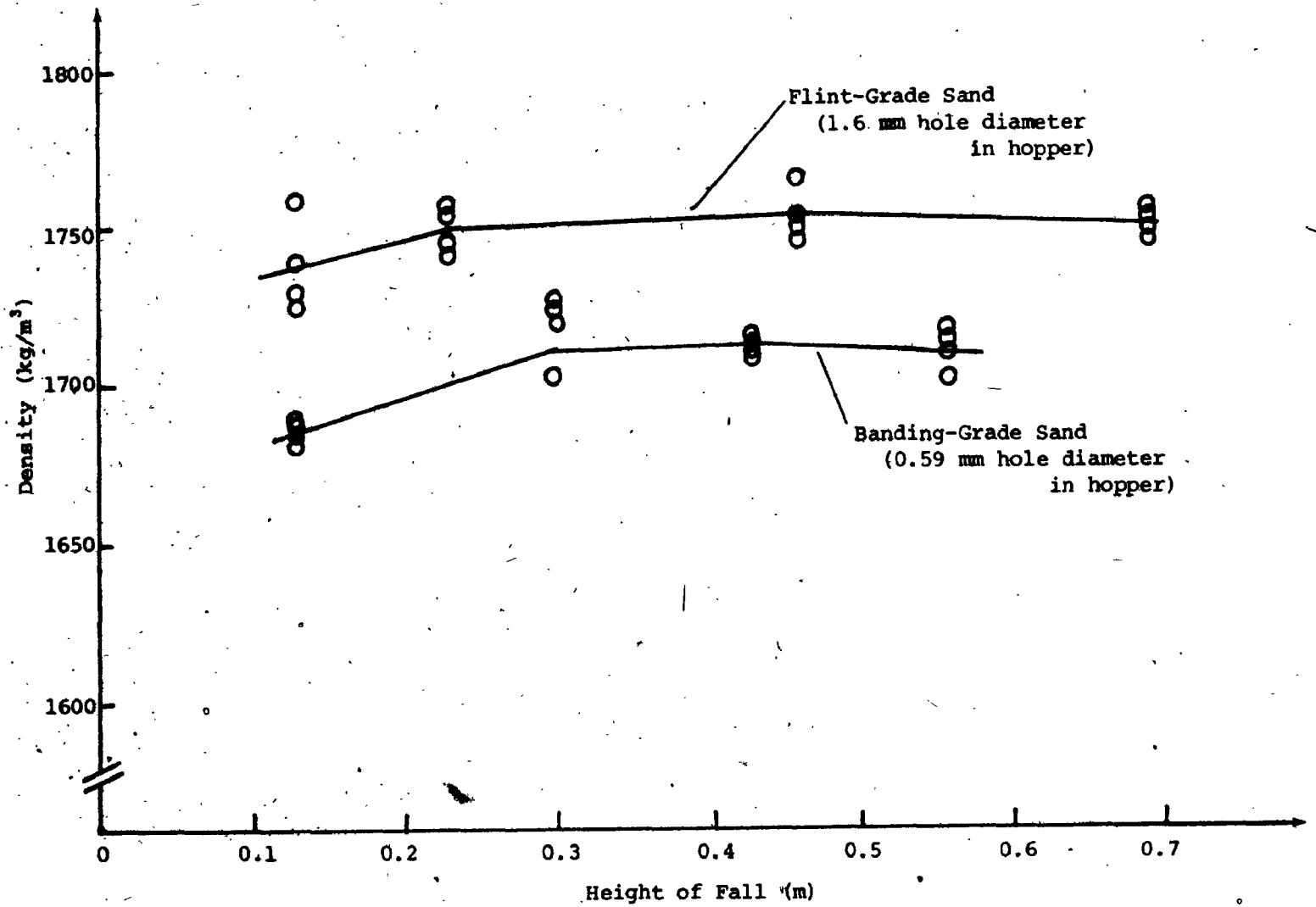

FIGURE 3.22

Graph of Placement Density versus Height of Fall

significant variable when the sand was allowed to fall through a plate drilled with a regular series of holes, similar to the method used in this research work. However, when the sand was deposited through a narrow rectangular opening, the density varied significantly with the height of fall. This was also observed by Shields *et al.* (1977), but the height of fall is less significant when a dense deposit of sand is being prepared.

For both types of sand the procedure for filling the plane strain tank was similar. The 0.05-m^3 capacity hopper was filled about three-quarters full with sand and was pushed manually back and forth at a uniform rate over the top of the apparatus. Each pass left a 4- or 5-mm layer of sand. The hopper was refilled when the sand was reduced to about one-third of the volume of the hopper. There were small variations in the sand elevation between the width of the walls of the tank, but they were less than 10 mm. When the sand reached a height of 0.97 m, the top surface was levelled with a smooth scraper, which removed about 5 mm of sand and left a plane surface for the test plate.

3.4.3. *Direct Shear Tests on Sand*

A number of direct shear tests were performed on the Flint-grade and Banding-grade sands. The sands were deposited in the direct shear box by the same method used in the plane strain apparatus, i.e., the sand was allowed to "rain" over the container from a height of 0.5 m. The effect of varying the density was not investigated.

Figure 3.23 shows the relationship between the maximum shear stress and normal stress for the two types of sand. The angle of internal friction was taken as 40 degrees for the Flint-grade sand and 36

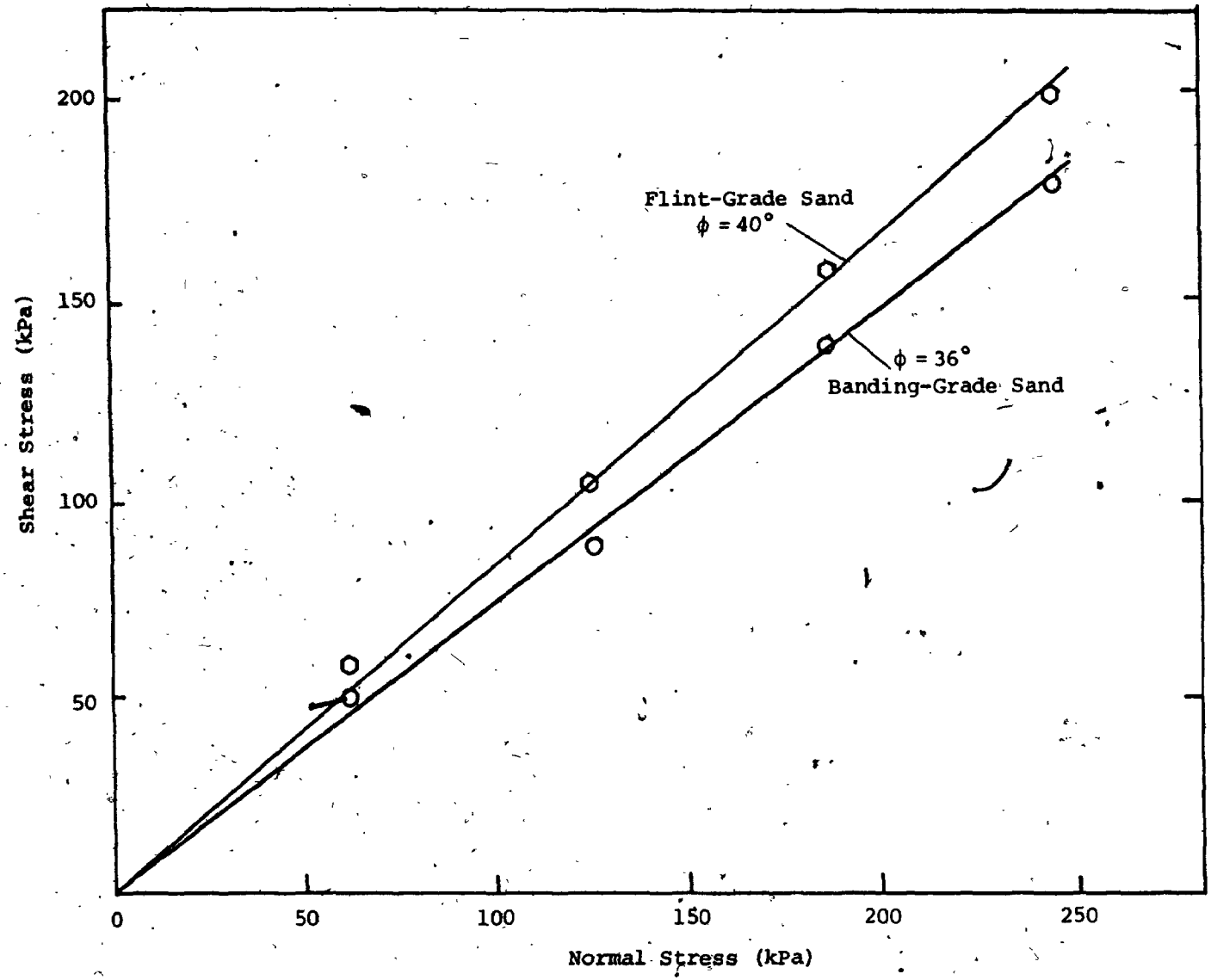

FIGURE 3.23
Direct Shear Test Results for Flint-Grade and Banding-Grade Sand

degrees for the Banding-grade sand. It was shown by Hasnain (1974) that for a sand with the same initial Relative Density the friction angle was dependent on the level of normal stress, especially for dense samples. Hence the use of a constant angle of internal friction is not strictly correct but will be used to provide an estimate of the bearing capacity of the sand.

4. TEST RESULTS AND DISCUSSION

4.1 *Introduction*

This section will present the results of the testing program of the interaction between a rigid steel plate and a cohesive or cohesionless soil medium. The experimental observations of the tests on sand will be presented first because they were intended to be preliminary trial runs ensuring that the apparatus functioned properly. The interaction between the plate and the sand will involve both settlement and contact stress distribution observations, as a function of load magnitude and loading cycle. A comparison will be made with previous observations of contact stress distributions on sand.

The results of a three-dimensional loading of the rigid square plate on a layer of cohesive soil will be presented in the following section. Although also intended as a preliminary test, the contact stress distribution proved interesting and will be compared with previous observations and theoretical predictions.

The principal experiment involving the plane strain loading of a rigid plate on a cohesive soil medium will then be presented. This will start with the pore water pressure increase and settlement of the clay in the test tank due to one-dimensional loading. Next, the immediate settlement of the test plate on the clay will be compared with predictions of several theoretical models, along with the immediate contact stress observations and pore water pressure increases. The settlement of the plate with time will be presented and discussed. The time-dependent response of the contact stresses will complete this section.

The results of two subsequent static loading tests on clay will then be presented to determine the effect of wall friction in the tank. The effect of magnitude of applied stress on contact stress distributions will also be discussed.

4.2 *Cohesionless Soil Medium*

4.2.1 *Introduction*

The Banding-grade and Flint-grade Ottawa sands can be ideally represented as cohesionless materials. All the experiments on sand were conducted in the "plane strain" apparatus previously described in Chapter 3. A total of five tests were conducted on Banding-grade sand and three tests on Flint-grade sand, after three previous trial tests were performed to become familiar with the operation of the apparatus. The sand was deposited by a "raining" technique described in Chapter 3 with the calibration results given in Tables 3 and 4. After each test *all* the sand was removed and re-deposited in a similar manner because it was found that removal of only *part* of the tank contents would produce load-deflection curves similar to re-loading curves.

In each test the average maximum applied stress was 147 kPa. Since the bearing capacity is at least of the order of 350 kPa (considering $\phi = 40°$) for the Flint-grade sand, the applied load can be considered to be within the *working* stress range. (See Appendix 10 for estimated bearing capacity of soil.) The load was recycled at least twice in each test.

At each load increment the observations consisted of recording the output of sixteen pressure transducers, four displacement transducers and one load cell. All of this information was read by the "B & F" data

acquisition system and printed on paper tape. Since each load cycle involved about ten recordings and three load cycles were performed, the amount of data generated was substantial. To facilitate the data processing, a computer program designated CONTAC was developed to reduce the amount of manual computations. A listing of the program and an example of the output is given in Appendix 11.

4.2.2 *Plate Settlement*

A typical load-deflection curve for the Banding-grade sand and Flint-grade sand are presented in Figure 4.1. The unloading and re-loading curves are also given, showing a substantial increase in the slope of the load-deflection curves. For both types of sand the method of deposition was essentially the same, producing load-deflection curves very similar to one another. The deflection at a maximum stress of 147 kPa averaged 7.6 mm for the Banding-grade sand and 6.0 mm for the Flint-grade sand. Re-cycling the load increased the maximum settlement by about 1.0 mm. The lower settlement for tests on Flint-grade sand can be attributed to the higher Relative Density measured during the density calibration tests.

The settlement was computed from the average of four displacement transducers located near each corner of the test plate. From the calculations given in Appendix 4, the plate can be considered rigid. Thus any difference in deflections can be attributed to either the inaccuracy of the displacement transducer or to the non-uniform settlement. It appears that there was some tilting of the plate, but the total angular rotation was always less than 0.5 degrees. The loading system was designed to apply a vertical load to the "T" bar, which was in turn

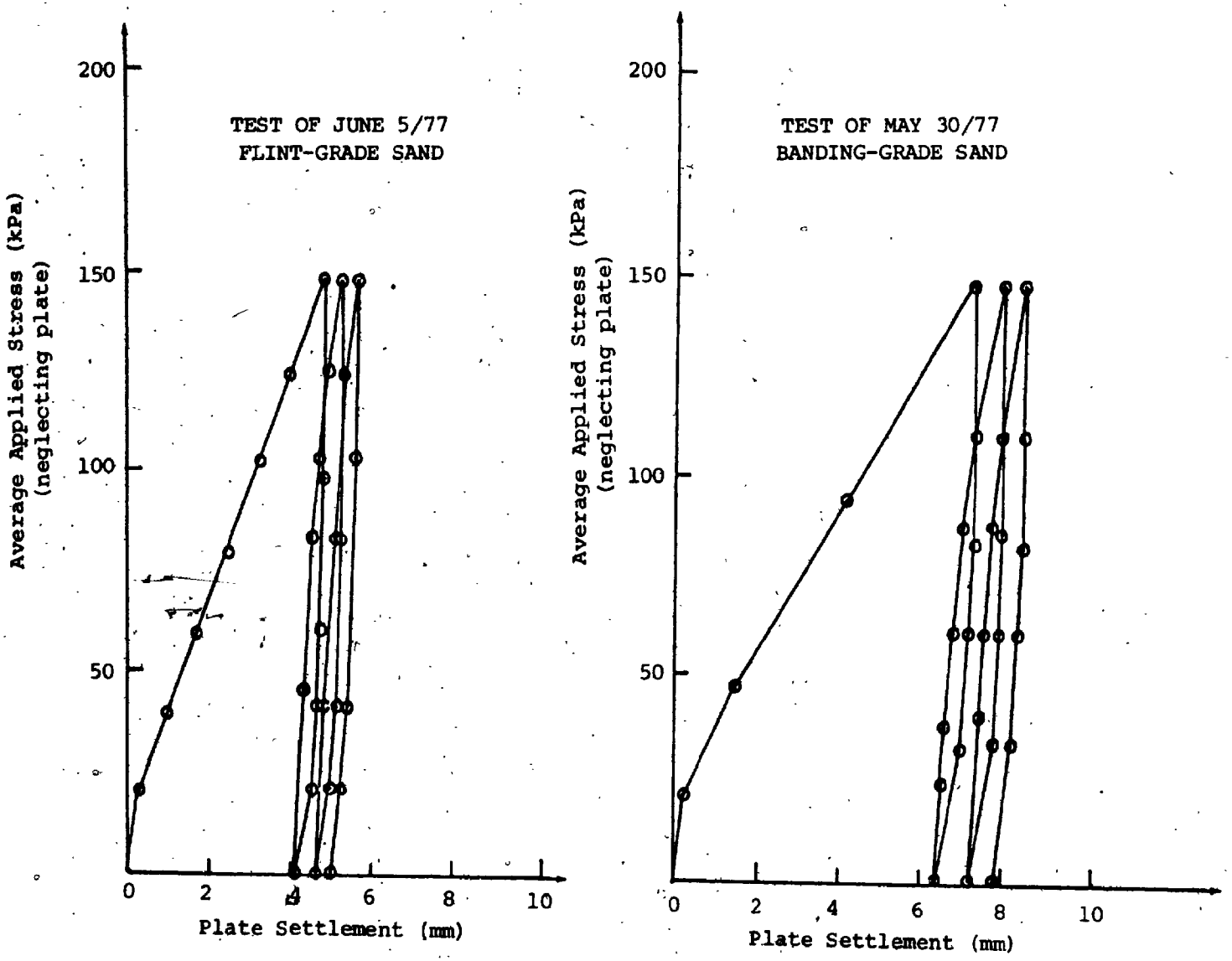

FIGURE 4.1

Typical Load Deflection Curves for Plate on Flint-Grade and Banding-Grade Sand

attached to the test plate by a threaded connection. The channel holding the "T" bar in place was monitored for movement, and the observed deflection was less than 0.03 mm. This implies that the threaded connection allows a small rotation, but this rotation is limited predominantly to the initial stress increments as the plate settles to fit the surface of the sand.

It is a difficult matter to predict the settlement of a footing resting on the surface of a granular material. Empirical methods are used with some degree of success, but they all require an estimate of the Young's modulus, E_s, (or compressibility) of the soil. Schmertmann (1970) has developed a widely used method making a simplifying assumption of the vertical strain induced beneath the foundation. The relative density of the Flint-grade and Banding-grade sand placed in the test tank can be considered to be medium dense. Terzaghi and Peck (1967) relate the relative density, D_R, of the sand to the number of blow-counts, N, from the standard penetration test. For D_R = medium, N ranges from 10 to 30 blows per foot, and for D_R = dense, N ranges from 30 to 50 blows per foot. Schmertmann (1970) used the empirical relationships E (tsf) = $2q_c$ and $q_c = 3.5$ N for clean, fine- to medium-grained sand, where q_c is the static cone bearing capacity. Using Schmertmann's (1970) method, assuming a constant compressibility modulus with depth, results in a predicted plate settlement of 7 to 20 mm for medium dense sand and 4 to 7 mm for dense sand. This can be compared with the observed settlement of 7.6 mm for the Banding-grade sand and 6.9 mm for the Flint-grade sand.

A very general comparison can be made with the summary of observed settlements compiled by Burland *et al.* (1977). In Figure 4.2 the ratio

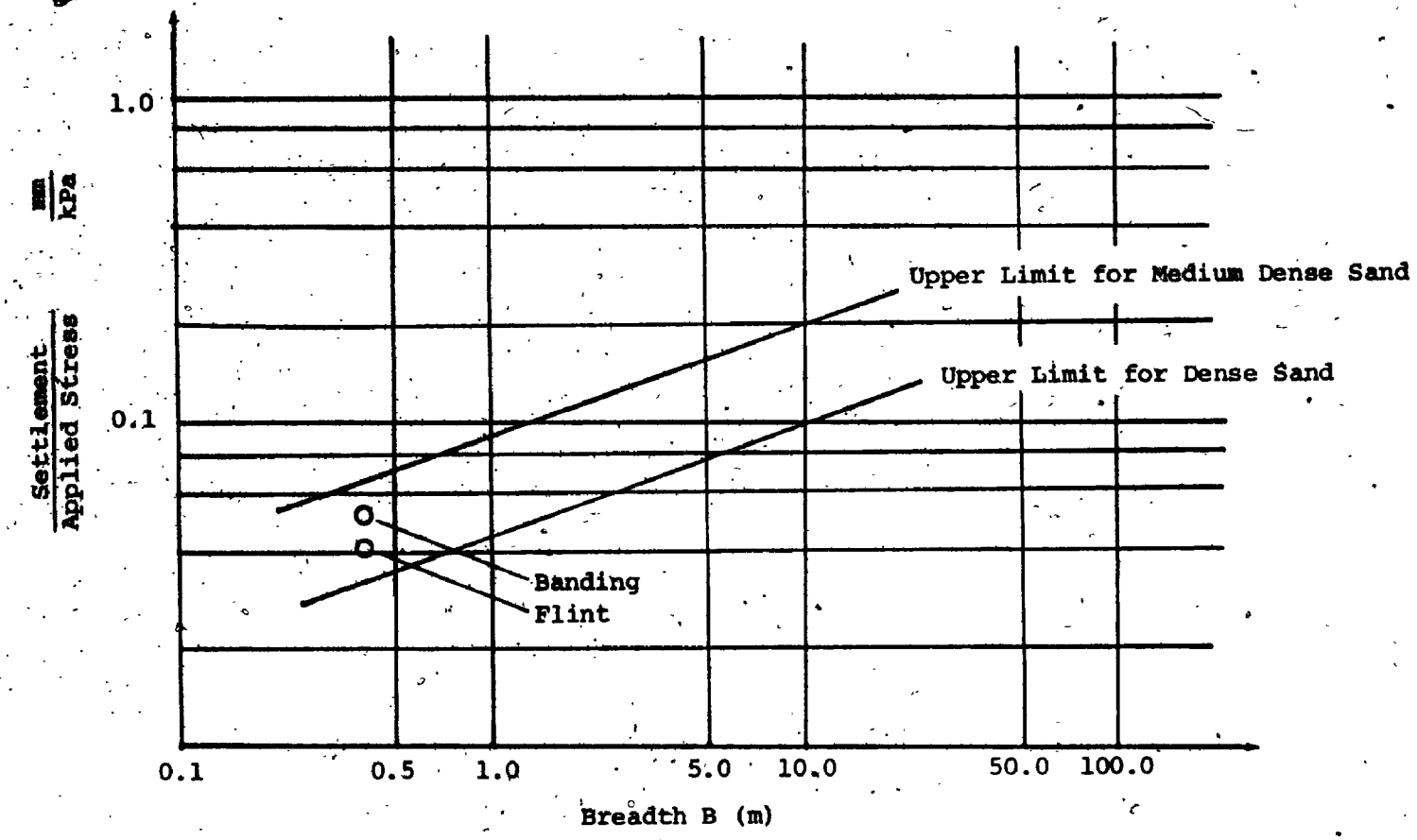

FIGURE 4:2

Comparison of Model Plate Settlement with Observed Settlement of Footings on Sand for Various Relative Densities (Burland *et al.*, 1977)

of observed settlement to applied stress is related to the footing breadth, with only the upper limits of settlement for medium dense and dense sand shown for clarity. The results for the average settlement of the plate on Flint-grade and Banding-grade sand are shown to lie in the range of medium dense sand, in agreement with the relative density determinations. This comparison is by no means conclusive because the limits are empirical upper limits that do not take into account the effect of the water table, relative depth of embedment or geometry of the foundation. The comparison does show that the observed settlements are comparable to existing observations, and illustrates the large scatter in footing settlement on granular soils.

4.2.3 *Contact Stress Distribution — Cohesionless Soil*

The contact stress distribution of primary concern is the distribution across the width of the idealized strip footing. Ideally, the contact stress distribution would be the same along the length of the strip footing, implying that the *shape* of the contact stress distribution will be the same along line A-A, B-B and C-C of Figure 3.1, and the *value* of the contact stress will be the same along D-D, E-E and F-F. The tests on sand were intended to check the validity of this assumption before the main test on a consolidating medium. The contact stress distribution was found to vary marginally along the length of the footing.

There are many ways of presenting the experimental results but only a few will be described. Figures 4.3, 4.4 and 4.5 summarize the output of all eight tests on sand. These results were obtained from an averaging process and are intended to establish trends, considered to be more important than absolute values of contact stress distributions.

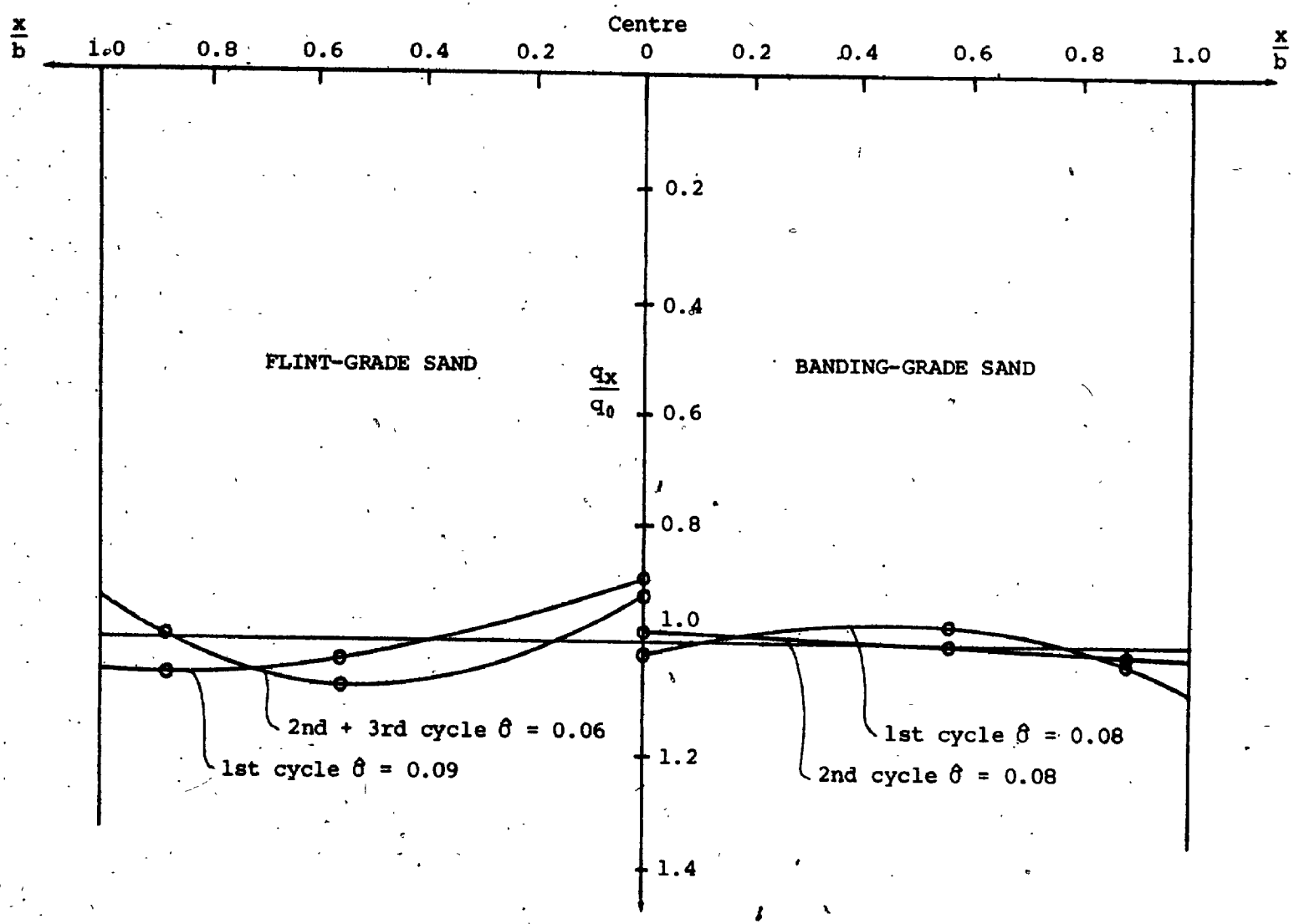

FIGURE 4.3

Summary of Tests on Sand, Maximum Applied Stress = 147 kPa

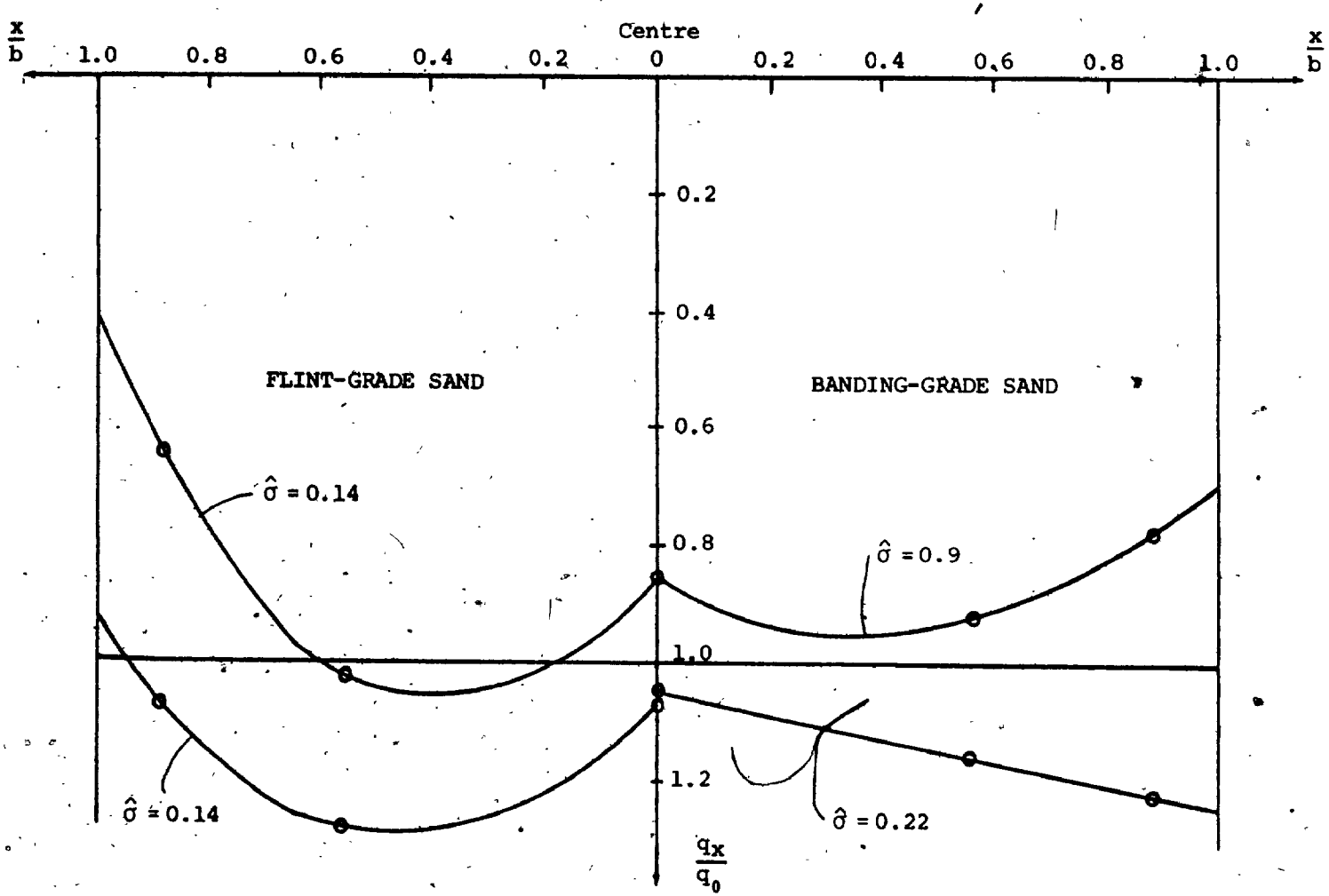

FIGURE 4.4

Summary of Highs and Lows During First Load Cycle

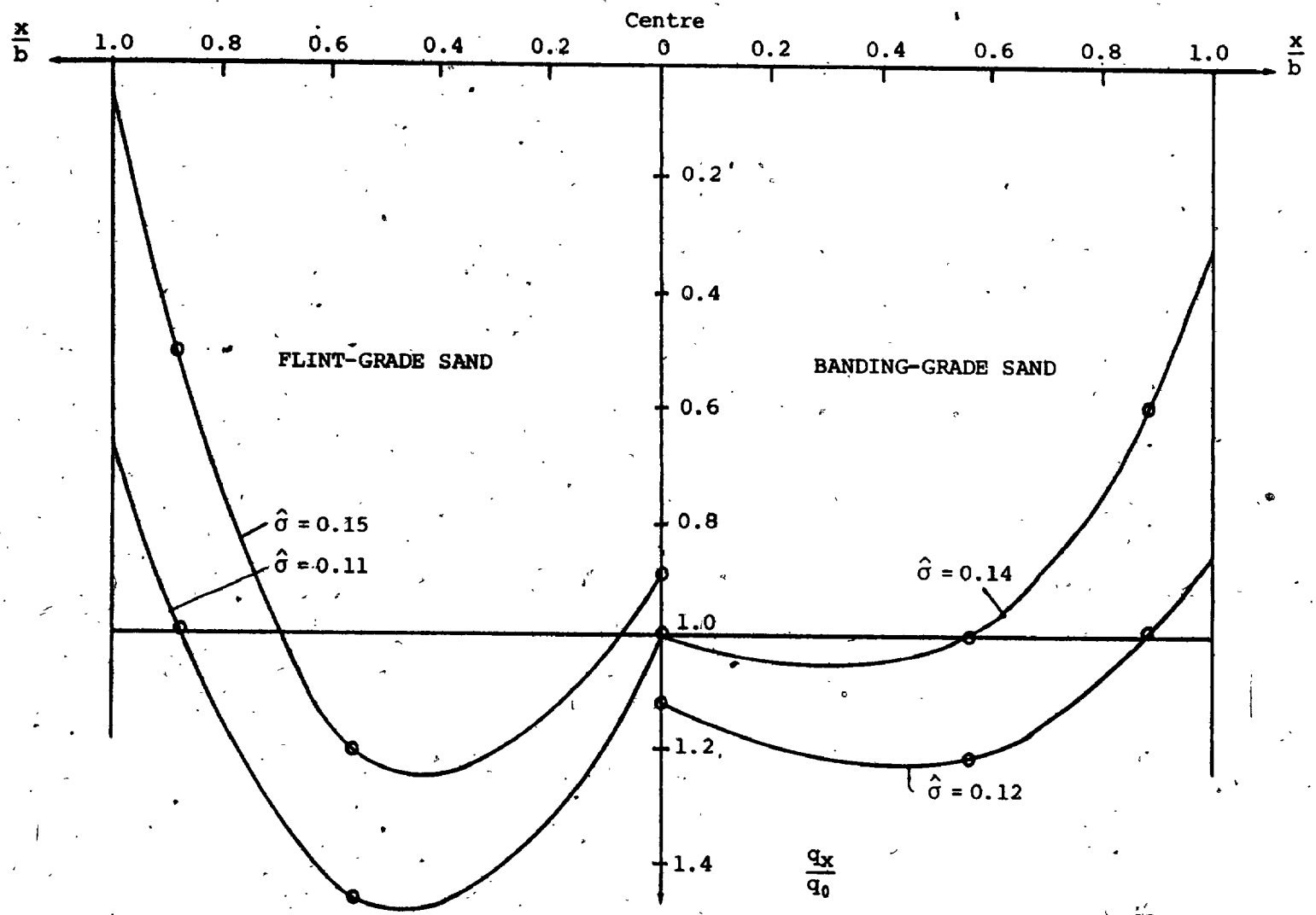

FIGURE 4.5

Summary of Highs and Lows During Second Load Cycle

The contact stress distribution presented will be applicable to any region A-A, B-B or C-C of Figure 3.1, since the variations along D-D, E-E or F-F were marginal. The small variations that occurred were taken into account by taking an average at each of three regions. In the "centre" region where the ratio of the distance x from the centre to half width b is equal to zero, the output of three pressure transducers can be averaged. At x/b equal to 0.56, hereafter called the "intermediate" region, five pressure transducers can be averaged. Similarly, five more pressure transducers can be averaged at the "edge" where x/b is equal to 0.88 (see Fig. 4.6).

A check can be made on the equilibrium of the system by comparing the measured contact stress beneath the plate with the applied stress. Each pressure transducer output represents the contact stress at a "point", so, strictly speaking, the total reaction stress acting beneath the plate cannot be determined unless assumptions are made regarding the contact area the pressure transducer is "assigned". Each pressure transducer was given a weighted percentage of the total area, as shown in Figure 4.7. For each stress increment, the output of each pressure cell was multiplied by its weighting factor and the sum of all these values was divided by sixteen, the number of pressure cells. This average value was then compared with the applied stress. A simple technique of summing all the pressure transducer outputs without using weighting factors produced an average contact stress that was within one percent of the previous method. This is due to the nearly uniform average contact stress observed in the sand tests, and may not be applicable when high stress gradients occur.

The relationship between reaction load and applied load appeared

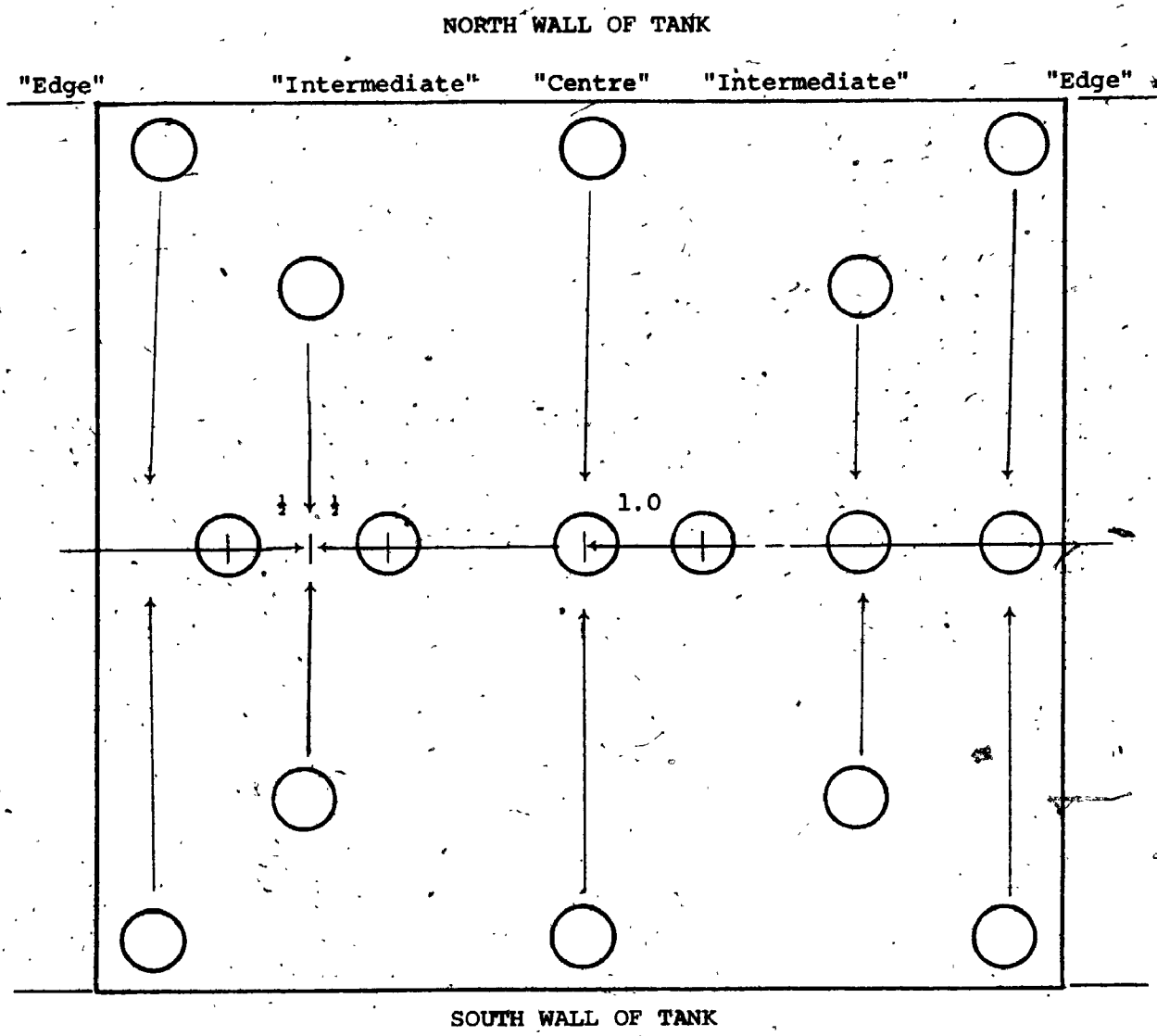

FIGURE 4.6

Method of Averaging of Contact Stresses for Plate on Sand

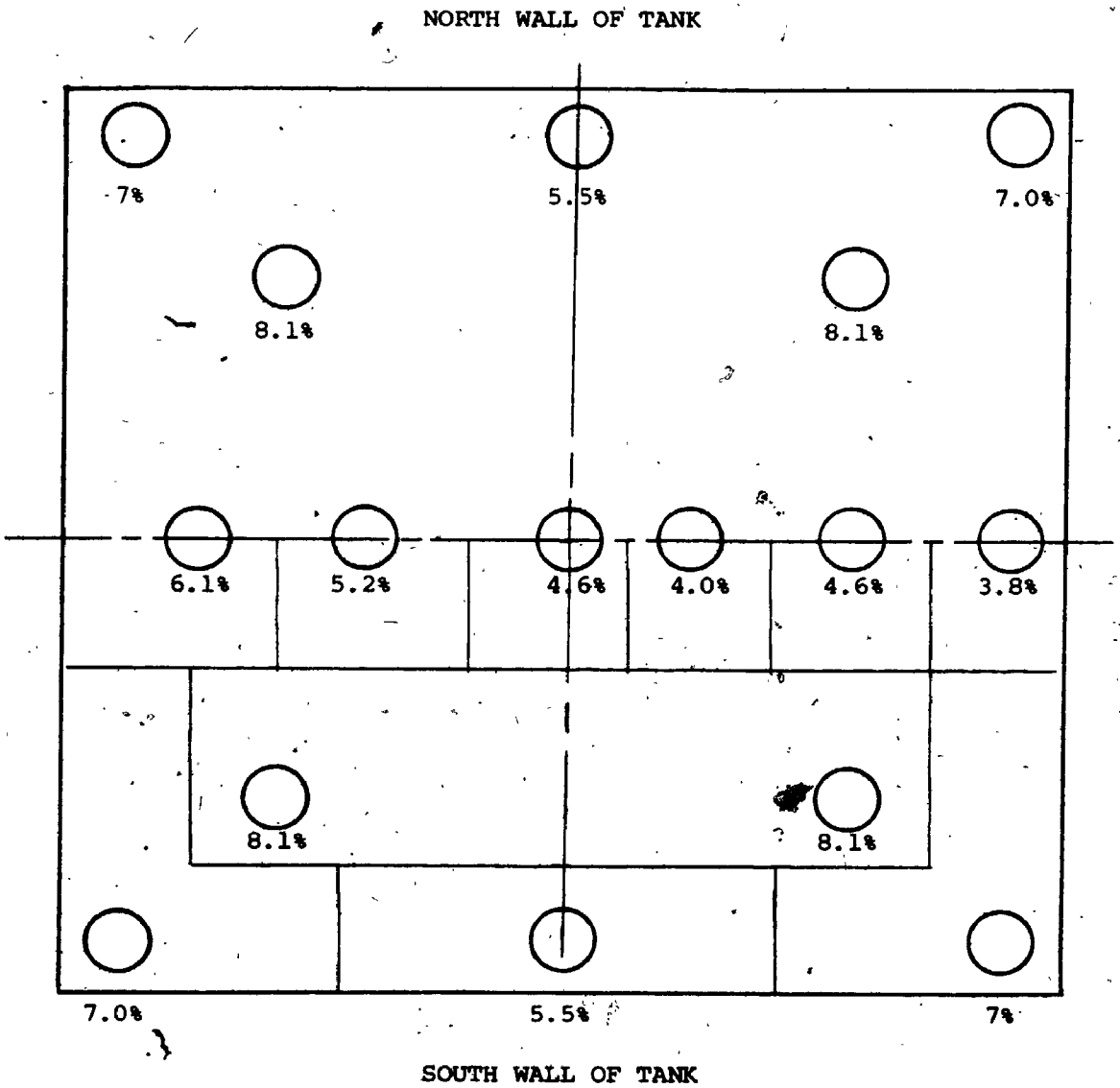

FIGURE 4.7

Weighted Percentage of Area on Plate for Each Pressure Transducer - Sand Tests

Result — Calculated Average Contact Stress was the Same as if Each Pressure Transducer had Equal Area

to depend on the magnitude of applied stress. For example, at a stress of 60 kPa the average reaction load may be 120 percent of the applied load but at 146 kPa the percentage may decrease to 107 percent. Increasing the applied stress tended to reduce the percentage of applied load measured by the contact pressure transducers. Since there was a wide variation in percentages between one test and another, and at each stress level, it was decided to *normalize* the results by dividing each pressure cell output by the average *measured* stress instead of applied stress. This method allows a comparison to be made between one experiment and another in terms of the average, but does not change the shape of the contact stress distribution.

Table 5 summarizes the results of all eight tests on sand. For each test the output was analyzed by the averaging process described. There is a large variation between one test and another, even for the same type of sand. For this reason another average was made using the Time Sharing Library program at Carleton University called POLYFIT.TSL. The normalized contact stresses and positions were input into the program, and a "best-fit" polynomial equation was generated, together with statistical data concerning the coefficient of multiple determination (R^2), standard error, $\hat{\sigma}$, and the sum of the squares of error. In all cases the highest R^2 value occurred when a quadratic equation was used, but in many cases a linear equation was comparable.

Figure 4.3 shows the computed best-fit curves of contact stress distribution occurring at a maximum stress of 147 kPa for both Flint-grade and Banding-grade sand. There is a trend towards slightly higher stresses at the "edge" than the "centre" for the first load cycle. For the second and subsequent cycles there is a redistribution of contact

TABLE 5

SUMMARY OF CONTACT STRESS DISTRIBUTIONS FOR SAND

(RESULTS OF EIGHT TESTS AVERAGED AND BEST QUADRATIC LINE COMPUTED FROM POLYFIT.TSL)

TEST	EDGE	INTER-MEDIATE	CENTRE LINE	EQUATION OF QUADRATIC LINE	R^2	STANDARD ERROR	SUM OF SQUARES OF STD. ERROR
(A) Maximum Load (147 kPa)							
1st cycle FLINT	1.065	1.036	0.895	$y = 0.89 + 0.35x - 0.18x^2$	0.51	0.09	0.048
2nd & 3rd FLINT	0.995	1.085	0.915	$y = 0.91 + 0.67x - 0.66x^2$	0.99	0.00	0.0002
1st cycle BANDING	1.046	0.946	1.073	$y = 1.07 - 0.56x + 0.61x^2$	0.66	0.04	0.018
2nd & 3rd BANDING	0.990	1.005	1.025	$y = 1.02 - 0.02x - 0.01x^2$	0.64	0.02	0.0007
(B) Range of Values Throughout First Cycle Loading							
Highs — FLINT	1.066	1.285	1.062	$y = 1.06 + 1.08x - 1.23x^2$	0.44	0.14	0.13
Lows — FLINT	0.6[illegible]6	1.036	0.844	$y = 0.84 + 1.33x - 1.77x^2$	0.67	0.13	0.11
Highs — BANDING	1.221	1.159	1.052	$y = 1.05 + 0.18x + 0.00x^2$	0.14	0.19	0.44
Lows — BANDING	0.782	0.920	0.839	$y = 0.83 + 0.51x - 0.65x^2$	0.07	0.22	0.60
(C) Range of Values Throughout Second Cycle Loading							
Highs — FLINT	0.995	1.464	0.984	$y = 0.98 + 2.33x - 2.64x^2$	0.84	0.11	0.09
Lows — FLINT	0.503	1.214	0.883	$y = 0.88 + 2.38x - 3.19x^2$	0.83	0.15	0.15
Highs — BANDING	0.989	1.223	1.116	$y = 1.11 + 0.77x - 1.04x^2$	0.45	0.11	0.17
Lows — BANDING	0.592	0.998	1.003	$y = 1.00 + 0.79x - 1.43x^2$	0.71	0.13	0.22

stress with a reduction at the "edge" and a corresponding increase in the "intermediate" and "centre" regions. This is more noticeable in the case of the Flint-grade sand.

It has been observed that the magnitude of the load, relative to the bearing capacity, has a marked influence on the contact stress distribution (see, for example, Murzenko, 1965; Ho and Lopez, 1968; Harti-Kainen, 1973). The stress applied in all the tests in this study can be considered to be within the "working" stress range. It was felt that within this range the shape of the contact stress distribution would remain similar. For this reason the normalized contact stress distribution of all the load increments during the first load cycle is presented in Figure 4.4, and for the second load cycle in Figure 4.5. For each test the minimum and maximum normalized contact stress observed at each region was recorded, as summarized in Table 5. These minimum and maximum values were then input into the POLYFIT.TSL program as before, and the best-fit curve was computed. By plotting the minimum and maximum contact stress curve a band is produced. The probability that the contact stress distribution lies within these band limits has not been computed, and the amount of data may be insufficient for statistically significant results, but it does illustrate the variability of the distributions that may occur. It should be noted that within this band equilibrium must hold, such that the area under the curve equals the applied stress.

When comparing the first and second cycles of Figures 4.4 and 4.5, it is observed that the contact stress is lower at the "edge" and higher in the "centre" and "intermediate" regions upon subsequent recycling of the load. Similar effects have been observed by previous researchers

for rigid foundations resting on compact and dense sands (see Murzenko, 1964; Ho and Lopez, 1968; Hartikainen, 1973). This effect can be explained if it is noted that the initially dense sand beneath the footing has a tendency to become less dense at the edges when a load is applied. Since the contact stress is dependent on the density of the soil, the contact stresses become higher in the centre region. If the soil was initially in a loose state, the application of the load would result in the sand becoming more dense directly below the plate and the contact stresses would be higher at the edges (see Krivorotov, 1976).

Two gradings of sand were used in these experiments to determine if the size of the grain affected the contact stress distribution. The results are not strictly comparable because the in-place relative densities of the two sands were not identical. With the relatively less dense Banding-grade sand the average edge contact stress tended to be lower than the Flint-grade results at the maximum stress of 147 kPa, but the difference is marginal.

One factor that should be considered in comparing the two grades of sand is the effect on the pressure transducer response. The pressure transducers were calibrated using a fluid pressure applied to the sensitive diaphragm 7.6 mm in diameter (see Plate 4). The average diameter, D_{50}, of the Flint-grade sand was 0.5 mm, and 0.2 mm for the Banding-grade sand. Hence there were, on the average, over six times as many soil grains in contact with the sensitive face when Banding-grade sand was used instead of Flint-grade. Since the contact of more grains would tend to produce a more uniform stress application to the pressure transducers, it was expected that there would be less scatter in the tests performed on Banding-grade sand, but the standard deviations of the

contact stress distributions are similar, as shown in Figures 4.4 and 4.5.

4.3 *Preliminary Test of Plate on Clay*

The opportunity to test the performance of the steel plate and pressure cells was made available at the start of the test program. A 1.2-m square rigid box had been filled with compacted clay to a depth of 0.4 m. The material was the same "Arnprior" clay used in later tests, except the method of compaction varied and the moisture content was considerably lower (28 to 30 percent). Instead of extruding the clay through a pug mill, the clay had been broken up into particles to pass a No. 4 sieve, and was then tamped in layers in the container. An experiment was performed by Moore (1977) for the case of a centrally loaded flexible plate (dimensions 360 mm × 360 mm) resting on cohesive soil. Since this experiment caused only minor disturbance to the bed of clay, the 50 mm × 378 mm square rigid steel plate was placed in the centre of the tank and loaded by means of the cantilever beam. Recordings were made for the load cell, sixteen pressure cells and plate deflections at five locations. Plate 7 illustrates the test set-up.

The load-deflection curve is shown in Figure 4.8, and the contact stresses across all diagonals are shown in Figures 4.9 and 4.10 at loads of 145 kPa and 200 kPa respectively. The initial load increments were applied in about ten-minute intervals, and the maximum load was left on for about four hours. Figure 4.8 shows some consolidation settlement taking place, but the measured contact stresses did not vary more than 5 or 10 kPa during this time.

Although only intended as a trial run, the results proved

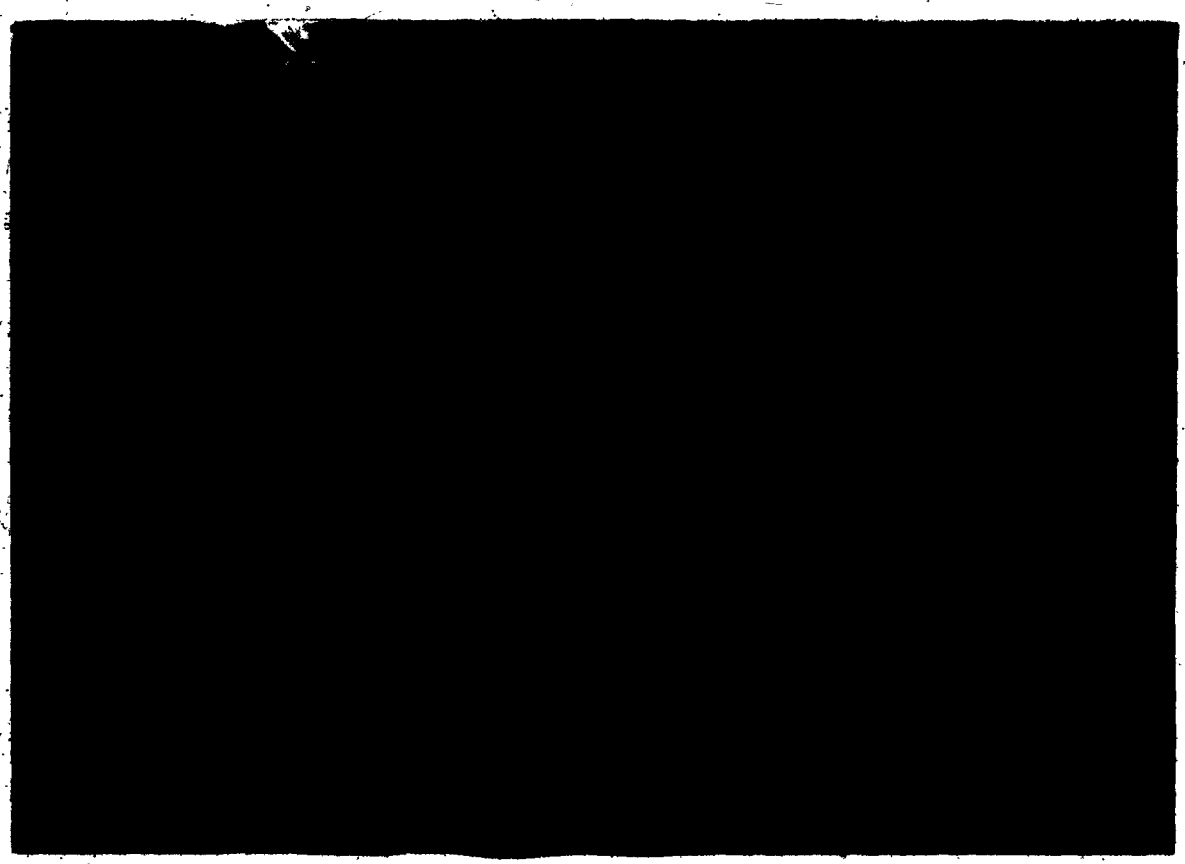

PLATE 7

Preliminary Test on Clay Layer

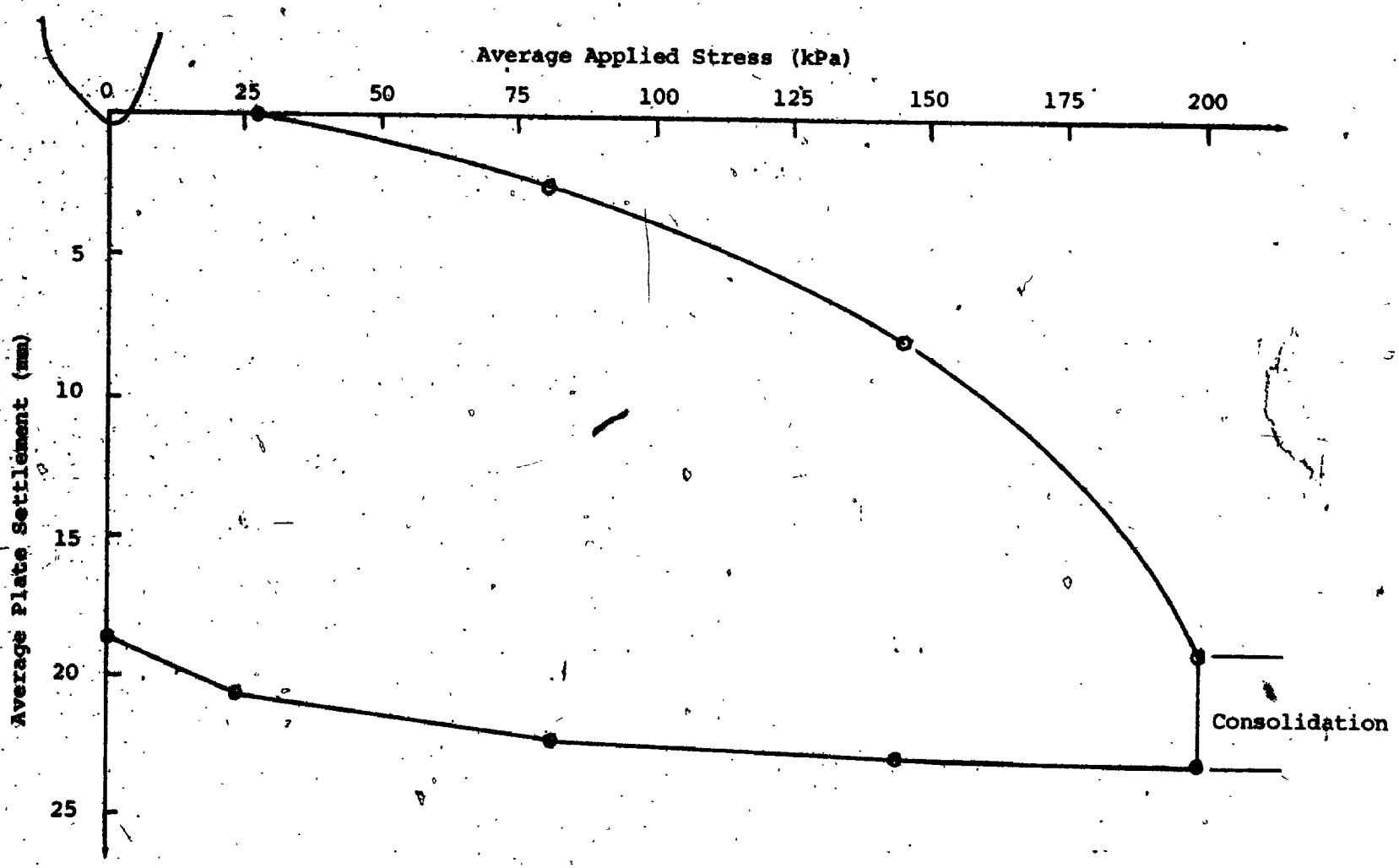

- FIGURE 4.8

Graph of Applied Stress versus Settlement for Preliminary Test on Clay

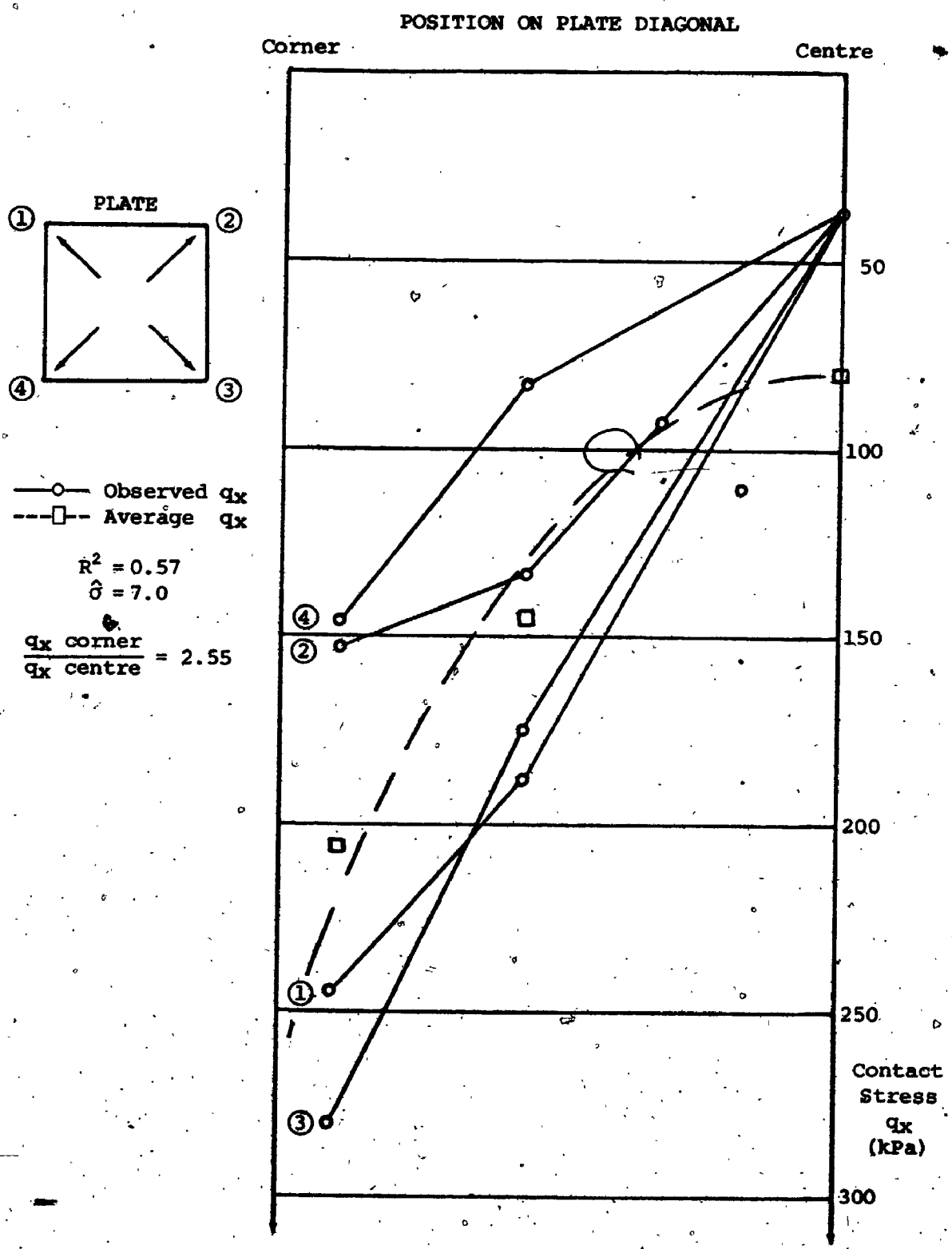

FIGURE 4.9
Contact Stress Distribution for Preliminary Test on Clay (q_0 = 145 kPa), Three-Dimensional Test Bed

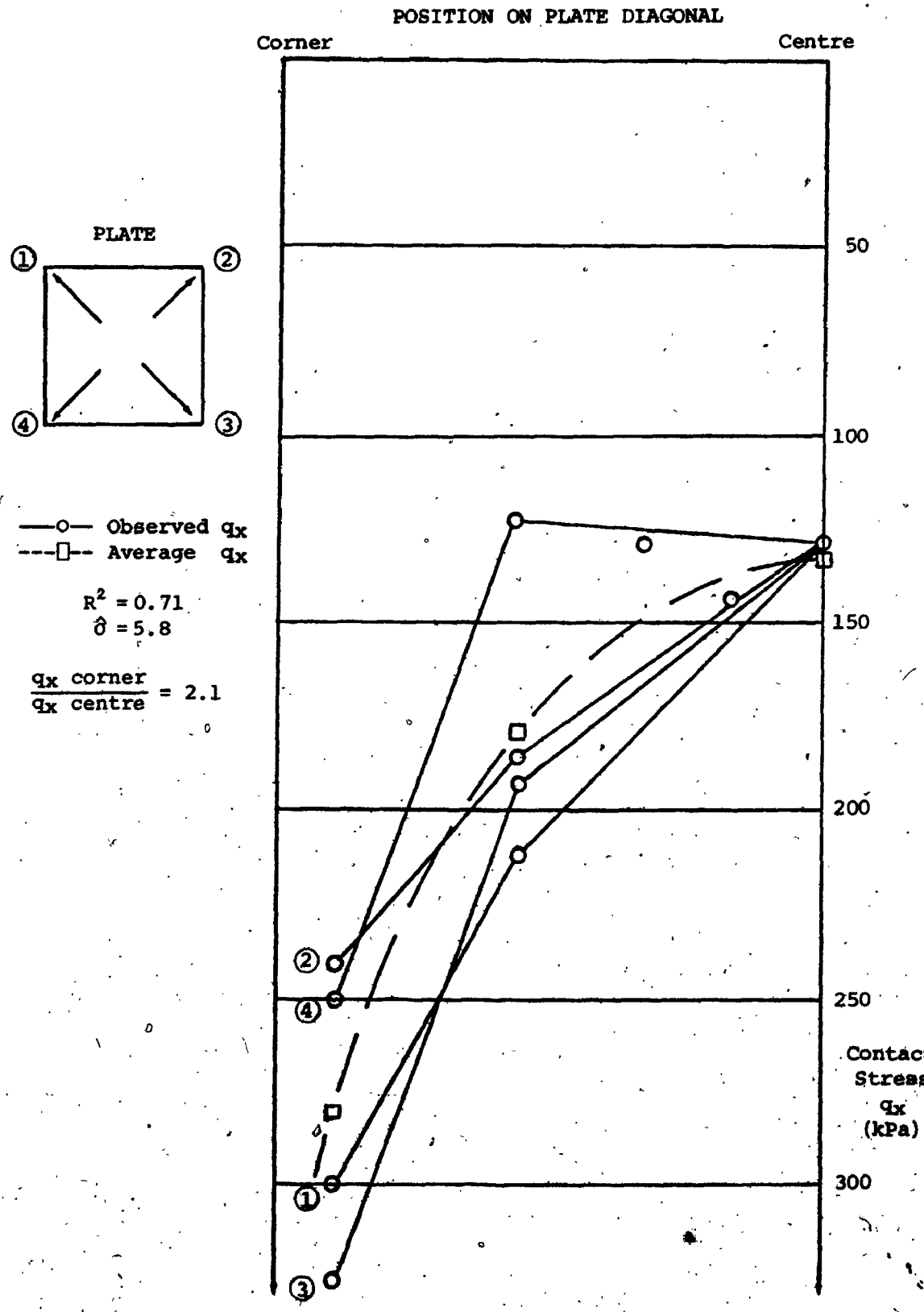

FIGURE 4.10
Contact Stress Distribution for Preliminary Test on Clay (q_0 = 200 kPa), Three-Dimensional Test Bed

encouraging. It can be seen that the contact stresses at the corners are substantially higher than at the centre region, but there is a relatively large variation at any one location. If the averages are plotted, the trend is that the corner contact stresses are over twice the centre region value. At a stress of 145 kPa this ratio of corner-to-centre contact stress is 2.6, but at 200 kPa the ratio is reduced to 2.1. In relation to the bearing capacity, these loads are approximately 40 percent and 60 percent respectively of the ultimate.

This test proved useful in outlining some of the problems that could be encountered in the main long-term test. It showed the importance of ensuring that the surface of the clay bed be level and plane, because at the initial loading stages there were local regions that registered substantially larger contact stresses than their equivalent locations on the test plate. These variations may have been due in part to the non-homogeneity of the clay bed or to the non-uniform settlement of the plate (up to 5 percent deviation from average). It also showed the necessity of using a recording system that was capable of reading all the instruments in a short period of time and printing the results on paper.

The test did not measure the deflections adjacent to the plate, nor was the effect of reloading the test plate investigated. The shear strength of the clay was approximately 50 kPa, with an average moisture content of about 28 percent. The effect of cohesion on the contact stress distribution can only be compared if several more tests are performed with different soil cohesion values.

4.4 *Plane Strain Test*

4.4.1 *Surcharge*

As explained in Section 3.3.5 it was possible that the method of placement of the clay in the plane strain tank produced small air cavities in the clay since the extrusion process produces cylindrical clay specimens (see Plate 8). A surcharge of 42 kPa was applied uniformly over the top of the test tank for a period of seven days. This was accomplished by placing a cotton cloth over the entire clay surface, followed by a uniform 10-mm layer of Flint-grade sand, 12.7-m thick plywood and two W8 x 24 wide flange beams. Using the lever arm of the loading apparatus, a force of 23.8 kN was applied to the top centre region of the test tank. The rigid steel beams ensured uniform settlement over the entire surface.

The average settlement was computed from four ± 76-mm displacement transducers positioned over the surface of the surcharge. A graph of the settlement versus load is given in Figure 4.11, and settlement versus time is given in Figure 4.12. The "immediate" compression of the top surface was 21.3 mm, due to the reduction in the air cavities. Since the surcharge loading resembles a one-dimensional compression test with Poisson's ratio equal to 0.5, there should be no immediate elastic settlement. The total surface consolidation amounted to 8.66 mm during the seven-day period. Upon unloading, the immediate rebound was 3.7 mm, followed by an expansion of 3.1 mm due to swelling (or delayed rebound caused by viscous drag on the side walls). The immediate rebound modulus E_r was 10,700 kPa, but if the total rebound (occurring within a 24-hour period) is taken into account, the secant modulus reduces to 5800 kPa. The actual E probably lies somewhere between the two values.

PLATE 8

"Arnprior" Clay Being Extruded from Pugmill

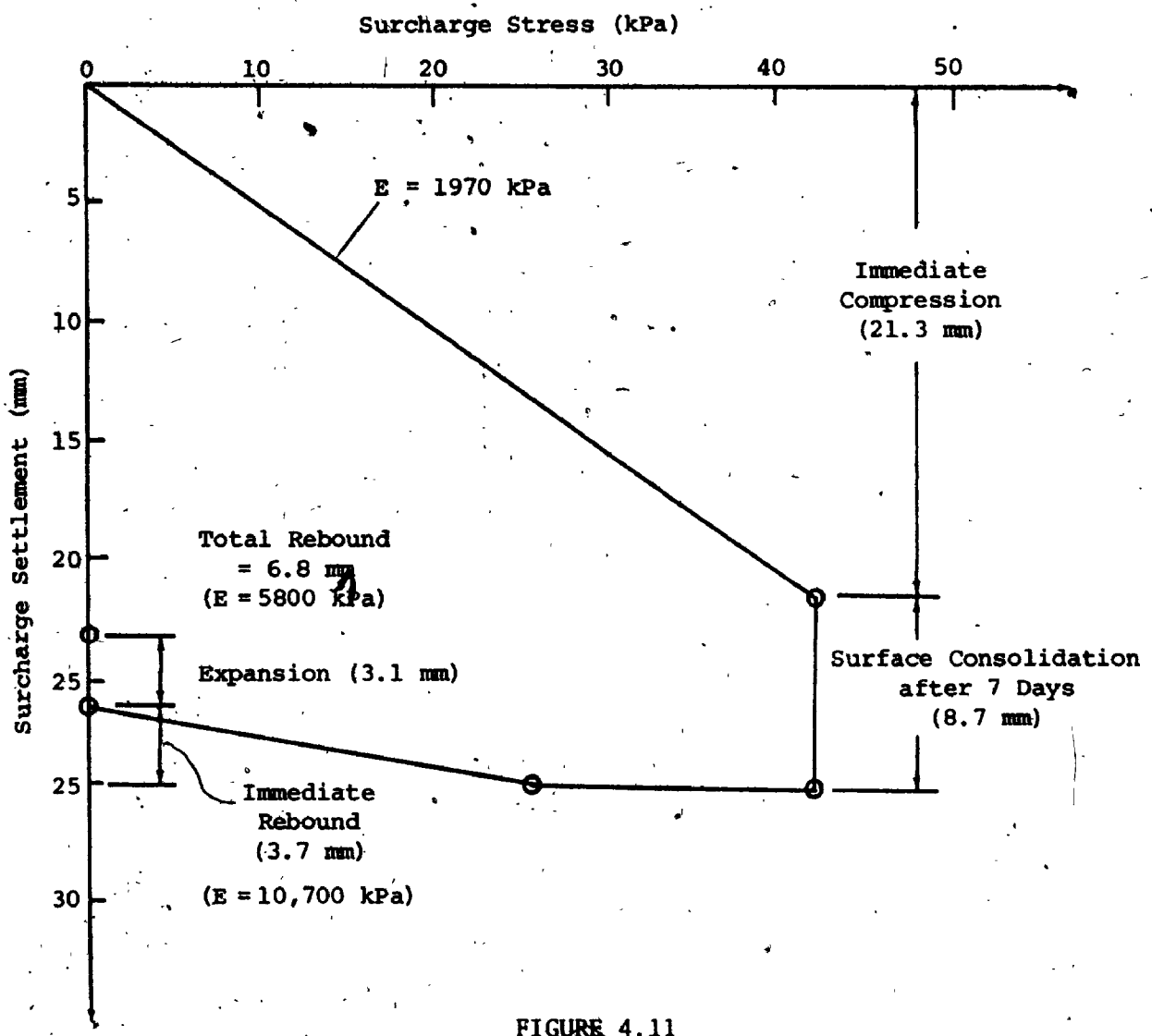

FIGURE 4.11

Settlement versus Stress due to Surcharge Applied before Plane Strain Test

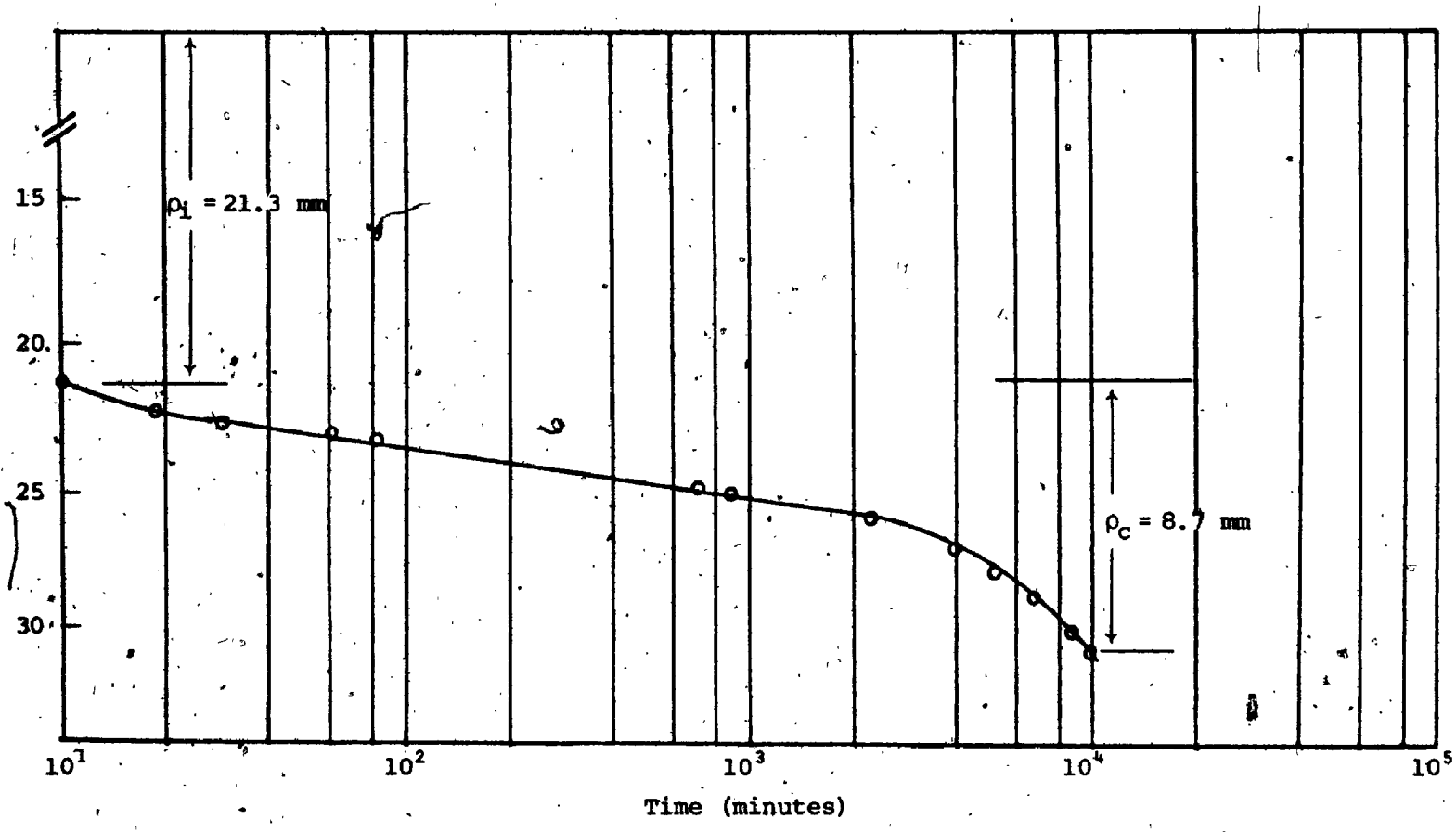

FIGURE 4.12

Graph of Surcharge Deflection versus Time in Plane Strain Test (q_0 = 42.1 kPa)

Applications of the surcharge enabled a check to be made on the functioning of the pore water pressure apparatus (see Plates 9 and 10). Since the pore pressure parameter B was found to be very close to 1.0, the pore pressures were expected to increase by the amount of the surcharge. The actual pore water pressure increase at all ten piezometer locations is shown in Figure 4.13 as a linear function of time. The time required to reach a peak value of pore water pressure varied from a few minutes to two hours, which may signify the presence of air in some of the piezometers.

The "immediate" peak increase in pore water pressure for all the piezometers is shown in Table 6, with the average maximum for the piezometers below centreline being 32.3 kPa, and 30.3 kPa for the piezometers beneath the edge. These represent 77 percent and 72 percent of the applied stress, for the "centreline" and "edge" piezometers, respectively.

There are several possible reasons for the pore water pressure response being lower than expected. Friction along the side walls would tend to reduce the stress transfer to the soil in the lower layers, but if this is true there should have been a clear gradient in the pore pressure distribution with depth. The assumption of one-dimensional compression requires that there be no lateral expansion of the side walls, but it was observed that at the top of the test tank the walls moved outwards about 0.25 mm when the surcharge was applied. This would cause the pore pressure increase to be lower. Probably the most significant cause of the lower pore water pressure response can be attributed to the measuring apparatus. Because 100 percent saturation could not be achieved, air may enter the piezometer cavity, and the pressure being

PLATE 9

Piezometer Placed in Clay

PLATE 10

Six-Chamber Pore Water Pressure Measuring Device

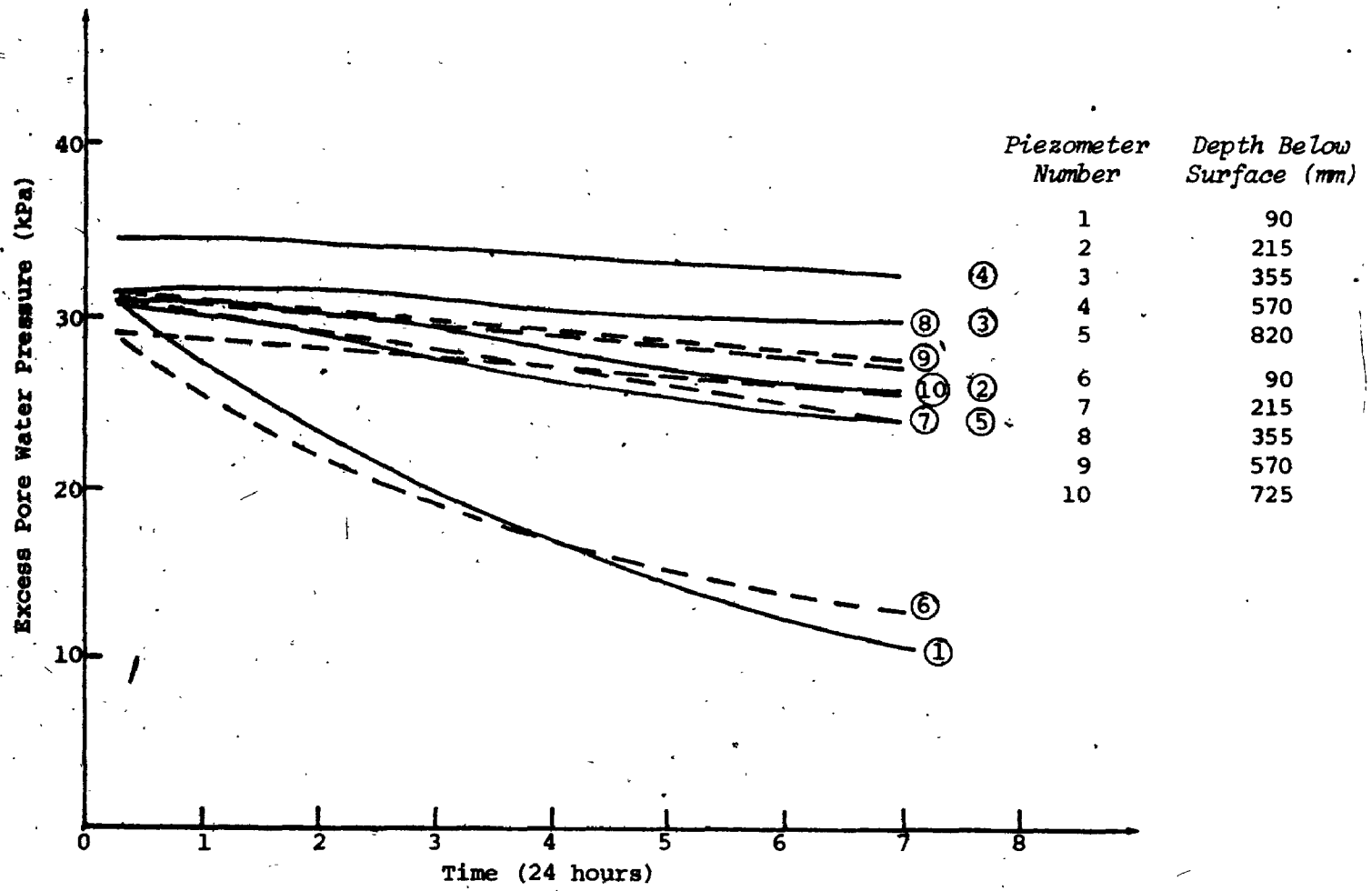

FIGURE 4.13
Centreline and Edge Pore Water Pressure Dissipation during Surcharge Loading of Plane Strain Tank

TABLE 6

IMMEDIATE PORE WATER PRESSURE OBSERVATIONS

PIEZOMETER NUMBER	z/b	SURCHARGE		PLATE LOAD Δu INITIAL (kPa)	IMMEDIATE Δu INCREMENT Δq_0 = 52.2 kPa	Δu MAXIMUM INCREMENT (kPa)	$\frac{\Delta u_{max}}{\Delta q_0}$
		MAXIMUM Δu (kPa)	Δu DISSIPATED (kPa)				
Centreline							
1	0.47	34.2	24.9	5.2	1.6	18.4	0.35
2	1.13	31.4	5.6	7.0	25.3	25.3	0.48
3	1.87	31.7	2.0	10.8	11.1	15.9	0.30
4	3.0	34.9	2.3	17.5	10.4	10.7	0.20
5	4.3	29.5	5.8	10.4	1.0	4.3	0.08
Average		32.3					
Edge							
6	0.47	29.6	17.8	0.3	7.5	7.5	0.14
7	1.13	31.3	8.1	0.8	12.8	14.9	0.29
8	1.87	30.6	3.2	3.5	13.2	14.4	0.28
9	3.00	30.4	2.9	5.7	14.1	14.2	0.27
10	3.80	29.4	3.4	5.1	13.5	13.6	0.26
Average		30.3					

measured by the transducers is a combination of the pore air and pore water pressure.

In Figure 4.13 the pore water pressure is plotted as a function of time for each piezometer location. As expected, the piezometers at the top of the clay layer dissipated the excess pore pressure sooner than the deeper piezometers because the drainage path was shorter. The time for 90 percent dissipation of the pore pressure in the bottom of the test tank was estimated to be several months, and unless this amount of time was spent there would be a variation in soil properties with depth. The surcharge was removed after seven days, before which some dissipation of pore water pressure in the top layer was produced, as shown in Figure 4.14. This graph provides useful information regarding the coefficient of consolidation, c_v, of the remolded clay. From Terzaghi's (1943) one-dimensional theory, the time factor is $T_v = c_v t/H^2$, which can be related to the degree of consolidation U. From the standard consolidation tests the total one-dimensional consolidation was estimated to be 56.0 mm (calculated on the basis of the observed excess pore water pressures). At the end of seven days the consolidation settlement was 8.7 mm, or 15.5 percent of the total predicted consolidation settlement. From Perloff (1975) the time factor, T_v, was given as 0.018. By assuming that the longest drainage path of the pore water pressure was equal to the thickness of the clay layer, the coefficient of consolidation was calculated to be 0.028 mm^2/sec. This value can be compared to the c_v values obtained from the standard one-dimensional consolidation tests, which ranged from 0.043 to 0.065 mm^2/sec. The lower observed c_v may, in part, be due to the sidewall friction in the tank reducing the rate of consolidation.

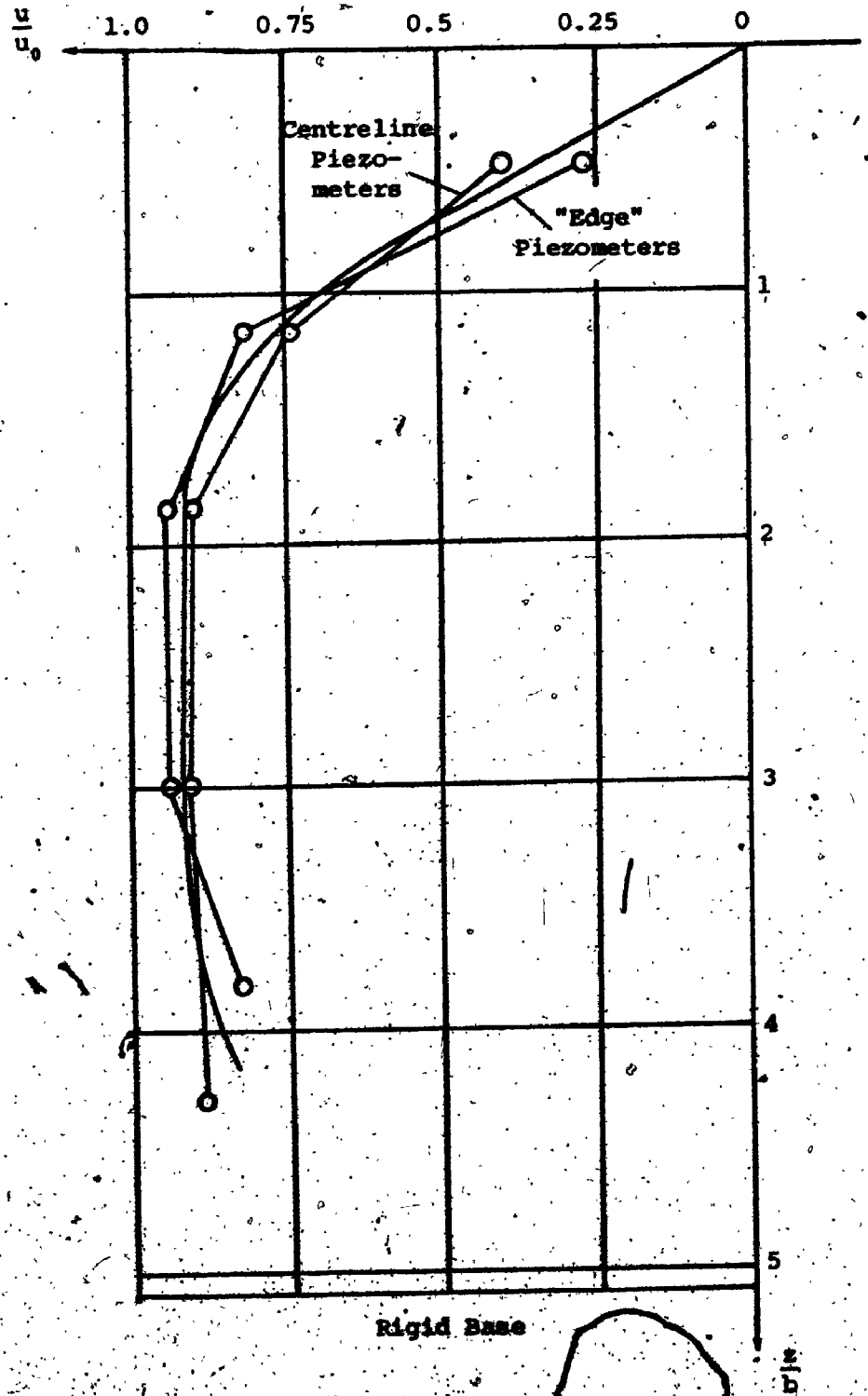

FIGURE 4.14

Degree of Pore Water Pressure Dissipation with Depth after Seven Days of Surcharge Loading of Plane Strain Tank

4.4.2 *Immediate Plate Settlement*

The application of load to the test plate in the plane strain experiment (see Plate 11) produced an immediate undrained settlement as shown in Figure 4.15. The stress was applied in three increments over a period of thirty minutes. For stresses less than the surcharge pressure of 42 kPa, the settlement resembles a reloading curve. When the load was applied in excess of this value, there was a substantial increase in slope of the curve. (This will be explained in terms of local yielding in the clay.)

A summary of several methods used to predict the immediate elastic settlement of a strip footing is presented in Appendix 12. This settlement is given in terms of the applied stress and Young's modulus. The general form of the immediate settlement equation is

$$\rho_i = \frac{q_o B}{E_u} (I)$$

as was introduced in Section 2.2.1. The amount of settlement is dependent on the method of determining the increase in stresses within the soil medium. The different methods give a range of influence coefficients, I, from 259 to 338 for the geometry used in the experiment, because different assumptions were made on the rigidity of the footing, and degree of roughness at the soil-foundation interface and the soil-rigid rough-base interface. With a flexible load the average settlement was computed by taking the average of the edge and centreline settlements. Taking the simple average of all the methods gives the relationship $\rho = 282\ q/E_u$ where ρ is in millimetres.

To predict the immediate undrained settlement an appropriate value of the undrained Young's modulus E_u must be chosen. This is usually

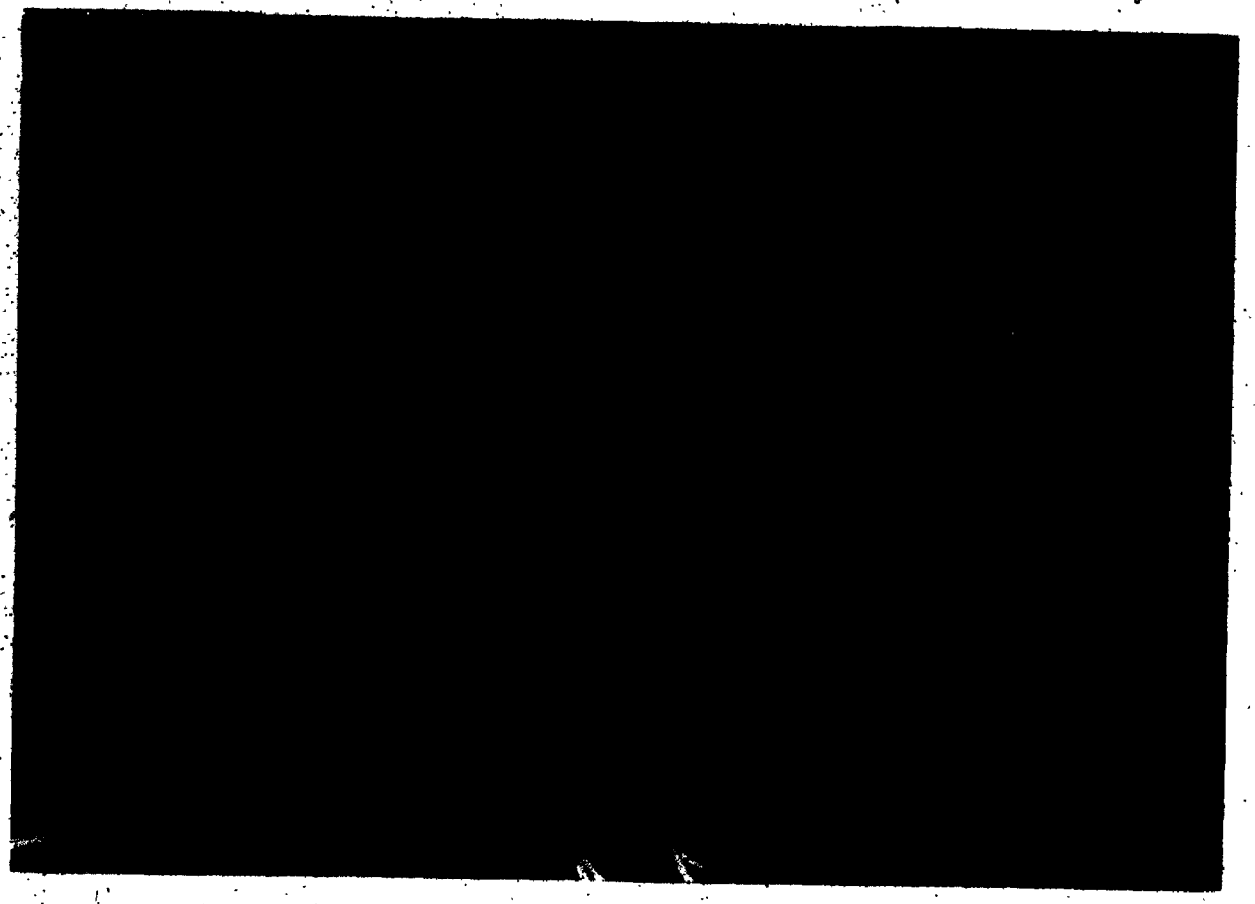

PLATE 11

Test Plate Installed over Plane Strain Apparatus
with Displacement Transducers in Place

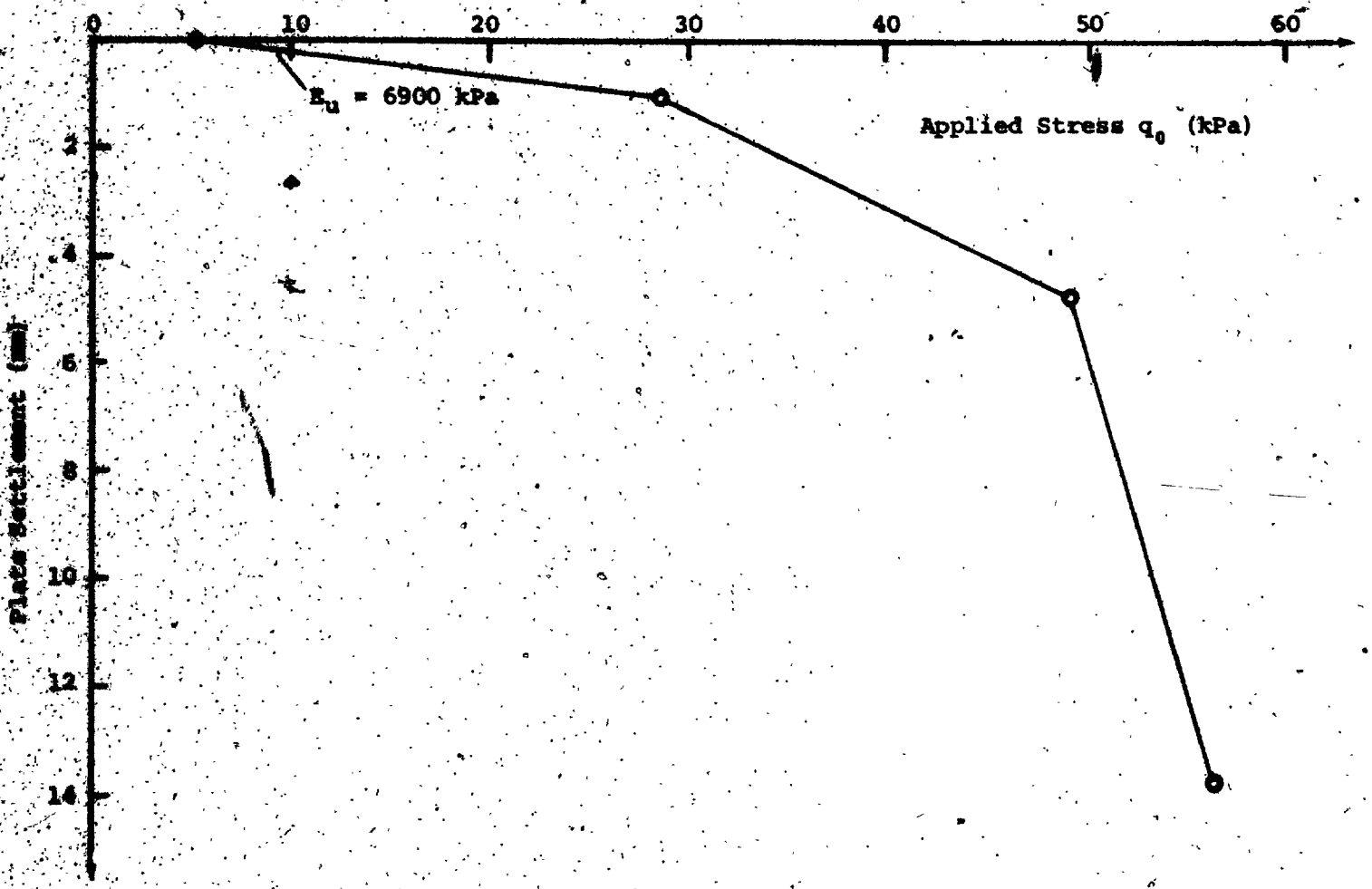

FIGURE 4.15

Initial Undrained Settlement during Plane Strain Test

determined in the laboratory from several variations of the triaxial test, but Figure 3.13 shows that the range of E_u values at any moisture content is not only large, but it also depends on the type of test and on the definition of E_u.

The undrained Young's modulus can be obtained from the immediate settlement of the clay during application of the surcharge in the plane strain test. (Using this value takes into account the presence of air cavities between the compressed extruded clay samples, and also any wall friction effects.) By assuming that the clay was strained equally throughout the layer, E_u was calculated as 1970 kPa. This is a relatively low value of E_u but is representative of a soft clay and compares with the values of E_u obtained from unconsolidated unconfined compression tests (Fig. 3.13). It also agrees with the E_u value obtained from the surcharge loading of the 0.3 m × 0.3 m × 0.4 m rigid box, which was 2500 kPa (see Fig. 4.16).

To compute the immediate settlement, a value of E_u was taken as 2000 kPa. When the surcharge was applied to the soil, the immediate surface deflection was 21.4 mm, followed by some consolidation settlement and then a rebound of 6.7 mm upon removal of the surcharge. (See Fig. 4.11.) Neglecting the consolidation settlement, the net permanent deflection was 21.4 - 6.7 = 14.7 mm.

The application of the surcharge compressed the soil and made it a stiffer material with a higher E_u value. During the plane strain test the loading of the plate at stress levels less than the surcharge pressure produced a load-deflection curve that resulted in a *rebound* curve (Fig. 4.15). When the surcharge stress was exceeded, the settlement increased substantially. It should be noted that the bearing capacity was

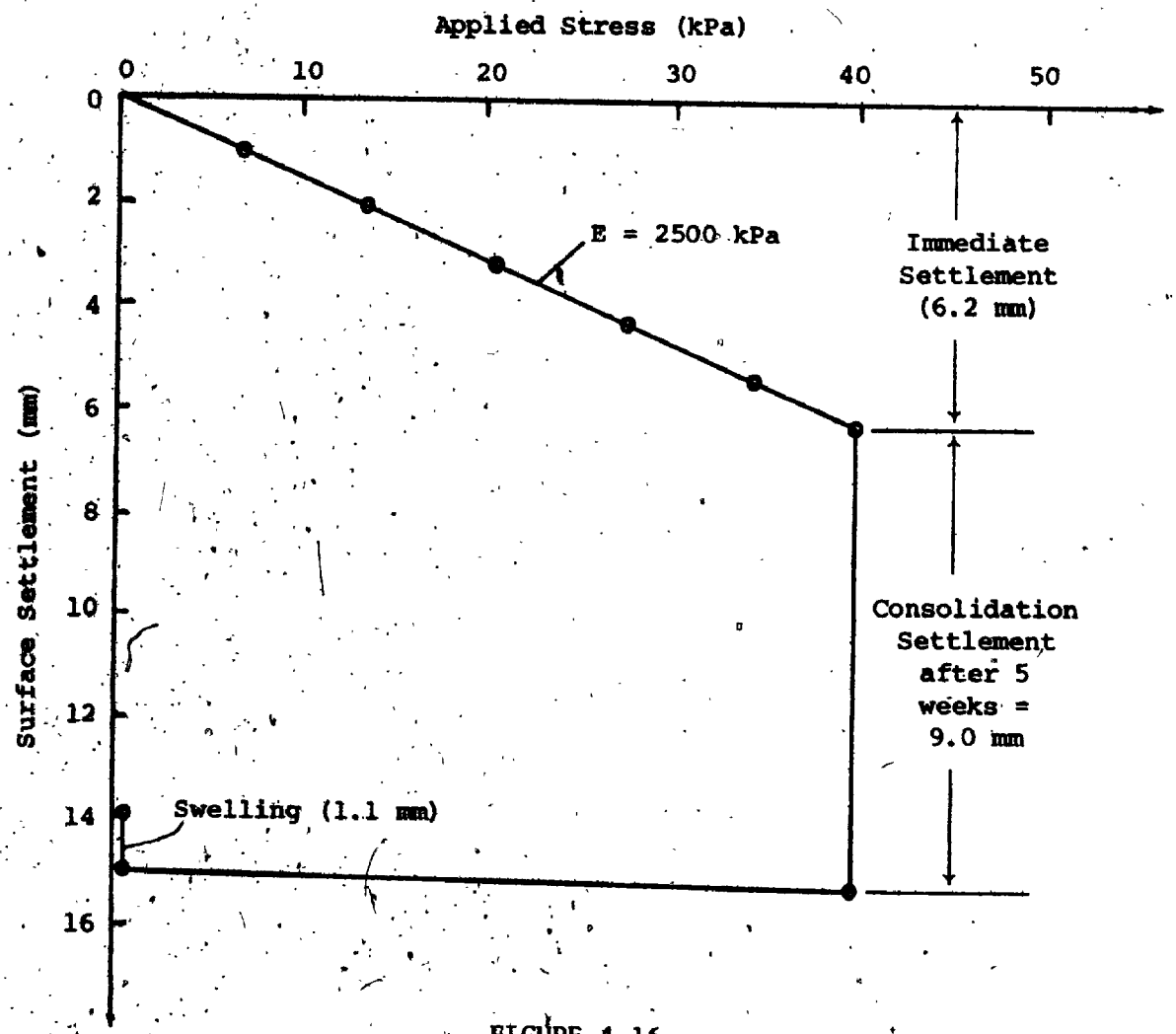

FIGURE 4.16

One-Dimensional Settlement in Control Box

estimated to be greater than 80 kPa (see Appendix 10). The problem can be explained if the soil was assumed to have a "virgin" E_u value as obtained during the surcharge loading.

In predicting the immediate settlement, reference is made to Figure 4.17. This figure takes into account the yielding of the soil as the applied stress approaches the bearing capacity and is based on the results of D'Appolonia *et al.* (1971). D'Appolonia *et al.* (1971) presented graphs relating S_R (the ratio of elastic settlement to actual immediate settlement with yielding) to the applied stress ratio, q_0/q_u, for various initial shear stress ratios, f, and layer depths, H/B. Figure 4.17 is derived from assuming a normally consolidated clay ($f = 0.75$) and $H/B = 1.5$. The analysis was for a uniformly loaded *flexible* strip footing; however, D'Appolonia *et al.* (1971) considered the results to be applicable to rigid strip footings.

If the surcharge had not been applied, the immediate settlement of the plate due to an applied stress equivalent to the surcharge stress (42 kPa) would have been ρ_1 in Figure 4.17. Assuming $E_u = 2000$ kPa, as obtained from the surcharge loading, $\rho_{el} = 282\ (42)/2000 = 5.9$ mm. This value represents the *elastic* settlement of the plate, assuming no yielding of the clay. To take into account yielding, the settlement ratio, $S_R = 0.53$, is employed. Hence $\rho_1 = 5.9/0.53 = 12.8$ mm. Similarly $\rho_2 = 23.9$ mm can be calculated for an applied stress of 52.3 kPa. For ρ_3 (see Fig. 4.17), which represents the reloading of the clay, reference is made to Figure 4.11 showing the surface rebound after the surcharge had been removed. The immediate secant E_u value was 10,700 kPa, but if the additional expansion of the soil with time is taken into account, E_u reduces to 5800 kPa. The actual value is probably in between these ranges,

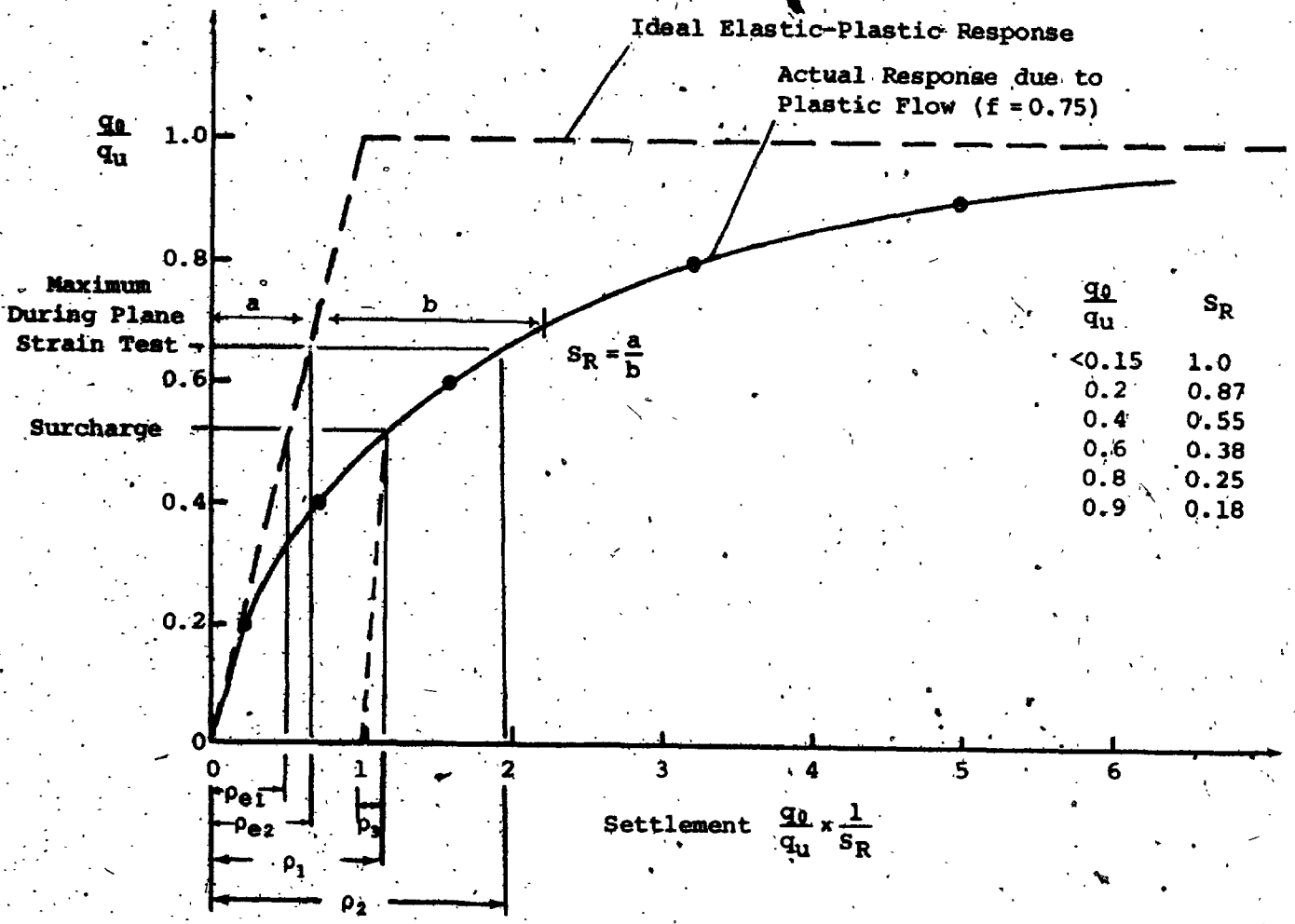

FIGURE 4.17
Idealized Load-Settlement Curve for Uniformly Loaded Flexible Strip Footing Resting on N/C Clay Layer with H/B = 1.5 (after D'Appolonia *et al.*, 1971)

so if these values are used as the bounds in the equation $\rho = 282\ q/E_u$, the predicted initial settlement, ρ_3, for a stress increment of 42 kPa will be 1.1 mm to 2.0 mm, assuming no plastic yielding of the soil.

By combining the above results, the total predicted immediate settlement of the plate during the plane strain test will be $\rho = (\rho_2 - \rho_1 + \rho_3) = (12.2$ to 13.1 mm). The observed immediate settlement due to the applied stress was 13.8 mm. This agreement is remarkable considering the difficulties in determining E_u and the uncertainties in the equation $\rho = 282\ q/E$. At higher stress increments, there was substantial local yielding, and to analyze the final total immediate settlement, the method of D'Appolonia *et al.* (1971) should be used. This method is highly sensitive to the degree of overconsolidation and estimate of bearing capacity.

4.4.3 *Surface Displacement Profile*

In addition to the settlement of the plate, the displacement of the surface adjacent to the plate was also observed during the initial loading stages for both the principal and subsequent tests. These results were compared with the theoretical case of a rigid strip footing resting on an isotropic homogeneous elastic half-space. The settlement of the surface relative to the centre of a *flexible* plate is well known (Gibson, 1967). For the case of a rigid plate, the technique employed in the calculation of contact stresses by superposition of uniform flexible loads also yields relative displacement influence factors. It is important to stress the fact that *relative* settlement is always used because the theory will give infinite settlement predictions at all points on the surface.

The relative settlement of the soil to the plate can be expressed as:

$$\rho_{soil} - \rho_{plate} = \frac{q_0 b}{2\pi G(0)} [I]$$

where q_0 = average uniform applied load
$G(0)$ = undrained shear modulus at surface
I = influence factor, dependent on distance from centreline to reference point.

A graph of influence factor (I) versus distance from centreline (x/b) is presented in Figure 4.18 for both the flexible and rigid cases. The relative surface displacement for both the principle test and second test is presented in Figures 4.19 to 4.22. More observations were made on the second test for small values of load, and it is here that the discussion will focus. The theoretical values of relative surface settlement were computed from a superposition technique given in Appendix 13. The results are plotted for each load increment and various values of undrained Young's modulus E_u (since the analysis has been for an incompressible medium $\nu = 0.5$ and $G = E/(2(1+\nu)) = E/3$).

The theory for an infinite strip predicts infinite surface displacement for all points, but the *shape* of the surface profile can be obtained. In Figure 4.20 with average load = 5.6 kPa, it can be seen that for $E_u = 6900$ kPa, there is good agreement between theory and observed relative settlement when $x/b < 1.75$. For $x/b > 1.75$ the surface does not deform, but the theory still predicts continuing displacement. For $E_u = 13,800$ kPa, there is agreement between the relative surface displacement at the end of the test tank ($x/b = 4.0$) for both the observed and theoretical calculations. For all other points with $x/b < 4.0$ there

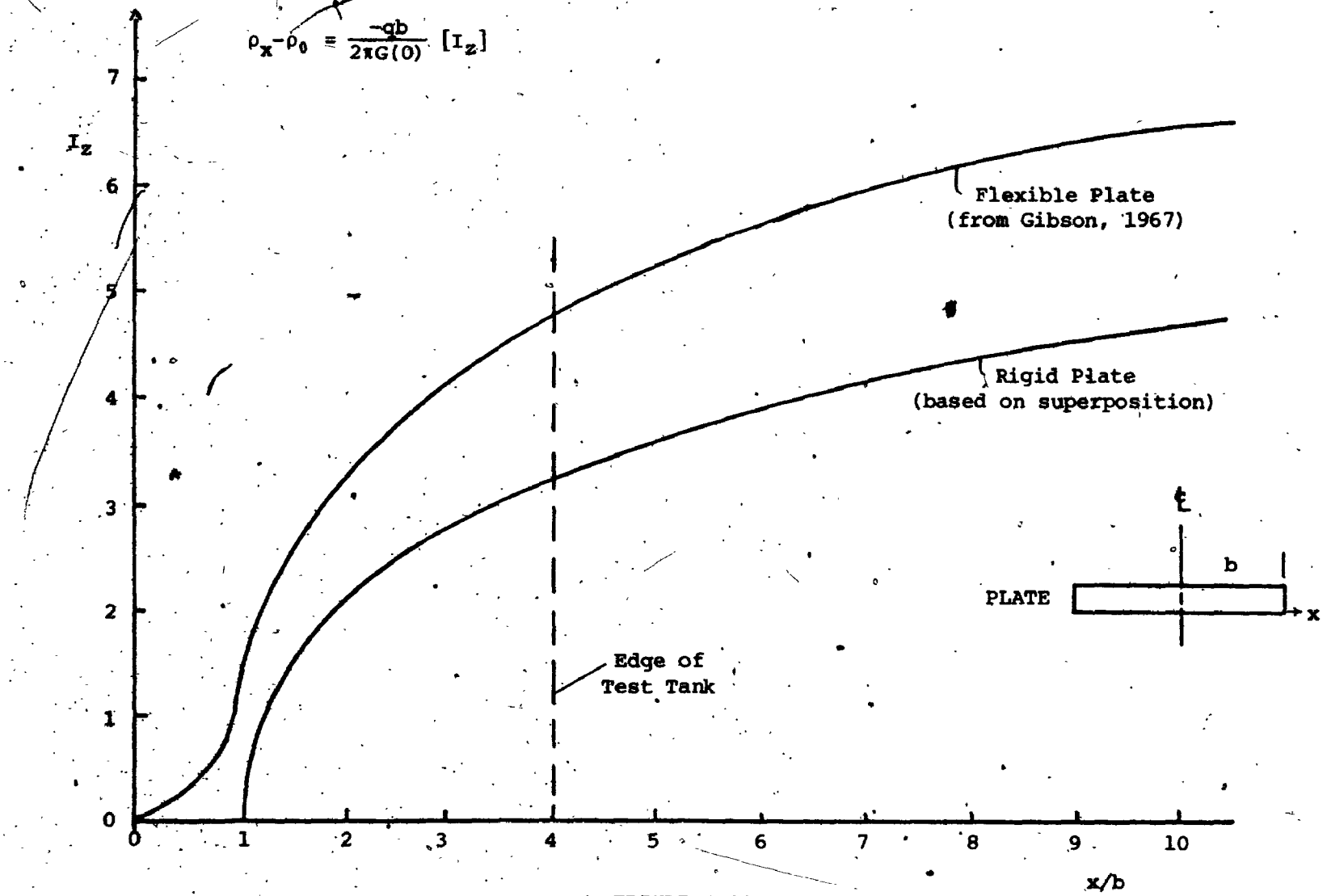

FIGURE 4.18
Surface Settlement Profile for Strip Footing

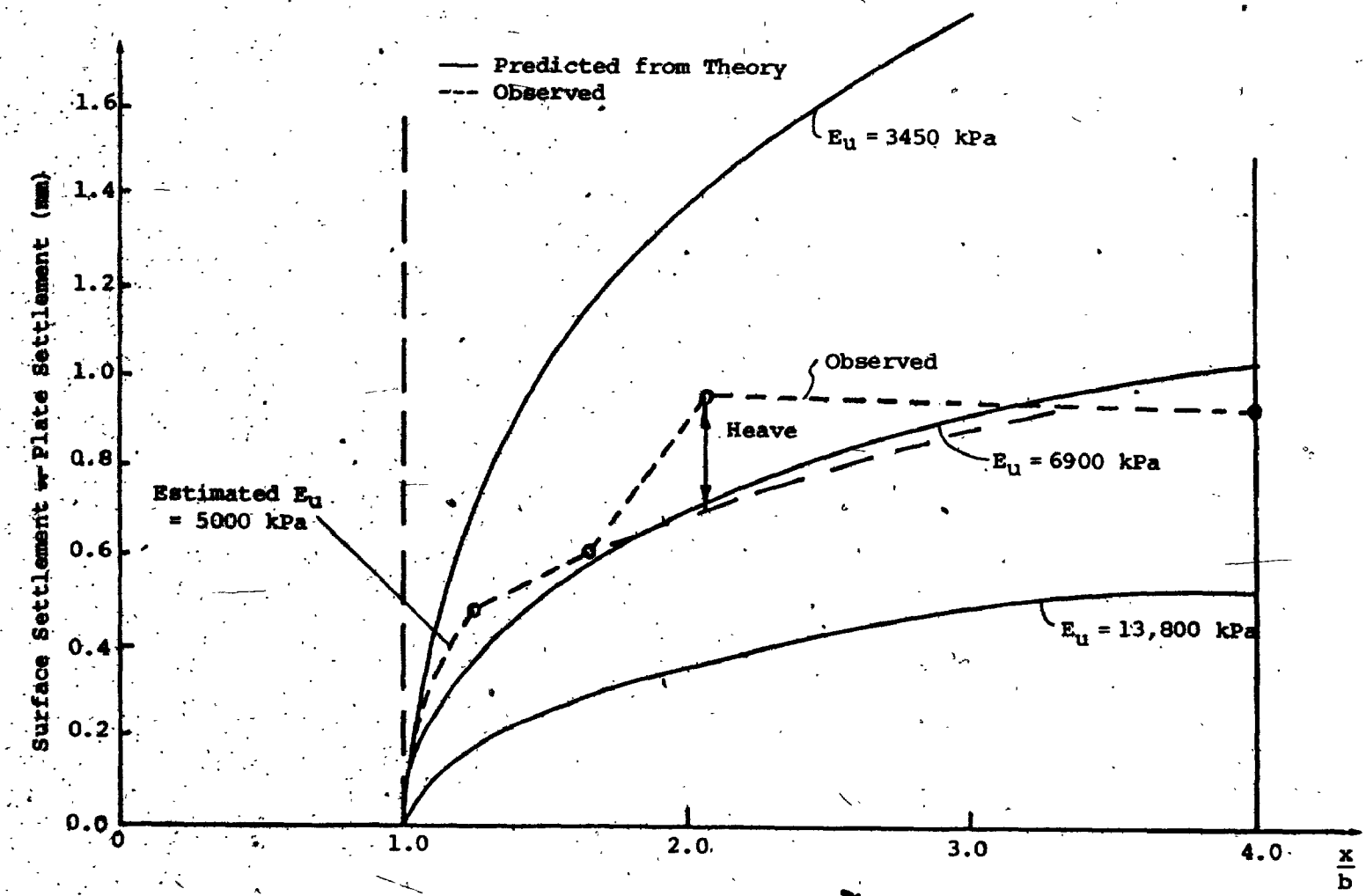

FIGURE 4.19
First Test on Clay, Surface Displacement Profile, Δq_0 = 24.6 kPa

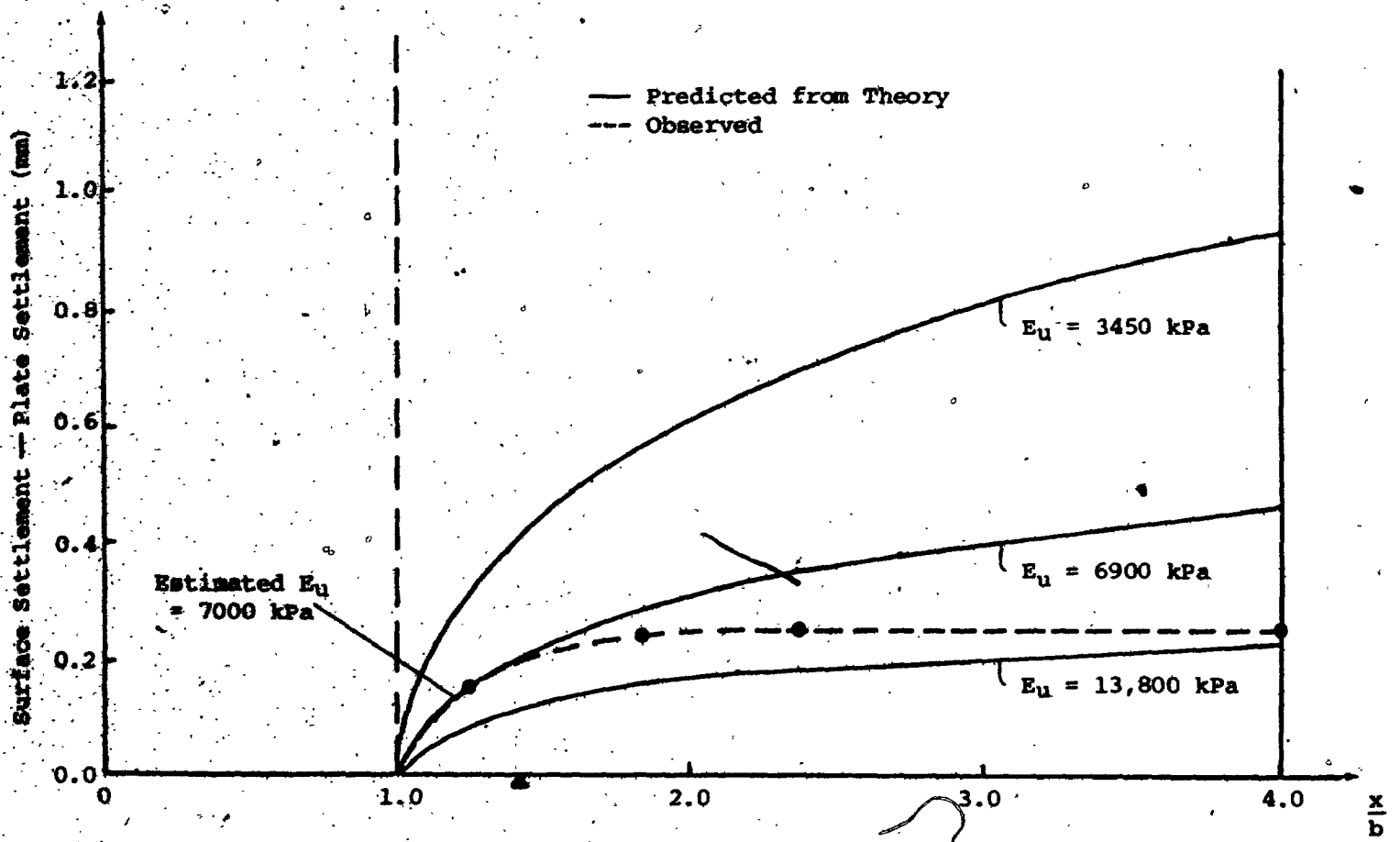

FIGURE 4.20
Second Test on Clay, Surface Displacement Profile, Δq_0 = 5.5 kPa

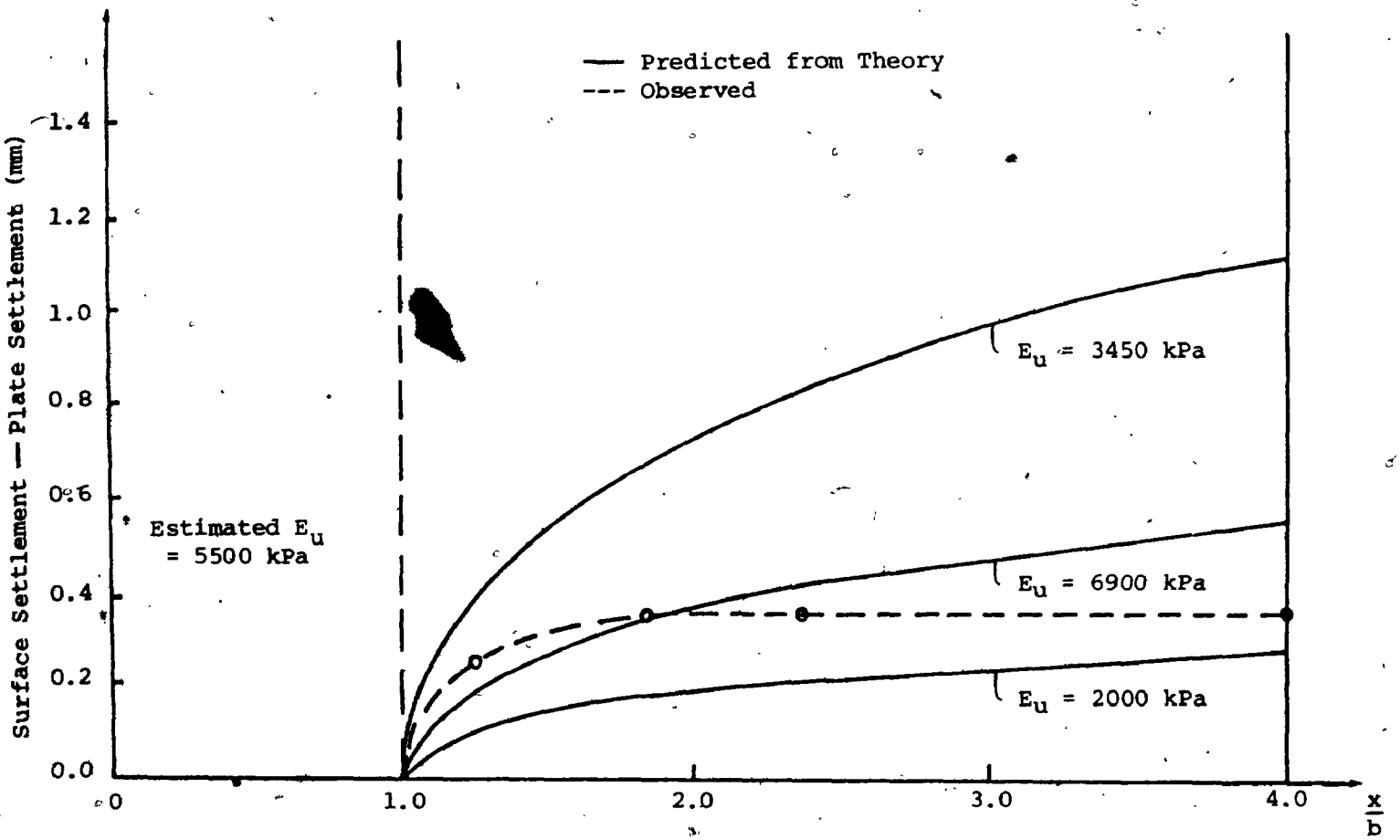

FIGURE 4.21
Second Test on Clay, Surface Displacement Profile, Δq_0 = 13.1 kPa

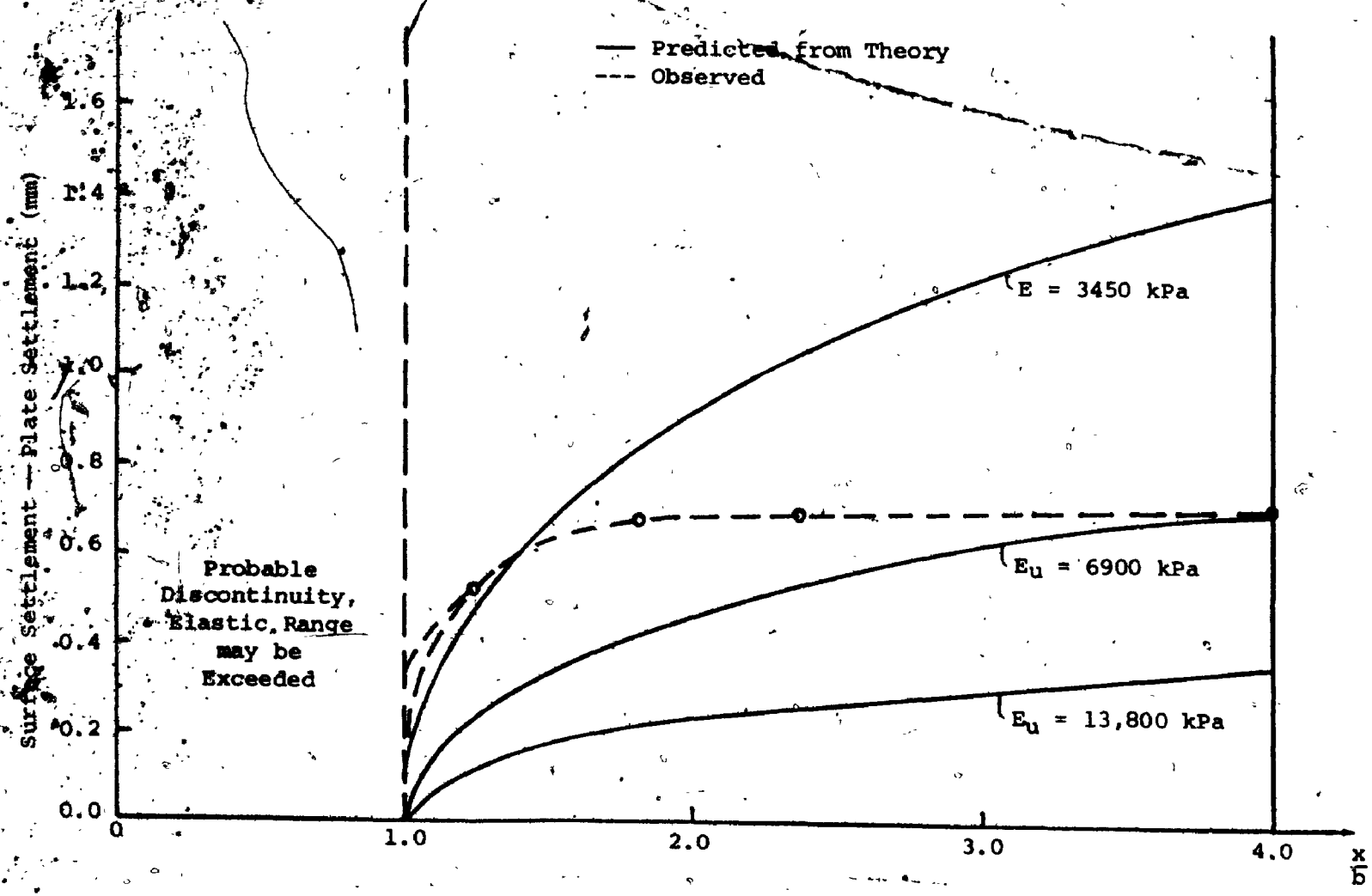

FIGURE 4.22
Second Test on Clay, Surface Displacement Profile, Δq_0 = 16.6 kPa

is a poor fit. Hence a choice can be made concerning the "proper" value of E_u that best fits the observed data.

Since the observed deflections appear more localized, it is felt that the correlation in the adjacent area of the plate should govern. This results in an initial value of E_u of 6900 kPa, in good agreement with the observed unloading modulus obtained from the surcharge application.

In Figure 4.21 for an average stress of 13 kPa, the best fit at the initial stages occurs when E_u is approximately 5500 to 6200 kPa. In subsequent loading increments, the best fit value of E_u continues to decrease, in agreement with a decreasing tangential modulus observed in the UU triaxial tests at higher stresses. For a load of 16.6 kPa (Fig. 4.22) a discontinuity may have occurred at the edge of the plate, and at stresses of 23.5 kPa and greater, a discontinuity was observed. The plate is now "punching" into the clay layer, and some heaving takes place.

The relative settlement for the first principal test is given in Figure 4.19 for a stress increment of 24.6 kPa. Near the plate, the use of E = 4800 kPa gives the best fit, if it is assumed that no discontinuity at the edge has occurred. Since the load is greater than the estimated cohesion of 15 kPa, and heaving is observed at x/b = 2, the elastic solution is not valid and it is unfortunate that more observations were not made at lower stress levels.

For small loads, there is good agreement between the observed surface displacement and the predicted displacement from elastic theory applied to a rigid strip footing. Most of the surface displacement appears to occur in a region less than 2b from the centre line of the

footing.

4.4.4 *Immediate Contact Stress Distribution*

The primary objective of this thesis was to measure the contact stress distribution beneath a rigid plate under plane strain conditions. For a clay medium there will be an initial contact stress distribution due to an applied load followed by a time-dependent response. The magnitude of the response was to be investigated. This section will discuss the contact stress observations made immediately after the plate was loaded, and the changes with time will be discussed separately.

The assumption of plane strain conditions implies that there will be no shear stresses acting on the x-y plane shown in Figure 3.1. For this condition to hold in the modeling, the walls must be rigid and frictionless. The rigidity of the walls was monitored throughout the experiment by dial gauges, and the maximum observed displacement was less than 0.08 mm at the level of the plate. The condition of frictionless walls is difficult to achieve in practice; however, attempts were made to minimize this factor by using highly polished stainless steel walls and a coating of silicone vacuum grease.

Ideally, the contact stress distribution between the walls would be uniform (i.e., independent of the y axis; see Figure 3.1) at each value of x/b. The actual distribution is shown in Figure 4.23. This graph was obtained by taking the average contact stresses at all the points across each position, i.e., six locations in the centre, two at each of the intermediate locations, and three adjacent to each wall. The range of values is also shown. It is apparent that the contact stresses are on the average substantially higher next to the wall,

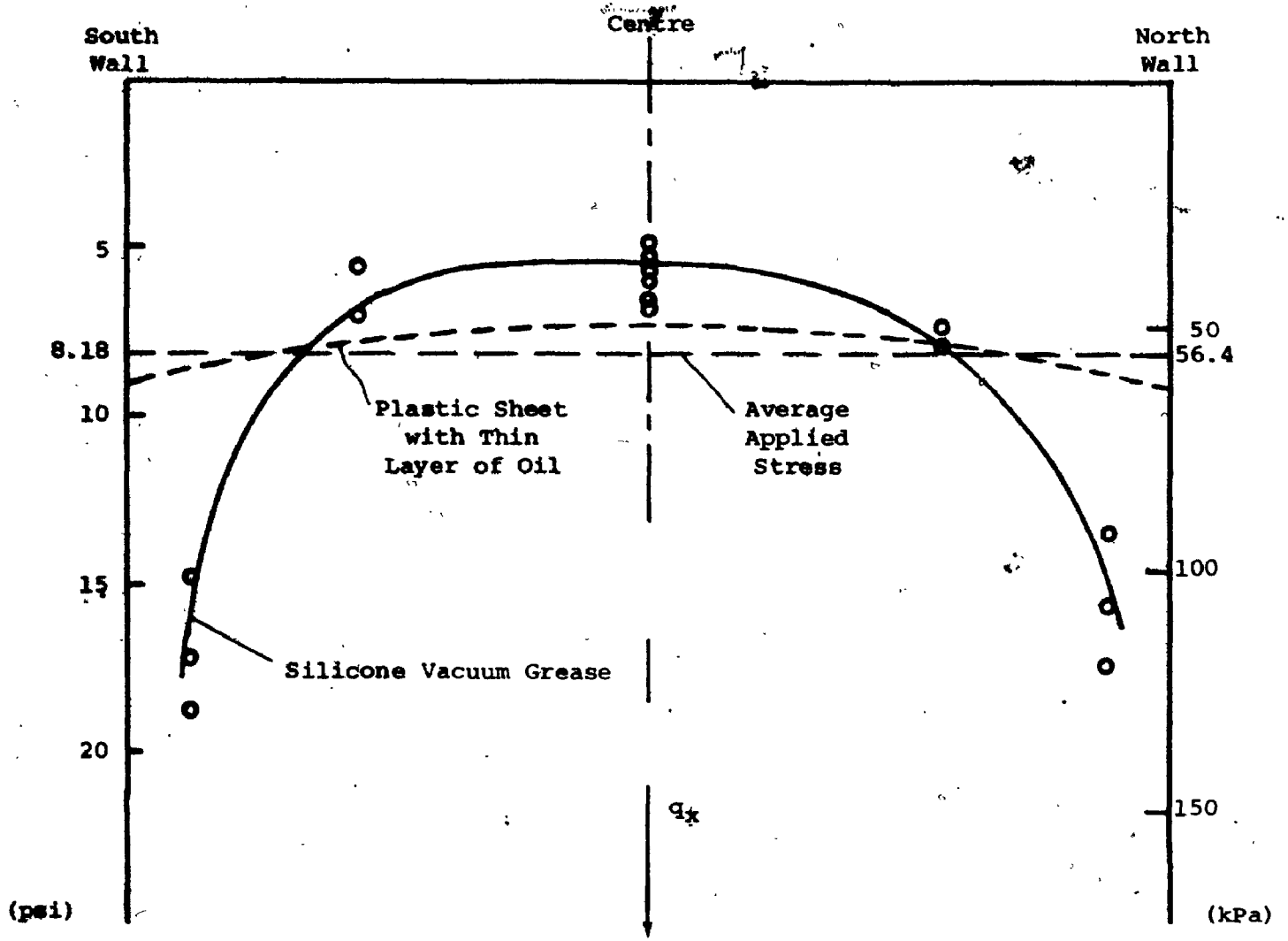

FIGURE 4.23
Contact Stress Distribution Between Walls of Plane Strain Apparatus

indicating the possibility of friction occurring between the soil and the stainless steel. The contact stress in the centre region is lower than the applied average contact stress. If there were no measurements made of the contact stress away from the centre, it may have been concluded that the pressure transducers were under-registering the actual contact stress, but this is not the case. A check was made of the measured contact stresses compared to the applied load. The data from the pressure transducers after the total stress was applied was entered into the program POLYFIT.TSL, and an equation of the average contact stress between the walls was generated. The integration of this equation produced a total average contact stress equal to 101.2 percent of the applied stress, which is within the accuracy of the measuring system. It can be concluded that the pressure transducers are viable devices for measuring the contact stress for a cohesive soil.

Although there are higher contact stresses adjacent the walls, the centre region of the test plate is still important because here the plane strain conditions may be considered to exist. The average contact stress in the centre region will be lower than the applied stress, but this can be taken into account by normalizing the observed contact stresses. Since each pressure transducer in the centre represents approximately 1/6 of the width of the plate, the normalizing process was accomplished by simply dividing the measured value by the average stress across the centre.

Figure 4.24 shows the contact stress distribution across the entire width of the centre area of the plate within a few minutes after load application. The absolute values are shown because the normalizing process does not change the shape of the curves. This graph is intended

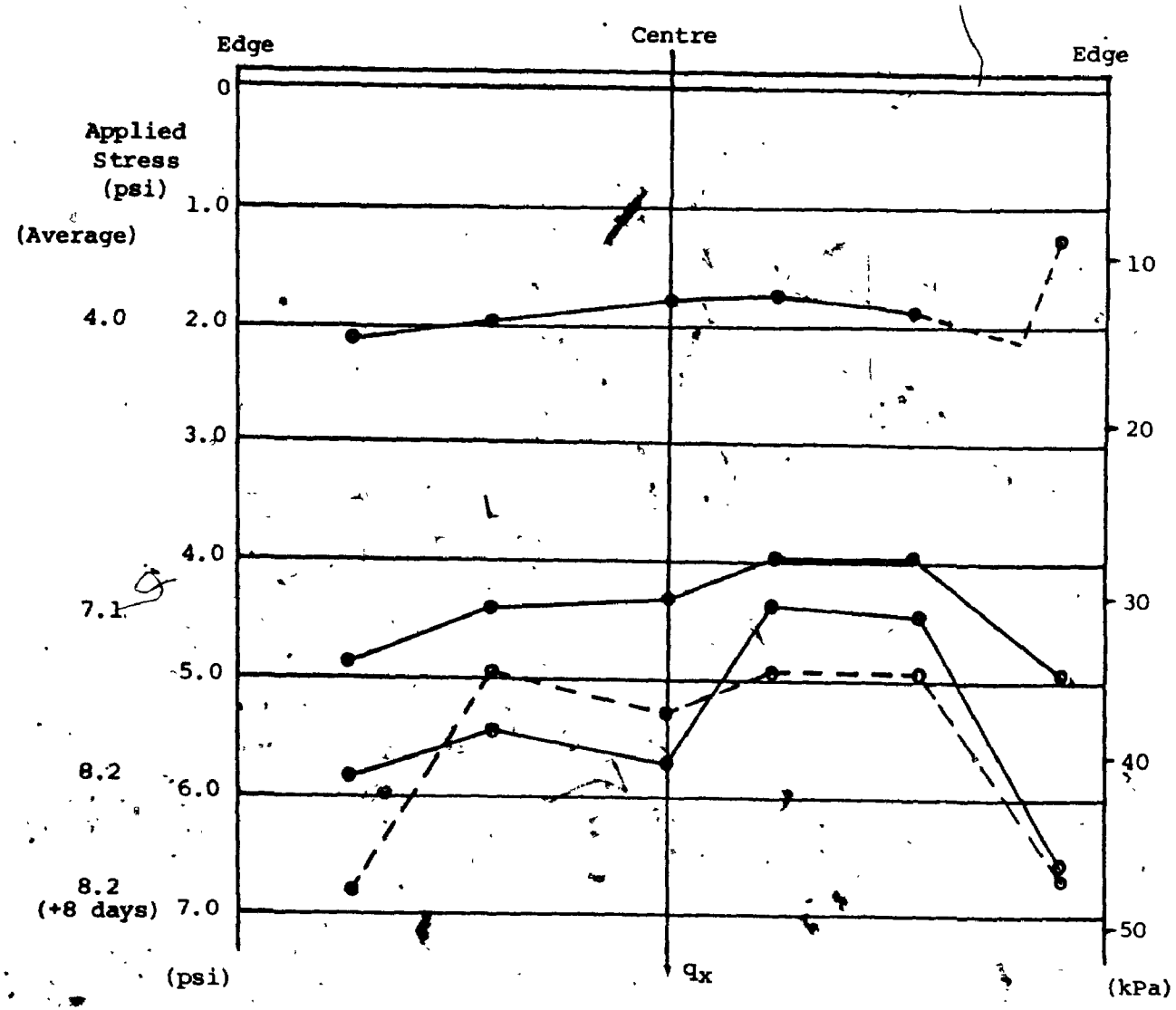

FIGURE 4.24
Immediate Contact Stress Distribution during Plain Strain Test, Centre Region of Plate

to show that the initial contact stress distribution may be irregular, as previously observed in the three-dimensional test on clay. Ideally the distribution would be symmetrical, enabling the superposition of all six pressure transducer locations for only half of the plate width b. Immediately after the load was applied, the distribution was irregular but within 24 hours this distribution became more symmetric. The initial non-uniformity may be due in part to the local non-homogeneity of the soil medium. With further plate settlement, these effects appear to be reduced.

The normalizing process can be used to show more clearly the *relative* distribution of contact stress. In Figure 4.25 the contact stress distribution due to the plate self-weight resembles the elastic distribution. The edges are up to 40 percent higher than average, with the centre region less than 80 percent of the mean. As the load is increased the pattern changes with the centre region taking a greater percentage of the load. This figure shows the initial irregular distribution, which becomes more symmetrical with time.

The contact problem of a rigid die acting on an elastic isotropic half-space under plane strain conditions gives the well-known result that the stresses tend to infinity at the edge. This singular behaviour occurs only if the corners are perfectly sharp. In a paper by Goodier and Loutzenheiser (1965) it is shown that the rounding of the corners by small parabolic or full circular arcs leads to a considerable reduction in the magnitude of the edge peak stress. This is illustrated in Figure 4.26, where the maximum peak contact stress will be only three times as great as average if the contact radius at the edge is 3.6 percent of the width of the plate. As this corner curvature increases, the peak stress

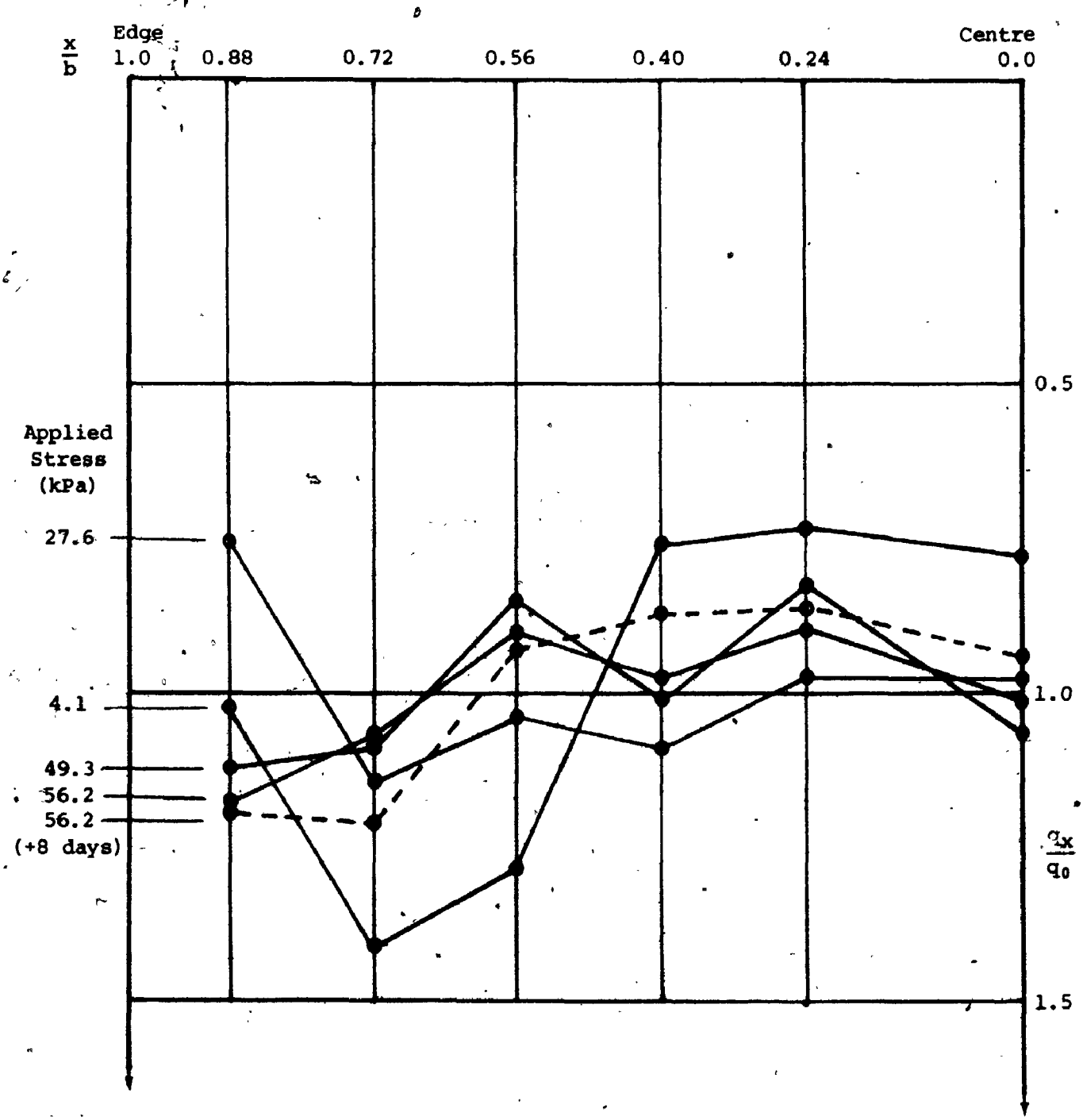

FIGURE 4.25

Initial Normalized Contact Stress Distributions During First Test on Clay

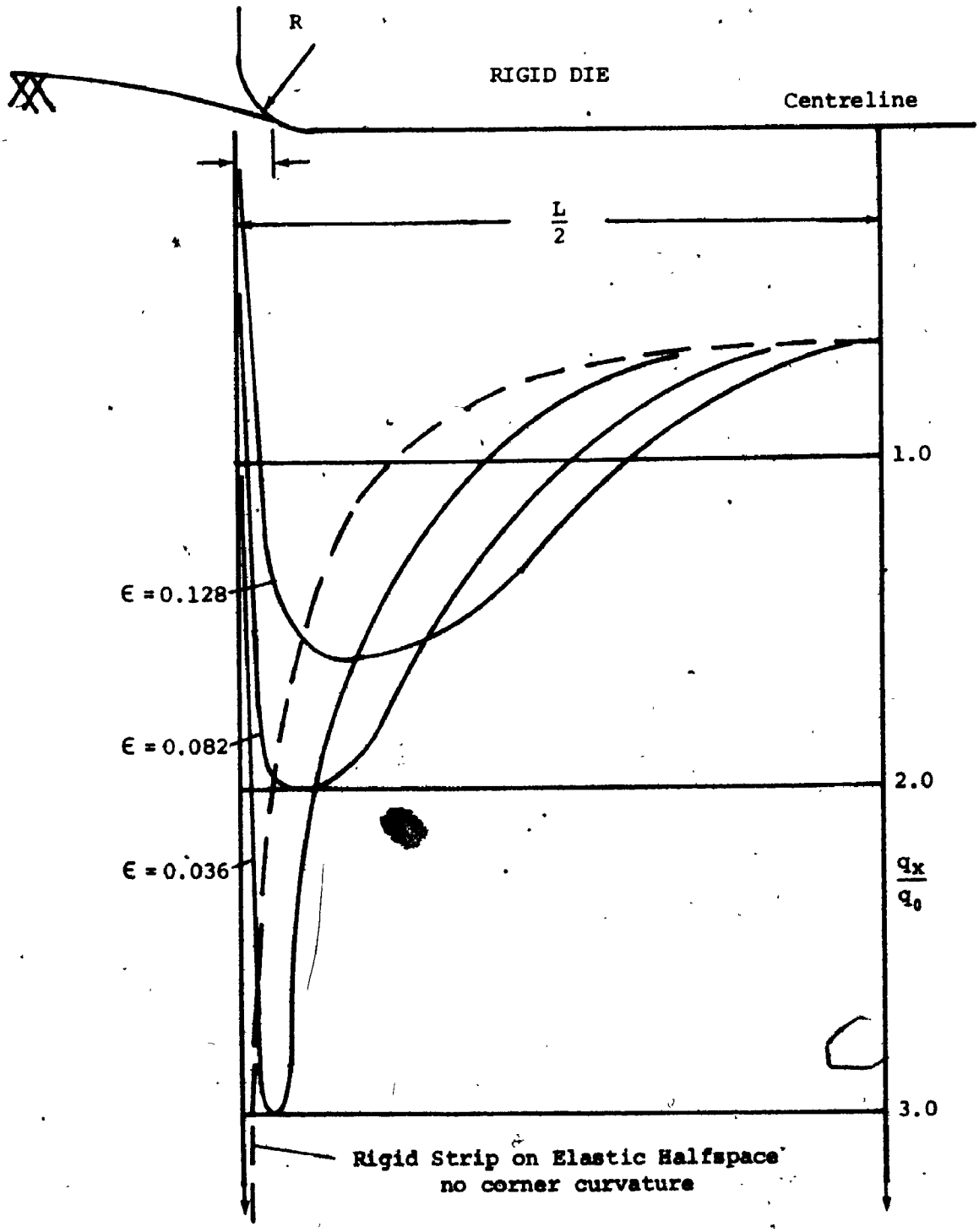

FIGURE 4.26

Graph of Contact Stress Distributions Beneath a Rigid Die, for Various Corner Curvatures (from Goodier and Loutzenheiser, 1965)

correspondingly decreases. A perfectly square corner will not occur in practice, so the edge singularity will not exist even for low stress ranges before local yielding can occur. It is one way of explaining the reason why local yielding produces lower peak stresses if the yielding is to be interpreted as an increase in corner curvature.

A comparison can be made between the observed contact stress distributions and those predicted by several theoretical models. As explained in the literature review on contact stresses, the edge stresses will approach infinity provided local yielding of the soil does not occur. In discussing the immediate contact stress distribution, it is necessary to estimate when local yielding of the soil first begins. With the method proposed by Schultze (1961) the yielding will occur even at small finite stress applications and the maximum contact stress will equal the bearing capacity of the soil. Section 4.5 will present the predicted contact stress distributions in more detail.

4.4.5 *Pore Pressure Response*

4.4.5.1 *Immediate Pore Water Pressure Response*

The prediction of excess pore water pressure due to an applied load first requires an assumption regarding the magnitude of the stress, applied stress distribution and rate of loading. The relationship between the applied stress and the stresses induced in the soil must then be determined. The final step involves establishing the relationship between these induced stresses and the excess pore water pressure. The process is complicated by the fact that the pore pressures are time-dependent, and the drainage paths that exist in the soil medium will control the build-up of pore pressures.

Pore water pressures were monitored in the main experiment of this study because it was an integral part of the total time-dependent behaviour of the soil medium. The purpose of the measurements were threefold: (1) to compare the observed immediate excess pore pressures with those predicted by available theories; (2) to provide an estimate of the total consolidation settlement; and (3) to determine the rate of dissipation of pore pressures and relate them to the change (if any) in the contact stress distribution.

The prediction of excess pore water pressures depend on the estimated change in the principal stresses due to an applied internal load. The changes in the principal stresses for the case of a uniformly loaded strip footing resting on an elastic half-space is obtained from elasticity theory. The basic formulation of the problem is given in Appendix 14, where a simple computer program, STRES2, was made to solve the equations and calculate the normal and principal stresses for any point in the soil medium. The results for the principal stresses below the centreline and edge of the plate are presented in Figures 4.27 and 4.28.

The distribution of applied stress is not uniform for the case of a rigid strip footing resting on an elastic layer. The measured contact stresses beneath the centre region of the test plate showed that the edge contact stress was approximately 125 percent of the average stress, versus 85 to 90 percent in the middle portion. (See Fig. 4.25.) This average stress in the centre should not be confused with the average applied stress over the entire plate. (As previously explained, friction on the walls may have lowered the contact stress in the centre region between the two walls.) For discussion purposes, a comparison will be made between the principal stresses produced by a fully flexible

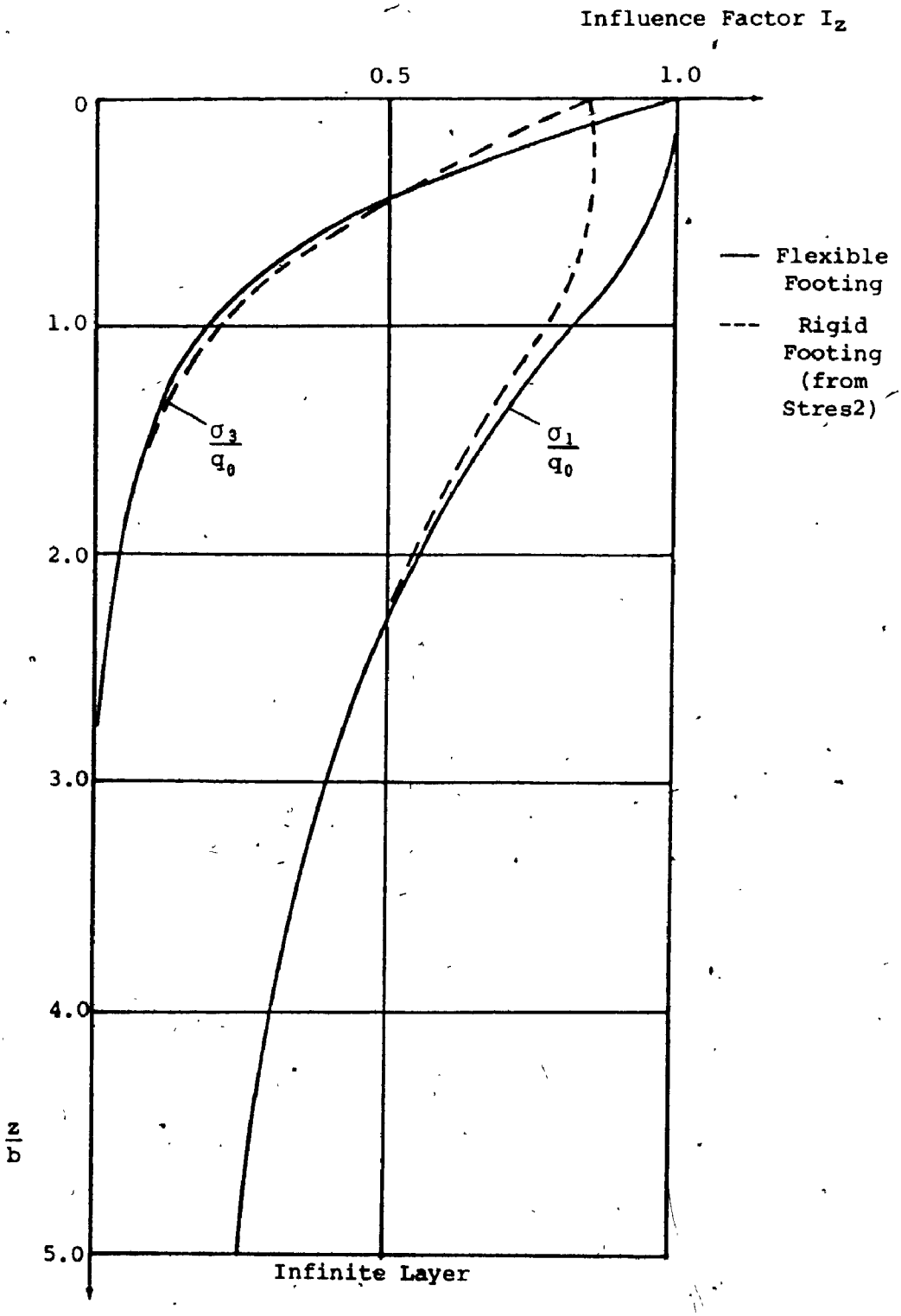

FIGURE 4.27
Centreline Influence Factors for Calculation of Principal Stresses Below Strip Footing

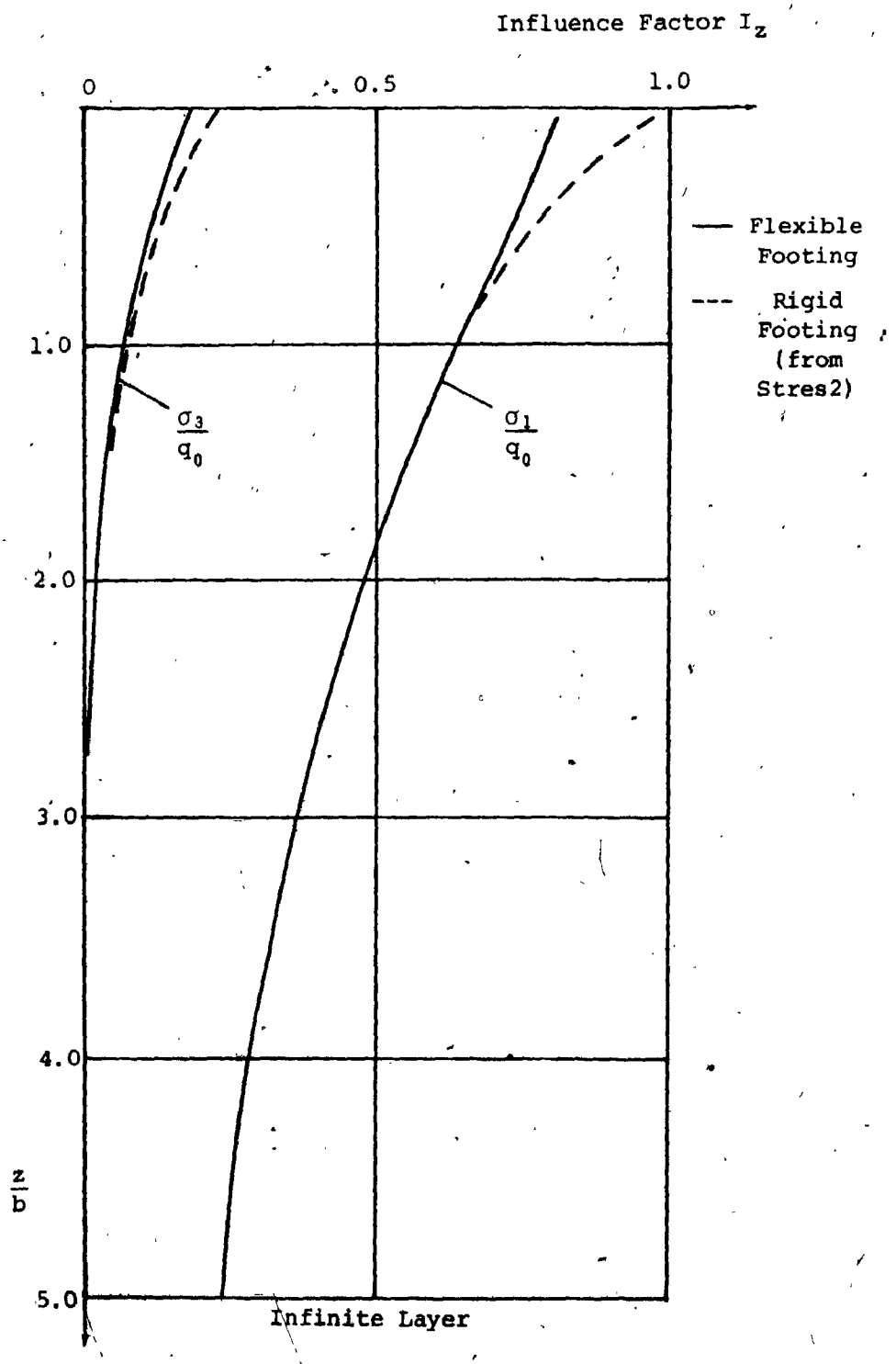

FIGURE 4.28
Edge Influence Factors for Calculation of Principal Stresses Below Strip Footing

footing and a rigid footing.

The computer program STRES2 (Appendix 14) was written to calculate the effects of a non-uniform strip load. This was accomplished by superimposing various uniform loads until the stress distribution resembled the case of a rigid footing. The results of this superposition technique are shown in Figures 4.27 and 4.28, for a contact stress distribution similar to that observed in the centre region of the plate. It is important to note that the effects of the rigid footing are most critical in the layer directly below the footing less than the width, 2b, after which the principal stresses are essentially the same for both flexible and rigid footings. Beneath the centreline the major principal stress, σ_1, for the rigid case is less than that of the flexible loading, whereas σ_1 at the edge of the footing is substantially higher than the flexible case. The large variation between the two cases is an important consideration in the prediction of the induced excess pore water pressure in the critical layer directly below the plate.

Several methods relating the change in principal stresses to increase in pore pressure have already been introduced in Chapter 2, and are summarized in Appendix 2. It was found by many researchers that the simplest and quite often the best correlation between predicted and observed pore water pressures was obtained if the pore pressures were predicted from the change in total octahedral stress, $\Delta\sigma_{oct}$, where

$$\Delta\sigma_{oct} = 1/3\ (\Delta\sigma_1 + \Delta\sigma_2 + \Delta\sigma_3)\ .$$

Hence $\Delta u = B\Delta\sigma_{oct}$, where B is the pore pressure parameter relating the compressibility of the water in the soil to the soil skeleton. For saturated or nearly saturated clays, $B \approx 1.0$. This equation is the more

3

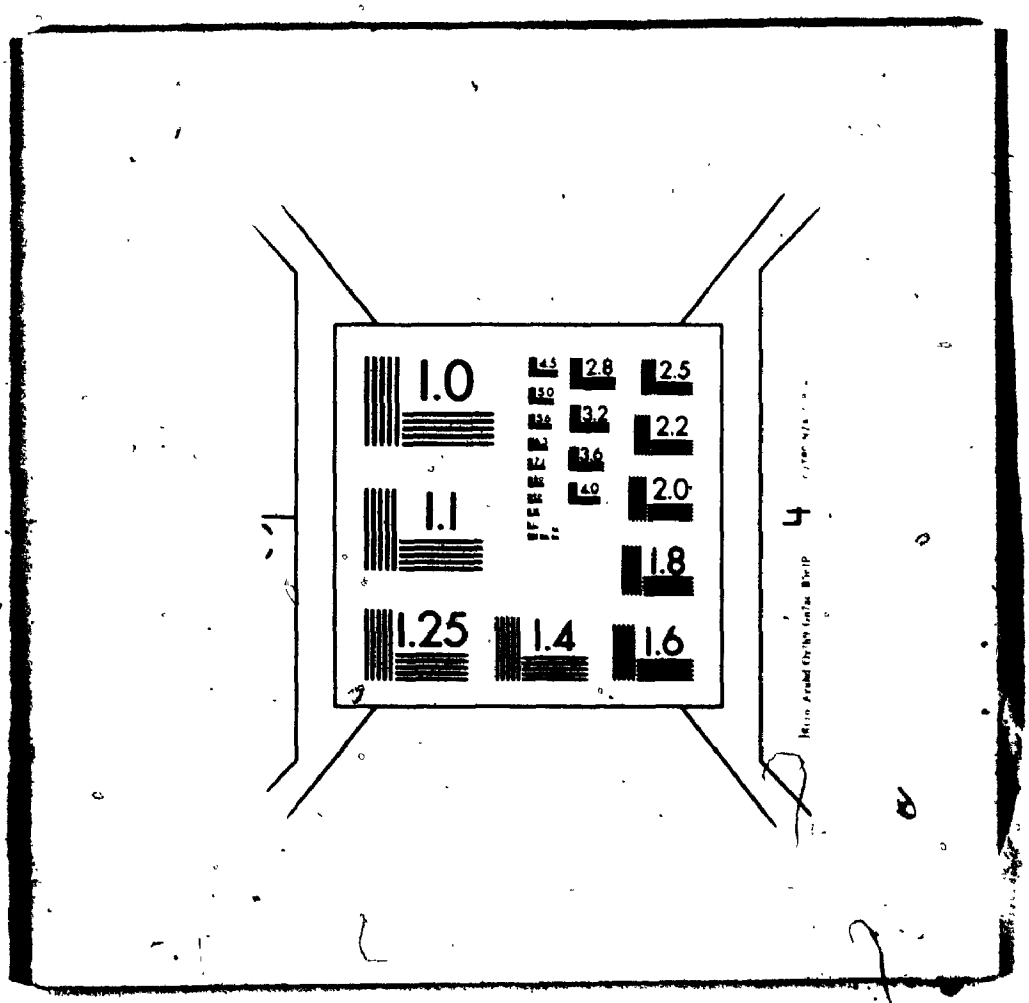

4

general form of the equation proposed by Skempton (1954), which is

$$\Delta u = B[\Delta\sigma_3 + A(\Delta\sigma_1 - \Delta\sigma_3)]$$

where A is the pore pressure parameter, determined experimentally from triaxial tests. A is found to be highly dependent on the over-consolidation ratio of the soil. Under plane strain conditions, Skempton's equation will be equal to the previous equation involving octahedral shear stress if A is $\frac{1}{2}$. For normally consolidated clays, the A value at failure has been found to range from 0.7 to 1.3, and for lightly over-consolidated clays the range is from 0.3 to 0.7 (Lambe, 1962). At strains less than failure the A parameter will be reduced. The experimental determination of A is also highly dependent on the rate of strain used in the triaxial test.

Figure 4.29 shows the estimated pore pressure parameter A as a function of depth below the surface. A range of values has been given because of the uncertainty involved in accurately determining the value. The soil near the surface has been assigned a lower value of A because there is experimental evidence that the clay has consolidated during the application of the surcharge (see Fig. 4.14). Below a depth b from the surface the clay is assumed to be normally consolidated. For an elastic material, A will be equal to $\frac{1}{2}$, so this has been taken as the median value.

With these estimated A values and the computed principal stresses based on a uniform strip load on an elastic half-space, an upper and lower bound to the immediate excess pore water pressure can be calculated as shown in Table 7. Figures 4.30 and 4.31 show the range of predicted $\Delta u/\Delta\sigma_0$ versus depth beneath the centreline and edge of the plate.

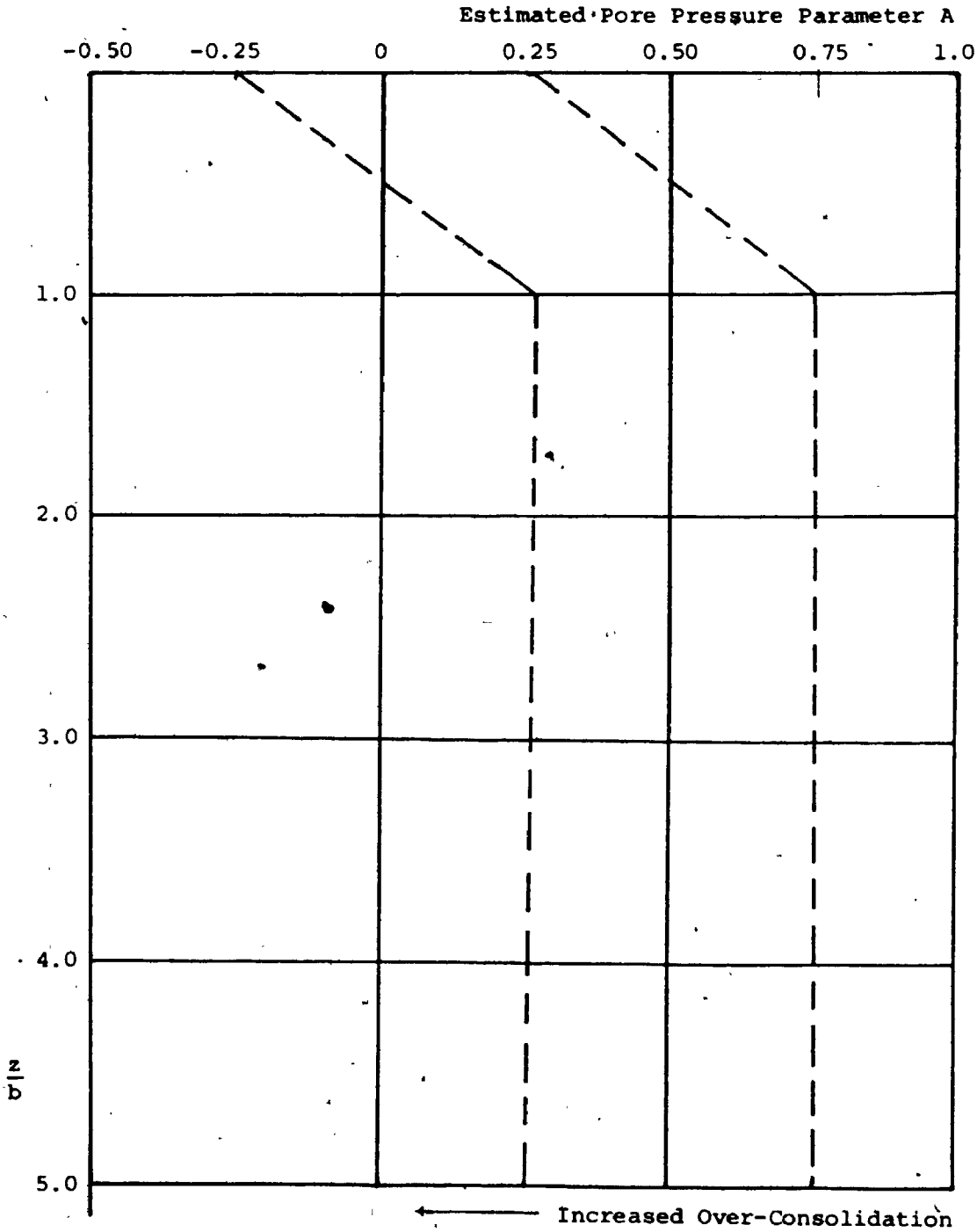

FIGURE 4.29
Estimated Pore Pressure Parameter A versus Depth Below Plate

TABLE 7

PREDICTED PORE WATER PRESSURES BELOW PLATE

POSITION z/b	BELOW CENTRELINE				BELOW EDGE			
	Principal Stress		*Pore Pressure Increment*		*Principal Stress*		*Pore Pressure Increment*	
	$\frac{\sigma_1}{q_0}$	$\frac{\sigma_3}{q_0}$	Upper Bound	Lower Bound	$\frac{\sigma_1}{q_0}$	$\frac{\sigma_3}{q_0}$	Upper Bound	Lower Bound
0.25	0.99	0.70	0.63	0.81	0.77	0.14	-0.02	0.38
0.5	0.96	0.45	0.45	0.71	0.73	0.11	+0.11	0.42
1.0	0.82	0.18	0.34	0.66	0.64	0.07	0.21	0.50
1.5	0.67	0.08	0.23	0.53	0.55	0.04	0.17	0.42
2.0	0.55	0.04	0.17	0.42	0.48	0.03	0.14	0.37
3.0	0.40	—	0.10	0.30	0.36	—	0.09	0.27
4.0	0.30	—	0.08	0.23	0.29	—	0.07	0.22
5.0	0.25	—	0.06	0.18	0.24	—	0.06	0.18

NOTE

(1) Centreline and edge principal stresses are based on *uniform* loading conditions, with infinite depth of layer.

(2) Pore pressure increments are based on estimated A parameters given in Figure 4.29 $\quad \Delta u = B[\Delta\sigma_3 + A(\Delta\sigma_1 - \Delta\sigma_3)]$.

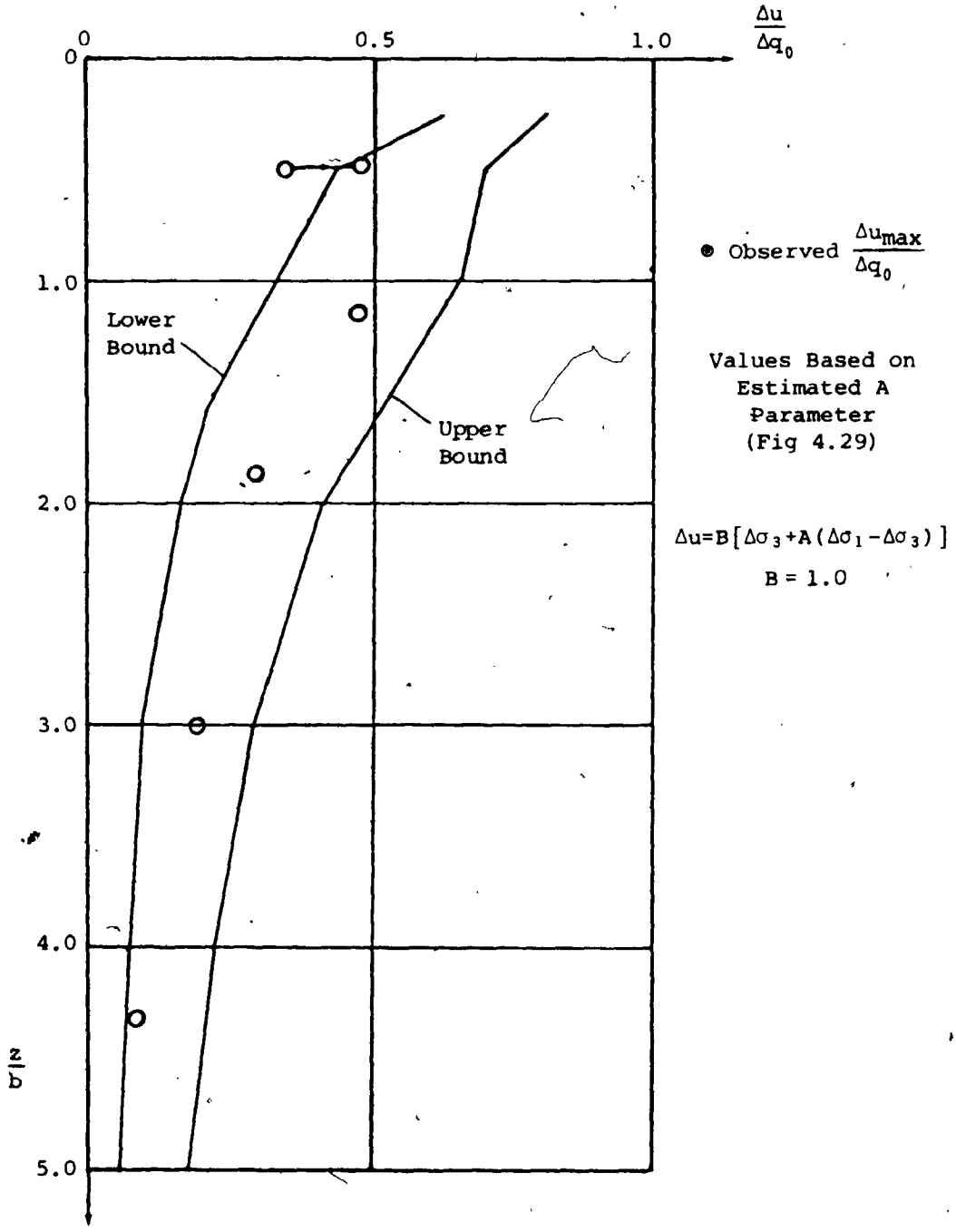

FIGURE 4.30
Predicted $\Delta u/\Delta q_0$ Below Centreline of Plate

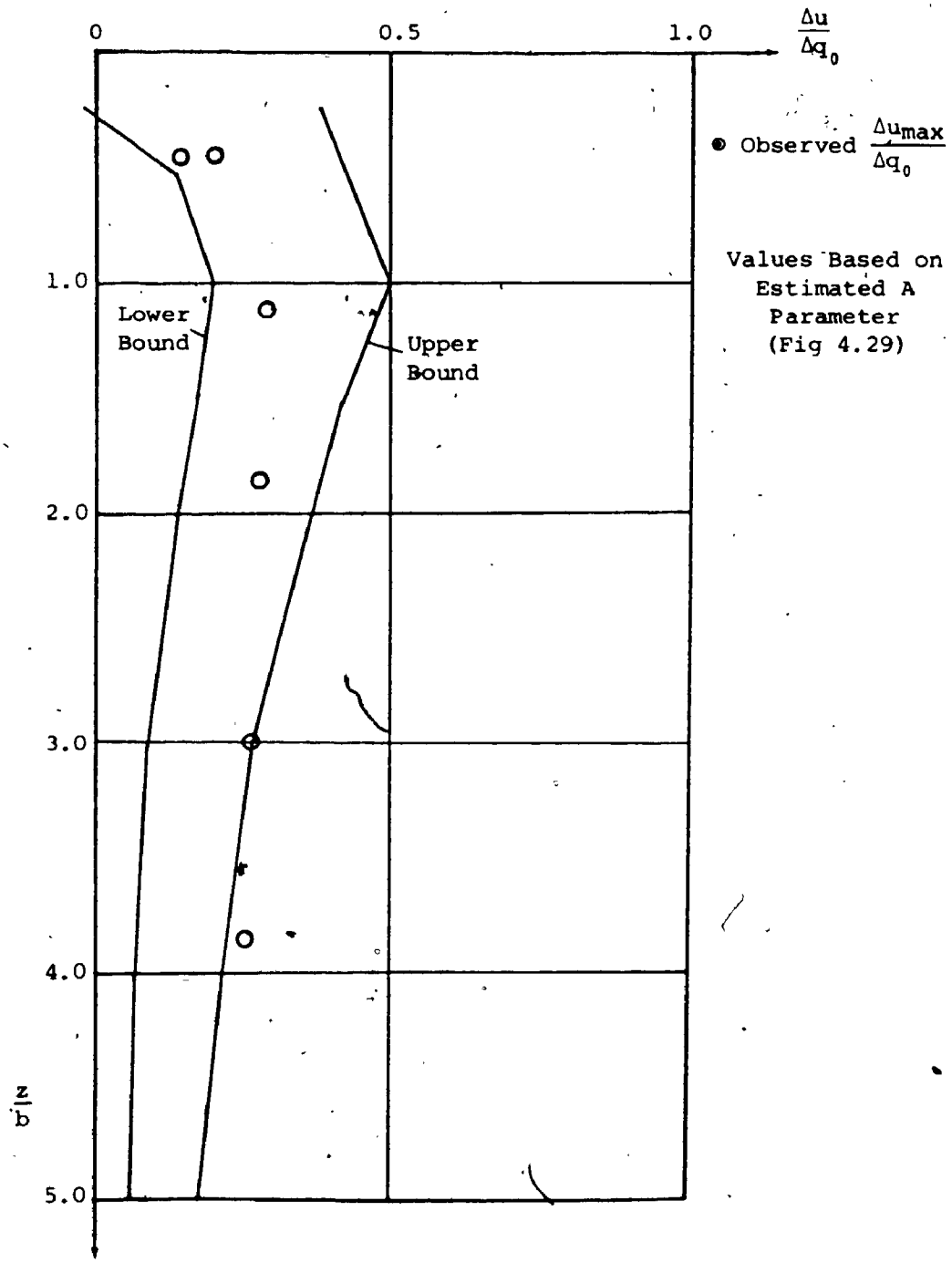

FIGURE 4.31
Predicted $\Delta u/\Delta q_0$ Below Edge of Plate

The immediate and maximum incremental pore pressures observed beneath the centreline and edge of the plate are summarized in Table 6. The delay in the observed maximum pore water pressure was variable, but usually less than two hours. By taking the maximum incremental pore pressure due to the plate loading and dividing it by the applied average stress, the results can be compared with the estimated pore pressure increase based on assumptions regarding the principal stress increments and A parameter (Figs. 4.30 and 4.31). The observed excess pore pressure beneath the centreline lies within the range of predicted values for all depths, and there is good agreement for the edge pore pressures for the upper layers.

Since predicting excess pore pressures on the basis of the increment in total octahedral shear stress has been found to provide good correlations, it is useful to compare the observed pore pressures with the calculated $\Delta\sigma_{oct}$. The calculation of $\Delta\sigma_{oct}$ is not as straightforward as might be expected in this model experiment because the boundary conditions are difficult to analyze. The applied stress distribution is non-uniform in the case of a rigid strip footing, and this has a significant effect on the soil within a depth 2b beneath the footing. The rigid rough base at a depth of 5b below the surface increases the stresses in the bottom layer. The vertical rough walls located at a distance 4b from the centre axis of the plate will tend to confine the soil and cause higher stresses.

Table 8 provides a summary of several methods used to calculate $\Delta\sigma_{oct}$ applicable to this problem and they are illustrated in Figures 4.32 and 4.33. Milović *et al.* (1970) and Poulos (1967) take into account the rigid rough base, showing substantially higher values of

TABLE 8

COMPARISON BETWEEN Δu AND $\Delta\sigma_{oct}$ COMPUTED BY VARIOUS METHODS

NO.	POSITION z/b	$\Delta u/\Delta q_0$ OBSERVED	$\Delta\sigma_{oct}/\Delta q_0$				
			Elastic	*Poulos*	*Milović* H/B=2	*Milović* H/B=3	*Superposition*
1	0.47	0.35	0.71	0.71	0.58	0.58	0.66
2	1.13	0.48	0.47	0.47	0.45	0.45	0.46
3	1.87	0.30	0.32	0.33	0.36	0.33	0.32
4	3.0	0.20	0.20	0.27	0.33	0.25	0.20
5	4.3	0.08	0.14	0.28	0.24	—	0.14
6	0.47	0.14	0.42	0.39			0.47
7	1.13	0.29	0.33	0.30			0.33
8	1.87	0.28	0.26	0.25			0.26
9	3.00	0.27	0.19	0.26			0.19
10	3.80	0.26	0.15	0.30			0.15

NOTE

(1) "Elastic" case based on uniform load applied to a flexible strip footing overyling a homogeneous isotropic elastic half-space.

(2) "Poulos" case based on Poulos (1967) for uniform load applied to a flexible strip footing overlying a homogeneous isotropic elastic layer, H/B = 2.5.

(3) "Milović" case based on Milović *et al.* (1970) for rigid rough strip footing on elastic layer with Poisson's ratio 0.45.

(4) "Superposition" case was based on superposition of uniform loads approximating a *rigid* strip footing (see Appendix 14).

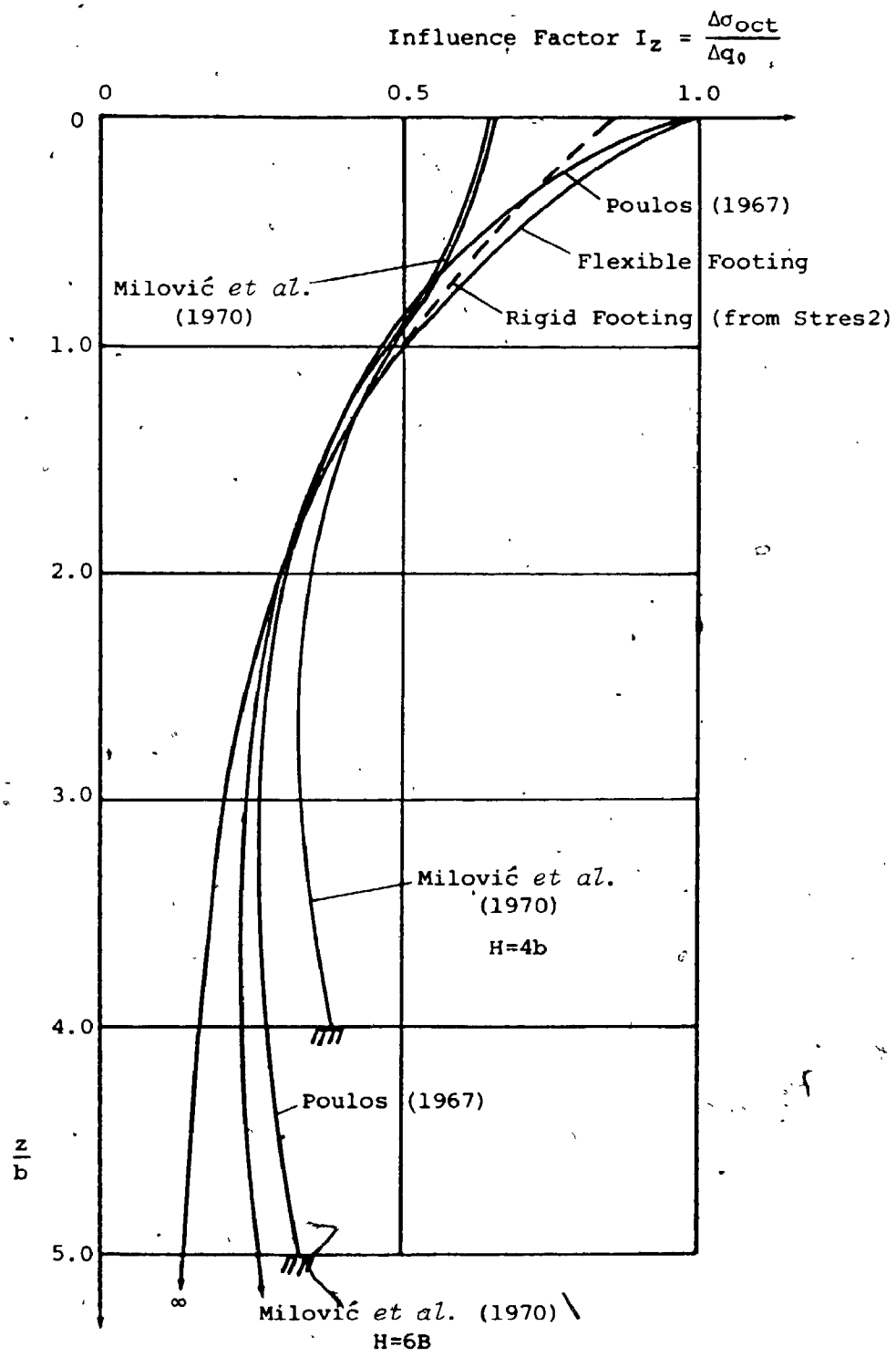

FIGURE 4.32
Centreline Influence Factor for Calculation
of Total Octahedral Normal Stress

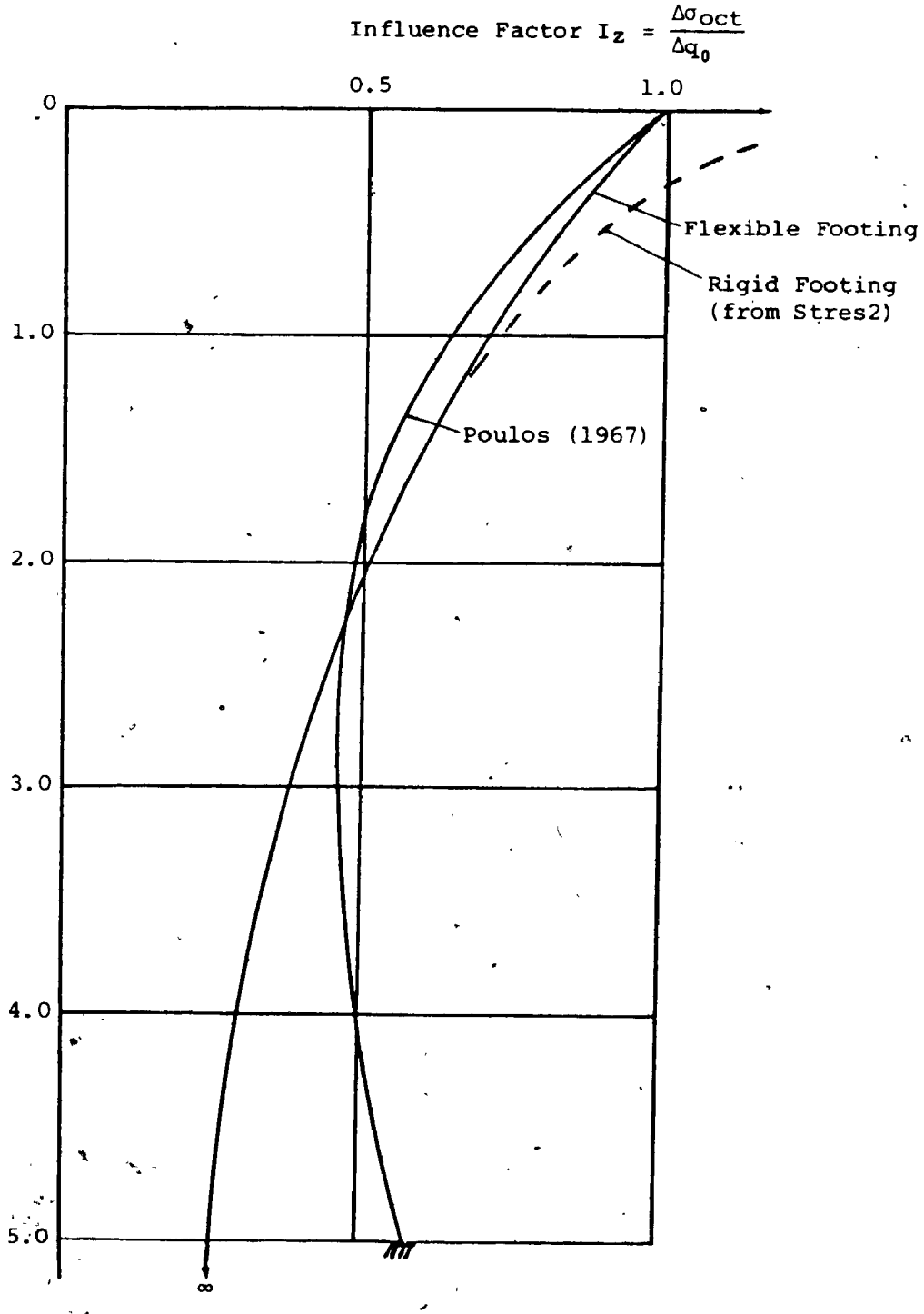

FIGURE 4.33
Edge Influence Factor for Calculation of
Total Octahedral Normal Stress

$\Delta\sigma_{oct}$ near the base. Milović *et al.* (1970) also analyzed the case of a *rigid* strip footing, and beneath the centreline the calculated $\Delta\sigma_{oct}$ values were much lower than the flexible case. Using the program STRES2 to calculate the increase in principal stresses results in an intermediate range of $\Delta\sigma_{oct}$ between those computed by a rigid and flexible strip footing. The best estimate of the induced $\Delta\sigma_{oct}$ would involve a combination of the results for a rigid strip footing and rough base, but Figures 4.32 and 4.33 serve to show the uncertainty involved in making an accurate prediction of $\Delta\sigma_{oct}$.

In Table 9 the A parameter has been back-figured from estimates of principal stresses and observed maximum pore water pressures. The principal stresses used in the computation are based on results developed for the stresses in an isotropic elastic half-space subjected to a strip load and do not truly represent the conditions of the present experiment. The calculated values of A all fall within the upper and lower range used in predicting the pore water pressure (Fig. 4.29).

The prediction of pore pressures on the basis of the increase in vertical stress due to the plate loading fails to take into account the effect of lateral expansion of the soil. Figure 4.34 shows the vertical stress increment with depth for both the centreline and edge of the strip footing. The observed increase in pore pressure is generally much less than predicted from the assumption that $\Delta u = \Delta\sigma_z$. The plane strain and two-dimensional conditions must be taken into account, as previously observed by several field observations (Lambe, 1962; D'Appolonia *et al.*, 1971; Moh *et al.*, 1972; Thamm, 1967).

TABLE 9

A PARAMETER BACK-FIGURED FROM OBSERVED PORE WATER PRESSURES

PRINCIPAL STRESS INCREMENTS CALCULATED FROM FLEXIBLE STRIP FOOTING ACTING ON ELASTIC ISOTROPIC HALF-SPACE
A = 0.5 (Elastic)

NO.	POSITION z/b	$\frac{\Delta\sigma_1}{\Delta q_0}$	$\frac{\Delta\sigma_3}{\Delta q_0}$	$\Delta u/\Delta q_0$ IF A = 0.5	OBSERVED $\Delta u/\Delta q_0$	A PARAMETER (DERIVED)
1	0.47	0.85	0.46	0.655	0.35	- 0.28*
2	1.13	0.73	0.17	0.450	0.48	+ 0.55
3	1.87	0.56	0.05	0.305	0.30	+ 0.49
4	3.0	0.40	0.00	0.200	0.20	+ 0.50
5	4.3	0.28	0.00	0.140	0.08	+ 0.29
6	0.47	0.88	0.14	0.510	0.14	0.00**
7	1.13	0.61	0.08	0.345	0.20	+ 0.40
8	1.87	0.49	0.03	0.260	0.28	+ 0.54
9	3.00	0.36	0.00	0.180	0.27	+ 0.75
10	3.80	0.30	0.00	0.150	0.26	+ 0.87

$$\Delta u = B[\Delta\sigma_3 + A(\Delta\sigma_1 - \Delta\sigma_3)]$$

If B = 1.0, then $A = \frac{\Delta u - \Delta\sigma_3}{\Delta\sigma_1 - \Delta\sigma_3}$

*NB If Δq_0 = average centre range stress, then $\Delta u/\Delta q_0 = 0.48$ (vs. 0.35)

Then A = 0.10 (still overconsolidated)

**Same as above. $\Delta u = \frac{7.5}{38.0} = 0.20$ (vs. 0.14)

Then A = 0.08

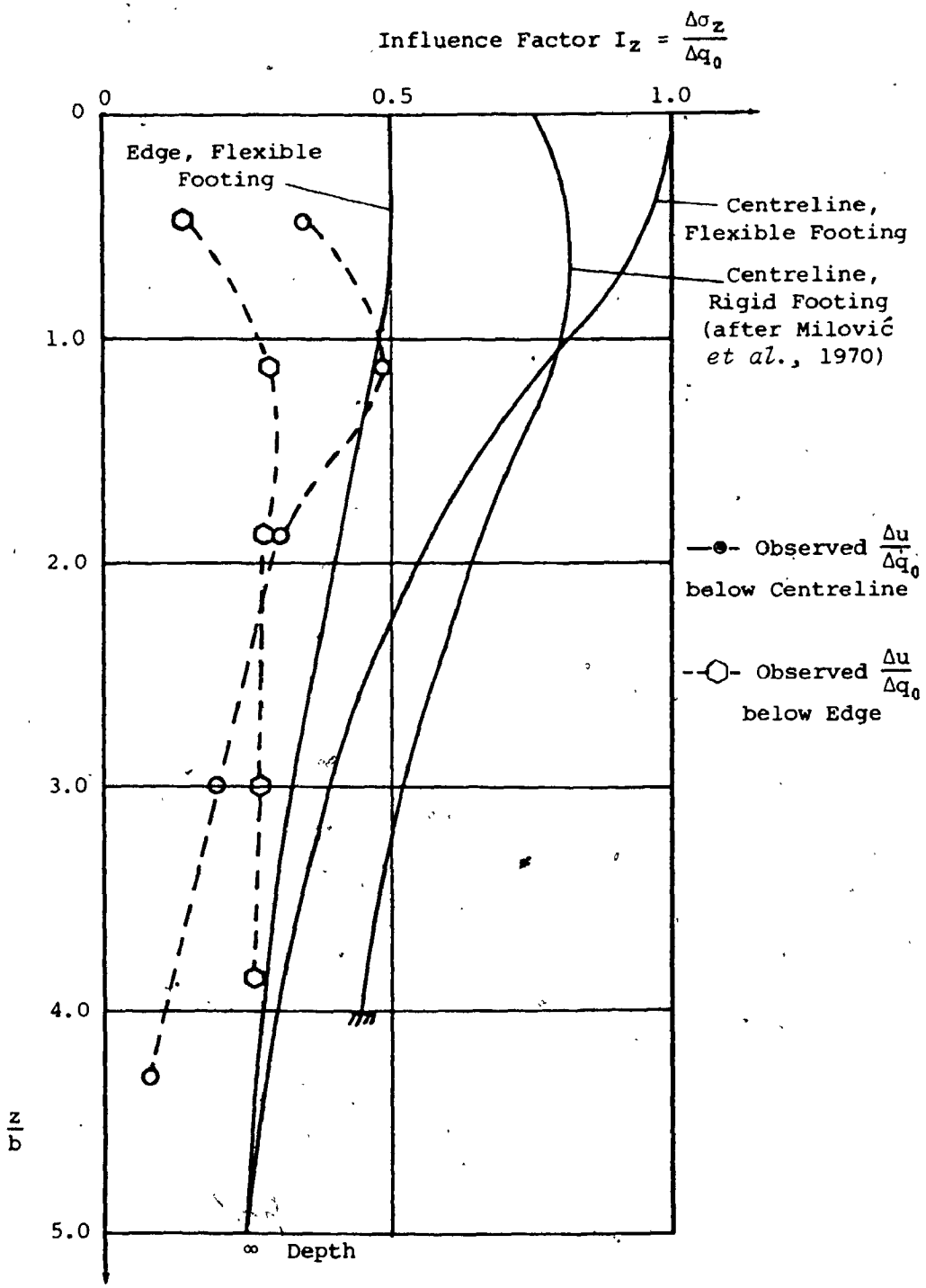

FIGURE 4.34
Influence Factors for Calculation of
Vertical Stress Below Plate

4.4.5.2 *Pore Water Pressure Dissipation*

The rate of dissipation of the pore water pressures from their peak values are given in Figures 4.35 and 4.36 for the piezometers below the centreline and edge of the test, plate, respectively. From these results it was found that:

(1) As the depth below the plate increases, the pore water pressures generally require more time to dissipate.

(2) The dissipation rates of the centreline and edge piezometers below the plate at equivalent elevations are very similar.

(3) The pore water pressure immediately below the plate centre required about twelve hours to reach a peak value. Burland and Roscoe (1969) observed that air trapped in the measuring system produced lower peak pore water pressures, but eventually the rate of dissipation of the pore water pressure coincided with the rates observed with similar saturated piezometers. Line A in Figure 4.35 was based on the observed maximum pore water pressure, but in line B the observed pore water pressure has been divided by the maximum pore water pressure predicted from assuming the soil was elastic and $\Delta u = \Delta\sigma_{oct}$. Line B provides a much better correlation with the other piezometers. In the previous discussion it had been shown that the consolidation of the upper clay layer during the surcharge application would have over-consolidated the soil and reduced the peak pore water pressure due to the plate. It has now been shown that the reduced peak pore water pressure may have been due to the delay in the measuring system. It is likely that both explanations are contributing factors, but it is difficult to separate the two phenomena.

(4) With the possible exception of the top centreline

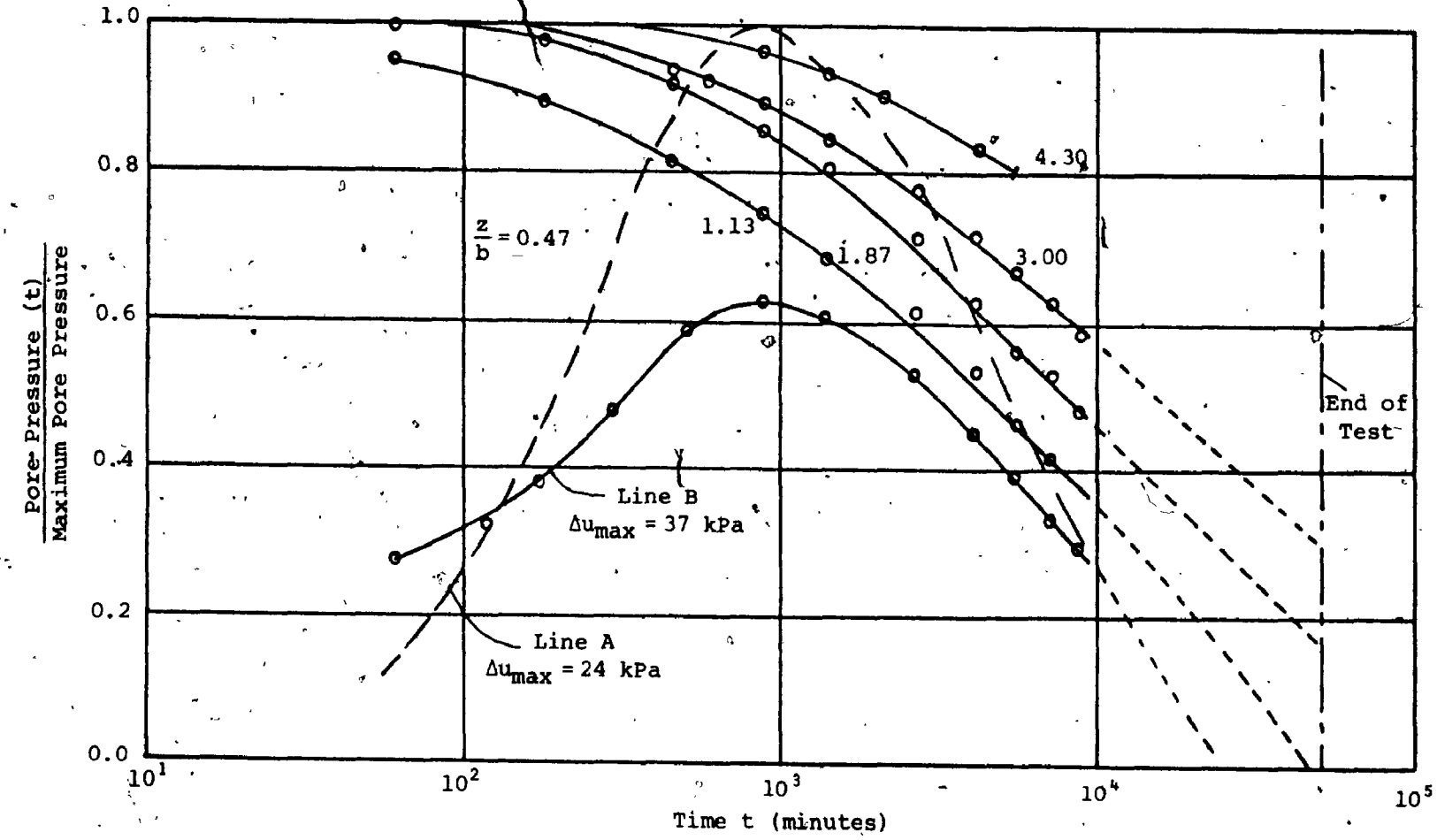

FIGURE 4.35
Dissipation of Pore Water Pressures Below Centreline of Plate

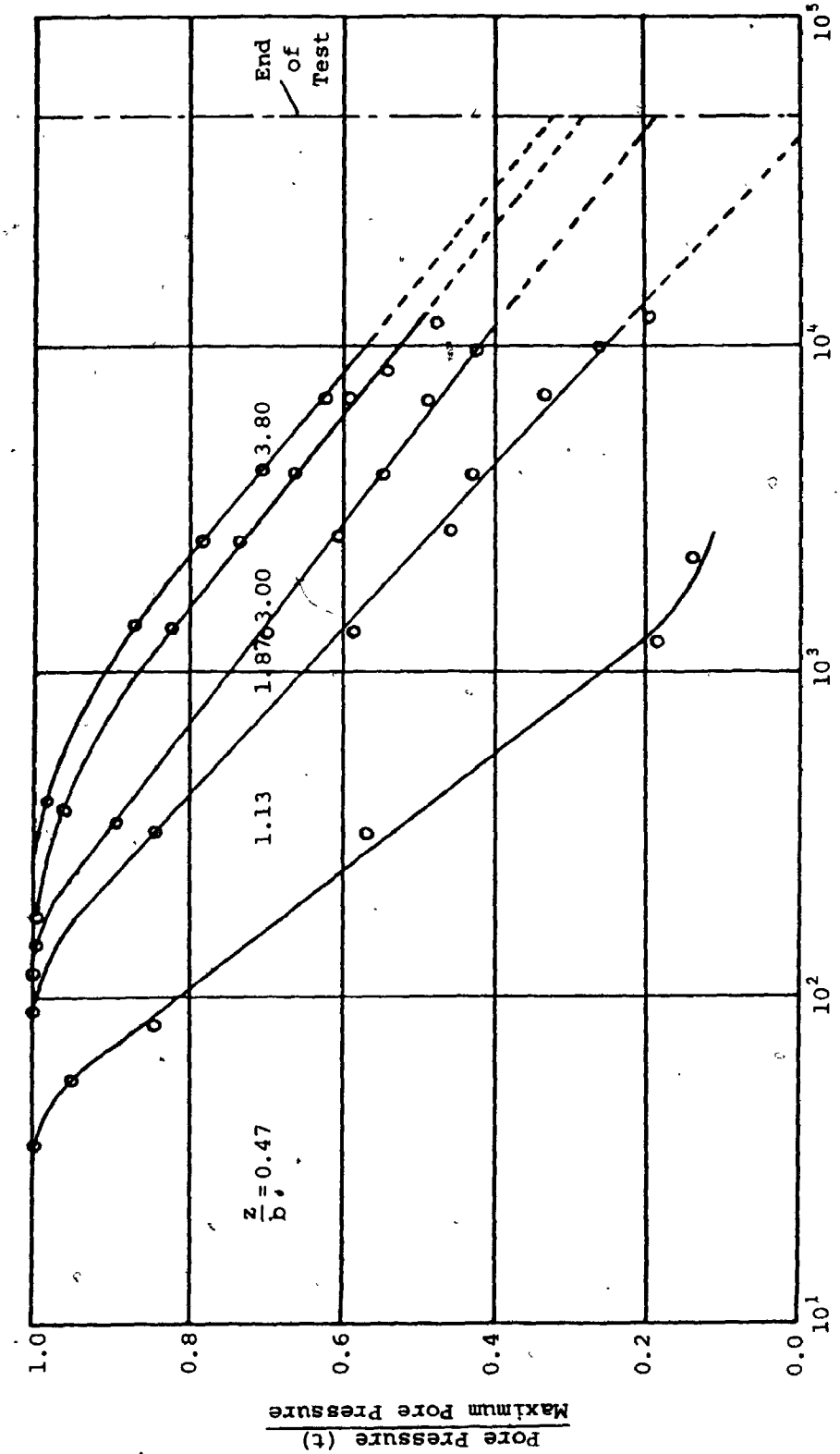

FIGURE 4.36
Dissipation of Pore Water Pressure Below Edge of Plate

piezometer, the pore water pressure systems appeared to function properly for various lengths of time. Generally, however, ten days after the plate loading the pore water pressures increased erratically, indicating the presence of air in the system. It is recommended in future tests that a larger piezometer tip be employed, to enable the piezometer to function for a longer period of time.

(5) By making an extrapolation of the curves, the pore water pressures in the upper layers are reduced to zero before the end of the test, and the pore water pressures in the lower layers are less than 30 percent of their maximum values. Since the primary consolidation settlement is related to the excess pore water pressure, it may be inferred that most of the consolidation settlement of the plate will have occurred at the end of the five-week test.

4.4.6 *Consolidation Settlement*

4.4.6.1 *Total Consolidation Settlement*

In the analysis of consolidation settlement, two aspects are of prime importance: (1) the degree of consolidation at any time; and (2) the total consolidation settlement expected. The degree of consolidation settlement at any time is difficult to predict and is highly dependent on the drainage conditions assumed in the model.

An estimate of the total consolidation settlement can be predicted from the results of the standard one-dimensional consolidation test. In this method the equation of the consolidation settlement of a finite layer can be represented as

$$\rho = H \frac{C_c}{1+e_0} \log \left(\frac{\sigma_0' + \Delta\sigma'}{\sigma_0'} \right)$$

where H = thickness of the layer
C_c = slope of the effective stress versus void ratio curve
e_0 = initial void ratio
σ_0' = initial average effective stress
$\Delta\sigma'$ = effective stress increment.

For the numerical calculations of consolidation settlement, the clay was divided up into eight layers, and the stress increment was taken from the middle of each layer. From the summation of the consolidation of each layer, the total consolidation settlement can be obtained.

From a series of standard one-dimensional consolidation tests, it was possible to determine an average value of the compression index, C_c. The void ratio-log effective stress curves are presented in Figures 3.16 to 3.20 and summarized in Table 2. The slope of the curves was highly dependent on the initial moisture content of the clay, but since the clay in the test tank was extruded at a consistent 39 percent (± one percent) the initial void ratio can be estimated at 1.15. Since remolded clay has been found to resemble normally consolidated clay, an average value of the compression index C_c can be obtained from the maximum slope of the void ratio-log effective stress curve. Taking the maximum slope represents the "virgin" portion of the clay e-log σ_0' curve, which is greater than the apparent recompression curve at low effective stress levels.

A summary of several methods used to predict the total consolidation settlement are presented in Table 10. The predictions are based on highly simplifying assumptions regarding the consolidation characteristics of the clay. It has been assumed that

— the soil behaves as normally consolidated clay;

TABLE 10

PREDICTED CONSOLIDATION SETTLEMENT
(mm)

DESCRIPTION	STRESS INCREMENT METHOD					
	(1) $\Delta\sigma_1$ Halfspace	(2) Δu Minimum	(3) Δu Maximum	(4) Δu Observed	(5) $\Delta u = \Delta\sigma_{oct}$	(6) $C*\Delta\sigma_1$
Predicted Consolidation Settlement ρ_c	52.2	23.5	41.9	20.7	36.4	34.0
Ratio $\frac{\rho_c}{(21.6\ mm)}$	2.42	1.09	1.94	0.96	1.69	1.57
Ratio $\frac{\rho_c}{(30.5\ mm)}$	1.71	—	—	$\frac{20.7 + 8.9}{30.5} = 0.97$	1.19	1.11

NOTE

(1) Observed consolidation settlement at the end of test = 21.6 mm.

(2) Total consolidation settlement due to surcharge and test plate = 30.5 mm.

— the compression index, C_c, is constant and equal to 0.306;

— the initial void ratio, e_0, is constant and equal to 1.15;

— the initial effective stress, σ'_0, is constant and equal to 20 kPa.

The assumptions used in the various methods presented in Table 10 are outlined as follows:

METHOD (1)

- $\Delta\sigma' = \Delta\sigma_1$ below plate centreline
- $\Delta\sigma_1$ was calculated from theory developed for a uniformly loaded strip footing resting on an isotropic elastic half-space (see Fig. 4.27)
- effect of rigid base and rigid footing not considered, but it is recognized that the differences in principal stresses can be significant.

METHOD (2)

- $\Delta\sigma' = \Delta u$ predicted below the plate centreline from the minimum estimated A parameter values (see Fig. 4.30).

METHOD (3)

- $\Delta\sigma' = \Delta u$ predicted below the plate centreline from the maximum estimated A parameter values (see Fig. 4.30).

METHOD (4)

- $\Delta\sigma' = \Delta u$ based on the maximum *observed* pore water pressure below the plate centreline (see Fig. 4.30).

METHOD (5)

- $\Delta\sigma' = \Delta u$
- $\Delta u = \Delta\sigma_{oct}$ below plate centreline (see Fig. 4.32)
- $\Delta\sigma_{oct}$ predicted from Poulos (1967) for a uniformly loaded strip footing resting on an isotropic elastic layer, $H/b = 5.0$.

METHOD (6)

- $\rho_c = C \times \rho_{c1}$, where ρ_{c1} is the predicted consolidation settlement from Method (1)

- C is a correction factor from Skempton and Bjerrum (1957)
- for A = 0.5 and H/b = 5, then C is given as 0.65

All of the methods are essentially similar but differ in one important aspect: the increase in effective stress.

The observed settlement versus time is plotted in Figure 4.37. At the end of five weeks, the total settlement minus the initial settlement amounted to 21.6 mm. It was difficult to assess whether or not 100 percent consolidation was achieved because there was no sharply defined portion indicating that secondary consolidation has begun. In the theoretical predictions of Davis and Poulos (1968, 1972), Gibson *et al.* (1970), Christian *et al.* (1972), Shanker *et al.* (1975) and Yamaguchi and Murakami (1976) relating the degree of consolidation, U, with various time factors, it was shown that the slope of the curves were essentially linear when U was greater than 50 percent and less than 90 percent. It was possible to estimate from the work by Davis and Poulos (1968) that the degree of consolidation was greater than 85 percent, using the c_v value obtained from the surcharge loading of the clay, and 0.3 for Poisson's ratio of the soil skeleton. For the purposes of comparison of the various methods, it is assumed that at the end of five weeks, the consolidation settlement was complete. In Table 10 the ratio of the predicted settlement to observed consolidation settlement is presented in the second row. The best correlation is found from the prediction of consolidation settlement on the basis of *observed* pore pressure increases. All of the other methods over-estimate ρ_c; the greatest discrepancy occurs in the method (1) (i.e., simplified one-dimensional method).

It should be recognized that during the application of the

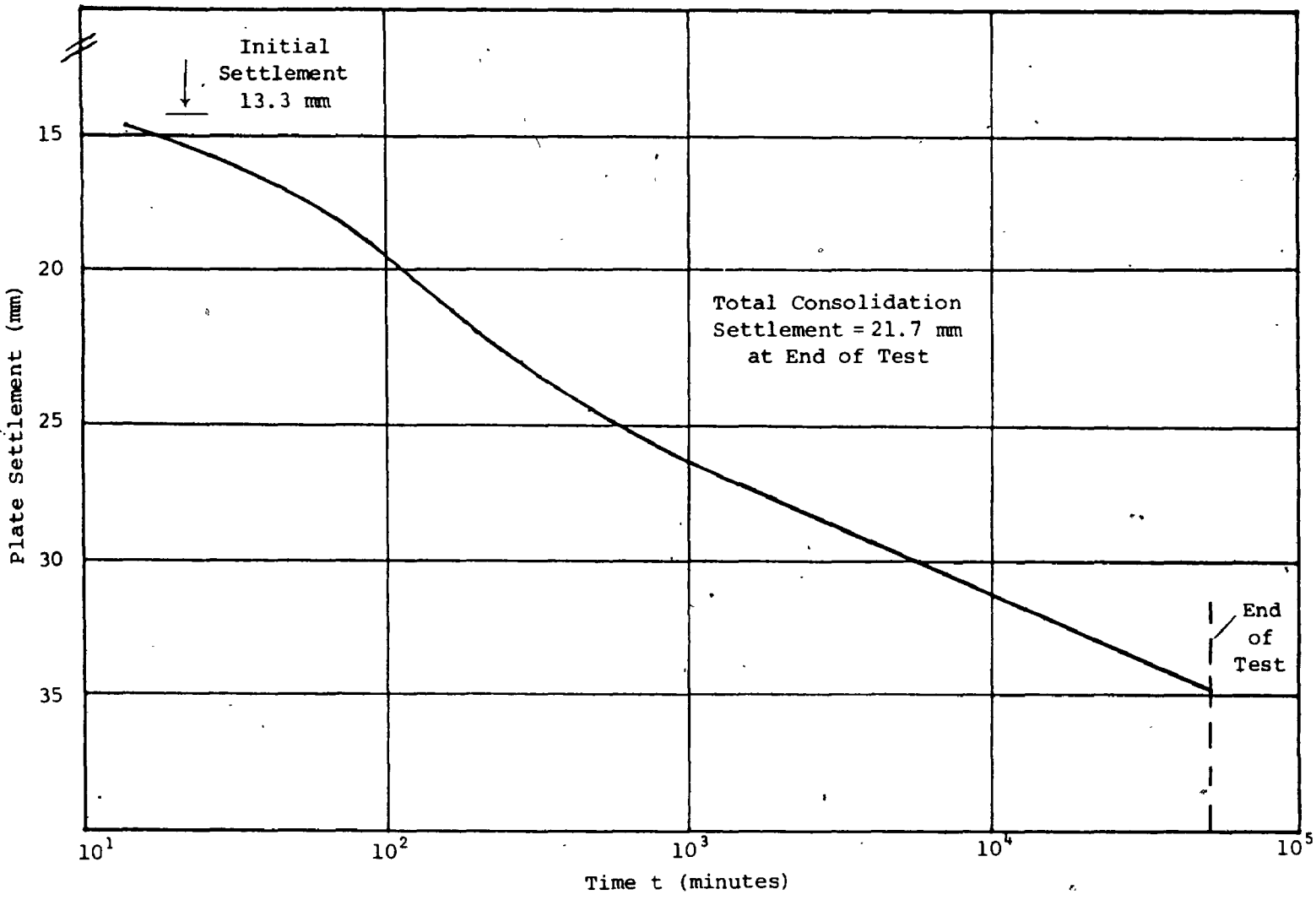

FIGURE 4.37
Consolidation Settlement during Plane Strain Test

surcharge, there was 8.9 mm of consolidation settlement primarily in the top layer of the soil. This can be taken into account by assuming this settlement would have occurred in the main test if no surcharge was applied. By dividing the predicted ρ_c values by the *total* ρ_c observed (21.6 mm + 8.9 mm) the assumption is made that the entire clay layer is normally consolidated. With this ratio, as shown in the third row of Table 10, the method (1) is again shown to greatly over-estimate ρ_c, but the prediction of settlement, ρ_c, from $\Delta u = \Delta\sigma_{oct}$ gives a better correlation. Since the consolidation process may be continuing, the ratio of ρ_c predicted / ρ_c observed would be reduced from the present 1.19, and provide an even better correlation.

These estimates of the consolidation settlement require an initial average effective stress to be estimated from the e-log (σ') curves. It is usually taken as being the point of intersection of the recompression curve and "virgin" loading curve, but it is apparent from Figures 3.16 to 3.20 that this value is not clearly defined in many cases. (In Figure 3.19 the sample had an initial moisture content greater than the moisture content of the clay in the test tank, so the "virgin" portion of the curve is more clearly defined at low effective stress levels.) Since e_0 can be assumed to range from 1.10 to 1.15, σ_0' ranges approximately from 20 kPa to 35 kPa in Figure 3.20. The choice of a σ_0' value has a significant effect on the calculation of total consolidation settlement. Using $\sigma_0' = 35$ kPa and $e_0 = 1.10$ in method (5) produces a total consolidation settlement of 24.4 mm. In comparison, using $\sigma_0' = 20$ kPa and $e_0 = 1.15$ produces $\rho_c = 36.4$ mm. It can be expected that all of the other methods would behave similarly and predict a lower consolidation settlement. Hence, the absolute value of predicted ρ_c is not known with

a high degree of certainty, and is sensitive to the initial conditions of the soil medium. The accurate determination of the initial effective stress is of major importance in undisturbed normally consolidated and over-consolidated clays taken from the field, but it is also found to be critical for the remolded clay used in this experiment.

Dr. Osler of McGill University has drawn attention to a method of determining the total settlement at the end of primary consolidation. Raymond (1965)* observed that in Terzaghi's (1943) theory of consolidation the pore water pressure-settlement relationship will be approximately linear when the pore water pressure-depth relationship resembles a parabolic distribution. Figure 4.37b shows a plot of pore water pressure versus plate settlement for various piezometer locations. By extrapolating the results the expected total settlement would have ranged from 24 to 25.5 mm. This can be compared with the observed total settlement of 21.6 mm at the end of the experiment. This method appears useful for providing an estimate of the primary consolidation settlement.

4.4.6.2 *Rate of Consolidation Settlement*

Much of the literature on consolidation settlement is concerned with the *rate* of settlement, and it has been found that the predictions are highly dependent on the assumptions regarding the drainage paths available for pore pressure dissipation (see Lee and Valliappan, 1974). The drainage paths in the plane strain apparatus are not clearly defined and at present there is no available analytical or numerical solution for the case of a *rigid* strip footing. In this experimental investigation

*Raymond, G.P. (1965) "Discussion: Two-stage construction of an embankment," Can. Geotech. Journal, 2, No. 3, 232-233.

the footing may be regarded as being impermeable, forcing the pore water below the plate to dissipate in some combination of lateral and vertical direction.

Davis and Poulos (1972) presented charts for the estimation of the rate of consolidation under two- and three-dimensional conditions incorporating various assumptions regarding the drainage paths available for pore water pressure dissipation. These results have been presented in Figure 4.38 for a uniformly loaded strip footing with a layer thickness 2.5 times the width of the footing. On the same graph the observed consolidation settlement during the principal test has been plotted, assuming 85 percent of the total consolidation settlement had occurred at the end of five weeks. The coefficient of consolidation was taken as ranging from 0.028 mm^2/sec (obtained from the surcharge loading) to

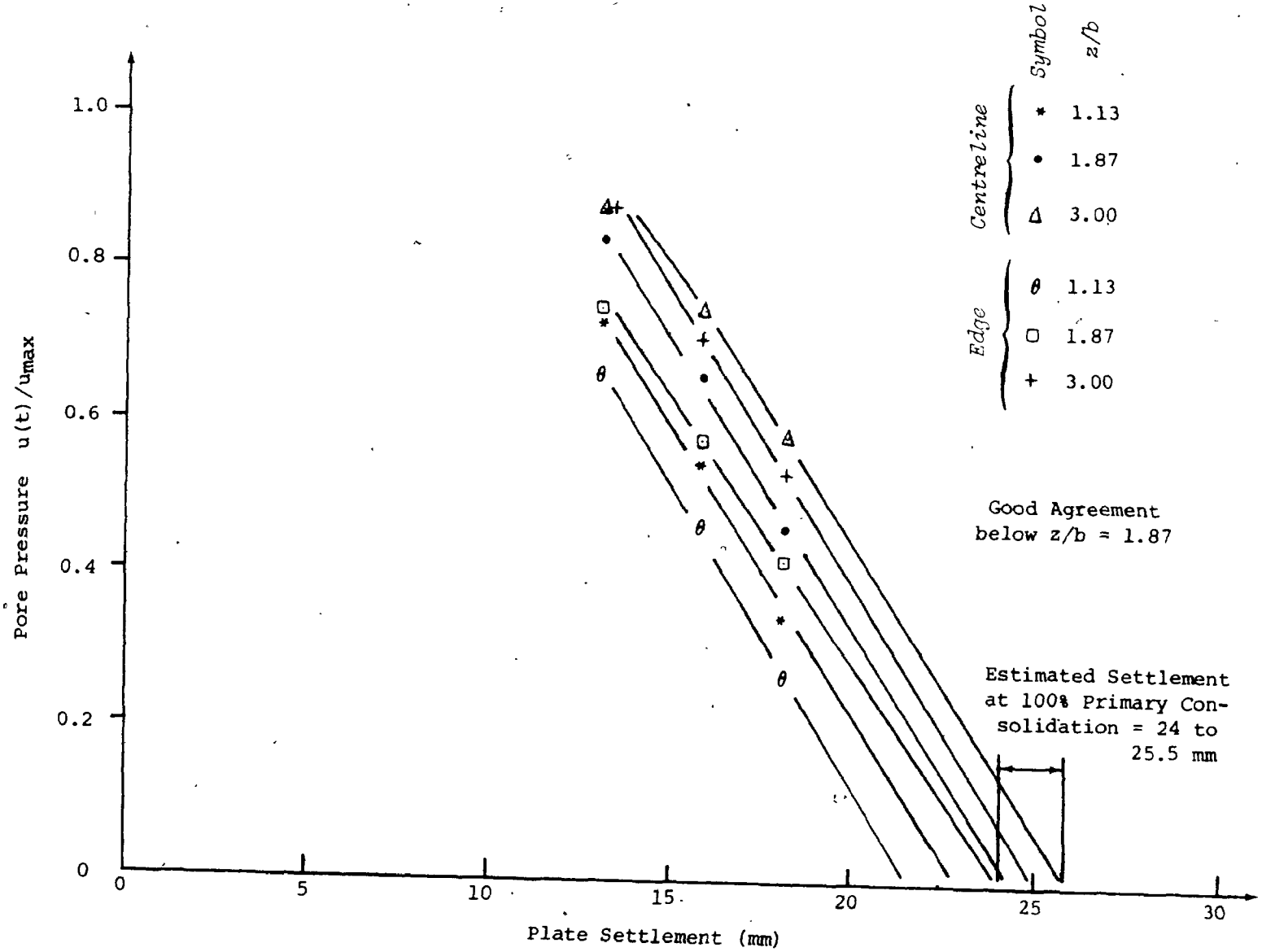

FIGURE 4.37b

Estimate of Primary Consolidation Settlement from Plot of Pore Pressure versus Settlement in Lower Portion of Clay Stratum

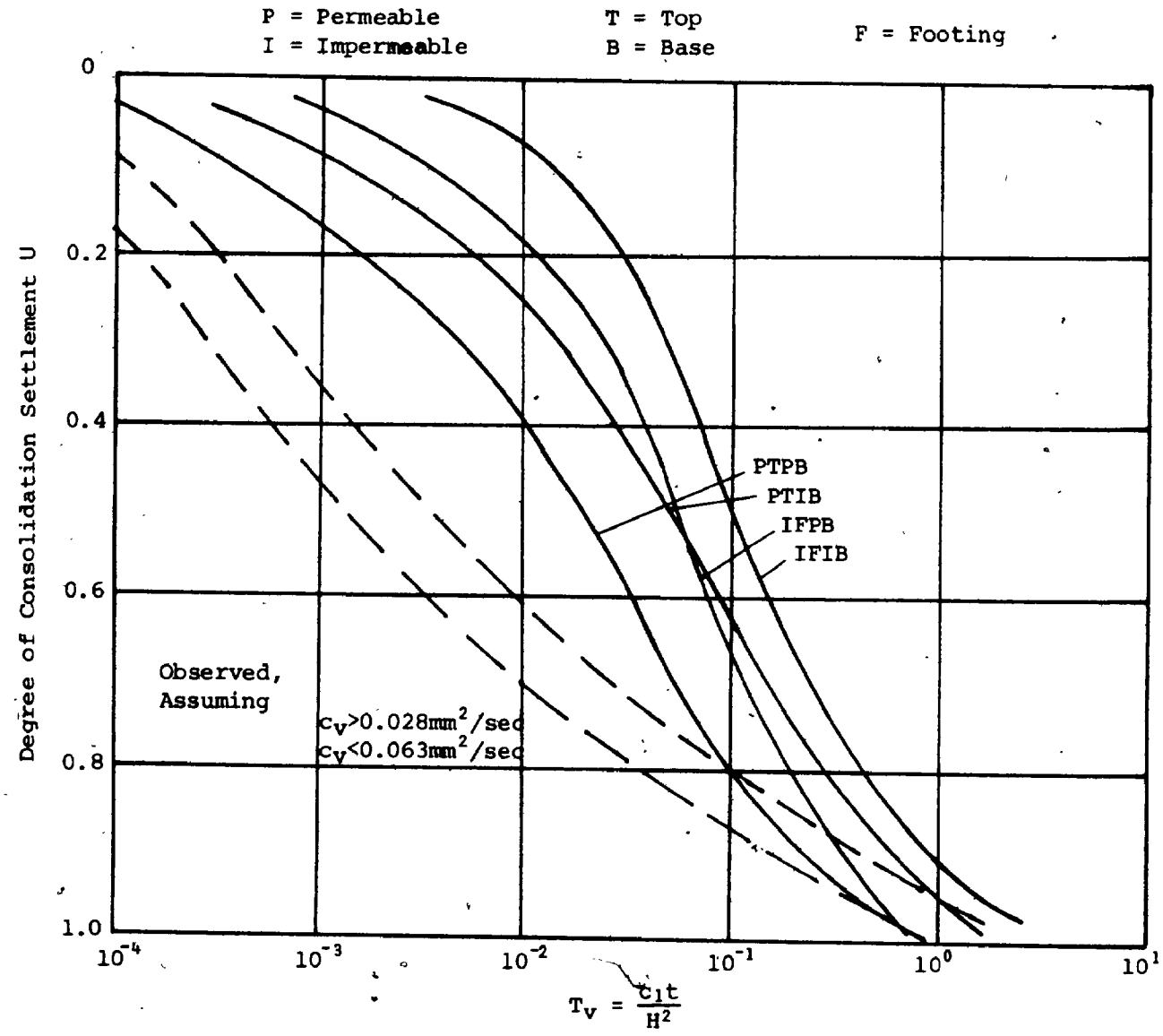

FIGURE 4.38
Degree of Consolidation Settlement With Time (after Davis and Poulos, 1972)

0.063 mm^2/sec (maximum obtained from the standard consolidation tests).

The observed rate of consolidation settlement appears to have been greater during the early stages of consolidation than any of the rates predicted by Davis and Poulos (1972). Shanker *et al.* (1975) similarly observed in model footings on a saturated clay that the experimental rate of consolidation was greater than the rate predicted by the three-dimensional theory of Biot (1941). Using a smaller value of layer thickness, H, in Figure 4.38 would have resulted in a shifting of the "observed" curves to the right, in better agreement with the values predicted by Davis and Poulos (1972). It is suggested that more experiments be performed before any conclusions are drawn from the results.

4.4.7 *Variation of the Contact Stress Distribution with Time*

The contact stresses were monitored in the plane strain apparatus for a period of five weeks, during which time the pore water pressures had substantially dissipated. The readings were taken every two minutes in the first hour after loading, at five-minute intervals in the next hour, ten-minute intervals for the next three hours, and every hour during the first few days. After this time readings were taken twice daily. The process was aided by the automatic timer on the data acquisition system.

The initial contact stress distribution in the centre region has already been presented in Figure 4.24, showing the asymetrical distribution immediately after loading. With 24 hours the distribution achieves a certain degree of symmetry, enabling a smooth curve to be fit to the points when all the locations are placed on one-half the plate width. As previously explained, the centre region has an average contact stress lower than the average total applied because of the possible

occurrence of wall friction. The centre results have been normalized in Figure 4.25 in order to show the relative magnitude of the contact stress with respect to position across the plate width. Each day the normalized contact stress distribution was plotted on the graph. At the end of the experiment it was found that although there were small fluctuations in the individual pressure cells, all the results were found to lie within the band shown in Figure 4.39.

The edge stresses are shown to be between 15 percent to 30 percent higher than the average stress. The middle region is between 80 percent and 95 percent of the average. The important point regarding the time-dependence of contact stresses is that there is no substantial re-distribution of the high edge stresses to the centre during consolidation, but neither is there a trend towards higher edge stresses. The major readjustment of the contact stress distribution occurred within the first 24 hours, after which the changes are relatively small. For example, the average centre stress varied from a high of 39.1 kPa to a low of 37.3 kPa which is a narrow range and comparable to the accuracy of the measuring system. A table of the daily observations is presented in Table 11, where it is shown that the edge contact stresses ranged from 1.10 to 1.30 of the average stress and the middle ranged from 0.81 to 0.94 of the average.

A plot of the individual pressure transducer outputs with time does not lead to a trend being observed (Fig. 4.40). The fluctuations may be considered to be due to environmental changes affecting the transducer output, such as small temperature and humidity fluctuations, and variations in supply voltage. As discussed previously, the total system is considered capable of measuring individual stresses to within ± 2 kPa

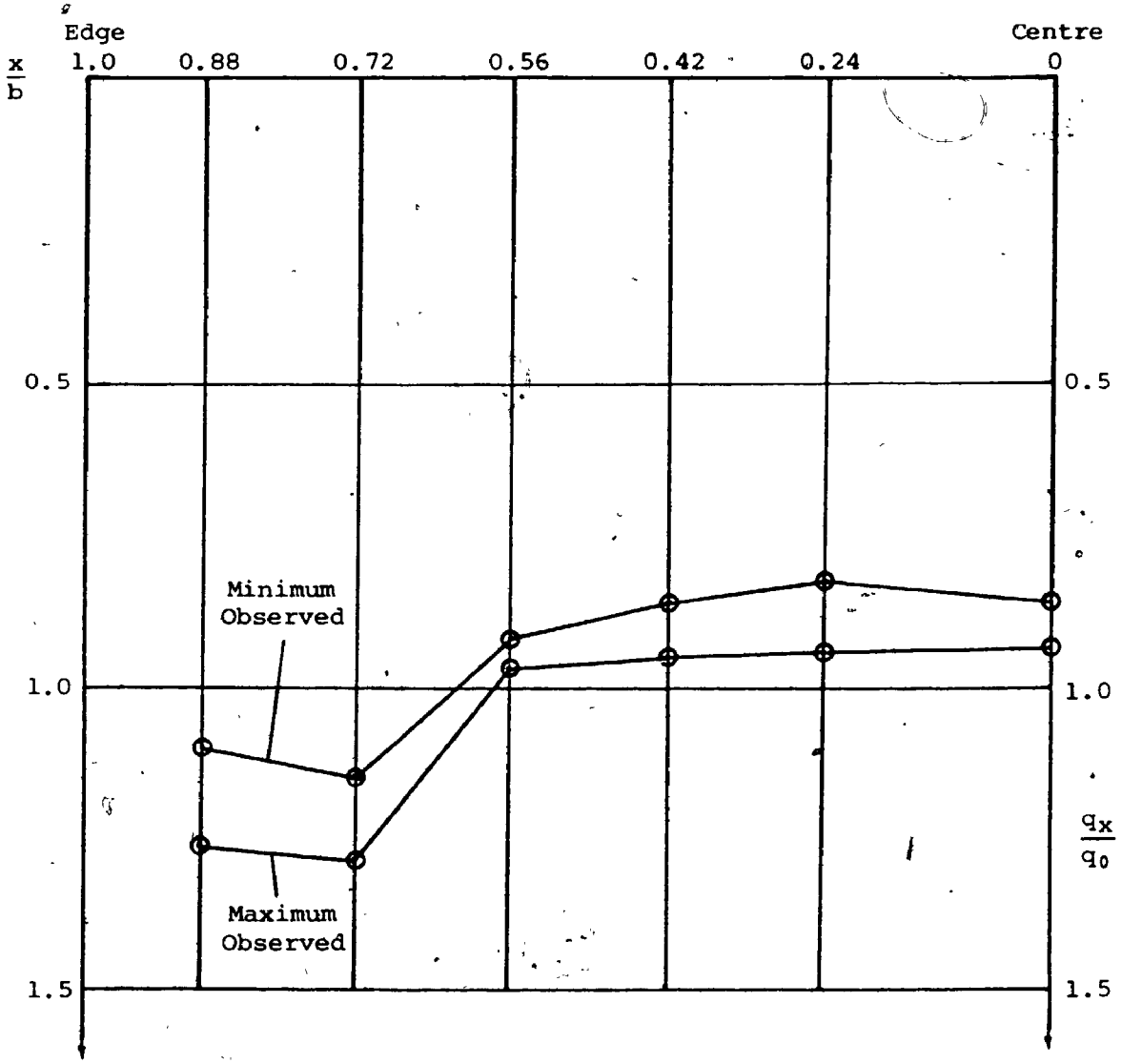

FIGURE 4.39

Normalized Contact Stress Distribution Throughout First Plane Strain Test

TABLE 11

CONTACT STRESS ACROSS CENTRELINE WITH TIME

UNITS OF kPa

NORMALIZED CONTACT STRESS = $\frac{\text{MEASURED } q_x}{\text{AVERAGE } q_0}$ (IN BRACKETS)

START AUG. 3 12 NOON

Date	Position x/b 0.88	0.72	0.56	0.40	0.24	0.0	Average q_0
Aug 4	42.8 (1.10)	47.8 (1.22)	36.2 (0.93)	37.3 (0.95)	36.8 (0.94)	33.3 (0.85)	39.1
5	43.7 (1.13)	46.9 (1.21)	36.1 (0.93)	37.1 (0.96)	35.2 (0.91)	32.8 (0.85)	38.6
6	44.5 (1.18)	45.1 (1.20)	36.2 (0.96)	36.5 (0.97)	31.1 (0.82)	32.8 (0.87)	37.7
8	44.0 (1.17)	43.5 (1.15)	36.1 (0.96)	36.2 (0.96)	32.2 (0.85)	34.5 (0.91)	37.7
9	45.5 (1.18)	44.9 (1.16)	36.9 (0.95)	35.7 (0.92)	33.2 (0.86)	36.0 (0.93)	38.7
10	46.3 (1.19)	46.0 (1.18)	36.1 (0.93)	34.6 (0.89)	33.8 (0.87)	36.3 (0.93)	38.8
11	46.0 (1.19)	47.1 (1.21)	36.1 (0.93)	33.8 (0.87)	33.5 (0.86)	36.3 (0.94)	38.8
17	49.0 (1.26)	47.0 (1.21)	37.1 (0.96)	32.8 (0.85)	32.5 (0.84)	34.5 (0.89)	38.8
19	47.4 (1.25)	47.3 (1.25)	36.4 (0.96)	32.0 (0.84)	30.9 (0.81)	34.2 (0.90)	38.0
20	48.5 (1.26)	48.0 (1.25)	36.8 (0.95)	31.7 (0.82)	31.7 (0.82)	34.6 (0.90)	38.6
22	46.7 (1.22)	48.6 (1.28)	36.6 (0.97)	31.7 (0.89)	31.5 (0.83)	32.3 (0.85)	37.9
23	47.6 (1.26)	47.9 (1.26)	36.6 (0.97)	31.5 (0.83)	30.6 (0.81)	33.3 (0.88)	37.9
Aug 24	47.0 (1.25)	47.5 (1.26)	36.2 (0.96)	31.3 (0.83)	30.8 (0.82)	33.2 (0.88)	37.7
25	47.4 (1.27)	48.6 (1.30)	36.4 (0.97)	31.9 (0.85)	31.3 (0.83)	33.3 (0.89)	37.5
26	47.0 (1.24)	47.2 (1.24)	36.1 (0.95)	32.4 (0.85)	31.6 (0.83)	33.0 (0.87)	37.9
27	44.8 (1.24)	45.3 (1.25)	35.9 (0.95)	33.1 (0.86)	31.5 (0.81)	33.1 (0.88)	37.6
29	44.8 (1.20)	45.3 (1.22)	35.9 (0.96)	32.3 (0.89)	30.2 (0.84)	33.3 (0.89)	37.3
30	45.4 (1.21)	47.3 (1.26)	35.5 (0.95)	32.6 (0.87)	30.7 (0.82)	33.7 (0.90)	37.5
31	44.4 (1.20)	45.7 (1.23)	35.4 (0.95)	32.4 (0.87)	31.6 (0.83)	33.4 (0.90)	37.1
Sept 1	43.9 (1.19)	46.6 (1.26)	35.2 (0.95)	32.2 (0.87)	30.7 (0.83)	33.3 (0.90)	37.0
2	42.9 (1.15)	48.4 (1.30)	35.1 (0.94)	32.3 (0.87)	31.1 (0.84)	33.3 (0.89)	37.2
3	41.7 (1.14)	48.3 (1.32)	34.5 (0.94)	31.6 (0.86)	30.8 (0.84)	33.1 (0.90)	36.6
6	40.0 (1.10)	46.9 (1.29)	34.5 (0.95)	32.3 (0.89)	30.2 (0.84)	33.3 (0.92)	36.2

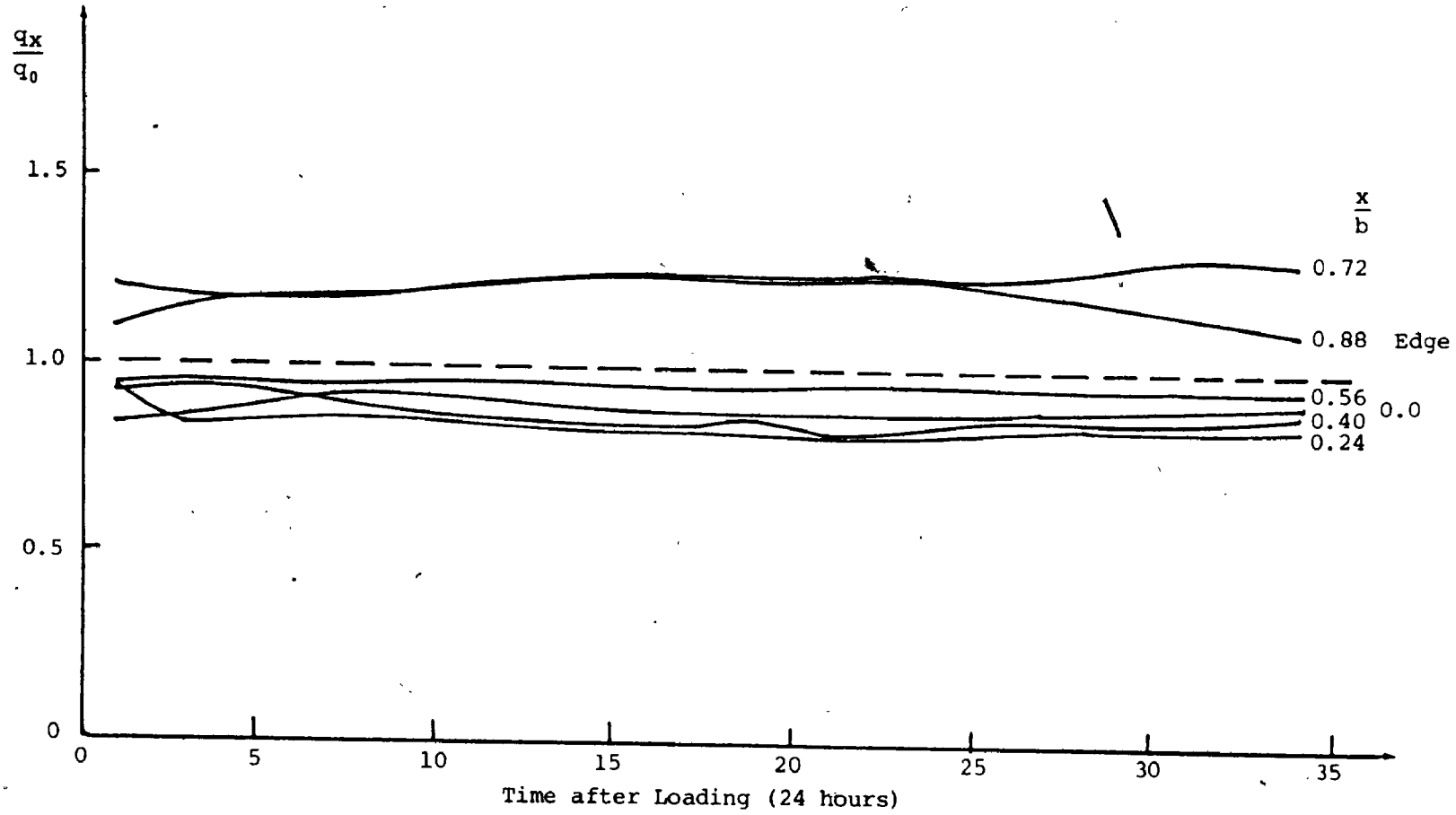

FIGURE 4.40
Contact Stress versus Time for Individual Pressure Transducers during First Plane Strain Test

at the stress range used in the experiments on clay (0 to 60 kPa average).

After the end of the five-week test, the plate was unloaded and then reloaded in small stress increments. The contact stress distribution across the centre region is plotted in Figure 4.41. The general shape of the reload contact stress distribution in the central section is similar to the first loading sequence, having higher edge contact stresses and lower stresses in the centre. The same degree of non-uniformity of contact stress distribution between the walls was observed during reloading.

When the test plate was removed the moisture content of the clay directly below the plate was about 4 or 5 percent lower than the initial moisture content of 39 percent directly below the plate. The variations in moisture content were less than one percent. The shear vane strength near the surface was uniformly about 50 percent higher than the shear strength of the soil adjacent the footing and at greater depth.

Huang (1976) and Brown (1977) studied the effect of visco-elastic soil behaviour on the performance of raft foundations, but there are relatively few theoretical studies of the time dependence of contact stress distributions during primary consolidation of the soil to compare with the experimental results. Huang (1976) showed that the contact stresses will increase at the edges and decrease at the centre as the raft settles. Brown (1977) showed that the outer columns of a structure will carry more of the load, indicative of higher edge contact stresses. In both cases the increases are moderate and are dependent on the initial relative flexibility of the raft to the soil medium. The studies are concerned with one form of secondary consolidation settlement, and

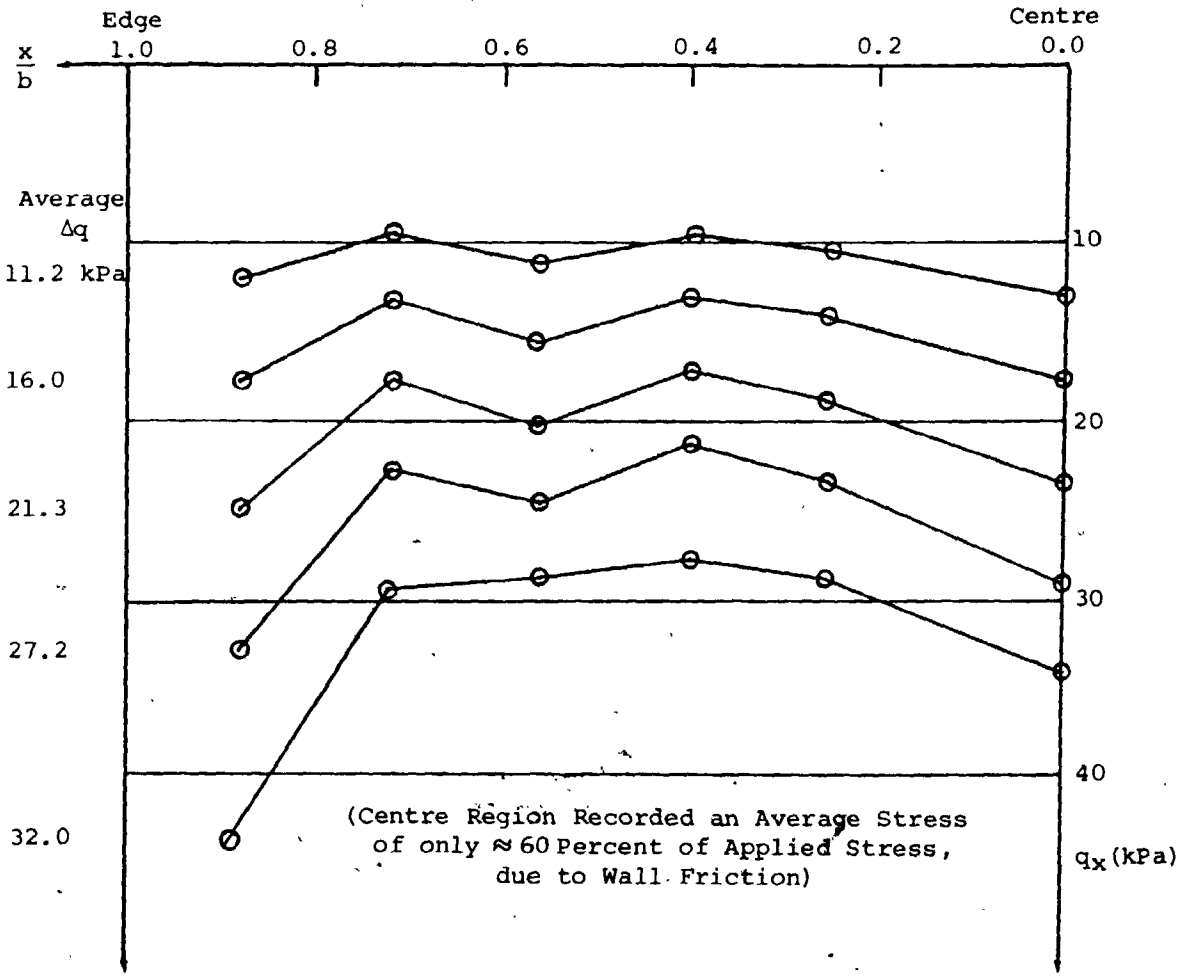

FIGURE 4.41

Incremental Contact Stress Distribution across Centre Region for Reloading of Plate after Five-Week Test on Clay

not with the changes in contact stress distributions due to the primary consolidation of the soil which is of direct importance in this investigation.

4.5 *Static Contact Stresses*

Two additional tests on clay using the plane strain apparatus were performed over a short period of time to acquire additional data on the immediate contact stress distribution. In the first subsequent test, the walls of the tank were removed and a 0.1-mm thick sheet of plastic placed between the stainless steel sheet and the clay layer (see Plate 12). The stainless steel had been cleaned and polished and a thin layer of light oil was spread over its surface. After replacing the walls, the top clay layer was removed and remolded to a depth of approximately 0.1 m. A surcharge of 62.8 kPa was applied to the surface similar to the surcharge used in the previous plane strain test, except that the duration of the load was less than two hours.

From the results of the main test in the plane strain apparatus, it was apparent that there was considerable side friction, causing the contact stress distribution beneath the plate to be high adjacent to the walls. Using the plastic sheet and thin layer of oil instead of silicone vacuum grease, the friction on the walls was considerably reduced. This was apparent in the second test during the application of the surcharge because the rebound of the surface amounted to 13.0 mm, compared to an initial deflection of 19.0 mm. In the first test the initial deflection was 21.3 mm with a smaller surcharge of 42.1 kPa, but the immediate rebound amounted to only 3.5 mm, followed by an additional 3.1 mm within 24 hours. The fact that the immediate rebound was a greater

PLATE 12

Removal of Side Wall of Plane Strain Tank for Placement of Plastic Sheet and Film of Oil

percentage of the initial deflection in the second test can be attributed in part to the reduced side wall friction.

After the surcharge was removed, the test plate was installed over the surface of the clay and left 24 hours to reduce any irregular surface profiles to a minimum. This step is necessary because the initial contact stresses were found to be highly dependent on small variations in the assumed plane surface. Since it was difficult to make the top surface as smooth as desired, the clay was sprinkled with a small amount of water, reducing its strength and resulting in a more uniform interface condition.

The load was then applied in a series of increments over a short period of time. Each load duration was less than 15 minutes, during which the contact stresses, plate settlement and surface profiles were recorded by the "B & F" system.

This test was useful in showing that the wall friction can be considerably reduced by using plastic sheeting and a thin layer of oil instead of silicone vacuum grease. This is illustrated in Figure 4.23, showing the average contact stress beneath the plate between the walls. The two methods employed to reduce the frictional effects along the sides of the container may be compared in the following manner:

AVERAGE NORMALIZED CONTACT STRESS BETWEEN WALLS
(q_x/q_0)

Method	*Location*		
	Adjacent Wall	Intermediate	Centre
Silicone Grease	2.07	0.84	0.70
Plastic Sheet and Oil	1.10	0.97	0.94

The wall friction can never be entirely eliminated but it is apparent that there are better methods than the use of silicone vacuum grease. This material was used by several researchers who reported that the friction between the soil and the walls of the container will be considerably less than it would be if no lubricant is used (Leonards and Girault, 1961; Burland and Roscoe, 1969).

The normalized contact stress distributions in the centre region at a stress of 52 kPa is shown in Figure 4.42. The contact stress in the centre is definitely higher than the edges, producing a parabolic distribution as would be expected under failure conditions or at high stress levels approaching failure. Since the estimated bearing capacity was greater than 80 kPa, the applied stress had produced extensive yielding of the clay at the edges of the plate. The plate was placed on a clay layer that was essentially the same material as used in the primary test, except for the remolded top layer 0.10 metres thick. Below this layer the clay may have consolidated directly beneath the plate resulting in non-uniform moisture contents and stress conditions. For this reason the contact stresses cannot be taken as representing those of rigid plate on a *homogeneous* elastic layer.

In the light of the above non-homogeneity, another test was performed on the clay in the plane strain apparatus, except this time the top 0.45 m of clay was removed. This left a layer of 0.52 m thick that was less influenced by the previous loading tests. The H/b ratio was reduced to 2.8 from 5.1. Shear vane tests (Fig. 4.43) showed that the clay at this depth had similar cohesive strength as the clay used at the start of the main five-week test.

The test plate was again installed in place, taking care that the

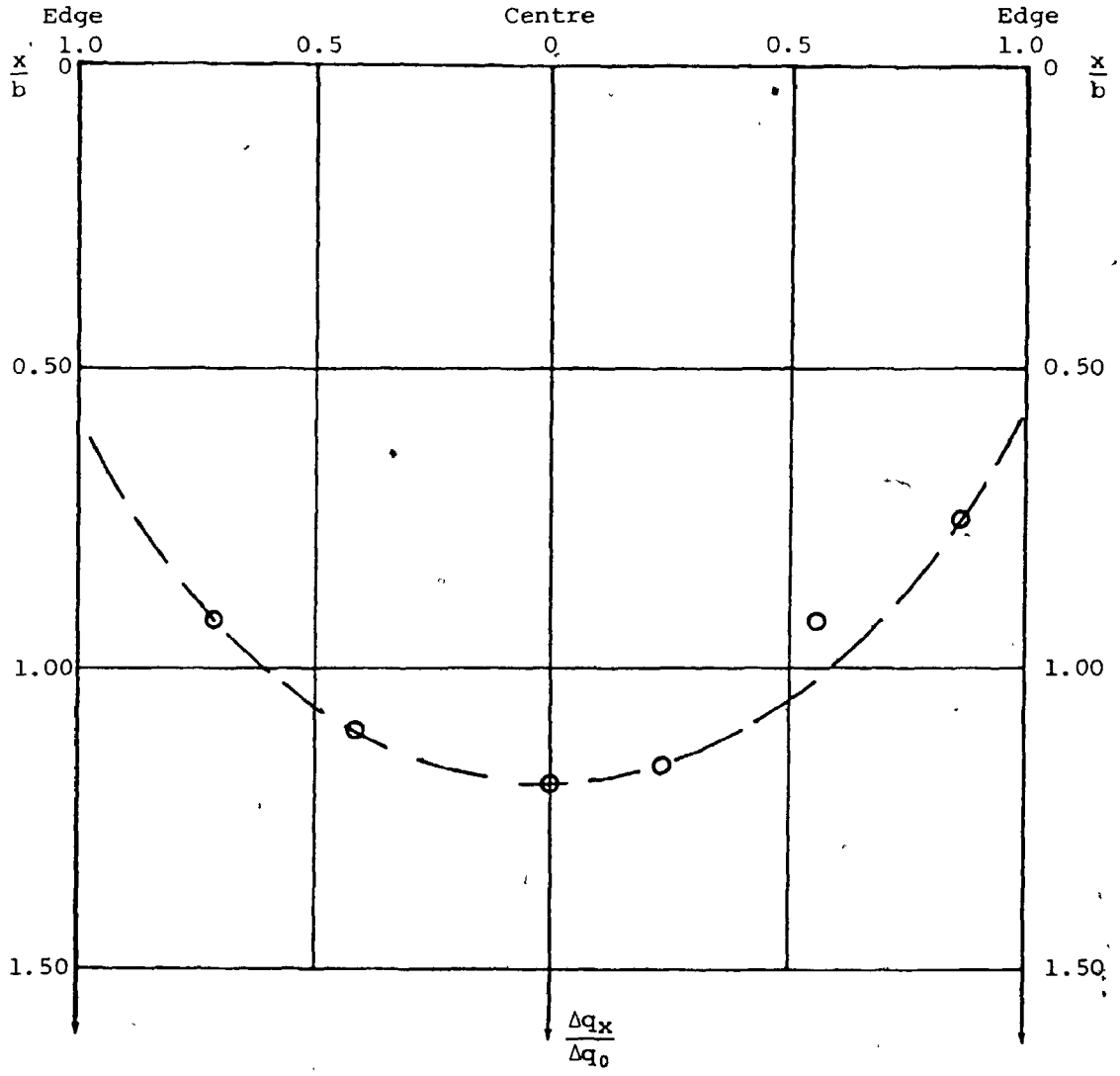

FIGURE 4.42

Contact Stress Distribution during Second Plane Strain Test, Δq_0 = 52 kPa

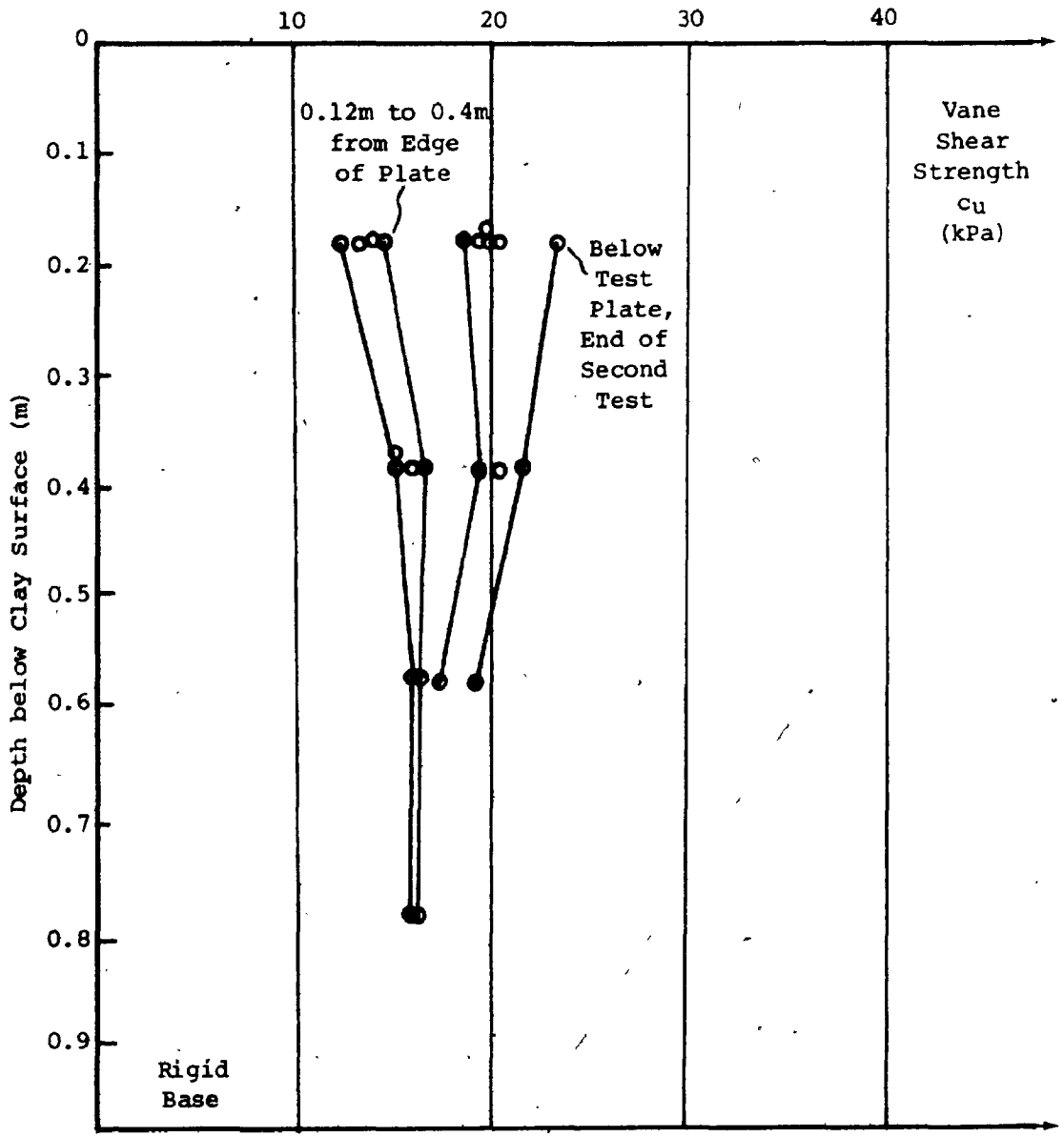

FIGURE 4.43
Vane Shear Strength Results from Plane Strain Apparatus

initial surface was as smooth as possible. Incremental loads were again applied and the contact stress and plate settlement recorded. With this test it was possible to determine the effect of the magnitude of load on the contact stress distribution. The incremental increase in contact stress with each increment in applied stress is plotted in Figure 4.44, normalized against the average applied stress in the centre region of the plate. These results prove very interesting in that at low stress levels the edge of the plate takes most of the incremental stress. The next stress increment is distributed more uniformly. With the third stress increment the centre carries most of the applied stress increment, with the edge contact stress increment less than half of the average. The load-settlement relationship is plotted in Figure 4.44a.

It was possible to take the results of the smooth curves obtained in Figure 4.44 and plot the relationship between the measured contact stress, q_x, and the average contact stress, q_0, for each of the six pressure transducers. If the contact stress was independent of the magnitude of the load, a series of straight lines would be produced. From Figure 4.45, the lines are curved because at higher stress levels local yielding at the edges of the plate causes the incremental contact stress to be distributed more in the centre region.

By summing the incremental contact stress distributions from Figure 4.45, the immediate contact stress distribution at different total applied stress levels can be obtained (Fig. 4.46). At low stress levels the edge contact stress is substantially higher than at the centre. As the load increases, the contact stress distribution becomes more uniform.

Since the clay used in the third test with $H/b = 2.8$ was in

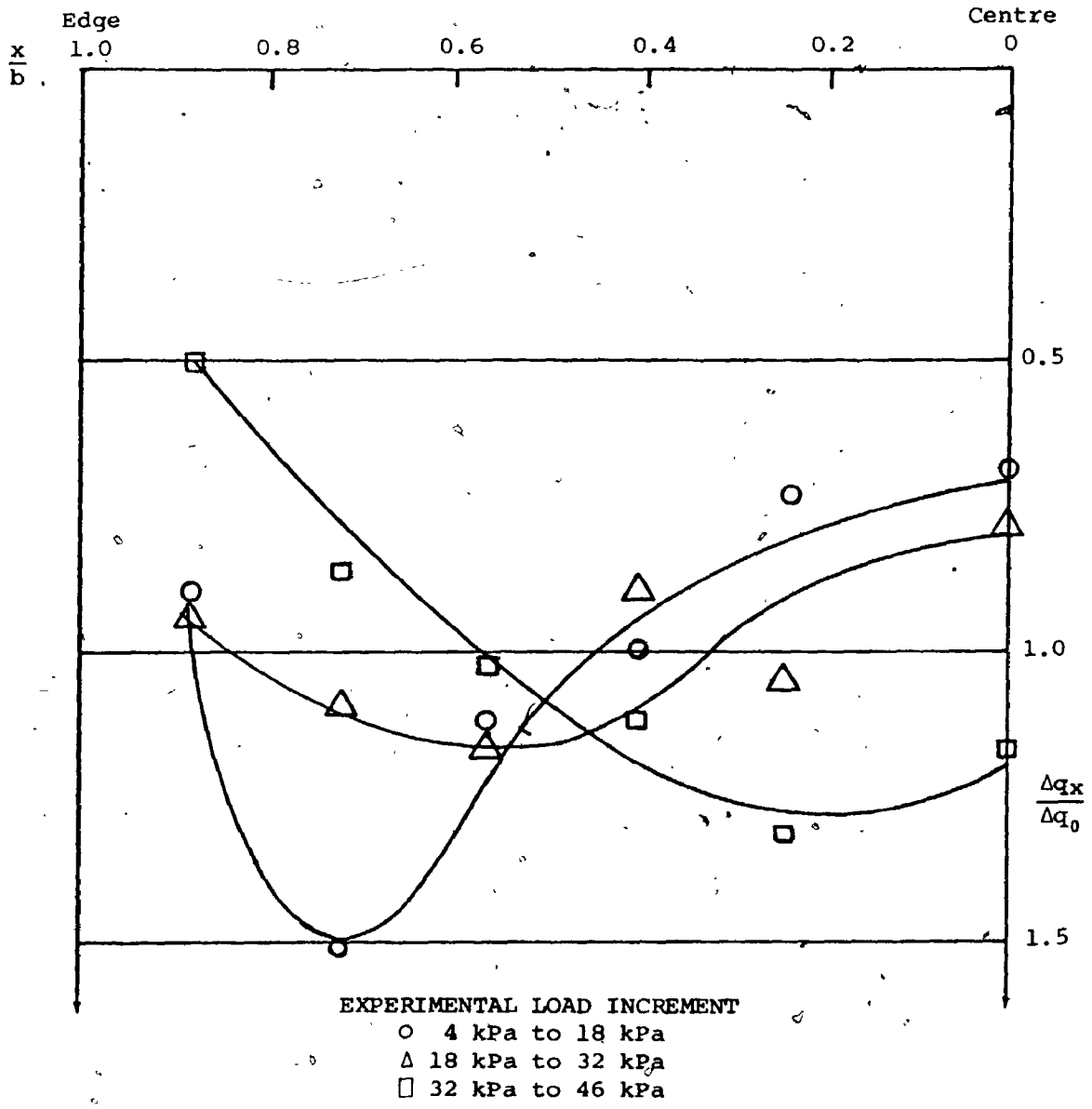

FIGURE 4.44

Incremental Contact Stress Distribution for Third Test on Clay

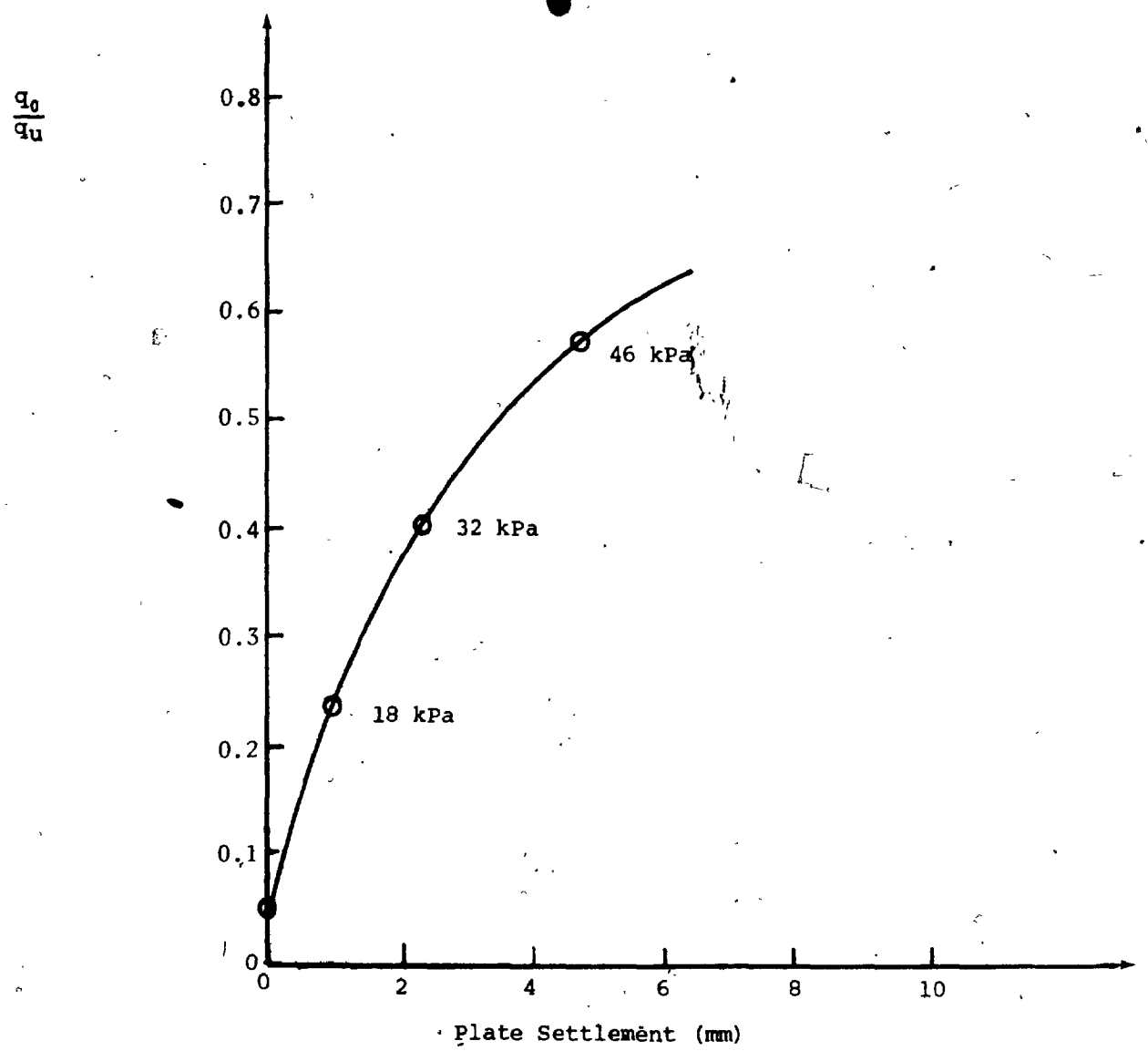

FIGURE 4.44b
Plate Settlement During Third Plane Strain Test

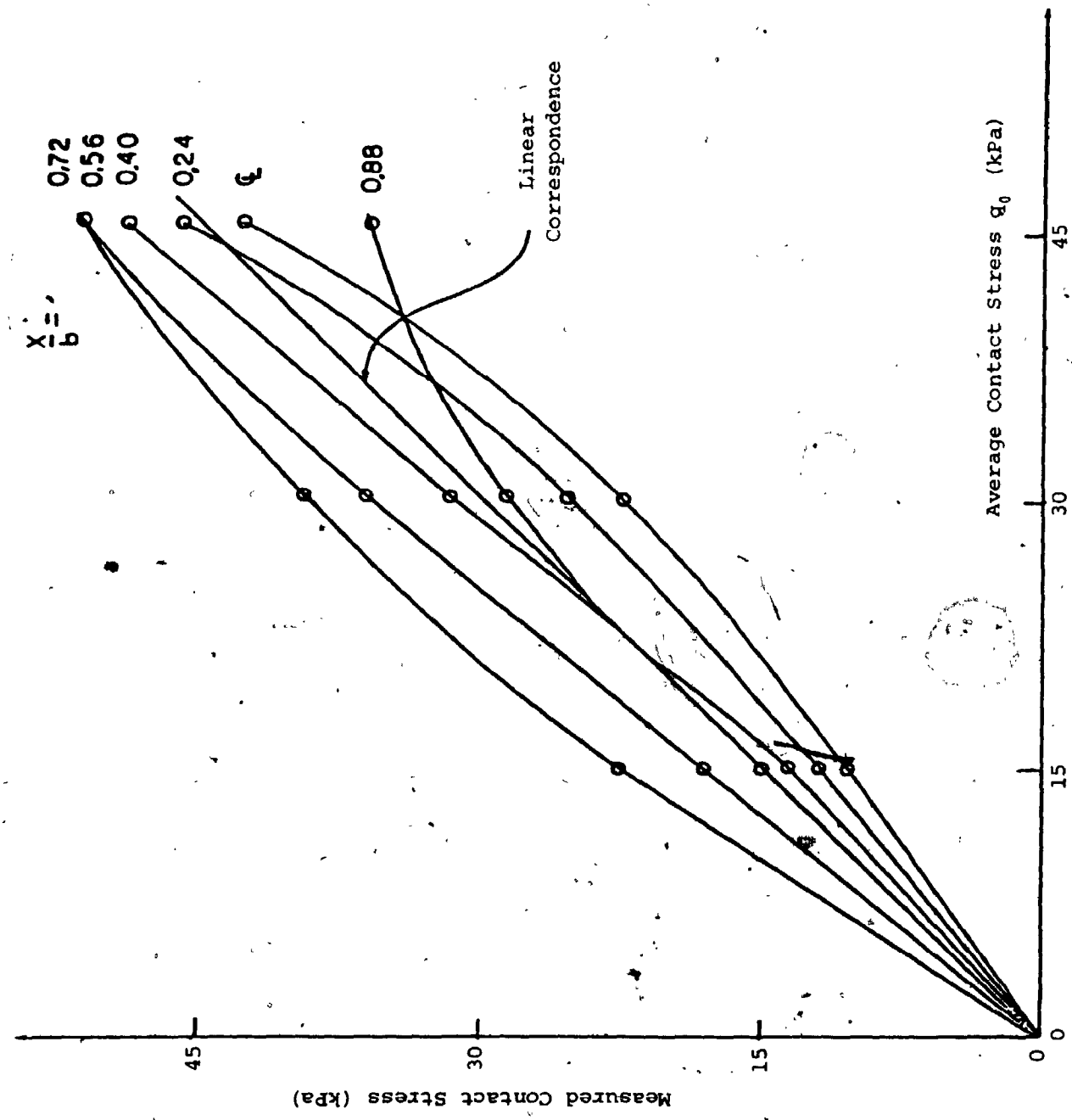

FIGURE 4.45 Measured versus Average Contact Stress from Third Test on Clay

practically the same condition as that used in the main test, the results can be compared. It has been shown (Fig. 4.39) that the centre strip contact stress distribution relating to the principal test had edge contact stresses approximately 50 percent greater than those of the centre. The average contact stress in this centre strip was about 39 kPa, compared to the total stress applied to the plate of 56.4 kPa. The side walls produced friction and increased the contact stresses adjacent to the walls, but within the centre strip it may be assumed that the walls have little influence. Hence, comparing Figure 4.39 with Figure 4.46, there is very good agreement in the contact stress distribution at a stress level of 39 kPa. The trend is still towards edge contact stresses about 50 percent higher than the centre. Relating this stress level to the bearing capacity (estimated to be greater than 80 kPa) the factor of safety is greater than two. Based on the experiments conducted (although limited) it becomes evident that at working stress levels the edge contact stresses will be substantially higher than their central values.

It has been observed in the past, and in this investigation, that the edge contact stresses are limited to a finite value because of either plastic yielding of the soil or corner curvature of the foundation. A comparison can be made with the predicted contact stress distribution for a rigid strip footing with plastic yielding at the edges, according to Schultze (1961) and Zeevaert (1972). Both methods are essentially the same for a purely cohesive material except that the magnitude of the limiting edge pressures are different. Schultze (1961), in agreement with Terzaghi (1943), assumes that the edge stress is fixed at a value equal to the average bearing capacity of the foundation (i.e.

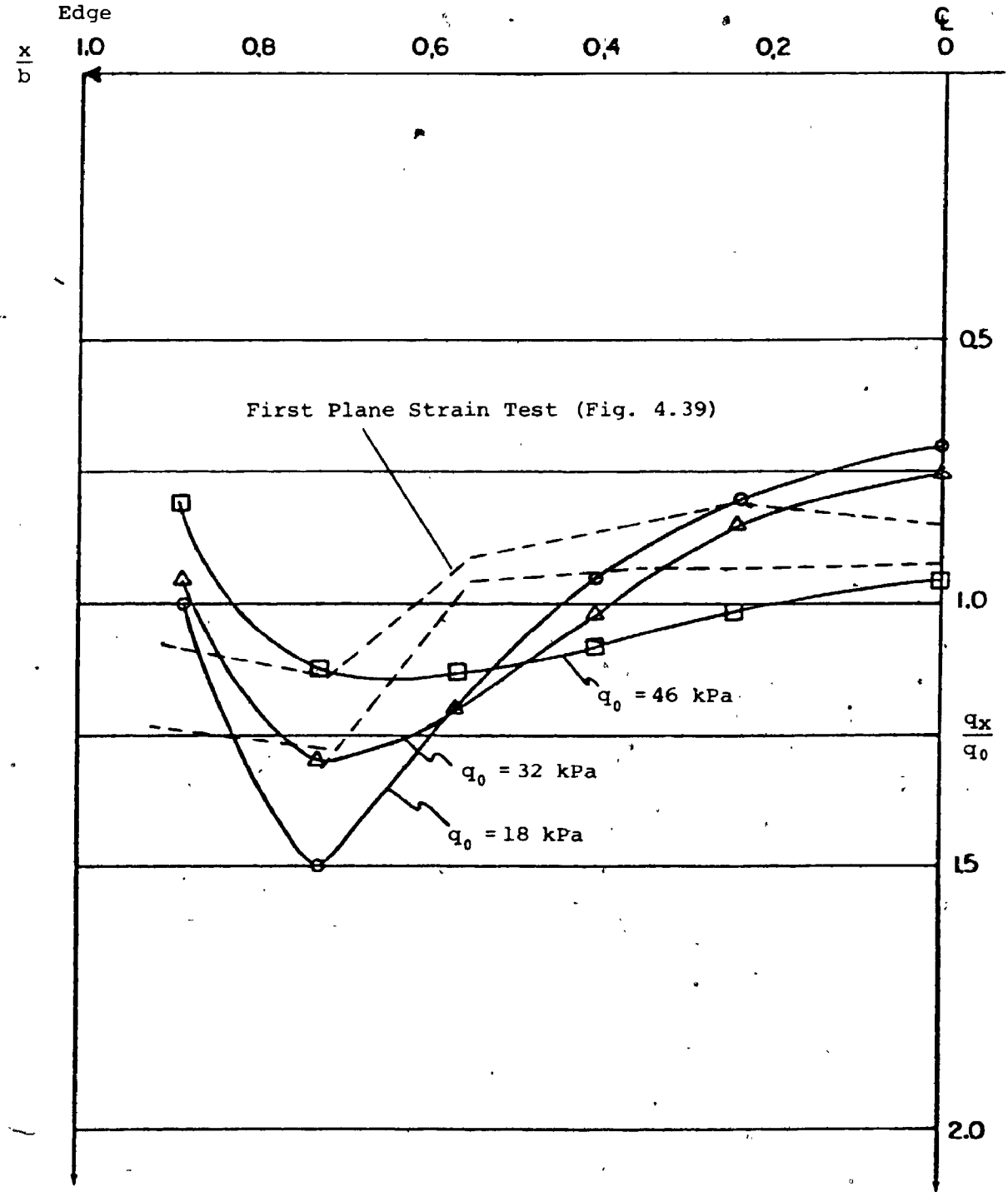

FIGURE 4.46
Summation of Incremental Contact Stress
Distributions during Third Test on Clay

5.14 c_u). As the applied stress increases, the centre region of the foundation has an increase in contact stress, while the edge stress remains constant. Zeevaert (1972) assumes that with a surface foundation, the edge contact stress is limited to 1.5 c_u, or only about one-third of the value chosen by Schultze (1961).

Hoeg *et al.* (1968), using a finite element technique, showed that local yielding at the edge of a shallow, rough rigid strip footing would first occur when the applied stress reached 2.3 c_u. At a stress level of about 3.1 c_u, the contact stress distribution was parabolic; this distribution remained constant as the load approached the bearing capacity value of 5.14 c_u. Theoretically, there should be some local yielding at the edge for any stress level. Chen (1975) showed that this was true in a finite element solution for a rough rigid strip footing on a thick layer of purely cohesive clay. When the load was about 15 percent of the bearing capacity, the contact stress distribution was essentially elastic. At 55 percent of the bearing capacity, the edge contact stresses were still 1.5 times the centre contact stress, but considerable yielding had occurred. It appears that the results from finite element analyses are highly dependent on the mesh configuration and boundary conditions, so the limiting edge contact stress will vary accordingly.

Figure 4.47 shows the different contact stress distributions that will be obtained from the methods given by Schultze (1961) and Zeevaert (1972). Line (1) represents the contact stress distribution for a rigid strip footing on an elastic half-space. In lines (2) and (3), the maximum edge stresses were taken as being equal to the estimated bearing capacity of the clay medium (81 kPa). A higher edge stress is given in

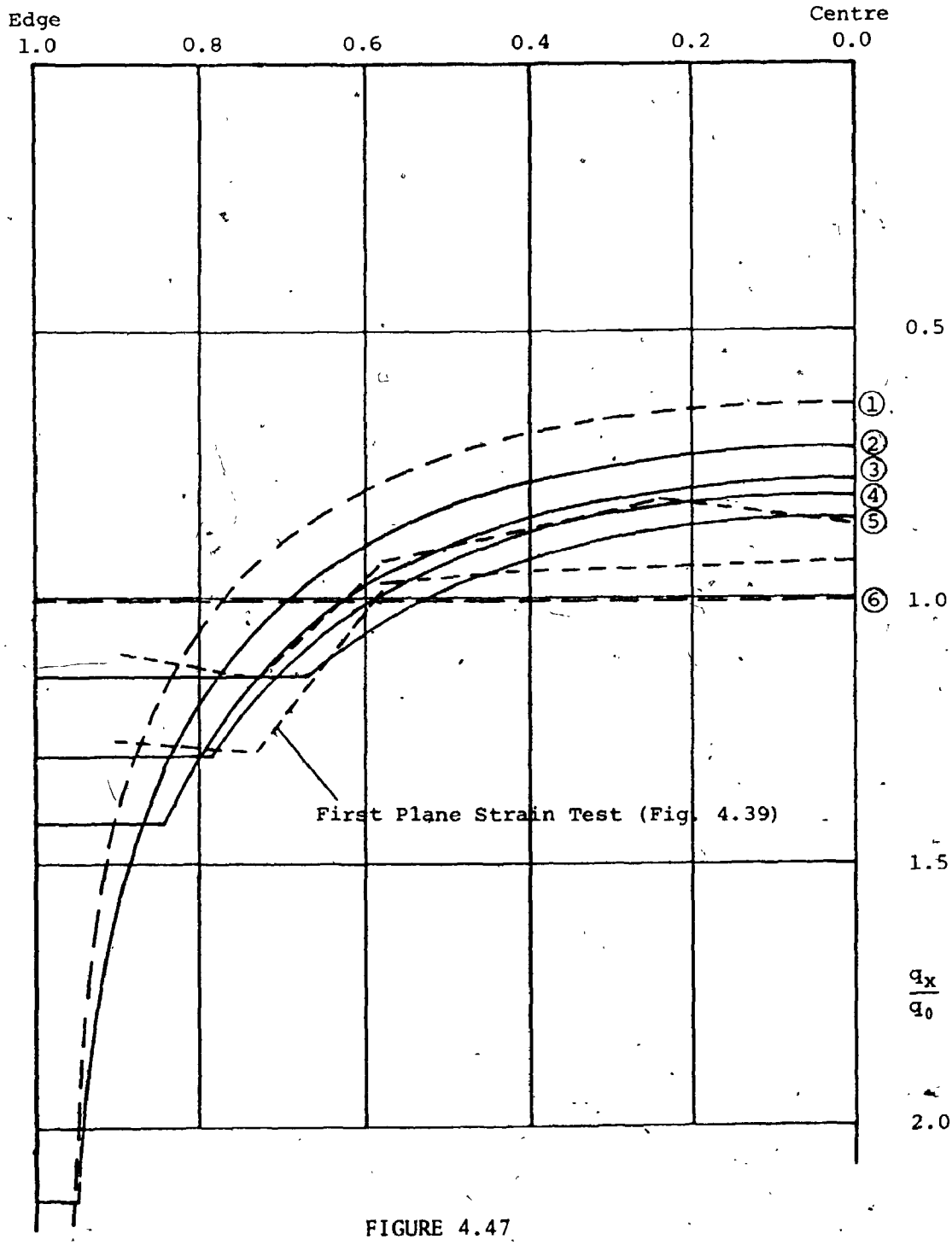

FIGURE 4.47

Contact Stress Distributions Predicted from Schultze (1961) and Zeevaert (1972)

line (2) because it was assumed that the applied stress was the same as the average stress in the centre portion between the walls of the tank (37.4 kPa). Line (3) was based on the average total stress applied to the plate (56.4 kPa). Lines (4) and (5) are computed from the observed maximum and minimum edge contact stresses in the plane strain test, to be compared with Figure 4.39. Line (6) is a uniform contact stress distribution that would have been computed on the basis of the maximum edge stress possible according to Zeevaert (1972).

The predicted contact stress distributions in Figure 4.47 depend on the assumptions regarding the maximum edge stress that will occur. Schultze (1961) relates this value to the bearing capacity, while Zeevaert (1972) uses a much smaller value. The extent of the local yielding will depend on the shear strength of the soil, but more experiments are required to clearly define the relationship between contact stress, shear strength and magnitude of load.

5. CONCLUSIONS AND RECOMMENDATIONS

5.1 *Summary and Conclusions*

An extensive review of literature related to the measurement of contact stress distributions beneath a structural foundation showed that the investigators were mainly concerned with the time-independent response of the soil reaction. In this study a model rigid strip footing was instrumented with sixteen pressure transducers capable of measuring the contact stresses beneath the foundation. A number of tests were performed on a cohesionless soil medium, but the principal study was directed towards the measurement of time-dependent contact stresses beneath a footing resting on a cohesive soil medium. Observations were also made on the induced pore water pressure response at different elevations in the soil layer, and on the footing settlement and surface profile of the soil medium. The following conclusions can be drawn:

(1) The contact stress distributions observed in this series of experiments differ substantially from the assumption of a uniform distribution.

(2) For both the sand and clay soil media the contact stress distribution depends on the magnitude of the applied load relative to the bearing capacity of the foundation.

(3) From these limited number of tests on a cohesive soil medium, it is apparent that the degree of cohesion enables there to be edge contact stresses substantially higher than the centre region, similar to that predicted by elastic theory. Local yielding of the soil at the edge of the foundation becomes an important

factor at higher applied stress levels.

(4) The immediate contact stresses can be predicted from the methods of Schultze (1961) or Zeevaert (1972) provided an estimate of the edge contact stress can be made. On the basis of the limited number of tests the edge contact stress is of the order of 1.5 to 3.0 c_u.

(5) Throughout the duration of the main test (five weeks) in the plane strain apparatus, the contact stress distribution was found to vary within a narrow band, the shape of which resembled the case of an elastic-plastic soil medium. The lack of substantial changes in the shape of the contact stress distribution is thought to be a characteristic of the soft clay used in the experiment.

(6) The contact stresses observed in the experiments on sand were found to be highly variable between one region and another, and between individual tests. In general, however, the contact stress distributions were shown to fall within a band that was similar in shape as those observed in previous studies on sand.

(7) The reloading of the rigid plate during the sand experiments resulted in a redistribution of contact stresses, with the contact stresses at the edge being reduced and being carried by the centre region.

(8) In general, the contact stress distributions for the two grades of sand were very similar. There was a slight tendency for the finer, relatively less dense sand to have lower contact stresses at the edge.

(9) The pressure transducers used in these experiments are capable of measuring the general shape of the contact stress distributions for a cohesive soil medium. There was a high degree of variability in the contact stress distributions for the cohesionless soil medium, which is more likely due to inhomogeneity of the soil rather

than instrument performance.

(10) The theoretical analysis used in this study showed that in comparison with the flexible foundation, the rigid foundation will produce substantially different stress changes in the soil, primarily in the soil layer less than the width of the footing below the foundation.

(11) The predictions of immediate settlement of the footing on clay are highly dependent on the assumptions regarding the boundary conditions of the soil medium. These predictions required an estimate of the Young's modulus of the soil. The best correlation between predicted and observed settlement resulted from the use of a Young's modulus derived from the surcharge loading of the clay layer. The immediate settlement can be predicted provided the yielding of the soil is taken into account.

(12) The magnitude of the total consolidation settlement can best be predicted from the basis of the observed porewater pressure increases. The use of the results of one-dimensional standard consolidation tests resulted in good agreement between the predicted and observed consolidation settlement. This has been observed in previous studies using a soft clay soil medium.

5.2 *Recommendations for Future Work*

This study has attempted to investigate a number of factors which are of importance to the soil foundation interaction problem. To date, only a limited number of experiments have been performed with model footings resting on cohesive soil media, and further research is necessary to clearly establish the trends observed in this study. It is recommended

that this initial program of research be continued, with the following suggestions for future work:

(1) It is suggested that more tests be performed on the cohesive soil medium to verify the observations of this investigation. In particular, it is suggested that the long-term loading of the plate be repeated under conditions of reduced sidewall friction and lower applied stress level.

(2) The problem of the time-dependent response of the contact stresses could be extended to different geometrical configurations, such as circular, square or rectangular foundations. Included in this section would be the dependence of the contact stress changes on the scale of the model footings.

(3) The relationship between the strength characteristics of the soil medium, the applied stress level, and the time-dependent response of the contact stress distribution deserves further investigation.

(4) Further research is required to determine how the thickness of deformable soil layer affects both the immediate and time-dependent response of the contact stress distributions.

(5) The conditions at the interface of the soil and foundation (such as degree of adhesion or pore water drainage) should be investigated for their effect on contact stress distribution.

(6) With most civil engineering projects, the load is applied to the soil over a period of time during which some degree of consolidation of the soil takes place. It is suggested that variations be made in the rate of loading of the model foundations to determine its effect on contact stress distributions.

(7) It is recommended that the flexibility of the

foundation be introduced in future research concerning contact stress distributions. Since the rigidity of the full-scale foundation can be expected to change with time, its influence on the contact stress distribution should be investigated.

(8) The effect of depth of embedment or overburden on both the static and time-dependent response of the contact stress distribution should be investigated.

REFERENCES

Akai, K. and Otsuki, H. (1974) "Model Studies on the Stress Distribution and the Bearing Capacity of Soil Ground," Soil and Foundations, Proc. JSCE, *223*, 99-107.

Akroyd, T.N.W. (1957) *Laboratory Testing in Soil Engineering*, Soil Mechanics Ltd., Great Britain.

American Concrete Institute, Committee 436 (1966) "Suggested Design Procedures for Combined Footings and Mats," Am. Concr. Inst. J., Oct. 1966.

A S T M (1973) *Annual Book of Standards*, Part 11, Articles D423-66, D424-69 and D854-58.

Atefi, H. (1975) Flexural Behaviour of Beams Resting on Elastic Media," Ph.D. Thesis, University of Aston in Birmingham, England.

Barden, L. (1962) "Distribution of Contact Pressure under Foundations," Geotechnique, *12*, 181-198.

-------- (1963) "The Winkler Model and Its Application to Soil," The Structural Engineer, *41*, No. 9, 279-280.

--------and McDermott, J.W. (1965) "Use of Free Ends in Triaxial Testing of Clays," J. Soil Mech. Found. Div., ASCE, *91*, SM6, 1-24.

Biernatowski, K. (1973) "The State of Stress and Displacement in the Contact Surface between a Rigid Foundation and Subsoil," Proc. 8th ICOSOMEF, Moscow, *1.3*, 15-18.

Biot, M.A. (1941) "General Theory of Three-Dimensional Consolidation," Journal of Applied Physics, *12*, 155-164.

Bishop, A.W. (1954) "The Use of Pore Pressure Coefficients in Practice," Geotechnique, *4*, 148-152.

-------- (1961) *Discussions in Proceedings*, Conf. on Pore Pressure and Suction in Soils, Butterworths, London.

-------- (1973) "The Influence on an Undrained Change in Stress on the Pore Pressure in Porous Media of Low Compressibility," Geotechnique, *23*, 435-442.

-------- (1976) "The Influence of System Compressibility on the Observed Pore Pressure Response to an Undrained Change in Stress in Saturated Rock," Geotechnique, *26*, No. 2.

--------, Alpan, I., Blight, G.E. and Donald, I.B. (1960) "Factors Controlling the Strength of Partly Saturated Cohesive Soils,"

Proc. Research Conf. on Shear Strength of Partially Saturated Cohesive Soils, ASCE, 503-532.

-------- and Henkel, D.J. (1962) *The Measurement of Soil Properties in the Triaxial Test*, 2nd ed., Edward Arnold Ltd., Great Britain.

--------, Kennard, M.F. and Penman, A.D.M. (1960) "Pore Pressure Observations at Selset Dam," Conf. on Pore Pressure and Suction in Soils, Butterworths, 91-102.

--------, Vaughan, P.R. and Green, G.E. (1969) "Report on Specialty Session, Pore Pressure Measurements in the Field and in the Laboratory," Proc. 7th ICOSOMEF, Mexico, *3*, 427-443.

Bobe, R., Hertwig, G. and Seiffert, H. (1977) "Foundation Slab Calculation Based on Measurements," 9th ICOSOMEF, Tokyo, *1*, 411-414.

Borodachev, N.M. and Tarikov, G.P. (1972) "Determination of the Reaction Pressure under a Foundation by Electrical Modelling Method," Soil Mech. Found. Eng., *9*, No. 6, 428-429.

Borowicka, H. (1936) "Influence of Rigidity of a Circular Foundation Slab on the Distribution of Pressures over the Contact Surface," 1st ICOSOMEF, Cambridge, Mass., *2*, 144-149.

Boswell, L.F. and Scott, C.R. (1975) "A Flexible Circular Plate on a Heterogeneous Elastic Half-Space: Influence Coefficients for Contact Stress and Settlement," Technical Note, Geotechnique, *25*, No. 3, 604-610.

Bowles, J.E. (1968) *Foundation Analysis and Design*, International Student Edition, McGraw-Hill, Inc., Japan, 91-96.

-------- (1970) *Engineering Properties of Soils and Their Measurement*, McGraw-Hill Book Co., New York.

Bozuzuk, M. (1970) "Field Instrumentation of Soil," Proc. Conf. Design and Installation of Pile Foundations and Cellular Structures, Lehigh University, Pa., 145-158.

-------- and Leonards, G.A. (1972) "The Gloucester Test Fill," Proc. Specialty Conf. on Performance of Earth and Earth-Supported Structures, Purdue Univ., Indiana, *1*, Part 1, 299-317.

Brown, P.T. (1974) "Influence of Soil Inhomogeneity on Raft Behaviour," Soils and Fdns. (Japanese Society of Soil Mechanics and Foundations Engineering), *14*, No. 1, 61-70.

-------- (1977) "Structure-Foundation Interaction and Soil Creep," 9th ICOSOMEF, *1*, 439-442.

Burland, J.B. (1969) "Foundations of Buildings on Clay," Proc. 7th ICOSOMEF, Mexico, 248-250.

--------, J.B., Broms, B.B. and DeMello, V.F.B. (1977) "Behaviour of Foundations and Structures," Proc. 9th ICOSOMEF, Tokyo, *2*, 495-546.

-------- and Roscoe, K.H. (1969) "Local Strains and Pore Pressures in a Normal Consolidated Clay Layer during One-Dimensional Consolidation," Geotechnique, *19*, No. 3, 335-356.

--------, Sills, G.C. and Gibson, R.E. (1973) "A Field and Theoretical Study of the Influence of Non-Homogeneity on Settlement," Proc. 8th ICOSOMEF, Moscow, *1*, 39-46.

Burn, K.N. (1963) "A Transducer to Measure Pore-Water Pressures in Soil Tests," Laboratory Shear Testing of Soils, ASTM Special Publication No. 361, 390-395.

Carrier, W.D. and Christian, J.T. (1973) "Rigid Circular Plate Resting on a Non-Homogeneous Elastic Half-Space," Geotechnique, *23*, No. 1, 67-84.

Chae, Y.S., Hall, Y.R. and Richart, F.E. (1965) "Dynamic Pressure Distribution beneath a Vibrating Footing," Proc. 6th ICOSOMEF, Montreal, *2*, 22-26.

Chamecki, S. (1956) "Structural Rigidity in Calculating Settlements," J. Soil Mech. Found. Div., ASCE, *82*, No. SM1, 1-19.

Chen, W. (1975) *Limit Analysis and Soil Plasticity*, Elsevier Scientific Publ. Co., Amsterdam, 169-210.

Cheung, Y.K. and Nag, D.K. (1968) "Plates and Beams on Elastic Foundations—Linear and Non-Linear Behaviour," Geotechnique, *18*, 250-260.

Chirarella, C. and Booker, J.R. (1975) "The Time-Settlement Behaviour of a Rigid Die Resting on a Deep Clay Layer," Q. Jl. Mech. Appl. Math., *28*, Pt. 3, 317-328.

Christian, J.T., Boehmer, J.W. and Martin, P.P. (1972) "Consolidation of a Layer under a Strip Load," J. Soil Mech. Found. Div., ASCE, *98*, SM7, 693-707.

Chummar, V. (1972) "Bearing Capacity Theory from Experimental Results," J. Soil Mech. Found. Div., ASCE, *98*, SM12, 1311-1324.

Converse, F.J. (1933) "Distribution of Pressure under a Footing," Civil Engineering, *3*, No. 4, 207-209.

Conway, H.D., Vogel, S.M., Farnham, K.A. and So, S. (1966) "Normal and Shearing Contact Stresses in Indented Strips and Slabs," Int. J. Engng. Sci., *4*, 343-359.

Crawford, C.B. (1961) "Engineering Studies of Leda Clay," in R.F.

Leggett, ed., *Soils in Canada*, Royal Society of Canada Special Publication No. 3, University of Toronto Press, Toronto, 200-217.

-------- (1963) "Pore Pressures within Soil Specimens in Triaxial Compression," in Laboratory Shear Testing of Soils, ASTM Special Publication No. 361, 192-199.

Crowser, J.C., Schuster, R.L. and Sack, R.L. (1974) "Settlement and Contact Pressure Distribution of a Mat-Supported Silo Group on an Elastic Subgrade," Proceedings of the Conference on Settlement of Structures, British Geotechnical Society, Pentech Press, Great Britain.

D'Appolonia, D.J., Lambe, T.W. and Poulos, H.G. (1971) "Evaluation of Pore Pressures beneath an Embankment," J. Soil Mech. Found. Div., ASCE, *97*, SM6, 881-897.

--------, Poulos, H.G. and Ladd, C.C. (1971) "Initial Settlement of Structures on Clay," J. Soil Mech. Found. Div., ASCE, *97*, SM10, 1359-1377.

Dascal, O. and Tournier, J.P. (1975) "Embankments on Soft and Sensitive Clay Foundation," J. Soil Mech. Found. Div., ASCE, *101*, GT3.

Davidson, D.P. (1975) "Environmental Influences on Pressure Transducer Performance," Measurement and Control, *8*, 273-278.

Davis, E.H. and Poulos, H.G. (1968) "The Use of Elastic Theory for Settlement Prediction under Three-Dimensional Conditions," Geotechnique, *18*, 67-91.

-------- and Poulos, H.G. (1972) "Rate of Settlement under Two- and Three-Dimensional Conditions," Geotechnique, *22*, No. 1, 95-114.

DeBeer, E.E. (1948) "Tests for the Determination of the Distribution of Soil Reactions underneath Beams Resting on Soil," Proc. 2nd ICOSOMEF, Rotterdam, *2*, 142-148.

-------- (1957) "The Influence of the Width of a Foundation Raft on the Longitudinal Distribution of the Soil Reactions," Proc. 4th ICOSOMEF, London, *1*, 269-274.

DeSimone, S.V. and Gould, J.P. (1972) "Performance of Two Mat Foundations on Boston Blue Clay," Proc. Specialty Conf. on Performance of Earth and Earth-Supported Structures, Purdue Univ., Indiana, *1*, Part 2, 953-980.

Doohan, J.P. (1975) "Earth Pressure Cells to Measure the Distribution of Shear and Normal Forces on a Footing," M.S. Thesis, Department of Civil Engineering, University of Ottawa, Ottawa, Canada.

Drnevich, V.P. and Hall, J.R. (1966) "Transient Loading Tests on a Circular Footing," J. Soil Mech. Found. Div., ASCE, *92*, SM6, 153-167.

Drupsteen, A.R. (1971) "Model Retaining Wall Investigation," 4th Year Undergraduate Project, Civil Engineering Dept., Carleton University.

Duncan, J.M. and Clough, G.W. (1971) "Finite Element Analyses of Port Allen Lock," J. Soil Mech. Found. Div., ASCE, *97*, SM8, 1053-1067.

Eden, W.J. and Crawford, C.B. (1957) "Geotechnical Properties of Leda Clay in the Ottawa Area," Proc. 4th ICOSOMEF, London, *1*, 22.

--------, McRostie, G.C. and Hall, J.S. (1973) "Measured Contact Pressures below Raft Supporting a Stiff Building," Canadian Geotechnical Journal, *10*, No. 2, 180-192.

Faber, Oscar (1933) "Pressure Distribution under Bases and Stability of Foundations," Structural Engr.

Farbar, G. (1977) "A Study of the Behaviour of Rigid Plate Anchors in an Elastic, Undrained, Isotropic Cohesive Soil Medium," 4th Year Undergraduate Project, Civil Engineering Dept., Carleton University.

Gerrard, C.M., Kurzeme, B.E., Andrews, D.C. and Topp, R. (1971) "Instrumentation of Raft Foundations in Perth," Proc. First Aust.-N.Z. Conf. Geomech., Melbourne, *1*, 361-368.

Gibson, R.E. (1963) "An Analysis of System Flexibility and Its Effect on Time-Lag in Pore Water Pressure Measurement," Geotechnique, *13*, No. 1, 1.

-------- (1967) "Some Results Concerning Displacements and Stresses in a Non-Homogeneous Elastic Half-Space," Geotechnique, *17*, No. 1, 56-57 with correspondence *18*, No. 2, 275-276, and *19*, No. 1, 160-161.

-------- (1974) "The Analytical Method in Soil Mechanics," 14th Rankine Lecture, Geotechnique, *20*, No. 2, 113.

-------- and Marsland, A. (1961) "Pore-Water Pressure Observations in a Saturated Alluvial Deposit beneath a Loaded Oil Tank," Conf. on Pore Pressure and Suction in Soils, Butterworths, London, 112-118.

--------, Shiffman, P.L. and Pu, S.L. (1970) "Plane Strain and Axially Symmetric Consolidation of a Clay Layer on a Smooth Impervious Base," Quart. J. Mech. and Appl. Math., *23*, 505-520.

-------- and Sills, G.C. (1971) "Some Results Concerning the Plane Deformation of a Non-Homogeneous Elastic Half-Space," Proc. Roscoe Memorial Symposium, Cambridge, G.T. Foulis & Co. Ltd., 564-572.

Goodier, J.N. and Loutzenheiser, C.B. (1965) "Pressure Peaks at the Ends of Plane Strain Rigid Die Contacts (Elastic)," Journal of Appl. Mech., ASCE, *32*, 462-463.

Gorbundv-Possadov, J.I. (1965) "Calculations for the Stability of a Sand Bed by a Solution Combining the Theories of Elasticity and Plasticity," Proc. 6th, ICOSOMEF, Montreal, *2*, 51-55.

Gosbell, K.B. (1970) "The Design, Instrumentation and Performance of the Perth Commonwealth Offices Raft Foundation," Proc. Symp. on Found. on Interbedded Sands, CSIRO, Aust., Div. of Applied Geomechanics, Melbourne, 99-106.

Graham, J. and Stuart, J.G. (1971) "Scale and Boundary Effects in Foundation Analysis," J. Soil. Mech. Found. Div., ASCE, *97*, SM11, 1533-1547.

Grasshoff, H. (1961) "Influence of Flexural Rigidity of Superstructure on the Distribution of Contact Pressure and Bending Moments in an Elastic Combined Footing," Proc. 5th ICOSOMEF, Paris, *2*, 300.

Guillet, G.R. (1967) *The Clay Products Industry of Ontario*, Ont. Dept. of Mines, I.M.R. #22, 141-143.

Hain, S.J. and Lee, I.K. (1974) "Rational Analysis of Raft Foundation," J. Geotechnical Eng. Div., ASCE, *100*, GT7, 843-860.

Hambley, E.C. and Roscoe, K.H. (1969) "Observations and Predictions of Stresses and Strains during Plane Strain of 'Wet' Clays," 7th ICOSOMEF, Mexico, *1*, 173-181.

Hanna, T.H. (1973) *Foundation Instrumentation*, Trans. Tech. Publications, Germany.

Harr, M.E. (1966) *Foundations of Theoretical Soil Mechanics*, McGraw-Hill, New York.

Hartikainen, J. (1973) "On the Distribution of the Vertical and Horizontal Contact Pressure Components under a Rigid Foundation," Proc. 8th ICOSOMEF, Moscow, *1.3*, 99-106.

Hasnain, M. (1974) "Shear Strength Characteristics of a Crushed Quartz Sand," M.Sc. Thesis, Dept. of Civil Eng., University of Ottawa, Ottawa.

Heil, H. (1969) "Studies on the Structural Rigidity of Reinforced Concrete Building Frames on Clay," Proc. 7th ICOSOMEF, Mexico, *2*, 115-121.

Henkel, D.J. (1960) "The Shear Strength of Saturated Remoulded Clays," Proc. Research Conf. on Shear Strength of Cohesive Soils, ASCE, 533-554.

-------- and Wade, N.H. (1966) "Plane Strain Tests on a Saturated Remoulded Clay," J. Soil Mech. Found. Div., ASCE, SM6.

Hilf, J.W. (1956) "An Investigation of Pore Water Pressure in Compacted Cohesive Soils," Tech. Memo. No. 654, United States Bureau of Reclamation.

Ho, M.M.K. and Lopes, R. (1969) "Contact Pressure of a Rigid Circular Foundation," J. Soil Mech. Found. Div., ASCE, *95*, SM3, 791-802.

Hoeg, K., Andersland, D.B. and Rolfsen, E.M. (1969) "Undrained Behaviour of Quick Clay under Load Tests at Asrum," Geotechnique, *19*, 101-115.

--------, Christian, J.T. and Whitman, R.V. (1968) "Settlement of Strip Load on Elastic-Plastic Soil," J. Soil Mech. Found. Div., ASCE, *94*, SM2, 431-445.

Holtz, W.G. (1973) "The Relative Density Approach—Uses, Testing Requirements, Reliability and Shortcomings," ASTM STP 523, 5-17.

Hooper, J.A. (1974) "Analysis of a Circular Raft in Adhesive Contact with a Thick Elastic Layer," Geotechnique, *24*, No. 4, 561-580.

Huang, Y.H. (1976) "FE Analyses of Rafts on Viscoelastic Foundations," Int. Conf. on Numerical Methods in Geomechanics, Virginia, ASCE, *1*, 463-474.

Hvorslev, M.J. (1976) "The Changeable Interaction between Soils and Pressure Cells; Test and Reviews at the Waterways Experiment Station," U.S. Army Engineer Waterways Experiment Station, Technical Report S-76-7.

Hwang, C.T., Morgenstern, N.R. and Murray, D.W. (1971) "On Solutions of Plane Strain Consolidation Problems by Finite Element Methods," Can. Geotech. Journal, *8*, 109-118.

Ingles, O.G. (1974) "Compaction" in *Soil Mechanics—New Horizons*, I.K. Lee, ed., Butterworth & Co. Ltd., London.

Juarez-Badillo, E. (1963) "Pore Pressure Functions in Saturated Soils," Proc. Research Conf. on Laboratory Shear Testing of Soils, ASTM Special Tech. Publication No. 361, 226-240.

Jumikis, A.R. (1969) *Theoretical Soil Mechanics*, Van Nostrand Reinhold Co., U.S.A.

Kaufman, R.I. and Sherman, Jr., W.C. (1964) "Engineering Measurements for Port Allen Lock," J. Soil Mech. Found. Div., ASCE, *90*, SM5, 221-247.

Koegler and Scheidig (1927) Referred to in Tschebotarioff, G.P. (1951) *Soil Mechanics, Foundations and Earth Structures*, McGraw-Hill Book Co., Inc., New York.

Kogan, B.I. and Satsuk, G.M. (1964) "Solution of Contact Problems of

the Mechanics of Non-Homogeneous Foundations by the Method of a Plate Analogy," Soil Mech. Found. Eng., No. 2, 79-84.

Krivorotov, A.P. (1972) "Experimental Investigations of the Change of Principal Stresses in Connection with Increased Load in a Sandy Foundation Bed beneath a Test Plate," Soil Mech. Found. Eng., *9*, No. 3, 141-144.

-------- (1976) "Change in Density of a Sandy Foundation Bed and its Effects on the Character of the Curve of Contact Pressures beneath a Rigid Plate," Soil Mech. Found. Eng., *13*, No. 4, 275-279.

-------- and Fedorov, V.K. (1973) "Contact Pressures under an Elevator Silo," Soil Mech. Found. Eng., *10*, No. 5, 296-299.

Ladd, C.C. (1964) Stress-Strain Modulus of Clay in Undrained Shear," J. Soil Mech. Found. Div., ASCE, *90*, SM5, 103-132.

-------- and Lambe, T.W. (1963) "The Strength of 'Undisturbed' Clay Determined from Undrained Tests," Proc. Laboratory Shear Testing of Soils, ASTM Special Publication No. 361, 342-371.

Lai, P.W. (1977) "Measurement of Density by Various Methods in a Cohesionless Quartz Sand," M.Sc. Thesis, Dept. of Civil Eng., University of Ottawa, Ottawa.

Lambe, W. (1962) "Pore Pressures in a Foundation Clay," J. Soil Mech. Found. Div., ASCE, *88*, SM2, 19-47.

-------- (1964) "Methods of Estimating Settlements," J. Soil Mech. Found. Div., ASCE, *90*, SM5, 43-67.

Laumans, Q. and Schad, H. (1976) "Calculation of Raft Foundations on Clayey Silts," Int. Conf. on Numerical Methods in Geomechanics, Virginia, ASCE, *1*, 475-488.

Lazebnik, G.E. (1970) "Investigation of Soil Pressure Distribution under Foundation Mats of Buildings," Soil Mech. Found. Eng., *7*, No. 6, 405-409.

-------- and Smirnov, A.D. (1964) "Measurement of Stresses under a Rigid Foundation Block in the Field," Soil Mech. Found. Eng., No. 2, 71-78.

--------, Smirnov, A.D. and Ivanov, D.G. (1973) "A Set of Instruments and Equipment for Measuring Soil Pressure," Soil. Mech. Found. Eng., *10*, No. 2, 116-121.

--------, Smirnov, A.D., Simakov, V.I. and Levadnyi, Y.M. (1966) "Measuring Stresses in Soils under Foundations," Soil Mech. Found. Eng., No. 5, 322-326.

Lee, I.K. and Harrison, H.B. (1970) "Structure and Foundation

Interaction Theory," Journal of the Structural Division, ASCE, *96*, ST2, 177-178.

-------- and Valliappan, S. (1974) "Analyses of Soil Settlement," in *Soil Mechanics—New Horizons*, I.K. Lee, ed., Newnes-Butterworths, London, 158-204.

Lee, K.L., Morrison, R.A. and Haley, S.C. (1969) "A Note on the Pore Pressure Parameter B," Proc. 7th ICOSOMEF, Mexico, *1*, 231-238.

LeLievre, B. and Vigneswaran, K. (1972) "Stresses beneath Strip Raft Foundations," Proc. 3rd S. E. Asian Conf. on Soil Engineering, Hong Kong, 289-293.

Lenczner, D. (1962) "Bending Moments and Pressures on Model Footings," Concrete and Constructional Engineering, *57*, 181-187.

-------- (1962) "Variation of Subgrade Modulus with Depth of Sand," Civil Engineering and Public Works Review, 210-212.

-------- (1963) "The effect of Flexural Rigidity of Footings and the Depth of Subgrade on the Distribution of Subgrade Modulus along the Length of Footings," SOLS-SOILS, *5*, 33-38.

Leonards, G.A. and Girault, P. (1961) "A Study of the One-Dimensional Consolidation Test," 5th ICOSOMEF, Paris, *1*, 213.

L'Herminier, R., Bachelier, M. and Soiero, F. (1957) "Investigation on the Foundation Raft for the First Atomic Reactor at Marcoule," Proceedings 4th ICOSOMEF, London, 307-311.

Likhovtsev, V.M. (1976) "Displacement and Contact Pressures for a Rigid Sunken Plate," Soil Mech. Found. Eng., *13*, No. 6, 414-419.

Malyshev, M.V., Zaretsky, Yu.K., Shirokov, V.M. and Cheremnikh, V.A. (1973) "Interaction of Rigid Foundations with a Base that Deforms Non-Linearly," Proc. 8th ICOSOMEF, Moscow, *1.3*, 155-160.

Massal'skii, E.K. (1964) "Experimental Study of a Flexible Beam on a Sand Foundation," Soil Mech. Found. Eng., No. 6, 344-347.

Milović, D.M., Touzot, G. and Tournier, J.P. (1970) "Stresses and Displacements in an Elastic Layer Due to Inclined and Eccentric Load over a Rigid Strip," Geotechnique, *20*, No. 3, 231-252.

Mineiro, A.J.C. (1973) "Pore Water Prediction under Plane Strain," Proc. 8th ICOSOMEF, Moscow, *1*, 275-279.

Mitchell, R.J. (1970) "On the Yielding and Mechanical Strength of Leda Clays," Can. Geotech. Journal, *7*, No. 3, 297-312.

Moh, Z., Brand, E.W. and Nelson, J.D. (1972) "Pore Pressures under a Bund on Soft Fissured Clay," Proc. Specialty Conf. on Performance

of Earth and Earth-Supported Structures," Purdue Univ., Indiana, *1*, Part 1, 243-271.

Moore, B.F. (1977) "An Investigation of Elastic Soil Settlement as Related to the Relative Rigidity of Raft Foundations," 4th Year Undergraduate Project, Civil Engineering Dept., Carleton University.

Muhs, H. and Bub, H. (1965) "Discussion Concerning a New Contact Stress Measuring Device," Proc. 6th ICOSOMEF, Montreal, 436-439.

Murzenko, Yu.N. (1969) "Experimental Results on the Distribution of Normal Contact Pressure on the Base of a Rigid Foundation Resting on Sand," Soil Mech. Found. Eng., No. 2, 69-73.

Mysholivskii, Y.S. and Khlopetskii, M.F. (1975) "Experimental Investigation of a Foundation Bed on a Rigid Underlying Layer," Soil Mech. Found. Eng., *12*, No. 4, 257-261.

Nwabuokei, S.O. (1976) "Measurement of Normal and Shear Stresses at the Base of a Rigid Footing Founded on Quartz Sand," M.Sc. Thesis, Department of Civil Engineering, University of Ottawa, Ottawa.

Okulova, M.N. (1968) "Stresses in Sandy Soils near a Loaded Ram," Soil Mech. Found. Eng., No. 4, 235-238.

Pahl, P.J. (1977) "Testing the Shape of Contact Pressure Curves," J. Soil Mech. Found. Div., *103*, GT7, 798-803.

Parkes, E.W. (1956) "A Comparison of the Contact Pressures beneath Rough and Smooth Rafts on an Elastic Medium," Geotechnique, No. 4, 183-189.

Parry, R.H. (1968) "Field and Laboratory Behaviour of a Lightly Overconsolidated Clay," Geotechnique, *18*, 151-171.

Paton, J. and Semple, N.G. (1961) "Investigation of the Stability of an Earth Dam Subject to Rapid Drawdown Including Details of Pore Pressures Recorded During a Controlled Drawdown Test," Conf. on Pore Pressures and Suction in Soils, Butterworths, 85-90.

Peck, R.B., Hanson, W.E. and Thornburn, T.H. (1974) *Foundation Engineering*, 2nd ed., John Wiley and Sons, New York.

Perloff, W.H. (1975) "Chap. 4: Pressure Distribution and Settlement," in *Fdn. Eng. Handbook*, eds. H.F. Winterkorn and H. Fang, Van Nostrand Reinhold, New York.

Poulos, H.G. (1967) "Stresses and Displacements in an Elastic Layer Underlain by a Rough Rigid Base," Geotechnique, *17*, No. 4, 378-410.

Radhakrishnan, N. and Reese, L.C. (1969) "Behaviour of Strip Footings

on Layered Cohesive Soils," Proc. Symposium on Application of Finite Element Methods in Civil Engineering, Vanderbilt University, Tennessee, 690-728.

Ramganatham, B.V., Remgaraju, V.R. and Pandian, N.S. (1973) "Contact Pressure beneath R. C. Test Footings," Proc. 8th ICOSOMEF, Moscow, *1.3*, 209-212.

Raymond, G.P. (1972) "The Kars (Ontario) Embankment Foundation," Proc. Specialty Conf. on Performance of Earth and Earth-Supported Structures, Purdue Univ., Indiana, *1*, Part 1, 319-340.

Richardson, A.M. and Whitman, R.V. (1963) "Effect of Strain Rate upon Undrained Shear Resistance of a Saturated Remoulded Fat Clay," Geotechnique, *13*, No. 4, 310-324.

Rivkin, S.A. and Gusenitsa, A.P. (1976) "Field Investigations of Distribution of Contact Pressures in Sands, Sandy Loams, and Ordinary Loams," Soil Mech. Found. Eng., *13*, No. 1, 12-15.

Saada, A.S. (1974) *Elasticity Theory and Applications*, Pergamon Press Inc., New York.

Sakurai, S. and Kitamura, Y. (1970) "Contact Pressure Distribution under Rectangular Rigid Foundation," Proc. Jap. Soc. Civ. Eng., No. 175, 59-73.

Sandford, J. (1976) "Accurate Pressure Transducers Keep Productivity High," Instruments and Control Systems, Oct., 39-46.

Schiffman, R.L. (1969) "The Influence of Adhesion of the Stresses and Displacements in an Elastic Halfspace," Highway Research Record No. 283.

--------, Chen, A.T. and Jordan, J.C. (1969) "An Analysis of Consolidation Theories," J. Soil Mech. Found. Div., ASCE, *95*, SM1, 285-312.

Schmertmann, J.H. (1970) "Static Cone to Compute Static Settlement over Sand," J. Soil Mech. Found. Div., ASCE, SM3, 1011-1043.

Schultze, E. (1961) "Distribution of Stress beneath a Rigid Foundation," Proc. 5th ICOSOMEF, Paris, *1*, 807-813.

Sedykh, E.K. (1964) "On the Diagram of Reaction Pressures under the Base of a Rigid Foundation," Soil Mech. Found. Eng., No. 3, 153-157.

Seed, H.B. (1965) "Settlement Analysis, A Review of Theory," J. Soil Mech. Found. Div., ASCE, *91*, SM2, 39-48.

Selig, E.T. and Ladd, R.S. (1973) "Evaluation of Relative Density Measurements and Applications," ASTM STP 523, 487-504.

Selvadurai, A.P.S. (1976) "The Response of a Rigid Circular Plate Resting on an Idealized Elastic-Plastic Foundation," Int. J. Mech. Sciences, *18*, 463-468.

-------- (1978) "Elastic Analysis of Soil-Foundation Interaction," *Developments in Geotechnical Engineering*, Vol. 19, Elsevier Scientific Publishing Company, New York.

Sergeev, I.T. and Savchenko, F.M. (1970) "Experimental Investigations of Soil Pressure on the Surface of an Anchor Plate," Soil Mech. Found. Eng., *9*, No. 5, 298-300.

Shanker, N.B., Rathman, M.V. and Rao, A.S. (1975) "Three-Dimensional Consolidation of a Saturated Clay under Model Footings," Soils and Foundations, *15*, No. 1, 88-92.

Shelyapin, R.S. and Sergeev, I.T. (1967) "Results of the Experimental Investigations of the Bending of Beams on Soil Bases," Soil Mech. Found. Eng., No. 2, 79-82.

Shields, D.H. and Bauer, G.E. (1975) "Determination of the Modulus of Deformation of a Sensitive Clay Using Laboratory and In-Situ Tests," Proc. of Conf. on In-Situ Measurement of Soil Properties, North Carolina, ASCE, *1*, 395-421.

--------, Scott, J.D., Bauer, G.E., Deschênes, J.H. and Barsvary, A.K. (1977) "Bearing Capacity of Foundations near Slopes," 9th ICOSOMEF, *1*, 715-720.

Shirokov, V.N. (1971) "Problem of a Rigid Punch on a Nonlinearly-Deforming Half-Space," Soil Mech. Found. Eng., *8*, No. 5, 309-312.

Sikso, H.A. and Johnson, V.C. (1965) "Pressure Cell Observations—Garrison Dam Project," J. Soil Mech. Found. Div., Proceedings, ASCE, *90*, SM5, 157-179.

Simons, N.E. (1974) "Normally Consolidated and Lightly Over-Consolidated Cohesive Materials," Review Paper Proc. Conf. Settlement of Structures, Cambridge, 500-530.

Skempton, A.W. (1954) "The Pore Pressure Coefficients A and B," Geotechnique, *4*, 143-147.

-------- and Bjerrum, L. (1957) "A Contribution to Settlement Analysis of Foundations on Clay," Geotechnique, *7*, 168-178.

Smith, I.M. (1970) "A Finite Element Approach to Elastic Soil-Structure Interaction," Canadian Geotechnical Journal, *7*, 95-105.

Smoltczyk, H.U. (1967) "Stress Computation in Soil Media," J. Soil Mech. Found. Div., ASCE, *93*, SM2, 101-124.

Snarskii, A. (1974) "Stresses and Displacements in the Soil under a

Circular Foundation," Soil Mech. Found. Eng., *11*, No. 5, 339-344.

Soderman, L.G., Kim, Y.D. and Milligan, V. (1968) "Field and Laboratory Studies of Modulus of Elasticity of a Clay Till," Highway Research Record No. 243, 1-11.

Sommer, H. (1965) "A Method for the Calculation of Settlements, Contact Pressures and Bending Moments in a Foundation Including the Influence of the Flexural Rigidity of the Superstructure," Proc. 6th ICOSOMEF, Montreal, *2*, 197-201.

Sutherland, H.B. and Lindsay, J.A. (1961) "The Measurement of Load Distribution under Two Adjacent Columns," 5th ICOSOMEF, Paris, *1*, 829-835.

Tavenas, F.A. (1973) "Difficulties in the Use of Relative Density as a Soil Parameter," ASTM STP 523, 478-483.

Teng, C.Y. (1949) "Determination of the Contact Pressure against a Large Raft Foundation," Geotechnique, *1*, 222-228.

Terzaghi, K. (1943) *Theoretical Soil Mechanics*, John Wiley & Sons, Inc., U.S.A.

-------- (1955) "Evaluation of the Coefficients of Subgrade Reaction," Geotechnique, *5*, No. 4, 297-326.

-------- and Peck, R.B. (1967) *Soil Mechanics in Engineering Practice*," 2nd ed., John Wiley & Sons, Inc., New York.

Tetior, A.N. and Litvinenko, S. (1971) "Foundations for Tower-like Structures," Proc. 4th Conf. on Soil Mechanics, Budapest, 819-827.

Thamm, B.R. (1976) "On Load Tests in Soft Clays," Int. Conf. on Numerical Methods in Geomechanics, Virginia, ASCE, *1*, 557-566.

Timoshenko, S. (1940) *Theory of Plates and Shells*, McGraw-Hill, New York.

-------- and Goodier, J.N. (1970) *Theory of Elasticity*, 3rd ed.,. McGraw-Hill, New York.

Tschebotarioff, G.P. (1951) *Soil Mechanics, Foundations and Earth Structures*, McGraw-Hill Book Co., Inc., New York.

Tsytovich, N. (1976) *Soil Mechanics*, Mir Publishers, Moscow, 85-122.

Vaughan, P.R. (1974) "The Measurement of Pore Pressures with Piezometers," in *Field Instrumentation in Geotechnical Engineering*, Butterworths, London, 411-422.

Verma, N.S. (1976) "One-Dimensional Compression and Pore Pressure Characteristics of Compacted Soils," Ph.D. Thesis, Department of

Civil Engineering, University of Ottawa.

Vesić, A.S. (1973) "Analysis of Ultimate Loads of Shallow Foundations," J. Soil Mech. Found. Div., ASCE, *99*, SM1, 45-73.

-------- and Johnson, W.H. (1963) "Model Studies of Beams Resting on a Silt Subgrade," J. Soil Mech. Found. Div., ASCE, *89*, SM1, 1-31.

Vinokurov, E.F., Makaruk, P.N. and Bol'Shedonov, I.I. (1964) "Investigation of the Character of Work of Foundation Blocks of Series II-03-02 on a Sand Foundation Bed," Soil Mech. Found. Eng., No. 6, 373-377.

Votava, Paul (1974) "Guide to Pressure Transducers," Instruments and Control Systems, Oct., 55-56.

Walker, B.P. and Whitaker, T. (1967) "An Apparatus for Forming Uniform Beds of Sand for Model Foundation Tests," Geotechnique, *17*, 161-167.

Williams, P.J. (1967) "Replacement of Water by Air in Soil Pores," The Engineer, Vol. 223, Feb. 24, 293-298.

Wood, L.A. and Larnach, W.J. (1974) "The Effects of Soil Structure Interaction on Raft Foundations," Proceedings of the Conference on Settlement of Structures, British Geotechnical Society, Pentech Press, Great Britain, 460-470.

Wu, T.H. (1976) *Soil Mechanics*, 2nd ed., Allyn and Bacon, Inc., Boston, U.S.A.

--------, Thayer, W.B. and Lin, S.S. (1975) "Stability of Embankment on Clay," J. Soil Mech. Found. Div., ASCE, 913-932.

Yamaguchi, H., Kimura, T. and Konno, H. (1968) "On the Contact Pressure Distribution between Rigid Loads and an Elastic Solid Underlain by a Rigid Boundary," Soils and Foundations, *8*, No. 3, 46-62.

-------- and Murakami, Y. (1976) "Plane Strain Consolidation of a Clay Layer with Finite Thickness," Soils and Foundations, Japanese Soc. of Soil Mech. and Fdn. Enrg., *16*, No. 3, 67-79.

Youd, T.L. (1973) "Factors Controlling Maximum and Minimum Densities of Sands," ASTM STP 523, 98-112.

Zeevaert, L. (1972) *Foundation Engineering for Difficult Subsoil Conditions*, Van Nostrand Reinhold Co., U.S.A., 294-334.

APPENDIX 1

SUMMARY OF RESEARCH CONCERNED WITH CONTACT STRESS BENEATH A FOUNDATION

Article	*Type**	*Material*	*Foundation*	*Geometry*	*Embedment*	*Contact Surface*	*Load*	*Remarks*
Koegler, Scheidig (1927)	M	Sand	Rigid	Circular 34 cm to 100 cm Dia.	Surface		Uniform	Effect of size of footing
Faber (1933)	M	Sand, Clay	Rigid	Circular 12" Dia.	With and Without Surcharge		Uniform Varied Magnitude	Effect of load, cohesion, embedment
Converse (1933)	M	Clay Loam	Rigid	3' square	4'	Rough	Uniform, Varied	Initially high corner stresses, at moderate load
Borowicka (1936)	T	Elastic	Variable Flexibility	Circular	Surface		Uniform	Effect of flexibility
DeBeer (1948)	M	Rhine Sand	Various Rigidities	Beams 1 m × 0.25 m	Surface Surcharge		Varied	Effect of flexibility
Teng (1949)	F	Volcanic Silty Clay	Flexible	Raft 180' × 68'	Shallow	Rough	Uniform	Contact stresses backfigured from settlement
Terzaghi (1955)	T	Sand, Clay	Rigid Flexible	Strip, Rectangular	Surface		Uniform	Factors affecting modulus of sub-grade reaction

* M = Model F = Field T = Theory

SUMMARY OF RESEARCH
(cont'd)

Article	*Type*	*Material*	*Foundation*	*Geometry*	*Embedment*	*Contact Surface*	*Load*	*Remarks*
Parkes (1956)	T	Elastic	Flexible	2-D Raft	Surface	Rough, Smooth	Variable	Effect of shear stress at interface
DeBeer (1957)	T	Elastic, inhomo-geneous	Rigid	Beam, Varied Size	Surface	Assumed Smooth	Uniform	Effect of shape of foundation, soil inhomogeneity
L'Herminier (1957)	F	Sand, Clay	Rigid	Raft, 29 m x 36 m	5 m	Rough	Uniform	Edge stresses large
Schultze (1961)	T F	Elastic Plastic	Rigid	Theory for strip foundation	Variable		Uniform Variable	Effect of cohesion, embedment load magnitude
Sutherland, Lindsay (1961)	F	Stiff Boulder Clay	Considered Rigid	2 Square Column Footings	Surface		Uniform, increased	Large variation in contact stress
Lenczner (1962 and 1963)	M	Sand	Degrees of Flexibility	Rectangular Plate 18" x 3"	Surface		Two-Point load, varied magnitude	Variation of subgrade modulus with plate flexibility and sand depth
Barden (1962)	T M	Elastic, inhomo-geneous	Flexible	Beam	Surface	Assumed Smooth	Variable	Effect of flexibility, load distribution, homogeneous and non-homogeneous anisotropy
Vesić (1963)	M	Silty Subgrade	Flexible, Intermediate, Rigid	Beam	Surface, 22" deep		Point loads, varied	Effect of flexibility, type of loading

SUMMARY OF RESEARCH
(cont'd)

Article	*Type*	*Material*	*Foundation*	*Geometry*	*Embedment*	*Contact Surface*	*Load*	*Remarks*
Barden (1963)	M	Sand	Flexible	Beam 36" x 4"	Surface		Point loads, varied	Effect of load distribution magnitude
Sedykh (1964)	T	Elastic Plastic	Rigid	2-D Plane	Surface	Rough	Uniform	Effect of load, soil cohesion
Kaufman, Sherman (1964)	F	Silty Clay, Sand	Considered Rigid	Canal Dock 135' x 1200'	[illegible]	Rough	Varied over time	Concave parabolic distribution
Sikso, Johnson (1964)	F	Clay, Shale	Rigid	Dam powerhouse 75'x134', and still basin	Some Embedment	Rough	Varied over time	High edge stresses
Lazebnik, Smirnov (1964)	M	Fine Sand or Loam	Rigid	Strip 60 x 180 cm	Surface	Measured 10 cm below footing	Uniform, varied magnitude	Effect of load
Kogan, Satsuk (1964)	M	Plexiglass	Rigid	Dam Models			Varied magnitude	Non-homogeneity, considered by plate analogy
Vinokurov *et al.* (1964)	M	Medium grain sand	Intermediate	Strip, 140 cm width	Surface and with surcharge		Centre, varied magnitude	Effect of load magnitude, surcharge

SUMMARY OF RESEARCH

(cont'd)

Article	*Type*	*Material*	*Foundation*	*Geometry*	*Embedment*	*Contact Surface*	*Load*	*Remarks*
Chae, Hall, Richart (1965)	M	Medium Grain Sand	Rigid	Circular 12" Dia.	Surface		Uniform, static & dynamic	Low stress levels, higher centre stresses
Murzenko (1965)	M	Compacted Sand	Rigid	Square 500 × 500 mm 700 × 707 mm	Surface	Slightly Rough	Varied, repeated	Effect of load, repeated load, size of footing
Gorbundov-Passadov (1965)	T	Sand Elastic-Plastic	Rigid	Plane footing	Surface	Rough	Constant, Uniform	Predict vertical, tangential stresses
Sommer (1965)	T	Elastic	Flexible	Beams, Slabs	Surface	Assumed Smooth	Varied along beam	Effect of flexibility of superstructure
Muhs, Bub (1965)	M	Loose Medium Dense Sand	Rigid	Strip 0.6 m wide	Only surface results presented	Some Adhesion	Uniform, varied	Effect of load, soil density, cyclic load
ACI #436 (1966)	T F	General	Flexible	General	Variable	Assumed Smooth	Variable	Suggested U.S. design code
Lazebnik *et al.* (1966)	M	Medium Dense Fine Sand	Rigid	Plate 1.2 m × 1.7 m Strip 2.85 m × 0.7 m	Surface		Uniform, varied	Compares interface and embedded pressure cells
Drnevich, Hall (1966)	M	Medium Sand	Relatively Rigid	Circular 12" Dia.	Surface		Uniform, static, dynamic	Effect of dynamic loading

SUMMARY OF RESEARCH

(cont'd)

Article	*Type*	*Material*	*Foundation*	*Geometry*	*Embedment*	*Contact Surface*	*Load*	*Remarks*
Shelyapin, Sergeev (1967)	M	Loose, Medium Dense Sand, Loam	Interme-diate	Beam	Surface		Uniform series of point loads, Varied	High edge stresses
Smoltczyk (1967)	T	Sand	Rigid	Plane Footing	Surface	Assumed Smooth	Uniform Varied	Statistical analysis
Cheung, Nag (1968)	T	Elastic, Inhomo-geneous	Flexible	Plates, Beams	Surface	Rough	Varied over area	FEM, effect of homogeneity, flexibility, load
Yamaguchi *et al.* (1968)	T M	Elastic, Homo-geneous	Rigid	Plane	Surface	Rough Smooth	Uniform, Varied	Effect of rigid base, Poisson's ratio, contact adhesion
Okulova (1968)	M	Fine sand, Medium Dense	Rigid	Square Ram 40 cm × 40 cm	20 cm depth		Uniform, Varied	High edge stresses
Heil (1969)	T	Consoli-dating	Flexible	Raft 2-D	Surface	Assumed Smooth	Varied over area	Effects of time, concrete creep
Ho, Lopez (1969)	M	Dense Sand	Rigid	Circular 6" Dia.	Surface + Embedment		Uniform, varied, repeated	Effect of load magnitude, embedment, cyclic load
Radhakrish-nam, Reese (1969)	M	2 Layered Clay	Rigid	Strip footing 21" × 1.5"	Surface		Uniform, Varied	FEM, effect of layered clay, load

SUMMARY OF RESEARCH

(cont'd)

Article	*Type*	*Material*	*Foundation*	*Geometry*	*Embedment*	*Contact Surface*	*Load*	*Remarks*
Lazebnik (1970)	F	Sand, Sandy Loam, Loam	Flexible	Mat Fdn., Ribbed Mat, Circular Ribbed Fdn.	5 m 11 m 5 m		Varied during construction, Non-uniform	3 cases, effect of load magnitude, distribution
Gosbell (1970)	F	Medium Dense Sand underlain by Clay	Considered Rigid	Raft 192'×86' ×5.5' thick	30'		Varied over time	High edge stress throughout loading
Milović *et al.* (1970)	T	Elastic	Rigid	Strip, rigid base	Surface	Rough	Inclined, Eccentric loading	FEM, effect of load, depth of layer, Poisson's ratio
Sakurai, Kitamura (1970)	T	Elastic	Rigid	Rectangular Raft	Surface	Rough or Smooth	Uniform	FEM, stress under entire raft
Gerrard *et al.* (1970)	F	Mainly Sand, Thin Clay Layers	1 Rigid 1 Flexible	Rafts 100'×100'×4' 100'×200'×7'	15' to 36'	Rough	Varied over time	Effect of raft flexibility
Duncan, Clough (1971)	T F	Silty Clay	Flexible Rigid	Canal Dock	61'	Rough	Varied over time	FEM analyses of Port Allen Dock
Tetior, Letvinenko (1971)	M	Fine Sand	Rigid	Annular	Surface		Eccentric, Varied Magnitude	Higher edge stresses

SUMMARY OF RESEARCH

(cont'd)

Article	*Type*	*Material*	*Foundation*	*Geometry*	*Embedment*	*Contact Surface*	*Load*	*Remarks*
Shirkov (1971)	T	Sand	Rigid	Circular	Surface	Assumed Smooth	Varied	Effect of shear deformation on contact stress
Krivirotov (1972)	M	Fine Sand	Rigid	30 x 75 cm 2-D	Surface	Assumed Smooth	Varied	Effect of load
Borodachev, Takirov (1972)	M	Electrical Modelling Method						Effect of geometry
Zeevaert (1972)	T	Elastic, Plastic	Rigid Flexible	Circular, Strip	Surface	Assumed Smooth	Uniform, Varied	Effect of soil, flexibility, geometry, load
Sergeev, Savchenko (1972)	M	Loose Medium Dense Sand, Loam	Flexible Rigid	Square anchor plate	1.2 m deep and deeper		Centre pullout	Effect of material, density, load, depth, flexibility
De Simone, Gould (1972)	F	Boston Blue Clay	Interme-diate	Mat Fdns. 60' x 220' 66' x 280'.	Embedded approxi-mately 30'		Varied over area	Contact stresses used in design
De Lievre, Vigneswaran (1972)	T	Linear Elastic Medium	Degrees of Flex-ibility	Strip Raft	Surface	Rough	Random Loading	FEM, effect of load, flexibility, soil layering
Lazebnik *et al.* (1973)	F	Compact Sand & Loam	Interme-diate	Circular Reservoir 5.5 m Dia.	Surface		Uniform Varied	Effect of magnitude of load, repeated load

SUMMARY OF RESEARCH

(cont'd)

Article	*Type*	*Material*	*Foundation*	*Geometry*	*Embedment*	*Contact Surface*	*Load*	*Remarks*
Eden, McRostie and Hall (1973)	F	Clay	Very Stiff	Raft	13'	Rough	Varied over time, surface	High edge stresses, remain high
Carrier, Christian (1973)	T	Elastic Inhomogeneous	Rigid	Circular Plate	Surface	Rough + Smooth	Uniform, Varied	FEM, effect of roughness, homogeneity
Malyshev (1973)	T	Sand	Rigid	2-D Plane	Surface + Embedment	Assumed Smooth	Varied	Effect of increased load, embedment
Hartikainen (1973)	M	Fine Sand Loose	Rigid	Square 30 × 30 cm	Surface + 50 cm	Assumed Smooth	Varied, reloaded	Effect of increased load, embedment
Biernatowski (1973)	T	Elastic, Plastic	Rigid	2-D Plane	Surface	Rough	Uniform, Varied	Effect of load, soil medium
Ranganthan (1973)	M	Sand	Flexible	Square 3' × 3'	Surface	Assumed Smooth	Varied	Backfigured from settlement
Krivorotov, Fedorov (1973)	F	Sand base over loam	Approx. Rigid	Raft-Silo 27 × 21 m	2 m Depth		Varied over time	Saddle-shaped, less than elastic theory
Crowser *et al.* (1974)	F	Dense silt, sand, gravel	Approx. Rigid	Mat	3 m		Varied over time	FEM backfigured High edge stresses
Akai, Otsuki (1974)	M	Sandy loam, also dense sand	Rigid	Circular 10 cm, 20 cm, 30 cm	Surface		Uniform, Static & Dynamic	Effect of load magnitude, repeated loads, material

SUMMARY OF RESEARCH

(cont'd)

Article	*Type*	*Material*	*Foundation*	*Geometry*	*Embedment*	*Contact Surface*	*Load*	*Remarks*
Wood, Larnach (1974)	T	Inhomo-geneous, Non-linear	Rigid to Flexible	Raft	Surface		Varied	FEM, effect of flexibility, load, soil cohesion
Hooper (1974)	T	Cohesive	Flexible	Circular Raft	Surface	Rough	Varied	Effect of roughness, flexibility, load magnitude
Snarski (1974)	T	Elastic Plastic	Rigid	Circular Plate	Varied Depth	Assumed Smooth	Varied	Effect of load magnitude, embedment
Brown (1974)	T	Elastic, Inhomo-geneous	Rigid Flexible	Rafts Footings	Surface	Assumed Smooth		Effect of inhomogeneity, flexibility
Mysholivskii, Khlopetskii (1975)	M	Medium Dense Sand	Rigid Flexible	Beams 1.2 m 1.8 m	Surface		Two-point loading, varied	Effect of rigid base, beam flexibility
Boswell, Scott (1975)	T	Elastic, Inhomo-geneous	Variable Flexibi-lity	Circular	Surface	Rough	Uniformly loaded	FEM, effect of inhomogeneity, flexibility
Chirarella, Booker (1975)	T	Consoli-dating Clay	Rigid	Circular	Surface		Uniformly loaded	Time-dependent response of contact stress distribution
Doohan (1975)	M	Sand	Rigid	Strip 12" wide	Surface	Rough	Varied	Cambridge cells modified

SUMMARY OF RESEARCH

(cont'd)

Article	*Type*	*Material*	*Foundation*	*Geometry*	*Embedment*	*Contact Surface*	*Load*	*Remarks*
Nwabuokei (1975)	M	Compact dense sand	Rigid	Strip 12" wide	Surface, adjacent slope	Rough	Varied	Effect of load, density
Rivkin, Gusenitsa (1976)	M F	Sand Sandy Loam Loam	Rigid	Circular	1 m		Varied	Field tests
Likhovtsev (1976)	T	Elastic	Rigid	Circular	Below Surface		Uniform	With embedment, stresses lower in centre, higher at edge
Krivorotov (1976)	M	Fine Sand	Rigid	Plate 0.3 m wide	Surface	Rough	Uniform, up to limit load	Effect of density
Laumans, Schad (1976)	T	Soft Clay	Flexible	Raft 2-D only	4 m	Rough	4 points, working and near failure loads	FEM, effect of drained, undrained analysis, load level
Pahl (1977)	T	Elastic	Flexible	Strip	Surface		Varied magnitude	Statistical estimate of the number of pressure cells required
Bobe *et al.* (1977)	F T	Elastic, Plastic	Variable Flexibility	30m × 61.6m Grain Silo	Shallow		Series of point loads	Effect of rigidity of foundation, soil yielding

APPENDIX 2

PORE PRESSURE EQUATIONS

(1) *One-Dimensional*

$$\Delta u = \Delta\sigma_z$$

= change in vertical stress

(2) *Skempton (1954)*

$$\Delta u = B[\Delta\sigma_3 + A(\Delta\sigma_1 + \Delta\sigma_3)]$$

where $\Delta\sigma_1$, $\Delta\sigma_3$ are changes in principal stresses

A,B are pore pressure parameters

(3) *Three-Dimensional*

$$\Delta u = 1/3(\Delta\sigma_1 + \Delta\sigma_2 + \Delta\sigma_3)$$

$$= \Delta\sigma_{oct}$$

(4) *Henkel (1960, 1966)*

$$\Delta u = \Delta\sigma_{oct} + a\Delta\tau_{oct}$$

where $\Delta\tau_{oct} = \Delta[(\sigma_1-\sigma_2)^2 + (\sigma_2-\sigma_3)^2 + (\sigma_3-\sigma_1)^2]^{\frac{1}{2}}$

$$a = \left(\frac{3A-1}{\sqrt{2}}\right)$$ from triaxial test

(5) *Bishop et al. (1961)*

unsaturated soil

$$\Delta u = \Delta u_a + \Delta u_w$$

$$\Delta u_a = B_a[\Delta\sigma_3 + A_a(\Delta\sigma_1 - \Delta\sigma_3)]$$

$$\Delta u_w = B_w[\Delta\sigma_3 + A_w(\Delta\sigma_1 - \Delta\sigma_3)]$$

(6) *Skempton (1960)*

dilatent soil

$$\Delta u = \frac{1}{\left[1+n\frac{C_w}{C_c}\right]} \left\{\frac{\Delta I_1}{3} + \frac{D}{3C_c}\left|(2\Delta I_1^2 - 6\Delta I_2)^{\frac{1}{2}}\right|\right\}$$

where ΔI_1 = change in first invariant

ΔI_2 = change in second invariant

C_w = compressibility of pore water

C_c = compressibility of soil skelton

D = parameter for dilatency

(7) *Juarez-Badillo (1963)*

$$\Delta u = \Delta\sigma + \alpha\sigma_c\left(\frac{\tau}{\tau_f}\right)^{\beta}$$

where $\Delta\sigma = 1/3(\Delta\sigma_1+\Delta\sigma_2+\Delta\sigma_3)$

σ_c = octahedral normal stress at which the specimen has been consolidated

$\tau = 1/3[(\Delta\sigma_1-\Delta\sigma_2)^2 + (\Delta\sigma_2-\Delta\sigma_3)^2 + (\Delta\sigma_3-\Delta\sigma_1)^2]^{\frac{1}{2}}$

τ_f = maximum octahedral shear stresses

α β, parameters

(8) *Mineiro (1973)*

plane strain testing

$$\Delta u = \frac{\Delta\sigma_1+\Delta\sigma_3}{2} + \sqrt{\frac{3}{2}}(A_t - 1/3)\, M_p\, |\Delta\sigma_1-\Delta\sigma_3|$$

where A_t = a parameter obtained from triaxial test

M_p = magnification coefficient

$$= \frac{\sqrt{3\,(3+\sin^2\phi')}}{3-\sin^2\phi'}$$

ϕ' = angle of internal friction obtained from plane strain tests

(9) *Bishop (1973)*

$$\frac{\Delta u}{\Delta \sigma} = 1/(1+\eta (C_w - C_s)/(C - C_s))$$

where η = porosity

C_w = compressibility of pore water

C_s = compressibility of soil skelton

C = bulk compressibility

(10) *Bishop (1976)*

$$\frac{\Delta u}{\Delta \sigma} = 1/\left[1+\eta \frac{(C_w - C_s)}{(C - C_s)} + \frac{V_L}{V}\left(\frac{C_w}{C - C_s}\right) + \frac{C_L + C_m}{V(C - C_s)}\right]$$

where η, C_w, C_s, C are same as above

C_L = compressibility of water in lines

C_m = compressibility of measuring instrument

V = sample volume

V_L = volume of water in lines .

APPENDIX 3

FIELD OBSERVATIONS OF PORE WATER PRESSURE MEASUREMENT

Article	*Type*	*Field Measurement*	*Predicted Δu Method*	*Predicted Δσ Method*	*Reasons for Discrepancies*
Bishop (1954)	Dam Stability	Not Given	$\Delta u = B[\Delta\sigma_3 + A(\Delta\sigma_1 - \Delta\sigma_3)]$	$\Delta\sigma_1 = f(h)$ h = height of overburden	A dependent on stress history, state of stress, rate of strain
Gibson, Marsland (1961)	Loaded Oil Tank	24 Piezometers	$\Delta u = \Delta\sigma_3 + A(\Delta\sigma_1 - \Delta\sigma_3)$ B = 1.0	circular uniformly loaded area, semi-infinite elastic medium	Firmer base, sampling disturbance, inhomogeneity
Paton, Semple (1961)	Rapid Drawdown in a Dam	5 Piezometers, Hydraulic	Same as Skempton (1954)	$\Delta\sigma_1 = f(h)$	Incomplete saturation
Bishop, Kennard, Penman	Dam Construction	78 Piezometers, Imperial College	$\Delta u = \Delta\sigma_z$	$\Delta\sigma_z = f(h)$	Dissipation of Pore Pressures, Inhomogeneity
Lambe (1962)	Preload for a tank	7 Casagrande Piezometers	$\Delta u = \Delta\sigma_3 + A(\Delta\sigma_1 - \Delta\sigma_3)$	$\Delta\sigma_1$, $\Delta\sigma_3$, From Elastic Analysis, stack of plates	Stress Changes? Lab Value of A?
	Levée for Flood Control	6 Open Tube Piezometers	$\Delta u = KA_f\Delta\sigma_1$	$\Delta\sigma_1$, From Uniform elastic halfspace	$A_f \propto$ OCR, $A_f \propto$ Depth, Δu Dissipation, Few Piezometers

FIELD OBSERVATIONS OF PORE WATER PRESSURE MEASUREMENT
(cont'd)

Article	*Type*	*Field Measurement*	*Predicted Δu Method*	*Predicted Δu Method*	*Reasons for Discrepancies*
Hoeg *et al.* (1969)	Preload for tank (two cases)	32 and 31 Piezometers	$\Delta u = \Delta\sigma_{oct} = 1/3(\Delta\sigma_1+\Delta\sigma_2+\Delta\sigma_3)$	Soil layered, but isotropic, linearly elastic, resting on rigid base	Good agreement in elastic range
D'Appolonia, Lambe, Poulos (1971)	Embankment	6 Electric 33 Hydraulic	(a) $\Delta u = \Delta\sigma_z$ (b) $\Delta u = \Delta\sigma_{oct}$ (c) $\Delta u = \Delta\sigma_{oct}+a\Delta\tau_{oct}$	(1) Homo. Elastic halfspace (2) Homo. Elastic Layer (3) FEM-LAB-Eu (4) FEM-Eu=1200 c_u	Δu Dissipation in top and bottom
Moh *et al.* (1969)	Embankment	52 Bishop Piezometers	$\Delta u = \Delta\sigma_{oct} + 3\alpha\Delta\tau_{oct}$ α Term is Small	Plane Strain, Homo. linearly elastic halfspace	Drainage during construction
Bozozuk, Leonards (1972)	Test Embankment	19 Open Standpipe Piezometers	$\Delta u = \Delta\sigma_{oct} + a\tau_{oct}$	Homo., Linear Elastic Isotropic, Plane Strain	Anisotropic Layers varying OCR
Raymond (1972)	Bridge Abutment	15 Piezometers	Not Predicted	FEM Method	Dissipation of PWP below crust, lateral drainage
Dascal, Tournier (1975)	Embankment	13 Piezometers	$\Delta u = f(h)$	Not Predicted	Not predicted but Pore Pressure Dissipation observed
Wu *et al.* (1975)	Embankment	18 Piezometers	$\Delta u = \Delta\sigma_z$ $\Delta u = \Delta\sigma_{oct}$ $\Delta u = \Delta\sigma_3+A(\Delta\sigma_1-\Delta\sigma_3)$ $\Delta u = \Delta\sigma_{oct}+a\Delta\tau_{oct}$	FEM Method, Linear and non-linear elasticity	Pore Pressure Dissipation, irregular construction pattern

APPENDIX 4

TEST PLATE RIGIDITY

(A) *Differential displacement of plate*

An estimate can be made of the differential displacement of the plate by simplifying the problem to the following configuration:

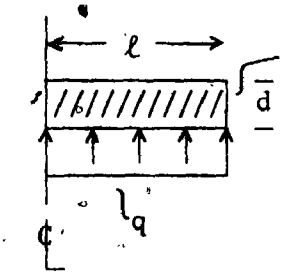

At end, $\rho_{max} = \frac{q\ell^4}{8EI}$

Assuming $q = 150$ kPa

$\ell = 0.19$ m

$E = 207 \times 10^6$ kPa

$I = \frac{bd^3}{12} = \frac{(1)(0.051)^3}{12}$ m^4

Hence $\rho_{max} = 0.011$ *mm* (0.00043 in).

Relative to the total plate settlement of 5 to 10 mm the differential displacement is small, and the plate can be considered to settle uniformly.

(B) *Relative rigidity*, K_r (Borowicka, 1938)

$$K_r = \frac{4}{3} \frac{(1 - \nu_s^2)}{(1 - \nu_b^2)} \frac{E_b}{E_s} \left(\frac{t}{B}\right)$$

For undrained loading: $\nu_s = 0.5$

$\nu_b = 0.3$

$E_b = 207 \times 10^6$ kPa

$E_s = E_u = 6.9 \times 10^3$ kPa

$t = 0.051$ m

$B = 0.38$ m

then $K_r = 80$

for $\pi < K_r < \infty$, Plate can be considered rigid.

For drained loading: $\nu_s = \nu' \leq 0.5$

$$E_s = E' = \frac{2(1+\nu')}{3} E_u$$

Letting $\nu' = 0.0$ then $E' = 0.67 E_u$

Now $K_r = 159$

The plate appears to be more rigid. From this method it follows that the contact stress distribution will tend to increase at the edges as the soil medium consolidates.

(C) *Relative rigidity*, K_r (ACI, 1966)

$$K_r = \frac{E' I_B}{E_s' b^3}$$

Letting E' = E for test plate = 207×10^6 kPa

E_s' = E' for soil = 4.6×10^3 kPa

I = Moment of Inertia of Plate = $t^3/12$

b = 0.19 m = 1.11×10^{-5} m^3

$K_r = 73$

for $K_r > 0.5$, Plate can be considered rigid.

APPENDIX 5

PRESSURE TRANSDUCER SPECIFICATIONS AND CALIBRATION

(A) *Pressure Transducer Specifications*

Kulite Semiconductor Products Ltd.
1039 Hoyt Avenue
Ridgefield, New Jersey

Model No. IPT-750-100

I	INPUT	
	Pressure Range	0-100 PSI (0-690 kPa)
	Operational Mode	Gauge
	Over Pressure	2 times maximum rating
	Rated Electrical Excitation	7.5 VDC
	Maximum Electrical Excitation	10 VDC
	Input Impedance	1200 ohm Nominal
II	OUTPUT	
	Output Impedance	500 ohm Nominal
	Full Scale Output (FSO)	100 mV Nominal
	Residual Unbalance	3% FSO
	Combined Non-linearity, Hysteresis and Repeatibility	0.5% FSO MAX
	Hysteresis	0.25% FSO MAX
	Repeatibility	0.1% FSO MAX
	Resolution	Infinite
III	ENVIRONMENTAL	
	Operating Temperature Range	-40°C to +120°C
	Compensated Temperature Range	27°C to 80°C
	Thermal Zero Shift	1%/FSO/55°C
	Thermal Sensitivity Shift	1%/FSO/55°C

(B) *Calibration of Pressure Transducers*

The sensitivity of the pressure transducers were supplied by the manufacturer, and are expressed in terms of millivolts output per volt input. All the pressure transducers had a recommended excitation voltage of 7.50 volts, and this value was used. The "B & F" data acquisition system could provide separate voltages to each of the pressure transducers. Modifications had to be made to the

"B & F" system to make the full scale output of ± 2000 micro-strain equivalent to approximately ± 690 kPa on the ×5 scale of the instrument. By reducing the scale multiplier to ×1, the ± 2000 micro-strain was equivalent to ± 140 kPa. Then each unit of micro-strain was measuring approximately 0.07 kPa, depending on the calibration factor of the individual transducer. When pressures greater than 140 kPa were to be measured, the scale adjustment could be increased to ×2, resulting in a full scale output of ± 280 kPa.

Each of the pressure transducers were calibrated several times by two methods, and the results were compared with the manufacturer's calibration constants. The first method involved placing the transducer into the pore water pressure cell shown in Fig. 3.9. The cell was modelled after a diagram given by Burn (1963) and it allows a fluid to enter the chamber containing the sensitive diaphragm of the transducer. The cell permits the de-aired water to be flushed free of air "pockets". Pressure was applied accurately by a system of mercury pots in the Soil Mechanics Laboratory, based on the method outlined in Bishop and Henkel (1962). For each pressure increment the output voltage was recorded. To determine the calibration constant, K, relating change in applied pressure to change in output voltage, the data was analyzed on the Time Sharing Library (TSL) program POLYFIT.TSL available at Carleton University to determine the best fit straight line through the points. The result was that the increment in applied stress, Δq_x, can be represented as $\Delta q_x = K\Delta V$, where ΔV is the change in voltage.

When the pressure cells are mounted in the test plate they are held in place by the brass collar that ensures the face of the transducer is flush with the bottom surface of the footing. To determine if the degree of tightening of the brass collar had an effect on the calibration constant, the pressure transducers were mounted in the test plate and the calibration chamber positioned over the face. The self-compensating mercury pot system again applied the pressure to the water, and a new set of data was generated. The new transducer in-place calibration constants were compared with the constants obtained previously, and were found to deviate by less than ±1 percent. They were also compared with the

manufacturer's calibration data, and the maximum deviation was ±2 percent, with the majority being less than ±1 percent. The calibration data is given in the following table. Although the manufacturer's method of calibration may have been more accurate, the calibration constants obtained in the laboratory were used in the analysis of the data.

PRESSURE TRANSDUCER CALIBRATION

Pressure Transducer Serial #	*Channel # on "B & F" Sand Tests*	*Channel # on "B & F" Clay Tests*	*Manufacturers' Calibration at 7.50 V Input 0-700 kPa Range*	*"Mercury" Calibration at 7.50 V Input 0-350 kPa Range*	*"Mercury" Calibration at 7.50 V Input 0-100 kPa Range*
			(psi/mv output)	*(psi/mv output)*	*(mV/psi)*
3148-4-176	26	11	0.749	0.758	0.713
2777-1-375	14	14	1.058	1.050	1.050
2777-1-376	17	28	1.003	1.007	1.000
2777-1-381	18	15	1.270	1.274	1.246
2777-1-383	11	26	1.190	1.202	1.200
2777-1-384	19	12	1.010	1.027	1.030
2777-1-478	10	21	1.159	1.162	1.148
2777-1-482	27	20	1.067	1.063	1.061
3326-3-11	24	18	0.997	1.005	0.974
3326-3-12	22	27	1.006	1.005	0.996
3326-3-14	20	13	1.010	0.987	1.009
3326-3-15	12	29	1.010	0.991	0.990
3326-3-16	23	25	0.995	1.000	0.985
3326-3-17	21	24	0.980	0.986	0.980
3326-3-18	13	23	0.998	0.992	0.984
3326-3-19	25	17	0.982	0.990	0.970
3112-3-366	—	31	1.003	0.988	0.99
3112-3-367	—	32	0.988	0.975	0.98
3112-3-368	—	33	1.031	1.017	1.02
3112-3-370	—	34	1.000	0.993	0.99
58406(10-1)	(0-10 psi range)	10	13.42	—	13.57
48407(10-2)	(0-10 psi range)	voltmeter	13.40	—	13.65

NOTE: (1) "Mercury" signifies that the stress was applied to the pressure transducer with a system of mercury pots in the laboratory.

(2) These "Mercury" test results were obtained when the pressure transducers were installed in the test plate. The calibration results obtained from using the pressure cell chambers of Fig. 3.9 or 3.10 differed by less than one percent.

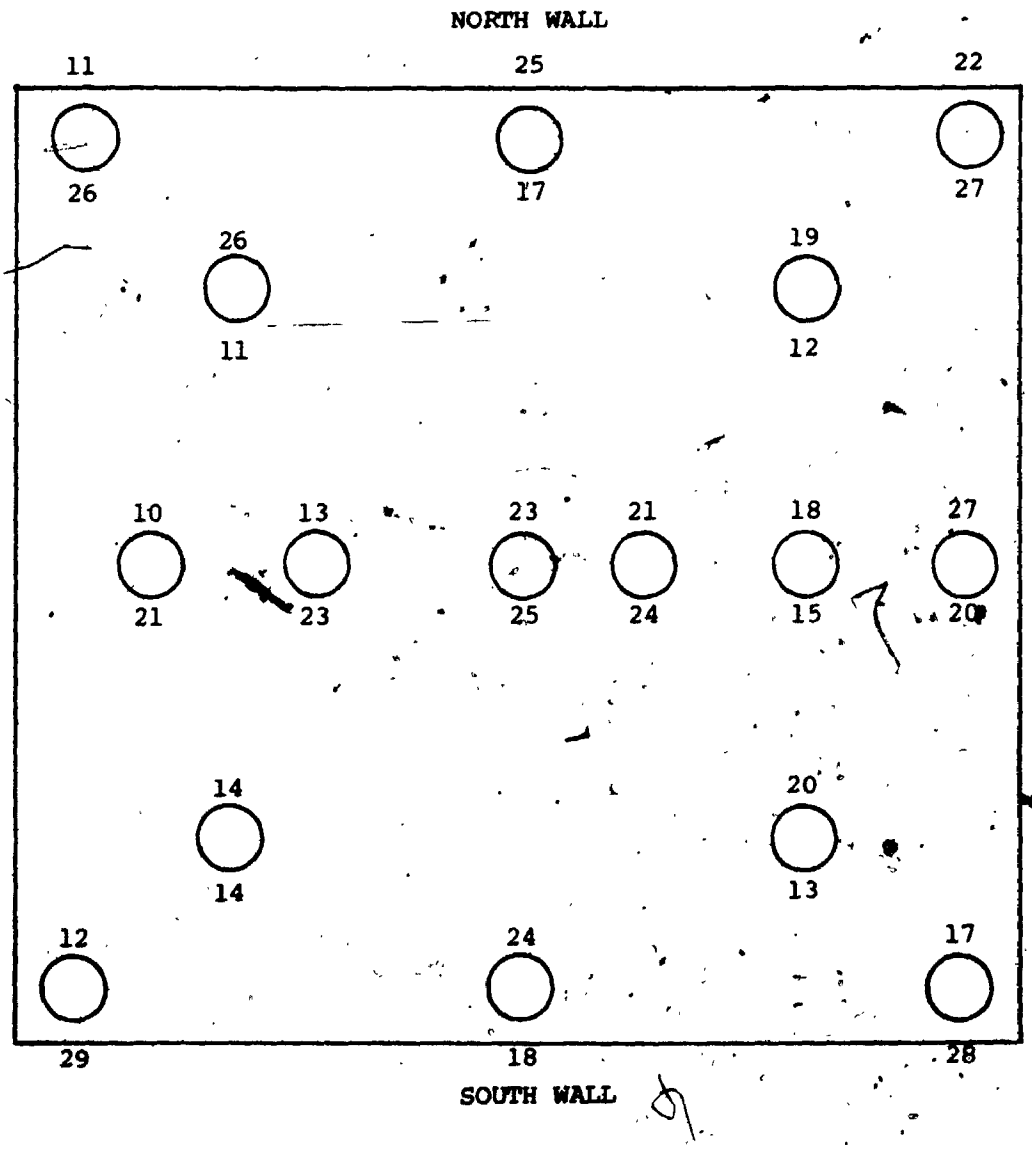

Key to Channel Locations on Test Plate

Sand Tests

Clay Test

APPENDIX 6

DISPLACEMENT OF PRESSURE TRANSDUCER DIAPHRAGM

The problem was analysed by Timoshenko (1940) for a uniformly loaded circular plate with clamped edges.

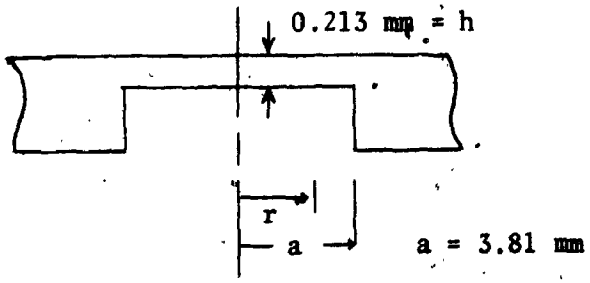

Equation of diaphragm displacement $w = \frac{q}{64D}(a^2-r^2)^2$

where q = load intensity

D = flexural rigidity = $\frac{Eh^3}{12(1-\nu^2)}$

Letting $E = 193\times10^6$ kPa

$\nu = 0.3$

$h = 2.13\times10^{-4}$ m

then $D = 1.71\times10^{-4}$ KN-m

Thus, for $q = 1$ kPa

$r = 0$ (centre)

then $w_{max} = 1.93\times10^{-8}$ m/kPa

By integrating the equation of the diaphragm deflection the displaced volume can be calculated as:

Volume displaced = 2.9×10^{-4} mm³/kPa .

The amount of deflection required for the registration of applied stress is calculated to be very small, and is in agreement with Hvorslev's (1976) recommendation that the rigidity of the pressure cell diaphragm be maximized in order to reduce the interference between the pressure cell and the soil.

APPENDIX 7

LOAD CELL SPECIFICATIONS AND CALIBRATION

(A) *Load Cell Specifications*

Interface, Inc.
7401 East Butherus Drive
Scottsdale, Arizona

Model 1210-AJ Precision Universal Load Cell

Load range	± 10,000 lb (± 44,500 N)
Input resistance	350.2 ohms
Output resistance	350.2 ohms
Recommended excitation	10 VDC
Maximum excitation	20 VDC
Maximum error band, computed on a best straight line through zero basis including non-linearity hysteresis and repeatability	± 0.020% FS
Compensated temperature range	-10°C to +46°C
Thermal zero shift	0.0002% FS/°C
Zero balance	0.1% FS
Compression output	*4.085* mV/V

(B) *Load Cell Calibration*

Load applied by INSTRON

Voltage input = 10.00 V

Load Applied (lb)	*Voltage Output (mV)*
1000	4.10
2000	8.20
3000	12.20
4000	16.20
4950	20.10
6000	24.20
7080	28.67
8000	32.50
9050	36.70
10000	40.60

From POLYFIT.TSL

Best fit straight line is

Voltage output (mV) = $(0.3428\times10^{-1}) + (0.4051\times10^{-2})$(Load (lb)).

Hence calibration constant (= slope of line) = 0.4051×10^{-2} *mV/lb*.

Compares with manufacturer's constant of 0.4086×10^{-2} *mV/lb*.

APPENDIX 8

DISPLACEMENT TRANSDUCER SPECIFICATIONS AND CALIBRATION

(A) *Specifications*

Hewlett Packard (Canada) Ltd.
1785 Woodward Drive
Ottawa, Ontario

Model 7DCDT-3000

Recommended excitation voltage	6.0 VDC
Maximum excitation	7.0 VDC
Full scale output (nominal)	5.0 VDC
Displacement range — full scale	± 3000 inches (± 75 mm)
Scale factor (nominal)	1.4 V/inch
Maximum non-linearity	± 0.5% FS
Temperature range	-54°C to +60°C
Weight of typical coil	200 gms
Dimensions	19 mm dia. × 267 mm long

(B) *Calibration of the Displacement Transducers*

A calibration constant for each of the displacement transducers (LVDT's) was obtained by supplying a constant 6.00 volt input to the transducer. The stainless steel core of the transducer was allowed to move within the LVDT, and its displacement was measured with a 0 to 2.000 inch dial gauge accurate to within ± 0.001 inch (± 0.03 mm). The relationship between the change in voltage and change in core position (or dial deflection) was established. The accuracy of the LVDT was given as ± 0.5 percent of full scale output. Similar to the discussion on pressure transducers, this implies an accuracy of ± 0.015 inch (± 0.4 mm) at each position of the core. The accuracy can be improved for smaller ranges, so a range of 0 to 1.2 inches (0 to 30 mm) was selected. As in most previous cases where a straight line had to be determined from a set of data, the program POLYFIT.TSL was used to get the "best-fit" linear relationship between the change in voltage output and change in core position.

For a 6.00 volt input, one-inch displacement results in a

change in voltage of

DCDT	#1	1.635 V
	#2	1.655 V
	#3	1.592 V
	#4	1.653 V
	#5	1.592 V

in the range of 0 to 1.0 inches.

APPENDIX 9

ARNPRIOR CLAY CHEMICAL AND MINERAL ANALYSIS

Dochart Brick and Tile Company, Ltd.
Arnprior, Ontario

from G.R. Guillet (1967)

(A) *Chemical Analysis — "Big Bank"*

SiO_2	56.46%
Al_2O_3	16.1
Fe_2O_3	7.30
CaO	3.59
MgO	3.72
Na_2O	2.53
K_2O	3.60
TiO_2	0.87
CO_2	0.14
H_2O+	2.20
H_2O-	3.18
SO_3	0.54
Total	100.1%
Loss on ignition	3.93
Soluble salts	0.65

(B) *Mineral Analysis — "Big Bank"*

	%
Non-Clay Minerals:	
Quartz	22
Calcite	not detected
Dolomite	not detected
Soda-Lime Feldspar	11
Potash Feldspar	2
Amphibole	0.5-5
Clay Minerals:	
Illite	abundant
Chlorite	trace
Montmorillonite	moderate

APPENDIX 10

BEARING CAPACITY OF A STRIP FOUNDATION

In foundation analysis, the two most important questions asked are generally: (1) is the design safe against bearing capacity failure? and (2) at working load levels, are the total and differential settlements tolerable? Although settlement considerations usually govern the design, the bearing capacity must be checked. It is common practice to relate the applied stress to the bearing capacity, and "working load levels" implies a "factor of safety" or ratio of bearing capacity to applied stress of 2.5 or greater. Factor of safety can also be defined in relation to the stress producing the first occurrence of local yielding at the edge of a stiff foundation (see for example Davis and Poulos, 1968; or D'Appolonia *et al.*, 1971).

A general formula for bearing capacity of q_u of a rigid strip footing embedded a depth D into a semi-infinite homogeneous soil mass can be represented as:

$$q_u = cN_c + \gamma DN_q + \tfrac{1}{2}\gamma_s BN_\gamma$$

where c = cohesive strength of the soil
γ_s = unit weight of the soil
B = width of strip footing
N_c, N_q, N_γ = bearing capacity factors.

This representation of bearing capacity is common to many authors, but the theoretical bearing capacity coefficients depend on the model being analysed. The most sensitive coefficient is N_γ, and many researchers have proposed values that vary substantially from one another.

For the undrained loading of a rigid smooth strip footing on a purely cohesive material, $q_u = (\pi+2)c_u$, as obtained from plasticity theory. For a rough interface condition this bearing capacity will increase to $5.7\,c_u$. At the end of consolidation, the bearing capacity can be determined in terms of the effective friction angle, ϕ', and c' parameters.

There is a problem in defining the criteria for bearing capacity failure because the load settlement curves are dependent on a number of factors, including the soil properties, the method of load application, and the rate of loading. Vesić (1973) describes three types of failure modes: (1) general shear failure; (2) punching shear failure; and (3) local shear failure. Under punching shear and local shear failure there is no well-defined ultimate load, and the point of failure is not clearly established. Arbitrary definitions of failure are often used, defining failure as that occurring when the settlement is equal to a certain percentage of the width of the footing or depth of embedment.

(A) *Bearing Capacity on Sand*

(1) BANDING SAND

From direct shear tests (Fig. 3.23) $\phi = 36°$

$$q_u = cN_c + \gamma D N_q + \tfrac{1}{2}\gamma B N_\gamma$$

Since $c = 0$
$D = 0$

then $q_u = \tfrac{1}{2}\gamma B N_\gamma$

From Chummar (1972) several theoretical and experimental results were presented from various authors. For $\phi = 36°$, N_γ ranged from 42 to 105, with most of the results in the range of 42 to 60. Vesić (1973) recommends a value of 56. The results of Shields *et al.* (1977) can be extrapolated to obtain $N_\gamma = 60$ for a strip footing resting on compact sand.

It is realized that there is uncertainty in the value of the angle of internal friction to be used in predicting N_γ because it was based on a limited number of direct shear tests. Shields *et al.* (1977) showed that the measured friction angle depended on the test method, such as the triaxial test, plane strain test or direct shear test. The estimate of bearing capacity is important in this investigation primarily in order to show that the stress applied to the foundation constitutes a working stress level.

Taking $N_\gamma = 60$, then $q_u = 200$ kPa. For a maximum applied stress of 147 kPa for the sand tests, the factor of safety was 1.4.

(2) FLINT SAND

From direct shear tests (Fig. 3.25) $\phi = 40°$

Again, from Chummar (1972), N_γ ranged from 85 to 210, with most of the values in the range of 85 to 110. Vesić (1973) recommended $N_\gamma = 109$. Shields *et al.* (1977) obtained $N_\gamma = 180$ for a dense sand medium.

Hence, the estimated value of q_u ranges from 275 kPa to 680 kPa.

For the tests on sand, the maximum applied stress was 147 kPa, which produces a factor of safety greater than 1.9.

(B) *Bearing Capacity on Clay*

From Vesić (1973)

$$q_u = cN_c + \gamma DN_q + \tfrac{1}{2}\gamma BN_\gamma$$

In this investigation

$c_u = 15$ kPa (see Section 3.3.7)

$N_c = 5.14$

$D = 0$

γ = effective unit weight = 12.84 kN/m^3

$B = 0.38$ m

$N_\gamma = 1.44$ (fn $\phi = 11°$, see Fig. 3.17)

Hence $q_u = 80.6$ kPa.

4 OF/DE 4

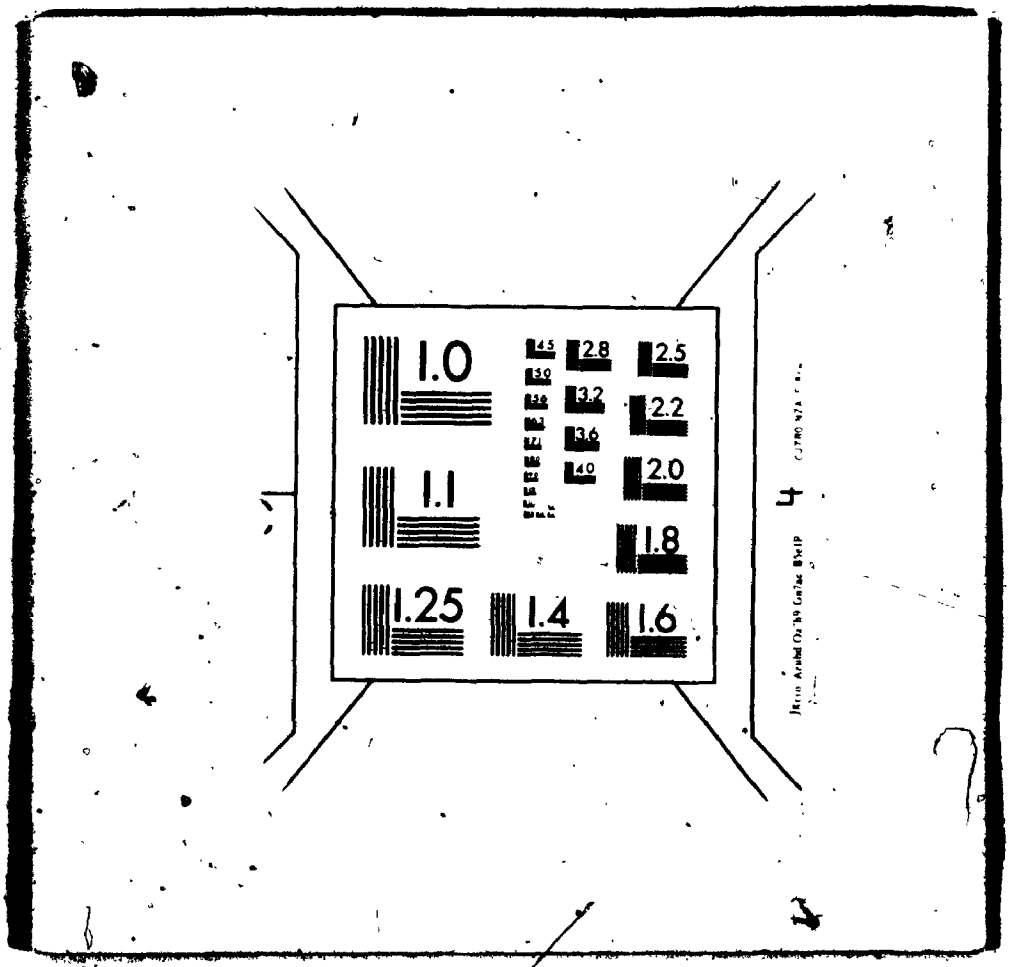

APPENDIX 11

COMPUTER PROGRAM CONTAC

This program was written to analyse the data obtained from the experiments that measured the contact stress distributions below the rigid test plate. The "B & F" data acquisition system recorded on paper tape the voltage output of the load cell, displacement transducers and pressure transducers. This data was stored in computer files in "raw" form until processed by the program CONTAC to produce meaningful results. All of the computations are basic arithmetical operations, which due to the amount of data generated, would have resulted in tedious calculations if performed by hand. Since the pressure transducers were positioned differently in the clay experiments, the channel numbers were also changed. The program for the clay tests was essentially the same as the one for the sand tests. A flow chart and computer printout are provided.

CONTAC FLOW CHART

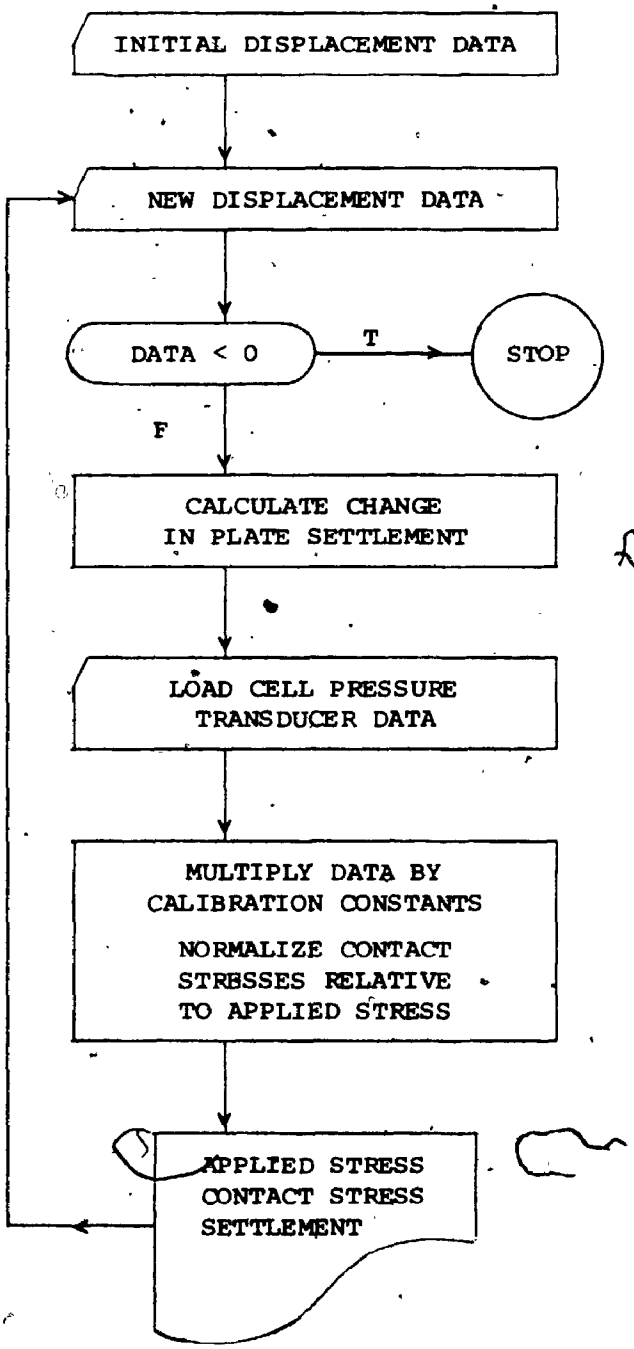

```
!EDIT CONTAC
EDIT HERE
*TYO-9999
   1.000 C      PROGRAM FOR REDUCING B&F DATA
   2.000 C      READ ORIGINAL DEFLECTIONS
   3.000        READ,D1,D2,D3,D4,D5
   4.000 C
   5.000 1      READ,C1,C2,C3,C4,C5
   6.000        IF(C1.LT.0.)GO TO 2
   7.000        C1=(C1-D1)/1.635
   8.000        C2=(C2-D2)/1.655
   9.000        C3=(C3-D3)/1.592
  10.000        C4=(C4-D4)/1.653
  11.000        C5=(C5-D5)/1.592
  12.000        SUMD=(C1+C2+C3+C4)/4
  13.000 C
  14.000        READ,C10,C11,C12,C13,C14
  15.000        READ,C15,C17,C18,C19
  16.000        READ,C20,C21,C22,C23,C24,C25,C26,C27
  17.000 C
  18.000        CON=1./(C15*0.0298)
  19.000 C
  20.000        C10=CON*C10/43.8
  21.000        C11=CON*C11/42.3
  22.000        C12=CON*C12/51.3
  23.000        C13=CON*C13/51.1
  24.000        C14=CON*C14/48.5
  25.000        C15=C15*0.0298
  26.000 C
  27.000        C17=CON*C17/50.4
  28.000        C18=CON*C18/40.0
  29.000        C19=CON*C19/49.5
```

```
   30.000          C20=CON*C20/48.1
   31.000          C21=CON*C21/51.6
   32.000          C22=CON*C22/50.4
   33.000          C23=CON*C23/50.8
   34.000          C24=CON*C24/50.9
   35.000          C25=CON*C25/51.5
   36.000          C26=CON*(C26-500.)/68.0
   37.000          C27=CON*C27/47.9
   38.000          SUM=C10+C11+C12+C13+C14+C17+C18+C19
   39.000          SUM=SUM+C20+C21+C22+C23+C24+C25+C26+C27
   40.000          SUM=SUM*100./16.
   41.000 C
   42.000          WRITE(108,90)
   43.000 90       FORMAT('************************************')
   44.000          WRITE(108,100)C15
   45.000          WRITE(108,101)
   46.000          WRITE(108,102)C11,C25,C22
   47.000          WRITE(108,103)C26,C19
   48.000          WRITE(108,104)C10,C13,C23,C21,C18,C27
   49.000          WRITE(108,103)C14,C20
   50.000          WRITE(108,102)C12,C24,C17
   51.000 C
   52.000 100      FORMAT(//'AVERAGE UNIFORM LOAD = ',F5.2,' PSI')
   53.000 101      FORMAT(//'CONTACT STRESS'/)
   54.000 C
   55.000 102      FORMAT(F6.3,11X,F5.3,13X,F5.3//)
   56.000 103      FORMAT(6X,F5.3,18X,F5.3//)
   57.000 104      FORMAT(3X,F5.3,2X,F5.3,2X,F5.3,1X,F5.3,1X,F5.3,1X,F5.3//)
   58.000 C
   59.000          WRITE(108,110)SUM
   60.000 110      FORMAT('PERCENTAGE OF APPLIED LOAD =',F6.2,' %')
   61.000          WRITE(108,105)C4,C1,C5,C3,C2
   62.000 105      FORMAT(/'DEFLECTIONS ARE =',/2F10.1,/5X,F10.1,/2F10.1//)
   63.000          WRITE(108,111)SUMD
   64.000 111      FORMAT('AVERAGE DEFLECTION = ',F7.1//)
   65.000          GO TO 1
   66.000 2        CONTINUE
   67.000          END
--EOF HIT AFTER 67.
*END

!
```

APPENDIX 12

SUMMARY OF INITIAL SETTLEMENT PREDICTIONS FOR STRIP FOOTING

Method	*Initial Settlement Equation*	*Conditions*	*Result (mm)*
Janbu *et al.* (1956) (from Bowles, 1968)	$\rho_i = \mu_1 \mu_2 \frac{qB}{E}[1-\nu^2][c]$	Rigid Base, B/h = 0.4 Flexible strip footing average ρ	$\rho_i = 277 \frac{q}{E}$
Poulos (1967)	$\rho_i = \frac{qH}{\pi E} I_{ST}$	Rigid Base Flexible strip footing $\nu = 0.5$ Edge or centreline	Centreline $\rho_i = 301 \frac{q}{E}$ Edge $\rho_i = 184 \frac{q}{E}$
Milović *et al.* (1970)	$\rho_i = \frac{qB}{E} I$	Rigid Base B/h = 0.4 interpolated Rigid strip footing $\nu = 0.5$ extrapolated	$\rho_i = 259 \frac{q}{E}$
Harr (1966)	$\rho_i = \frac{c_d' qB(1-\nu^2)}{E}$	Rigid Base, smooth or rough contact Flexible strip footing Edge or centreline	Centreline $\rho_i = 400 \frac{q}{E}$ Edge $\rho_i = 277 \frac{q}{E}$
Superposition	$(\rho_{plate} - \rho_{edge}) = \frac{qB}{\pi G}[I]$	Settlement relative to end wall Rigid strip footing $\nu = 0.5$	$\rho_p - \rho_e = 295 \frac{q}{E}$ Average I = 282

APPENDIX 13

EXPLANATION OF PROGRAM DELTAH FOR COMPUTATION OF CONTACT STRESSES BENEATH A RIGID PLATE

The solution for the settlement profile of a strip load on an isotropic homogeneous elastic halfspace has been used to compute both the settlement profile and contact pressure of a *rigid* strip footing. The relative settlement solution for an incompressible medium with Poisson's ratio of 0.5 was given by Gibson (1967) for the case of Young's modulus E increasing linearly with depth. The special case of a uniform modulus E was also presented, and was used in this analysis.

The theoretical results show that the settlement at all points of the medium is infinite. To overcome this problem, the settlement can be represented as the relative settlement of a point with reference to another point, by substracting an "infinite constant". Usually the reference point is taken as the centreline of the strip load, but this is purely arbitrary. The result is that the surface settlement of a point relative to the centre can be represented as

$$\rho(x,0) - \rho(0,0) = -\frac{qb}{2\pi G(0)}\left[\left(1+\frac{x}{b}\right)\ell n\left|1+\frac{x}{b}\right| + \left(1-\frac{x}{b}\right)\ell n\left|1-\frac{x}{b}\right|\right]$$

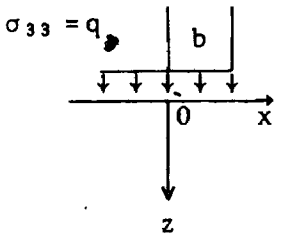

where $\rho(x,0)$ = settlement at point (x,0)

$\rho(0,0)$ = settlement at point (0,0)

q = local intensity of load

b = one-half strip width

$G(0)$ = shear modulus at surface $= \frac{E}{2(1+\nu)}$

x/b = relative position of surface point with respect to strip width

The above solution results in maximum settlement occurring at the centre of the strip. Uniform stress application results in a uniform contact stress distribution, but non-uniform settlements. The problem of a rigid strip footing can be approximated by a superposition technique, similar to that used by Conway *et al.* (1966) and Yamaguchi *et al.*

(1968). The contact width is divided into several intervals, and each interval is assumed to have a uniform stress distribution. The intervals can be equally spaced or they can vary in width. For the simplest case of equal intervals the vertical deflections at the centre of the intervals can be expressed in terms of the contact stress $p_1, p_2, p_3, \ldots p_r$, and by superimposing a series of uniform loads over a portion of the strip width a set of η simultaneous equations are produced. A further constraint imposed on the system is that all interval deflections must be equal. This results in $(\eta+1)$ unknowns, i.e. η interval contact stresses and one unknown deflection. By considering the overall equilibrium of the foundation, the total stress applied must equal the total reaction stress. Hence the $(\eta+1)$ simultaneous equations can be solved, resulting in a contact stress distribution across the plate approximating that of the elastic solution given by

$$q_x = \frac{2q_0}{\pi\sqrt{1-(x/b)^2}}$$

The results of this program can also be used to calculate the stress distribution within the elastic medium.

FLOW CHART OF PROGRAM DELTAH

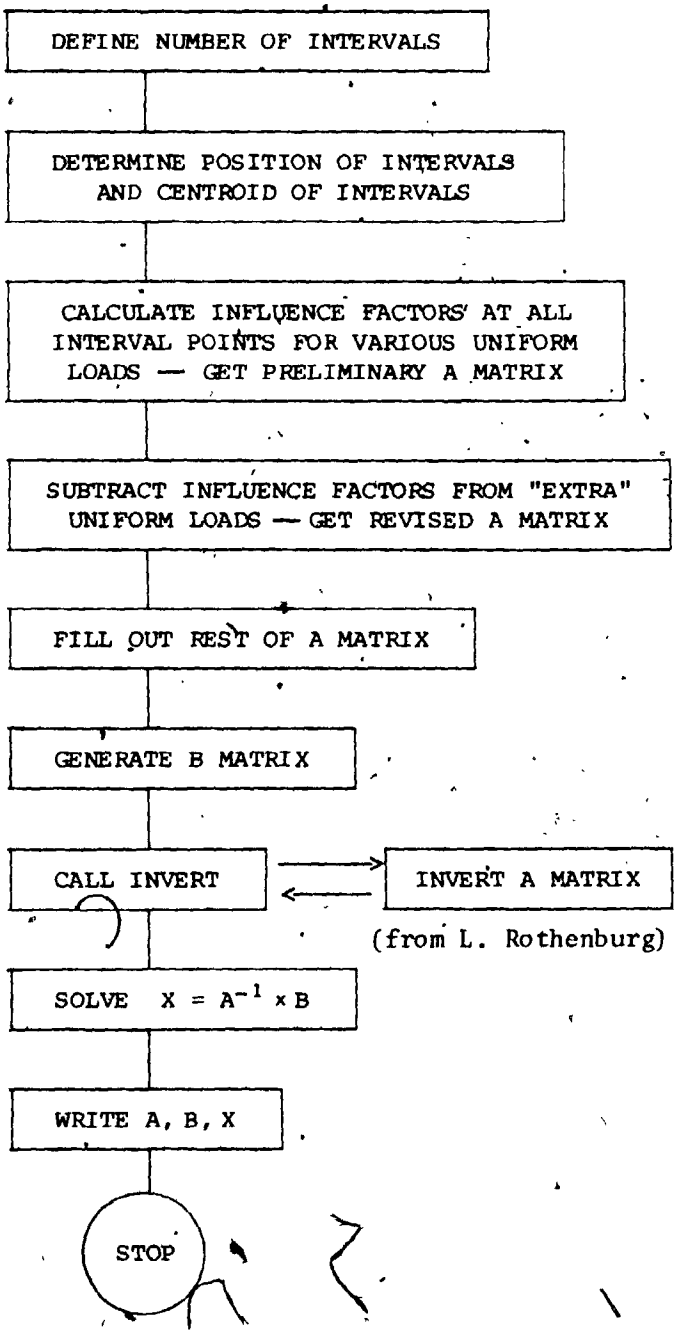

CONTACT STRESS RESULTS

— results of DELTAH —
— interval based on *centroid* —

Pts	*Left Side of Interval XI(I)*	*Centroid X(I)*	q_x/q_0	*ρ(ref. 4*b)*
3	0.50000	0.29683	0.78954	3.25825
	0.86603	0.71507	0.86312	
	1.00000	0.96671	2.15942	
6	0.25882	0.15046	0.78589	3.24327
	0.50000	0.38899	0.79531	
	0.70711	0.61170	0.83889	
	0.86603	0.79468	0.97157	
	0.96593	0.92433	1.32239	
	1.00000	0.99149	4.24182	
10	0.15643	0.09054	0.78550	3.24167
	0.30902	0.23757	0.78748	
	0.45399	0.38497	0.79577	
	0.58779	0.52393	0.81616	
	0.70711	0.65023	0.85762	
	0.80902	0.76098	0.93618	
	0.89101	0.85297	1.08481	
	0.95106	0.92404	1.39068	
	0.98769	0.97243	2.05990	
	1.00000	0.99692	7.04628	

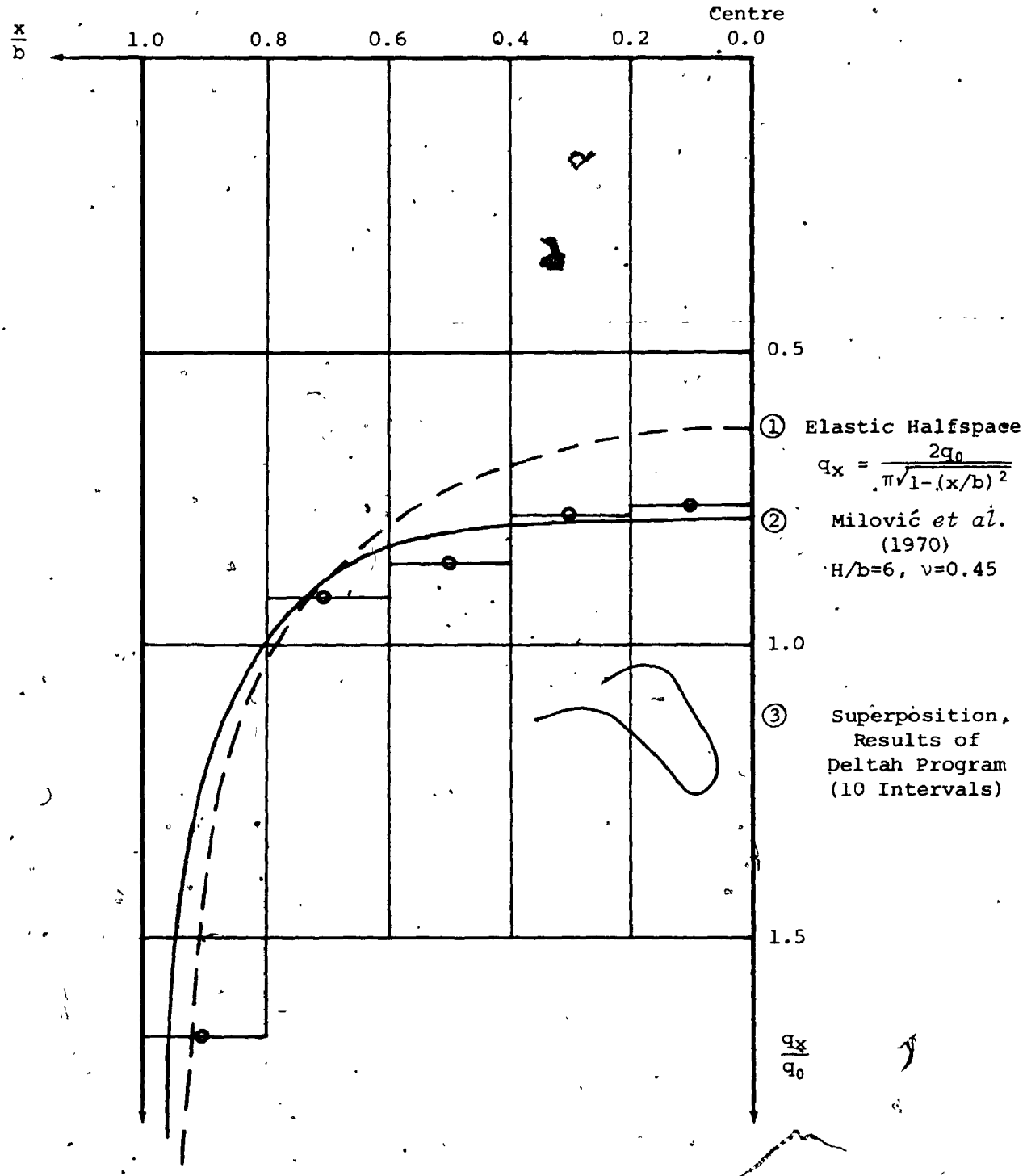

Comparison of Contact Stress Distribution
Beneath a Rigid Strip Footing

```
*EDIT DELTAH
*TYO-999
    1.000 C     PROGRAM TO COMPUTE CONTACT PRESSURES UNDER A RIGID PLATE
    2.000       DIMENSION A(4,4),B(4,1),BB(4,1),X1(4),X(4),XW(4)
    3.000       INTEGER I1(4),I2(4)
    4.000 C     FIX NUMBER OF INTERVALS
    5.000       NP=3
    6.000       WRITE(108,42)NP
    7.000 42    FORMAT(' NUMBER OF INTERVALS = ',F10.1)
    8.000 C     CALCULATE POSITION OF INTERVALS
    9.000       PI=3.14159265
   10.000       DO 1 I=1,NP
   11.000       N=I
   12.000 C     LET X1(I) DIVIDE INTERVAL WIDTHS
   13.000       X1(I)=SIN((PI*N)/(2*NP))
   14.000 1     CONTINUE
   15.000       WRITE(108,43)
   16.000 43    FORMAT('INTERVAL POSITIONS ARE = ')
   17.000       WRITE(108,5)(X1(I),I=1,NP)
   18.000 5     FORMAT(/10F10.5)
   19.000 C     CALCULATE CENTROID OF INTERVAL
   20.000       XM=0
   21.000 C     LET X(I) BE CENTROID OF INTERVAL
   22.000       DO 2 I=1,NP
   23.000       XW(I)=X1(I)-XM
   24.000       XM=X1(I)
   25.000       X(I)=SQRT(1.-(2.*NP*XW(I)/PI)*(2.*NP*XW(I)/PI))
   26.000 2     CONTINUE
   27.000       WRITE(108,44)
   28.000 44    FORMAT(' CENTRE OF INTERVALS ARE = ')
   29.000       WRITE(108,6)(X(I),I=1,NP)
   30.000 6     FORMAT(10F10.5/)
   31.000 C     COMPUTE FIRST GENERATION OF A MATRIX
   32.000       DO 3 J=1,NP
   33.000       BA=X1(J)
   34.000       DO 4 I=1,NP
   35.000       XDB=X(I)/BA
   36.000       XEDB=100/BA
   37.000       A(I,J)= (-1.)*((1+XDB)*ALOG(ABS(1+XDB))
   38.000      1 +(1-XDB)*ALOG(ABS(1-XDB)))
   39.000       A(I,J)=A(I,J)+((1.+XEDB)*ALOG(ABS(1.+XEDB))
   40.000      1 +(1.-XEDB)*ALOG(ABS(1.-XEDB)))
   41.000 4     CONTINUE
   42.000 3     CONTINUE
   43.000 C     REVISE A MATRIX
   44.000       DO 20 JJ=1,NP
   45.000       J=(NP+1)-JJ
```

```
46.000          JM=J-1
47.000          IF(JM.LT.0.5)GO TO 10
48.000          DO 21 I=1,NP
49.000          A(I,J)=A(I,J)+(-1.)*A(I,JM)
50.000 21       CONTINUE
51.000 20       CONTINUE
52.000 10       CONTINUE
53.000 C        FILL OUT REST OF A MATRIX
54.000          WRITE(108,41)
55.000 41       FORMAT(' A MATRIX = ')
56.000          NPP=NP+1
57.000          DO 31 I=1,NP
58.000 31       A(I,NPP)= -1.0
59.000          DO 32 J=1,NP
60.000 32       A(NPP,J)=XW(J)
61.000          A(NPP,NPP)= 0.0
62.000          WRITE(108,7)NPP,((A(I,J),J=1,NPP),I=1,NPP)
63.000 7        FORMAT(N(F10.5))
64.000 22       CONTINUE
65.000 C        GENERATE B MATRIX
66.000          B(NPP,1)=1.0
67.000          DO 40 I=1,NP
68.000 40       B(I,1)= 0.
69.000          WRITE(108,33)
70.000 33       FORMAT(' B MATRIX = ')
71.000          WRITE(108,34)(B(I,1),I=1,NPP)
72.000 34       FORMAT(F10.5)
73.000 C        INVERT A MATRIX
74.000          N=NPP
75.000          CALL INVERT(A,N,I1,I2)
76.000 C        SOLVE  FOR X=A(INVERSE)*B
77.000          DO 50 I=1,NPP
78.000 50       BB(I,1)=0.
79.000          DO 60 I=1,NPP
80.000          DO 60 J=1,NPP
81.000 60       BB(I,1)=BB(I,1)+A(I,J)*B(J,1)
82.000          WRITE(108,35)
83.000 35       FORMAT('SOLUTION TO AX = B IS ')
84.000          WRITE(108,34)(BB(I,1),I=1,NPP)
85.000 C
86.000          END
87.000 C        SUBROUTINE FOR INVERTING A MATRIX
88.000 C        FROM L. ROTHENBURG
89.000          SUBROUTINE INVERT (A, N, I1, I2)
90.000          INTEGER I1(N), I2(N)
91.000          DIMENSION A(N,N)
92.000          M=N
93.000          PREC=1.E-5
94.000          TEST=0.0
95.000          DO 1 I=1,M
96.000          I2(I)=0
```

```
 97.000          DO 1 J=1,M
 98.000    1     TEST=TEST+A(I,J)*A(I,J)
 99.000          TEST=PREC*(TEST)**0.5/M
100.000          DO 9 K=1,M
101.000          BIG=0.0
102.000          DO 3 I=1,M
103.000          IF (I2(I) .NE. 0) GO TO 3
104.000          DO 2 J=1,M
105.000          IF (I2(J) .NE. 0) GO TO 2
106.000          T=ABS(A(I,J))
107.000          IF (T .LE. BIG) GO TO 2
108.000          BIG=T
109.000          IROW=I
110.000          JCOL=J
111.000      2   CONTINUE
112.000      3   CONTINUE
113.000          IF (BIG .LE. TEST) WRITE(6,100) ; STOP
114.000          I1(K)=JCOL
115.000          I2(JCOL)=IROW
116.000          IF (JCOL .EQ. IROW) GO TO 6
117.000          DO 5 J=1,M
118.000          TEMP=A(IROW,J)
119.000          A(IROW,J)=A(JCOL,J)
120.000      5   A(JCOL,J)=TEMP
121.000      6   PIV=1.E0/A(JCOL,JCOL)
122.000          DO 7 J=1,M
123.000          IF (J .NE. JCOL) A(JCOL,J)=PIV*A(JCOL,J)
124.000      7   CONTINUE
125.000          A(JCOL,JCOL)=PIV
126.000          DO 9 I=1,M
127.000          IF (I .EQ. JCOL) GO TO 9
128.000          PIV=-A(I,JCOL)
129.000          DO 8 J=1,M
130.000          IF (J .NE. JCOL) A(I,J)=A(I,J)+PIV*A(JCOL,J)
131.000      8   CONTINUE
132.000          A(I,JCOL)=PIV*A(JCOL,JCOL)
133.000      9   CONTINUE
134.000          DO 11 K=1,M
135.000          I=M+1-K
136.000          JCOL=I1(I)
137.000          IROW=I2(JCOL)
138.000          IF (IROW .EQ. JCOL) GO TO 11
139.000          DO 10 I=1,M
140.000          TEMP=A(I,IROW)
141.000          A(I,IROW)=A(I,JCOL)
142.000     10   A(I,JCOL)=TEMP
143.000     11   CONTINUE
144.000    100   FORMAT(/,'*****MATRIX IS SINGULAR*****')
145.000          RETURN
146.000          END
--EOF HIT AFTER 146.
*
```

APPENDIX 14

COMPUTER PROGRAM STRES2

The computer program STRES2 was written to compute the stresses within a homogeneous isotropic elastic halfspace when subjected to a series of uniform strip loads. The solution for a uniformly loaded strip footing is available in many texts (see for example Tsytovich, 1976; Saada, 1974; Jumikis, 1969). The following reference system was used in the analysis:

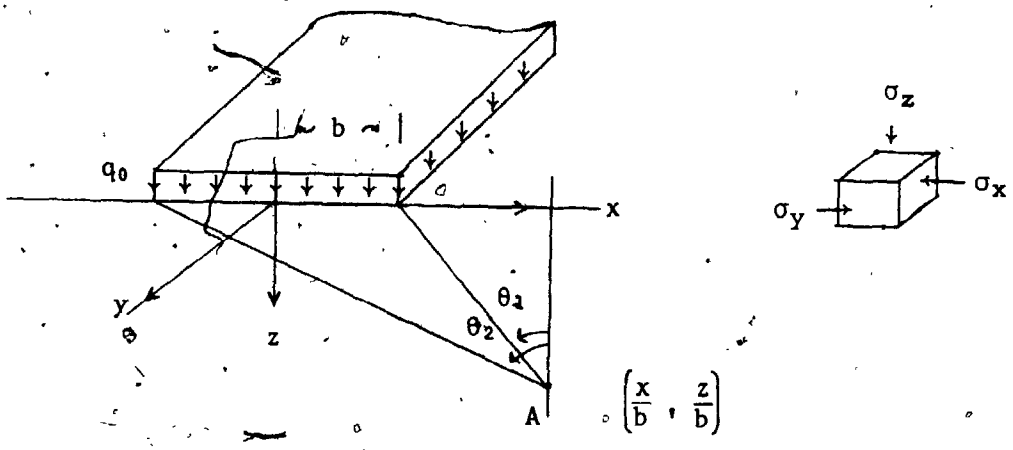

At any arbitrary point A with the soil medium,

Normal stress $$\sigma_z = \frac{2q_0}{\pi}\int_{\theta_1}^{\theta_2}\cos^2\theta\, d\theta = \frac{q_0}{2\pi}\left[2(\theta_2-\theta_1) + (\sin 2\theta_2 - \sin 2\theta_1)\right]$$

$$\sigma_x = \frac{2q_0}{\pi}\int_{\theta_1}^{\theta_2}\sin^2\theta\, d\theta = \frac{q_0}{2\pi}\left[2(\theta_2-\theta_1) - (\sin 2\theta_2 - \sin 2\theta_1)\right]$$

$$\sigma_y = -\nu(\sigma_z+\sigma_x)$$

$$\sigma_{xz} = \sigma_{zx} = \frac{q}{\pi}\int_{\theta_1}^{\theta_2}\sin 2\theta\, d\theta = \frac{q}{2\pi}\left[\cos 2\theta_1 - \cos 2\theta_2\right]$$

The principal stress can be calculated from

Major principal stress $$\sigma_1 = \frac{q_0}{\pi}\left[(\theta_2-\theta_1) + \sin(\theta_2-\theta_1)\right]$$

$$\sigma_2 = \frac{q_0}{\pi}\left[(\theta_2-\theta_1) - \sin(\theta_2-\theta_1)\right]$$

$$\sigma_3 = -\nu(\sigma_1+\sigma_2)$$

where θ_1,θ_2 are the radian angles shown in the reference system.

$$\theta_1 = \tan^{-1}\left(\frac{x-b}{z}\right)$$

$$\theta_2 = \tan^{-1}\left(\frac{x+b}{z}\right)$$

These equations for a uniformly loaded strip have been derived from the integration of the solution for a single concentrated linear load. Since the principle of superposition applies it is possible to compute the stress increases within the elastic medium for any arbitrary loading condition. The computer program STRES2 adds the incremental stresses due to a series of uniform strip loads. The width of the footing is divided into equal intervals, with each interval being assigned a uniform contact stress. It was possible to make the contact stress distribution resemble the contact stress distribution expected from a *rigid* strip footing by making the edge contact stress higher than the centre region.

The computer program calculates the normal and principal stresses for any point within the soil medium, but the results for the distribution below the centre axis and footing edge were of primary importance. The estimate of incremental stresses could then be used in comparing the observed pore pressure increases with several theoretical models.

Several contact stress distributions were used, based on the results of the computer program DELTAH, and on the observed contact stress distribution in the experiment. Equilibrium has been ensured, and the edge contact stress has been limited to a finite value in agreement with the concept of local yielding at the edge occurring in practice. It was found that the rigid footing had an influence predominately within a layer less than 2b from the surface, after which the rigid and flexible solutions were essentially similar. Some of the results of the program are shown in Fig. 4.27 and 4.28.

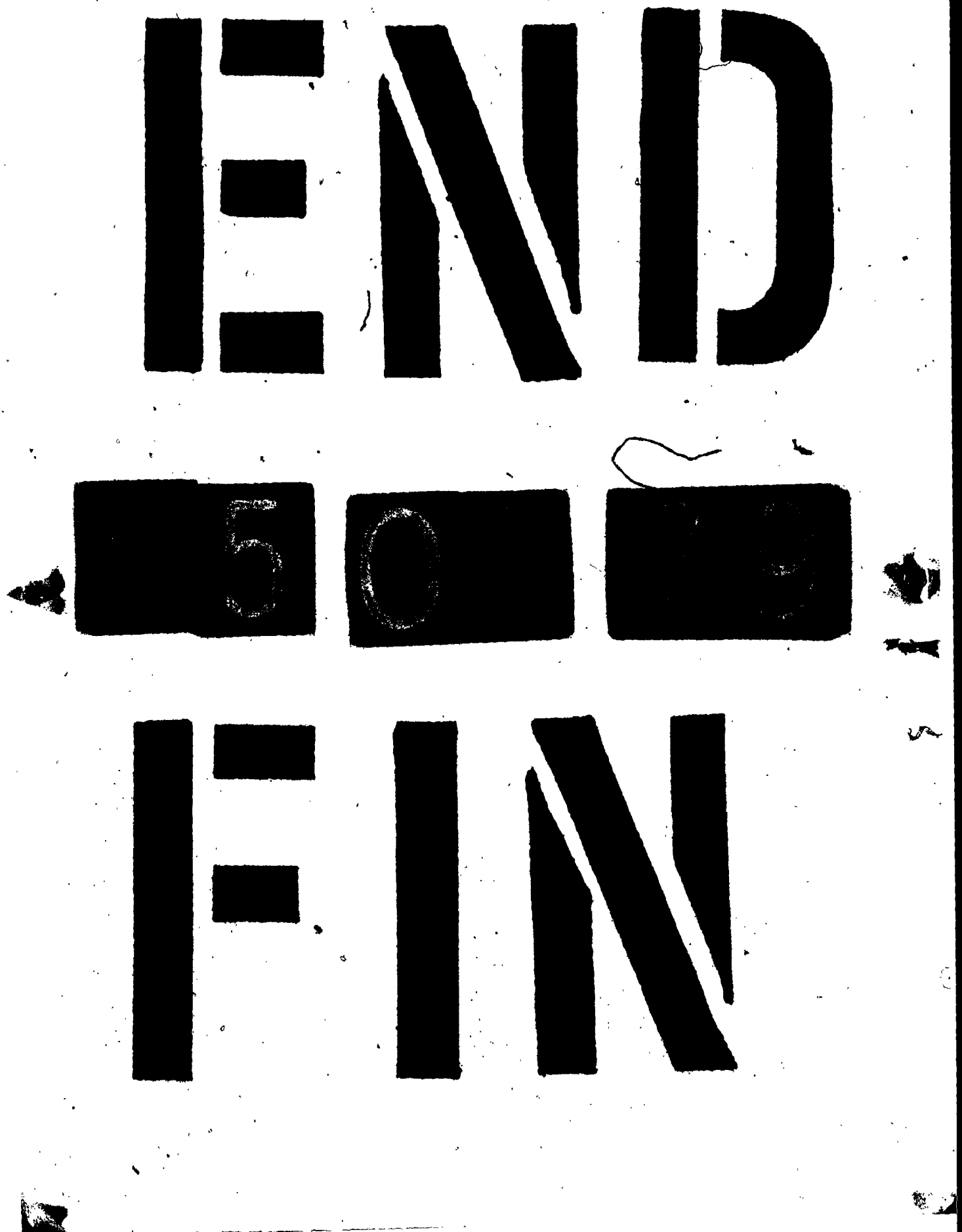
END
THE